Investigation of the role of WIPI2 in autophagosome formation: Functional characterisation of the WIPI2-Atg16L1 interaction

Hannah Clare Dooley

University College London

and

Cancer Research UK London Research Institute

PhD Supervisor: Sharon Tooze

A thesis submitted for the degree of

Doctor of Philosophy

University College London

July 2014

Declaration

I, Hannah Clare Dooley, confirm that the work presented in this thesis is my own. Where information has been derived from other sources, I confirm that this has been indicated in the thesis.

Abstract

Macroautophagy, here called autophagy, is a catabolic process that is required for cell homeostasis and cell survival under nutrient starvation, as well as development and immunity in higher eukaryotes. Characterised by the formation of double membrane-bound vesicles, termed autophagosomes, macroautophagy results in degradation of intracellular proteins in the lysosome. Autophagy initiation leads to the formation of a double membrane phagophore, which expands and sequesters cytoplasm components before autophagosome closure and fusion with endosomes and lysosomes.

Autophagosome formation requires the sequential and concerted action of a number of core autophagy proteins. First identified in yeast, characterisation of mammalian autophagy proteins has shed light on the molecular mechanisms of autophagy initiation and phagophore expansion. However, a number of key questions remain unanswered, including what the functions of the core autophagy proteins mAtg9 and WIPI2 are. mAtg9 is the only transmembrane protein required for autophagy while WIPI2 is a PtdIns(3)P-binding protein. To address the function of these proteins, I used and explored immunoprecipitation - mass spectrometry based approaches to identify and characterise novel interactors. I showed that mAtg9 binds transferrin receptor and this interaction supports a model whereby mAtg9 traffics from a tubular-vesicular mAtg9 compartment, with recycling endosome-like characteristics, to support autophagosome formation. β-propeller proteins such as WIPI2 frequently act in mediating protein-protein interactions and so WIPI2 may recruit autophagy proteins to the PtdIns(3)P-positive site of autophagosome formation. I characterised the Atg16L1-WIPI2b interaction and investigated possible regulation of WIPI2 function by phosphorylation. I used immunoprecipitation to map the interacting regions of WIPI2b and Atg16L1 and to demonstrate that these proteins interact directly. I produced binding mutants of each protein and subsequently characterised the function of Atg16L1-WIPI2b binding, showing that the interaction is required for starvation- and pathogen-induced autophagy. Preliminary data was also obtained on the phosphorylation of the C-terminus of WIPI2 as a possible mechanism of WIPI2 function regulation. I propose a model in which WIPI2b is a PtdIns(3)P effector protein required for recruitment of the Atg12–5-16L1 complex to the site of autophagosome formation and LC3 lipidation.

Acknowledgement

First and foremost, I would like to thank my supervisor Sharon Tooze for her continuous support and encouragement throughout my PhD in relation to life both in and outside of the lab, especially during the publication of my work and writing my thesis. I have learnt a huge under her guidance and count myself extremely fortunate to have worked under such an inspiring scientist over the past four years.

A special thank you to Michael Wilson at the Babraham Institute, whose structural analyses and insights during the WIPI2 project have been invaluable and who has been a pleasure to collaborate with. Also thank you to Stephen Girardin and Dana Philpott for hosting me in their labs in Toronto, and to Matt and Ivan for teaching me how to use *Salmonella* while I was there. I would also like to acknowledge The Bogue Research Fellowships for funding my trip to Canada.

To my examiners Nickolas Ktistakis and Jon Lane – thank you for being so accommodating when we had to re-schedule my viva at late notice and for reading my thesis so quickly.

I am indebted to the core facilities at the LRI: to the equipment park, mass spectrometry facility and antibody production unit. Additionally, thank you to Brenda for her hard work in keeping our floor running smoothly.

I would like to thank my thesis committee: Giampietro Schiavo, Almut Schulze and Peter Parker for their useful inputs and contributions.

Past and present members of the SPW lab, thank you for making the past four years of my life so fantastic. Thank you all for useful discussions and for being eternally generous with your time, expertise and reagents. Thank you to Hannah Polson and Andrea Orsi for their work on WIPI2 and mAtg9, respectively, that I was fortunate enough to continue. Thank you to Chris for putting up with a continuous barrage of, mainly cloning-related, questions. Similarly, thanks to Martina for putting up with the same questions when I didn't get the answer that I wanted from Chris (i.e. the short protocols!) and for being such a great bench mate. Thank you to Delphine and Eyal for being such lovely people and to Harold for always knowing where things are and for being so calm amongst the chaos. A massive thanks to Minoo for always looking out for me (and my health) and for all her hard work on the WIPI2 paper. Finally, thank you to

Justin for being the best PhD-buddy I could possibly ask for and for providing a constant source of entertainment. I will miss you all!

Thank you to all my family for taking an interest in my work – Mum, I am sorry that this thesis doesn't have a more exciting story line! Thank you to both Mum and Dad for always believing in me; I wouldn't be where I am today without your love, encouragement and support. Thank you to my sister, Charlotte, for putting up with me over the years and for always being at the end of the phone when I need to talk. Last but certainly not least, I would like to thank Rob for being there for me, for his patience and understanding, and for making my days brighter.

Table of Contents

Table of figures

List of tables

Abbreviations

2GL9	GFP-LC3 stably transfected HEK293A cells
Atg	Autophagy related
AMPK	5’ adenosine monophosphate-activated protein kinase
BATS	Barkor/Atg14L autophagosome targeting sequence
CMA	Clathrin mediated autophagy
DAG	Diacylglycerol
DFCP1	Double FYVE-containing protein 1
DMEM	Dulbecco’s modified Eagle’s Medium
DSP	Dithiobis[succinimidyl propionate]/ Lomant’s reagent
EBSS	Earle’s balanced salt solution
ELISA	Enzyme-linked immunosorbent assay
EDGR	Epidermal growth factor receptor
ER	Endoplasmic reticulum
ERGIC	ER-Golgi intermediate compartment
FBD	FIP200 binding domain
FIP200	FAK family kinase-interacting protein of 200 KDa
GAP	GTPase activating protein
GATE-16	Golgi-associated ATPase enhancer of 16kDa
GABARAP	GABA receptor-associated protein
GEF	GTPase exchange factor
GFP	Green fluorescent protein
HEK293A	Human embryonic kidney 293A cells
HOPS	Homotypic fusion and protein sorting
Hsc70	Heat shock cognate 70 protein
IP	Immunoprecpitation
KD	Knockdown
KO	Knockout
LAMP	Lysosome-associated membrane protein
MAP-LC3 (LC3)	Microtubule-associated protein 1 light chain 3
mAtg9	Mammalian Atg9

MEF	Mouse embryonic fibroblast
mTOR	Mechanistic target of rapamycin
MOI	Multiplicity of infection
NBR1	Neighbour of BRAC1 gene 1
NDP52	Nuclear domain protein 52
OPTN	Optineurin
PAS	Pre-autophagosomal structure
PBS	Phosphate buffered saline
PCR	Polymerase chain reaction
qPCR	Quantitative polymerase chain reaction
PE	Phosphatidylethanolamine
PROPPIN	β-propellers that bind phosphoinositides
PtdIns(3)P	Phosphatidylinositol 3-phosphate
Raptor	Regulatory associated protein of mTOR complex
Rheb	Ras homologue enriched in brain
RISC	RNA-induced silencing complex
SCV	*Salmonella* containing vesicle
SDM	Site directed mutagenesis
SDS	Sodium dodecyl sulfate
SEM	Standard error of the mean
siRNA	Small interfering RNA
SNARE	SNAP (Soluble NSF Attachment Protein) receptor
Stx13	Syntaxin 13
TBK1	TANK binding kinase 1
TfR	Transferrin Receptor
TTSS	Type three section system
TGN	Trans Golgi network
Ubl	Ubiquitin like
ULK	Unc-51 like autophagy activating kinase
V-ATPase	Vacuolar-type H^+-ATPase
WIPI	WD repeat domain phosphoinositide-interacting
WT	Wild type

Publications

Wilson MI, Dooley HC and Tooze SA. 2014. WIPI2b and Atg16L1: Setting the stage for autophagosome formation. *Biochem Soc Trans*. In Press.

Dooley HC, Razi M, Polson HE, Girardin SE, Wilson MI and Tooze SA. 2014. WIPI2 links LC3 conjugation with PI3P, autophagosome formation, and pathogen clearance by recruiting Atg12–5-16L1. *Mol Cell*, 55, 238-52.

Lamb CA, Dooley HC, and Tooze SA. 2013. Endocytosis and autophagy: Shared machinery for degradation. *Bioessays*, 35, 34-45.

Orsi A, Razi M, Dooley HC, Robinson D, Weston AE, Collinson LM, and Tooze SA. 2012. *Mol Biol Cell*, 23, 1860-73.

Chapter 1. Introduction

1.1 Protein degradation

Proper cell function is achieved through transcriptional control of protein synthesis combined with protein turnover via protein degradation. Although this paradigm is well established now, it has not always been the case. For many years it was thought that the proteins of a cell were stable and not actively degraded. Work by Rudolf Schoenheimer in the late 1930s demonstrated that radioactive nitrogen was incorporated into the tissue of rats after feeding with ^{15}N-labelled tyrosine while non-labelled protein was excreted, showing for the first time that ingested protein is not just required for metabolism, but is required for forming new proteins after protein degradation (Ciechanover, 2005). This idea of protein flux was controversial and it was not until the notion of a half-life of a protein was demonstrated that it was widely accepted.

Numerous landmark discoveries in the past 70 years have built up a complex picture of protein degradation. Both bulk and specific protein degradation occurs within the cell and is essential, in combination with regulated gene expression, for almost all cellular processes, from modulation of the proteome to enable adaption to changes in extracellular conditions, to cell differentiation, cellular homeostasis, protection against starvation, defence against pathogens and cell division. There are two major protein degradation pathways: lysosome- and proteasome-mediated degradation (Figure 1.1). Both of these pathways are tightly controlled and dysfunction of either results in serious pathologies.

1.1.1 Lysosome-mediated protein degradation

The lysosome was discovered in the laboratory of Christian de Duve when it was demonstrated that the enzymatic activity of the cellular fractions containing acid phosphatase increased following treatments that caused membrane disruption (Sabatini and Adesnik, 2013). Further characterisation of these cellular fractions revealed the presence of other hydrolases, all of which have a low optimal pH, and led to the theory of a membrane-bound organelle that was specialised for degradation of macromolecules.

De Duve termed this organelle the lysosome (De Duve and Wattiaux, 1966). This discovery was achieved by biochemical means only; no microscopy was utilised in this initial characterisation of the lysosome. Further work by de Duve's team and others using electron microscopy subsequently confirmed that lysosomes were dense, membrane bound organelles with an acidic pH.

Subsequent morphological studies from numerous researchers began to shed light on how extracellular and intracellular proteins and other macromolecules are degraded. Studies following extracellular markers showed that material was endocytosed into single membrane-bound vesicles, which did not stain for lysosomal acid hydrolases, but which fused with lysosomes at later stages (De Duve and Wattiaux, 1966). Endocytosis of extracellular and plasma membrane bound material and subsequent membrane trafficking events resulting in degradation of endocytosed material will not be discussed any further; I will instead concentrate on degradation of intracellular material.

Morphological studies revealed the presence of acid phosphatase-stained, single membrane-bound organelles that contained cellular components such as bulk cytoplasm, endoplasmic reticulum (ER), and mitochondria (Ohsumi, 2014). Bulk cytoplasm and organelles were also seen in acid phosphatase negative double membrane-bound organelles, termed autophagosomes (De Duve and Wattiaux, 1966). We now know that a double membrane forms around bulk cytoplasm or organelles before self-fusing and subsequently fusing with the lysosome to form a degradative autolysosome, in which macromolecules are broken down and the resulting products are released into the cytoplasm for reuse. This process is termed macroautophagy, or simply autophagy, and will be discussed in more detail in subsequent sections.

Macroautophagy and the endocytic pathway are the major pathways by which material is delivered to the lysosome. However, there are an additional two forms of delivery, both types of autophagy, named microautophagy and chaperone-mediated autophagy (CMA). Intra-lysosomal vesicles have been identified in mammals and in yeast, and are thought to be a product of microautophagy (De Duve and Wattiaux, 1966, Li et al., 2012). Non-selective microautophagy involves the direct engulfment of cytoplasmic cargo at the surface of the lysosome through the formation of a finger-like insertion into the lysosome or vacuole (Mijaljica et al., 2011). Constriction of the neck

of this figure-like tube results in pinching off of a microautophagic vesicle into the lumen of the lysosome or vacuole. This microautophagosome and its contents are subsequently degraded, as for macroautophagosomes. Selective degradation of mitochondria, peroxisomes and the nucleus by microautophagy (micromitophagy, micropexophagy and micronucleophagy, respectively) have been seen in some yeast types (Mijaljica et al., 2011). This selective degradation is thought to occur either through the formation of finger-like projections by the microautophagosome around the organelle (as for micropexophagy) or through piece-meal digestion of small fragments of the organelle in contact with the vacuole (as for micronucleophagy) (Li et al., 2012). Selective micronucleophagy has not been observed in mammals. The function of microautophagy in mammals is unclear; it is thought to be required for survival during starvation, although there is no direct evidence for this (Li et al., 2012, Mijaljica et al., 2011). A more widely accepted, but not necessarily the only, function of microautophagy is in the regulation of lysosome size. After macroautophagosome-lysosome fusion results in increased lysosome size, invagination and pinching off of the lysosome membrane by microphagy acts in organelle homeostasis (Mijaljica et al., 2011).

As well as delivery to the lysosome via membrane deformation and fusion events, certain proteins can be transported across the surface of the lysosome by chaperone-mediated autophagy (CMA) (Orenstein and Cuervo, 2010). CMA involves the targeted degradation of peptides containing a pentapeptide CMA consensus motif. This motif is recognised by the cytosolic protein chaperones, including heat shock cognate 70 protein (Hsc70). CMA substrates then bind the CMA receptor, lysosome-associated membrane protein type 2A (LAMP-2A), on the lysosome surface. LAMP-2A subsequently oligomerises and allows translocation through the lysosome surface. Although constitutively active, CMA is upregulated during periods of cellular stress such as starvation and stress causing protein damage, similarly to macroautophagy (Orenstein and Cuervo, 2010). However, CMA is upregulated at a later stage of starvation than macroautophagy, suggesting that cells may switch from a global protein degradation to a targeted degradation mechanism, therefore ensuring that cells are not damaged by over-digestion of intracellular proteins and instead that only superfluous or unrequired proteins are targeted for degradation and recycling.

1.1.2 Proteasome-mediated protein degradation

The discovery of lysosome-mediated protein degradation provided an explanation for how a cell could mediate intracellular protein and macromolecule degradation but not cause widespread damage, as would be caused by cytosolic hydrolases. However, the pathways described above did not provide an explanation for protein degradation seen in rabbit reticulate lysate, which contains no lysosomes, and other systems where lysosomal inhibitors had been used (Ciechanover, 2005). Investigations led to the discovery of the ubiquitin-proteasome system. Ubiquitin is a small protein, consisting of 76 amino acids, that is covalently bonded to a lysine residue in a target protein. Addition of a polyubiquitin chain containing lysine-48 linkages between ubiquitin molecules results in protein targeting to the proteasome (Ciechanover, 2005). Addition of ubiquitin to a protein involves a cascade of enzymatic reactions: activation of ubiquitin by an ubiquitin-activating enzyme (E1 enzyme) is followed by transfer of the ubiquitin molecule to the active site of an ubiquitin conjugation (E2) enzyme. The final step is the recognition and bringing together of the E2 enzyme and the target protein by a specific ubiquitin ligase (E3 enzyme), which catalyses the transfer of ubiquitin from the active site of the E2 enzyme to the target protein. Following polyubiquitination, a protein is recognised by the proteasome – a barrel-shaped complex comprising of two end ‘caps’ that recognise ubiquitinated proteins and, after protein unfolding, allow entry into the core of the barrel. The core of the proteasome contains proteolytic activity and catalyses protein degradation at the protease active sites. Due to regulation of protein entry into the proteasome barrel by the cap domains, protein degradation can occur in the cytoplasm without causing widespread cellular damage (Ciechanover, 2005). The large number of different E3 enzymes present in cells allows this process to be highly specific and tightly regulated, resulting in the ubiquitin-proteasome system functioning in a huge number of tightly controlled cellular processes including cell cycle control and gene transcription.

My PhD project involves determining the function of WIPI2 in macroautophagy. Consequently, other forms of protein and macromolecule degradation will not be discussed further.

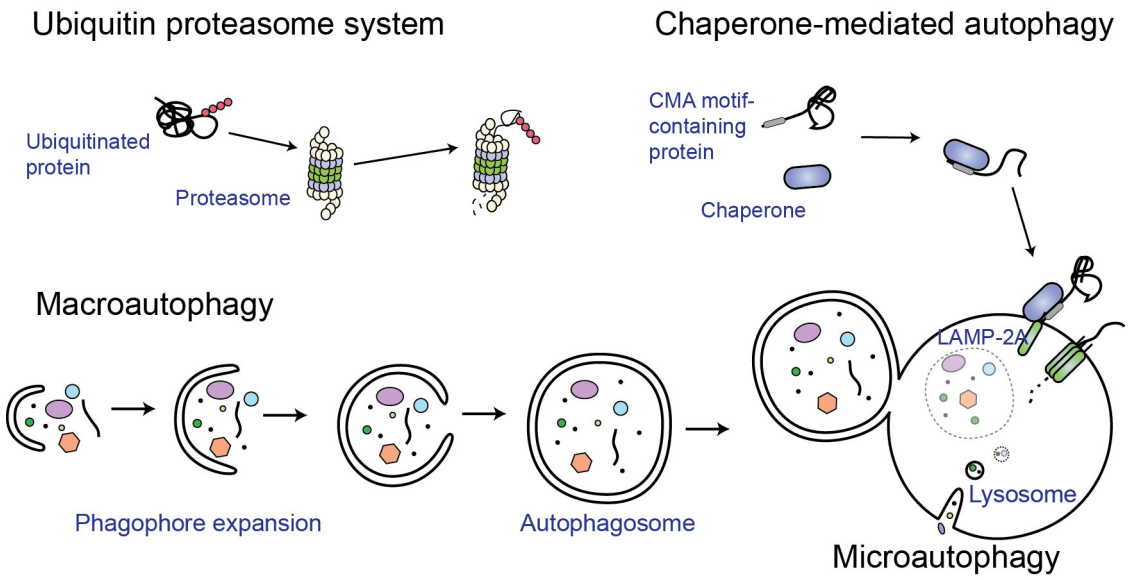

Figure 1.1 Intracellular protein degradation

Intracellular proteins can be degraded via lysosome- and proteasome-mediated protein degradation pathways. Lysosome-mediated intracellular protein degradation is termed autophagy (macroautophagy, microautophagy and chaperone-mediated autophagy).

1.2 Macroautophagy

Macroautophagy (hereafter called autophagy) is a cellular catabolic process that is conserved amongst all eukaryotes: from yeast to man. Literally meaning 'self-eating', autophagy is characterised by the nucleation and expansion of a double membrane (called a phagophore or isolation membrane) that surrounds bulk cytoplasm or organelles, before self-fusing to become an immature autophagosome. The outer membrane of the autophagosome subsequently fuses with organelles in the endocytic pathway, including endosomes, but most importantly lysosomes, forming a degradative autolysosome/mature autophagosome. As discussed previously, the lysosome lumen is acidic and contains numerous hydrolytic enzymes. Therefore, autophagosome-lysosome fusion results in the degradation of the autophagosome contents. Degradation products include amino acids and other macromolecules, and these are released into the cytosol

for reuse. Autophagy occurs in basal conditions, ensuring that old and damaged organelles and long-lived proteins are turned over, and is upregulated in response to cell stress such as amino acid starvation to promote cell survival. During starvation the macromolecules degraded via autophagy are reused for processes such as synthesis of essential proteins.

Although autophagy was originally characterised by electron microscopy in mammalian tissue and cells, the molecular components required for autophagy were first identified in yeast. Nitrogen starvation results in *Saccharomyces cerevisiae* sporulation and meiosis, indicating that nitrogen depletion results in a global turnover of protein in these cells in order to dramatically change their state. Consistently, Yoshinori Ohsumi found that *S. cerevisiae* mutants with impaired vacuole function accumulated autophagic bodies within the vacuoles after nitrogen starvation (Ohsumi, 2014). Ohsumi's group used this accumulation of autophagic bodies (which was visible under light microscopy) as a read-out for gene mutants with an autophagy defect. Looking for mutants that failed to accumulate autophagic bodies in the vacuole after nitrogen starvation, they found the first autophagy defective mutant, *apg-1* (Tsukada and Ohsumi, 1993). This mutant died during long-term nitrogen starvation and this phenotype became the basis for a primary screen for autophagy mutants. Mutants obtained using this primary screen were verified using light microscopy to check for an accumulation of autophagy bodies in the vacuole and complementation analysis of over 100 verified mutants showed 15 complementation groups (Tsukada and Ohsumi, 1993). This list of mutants was added to by other groups using other readouts, including those screening for the Cvt pathway in which α-aminopeptidase I (Ape1) is delivered to the vacuole (Harding et al., 1995). The Cvt pathway involves sequestering specific cargo inside a double membrane-bound vesicle before delivery to the vacuole. The Cvt pathway and autophagy are morphologically similar and many of the genes identified in the screen for Cvt mutants are the same as those identified for autophagy. Cvt is used as a model for selective autophagy, although the pathway is not found in higher eukaryotes. Over 30 autophagy-related (ATG) genes in *S. cerevisiae* have now been identified, representing bulk and selective autophagy. Of these, 18 are considered 'core' autophagy genes that are required for both starvation-induced and selective autophagy and are highly conserved.

Gene isolation and characterisation of the proteins identified in yeast screens have not only advanced our understanding of autophagy in yeast, but have also been extremely informative for research on autophagy in higher eukaryotes. A number of homologues of *S. cerevisiae* autophagy proteins are thought to perform the same or similar functions in mammals, mice and other eukaryotes (Table 1.1). A recent screen for *Schizosaccharomyces pombe* autophagy genes has shown that the mechanism of autophagy is similarly conserved in other yeast (Sun et al., 2013).

The autophagy machinery identified by genetic screens falls into a number of functional groups. These are the Atg1 kinase complex, the PtdIns(3) kinase complex, PtdIns(3)P binding proteins (the Atg18-Atg2 complex), the ubiquitin-like conjugation systems and Atg9. Hierarchical analysis has demonstrated that these systems are recruited to the site of autophagosome formation in a sequential and concerted manner (Suzuki et al., 2007), and this hierarchy of action is well conserved in mammalian autophagy (Itakura and Mizushima, 2010). The autophagosome formation site in yeast is termed the pre-autophagosomal structure (PAS). Autophagy machinery is held in an inactive state by target of rapamycin (TOR), a serine/threonine kinase that phosphorylates and inactivates the Atg1 kinase complex (Kamada et al., 2000). TOR is inactivated by nitrogen starvation, releasing the inhibitory phosphorylation of Atg1 and Atg13, and allowing Atg1 kinase complex formation and translocation, along with the Vps34 type III PtdIns(3)P kinase complex II (Atg14-containing complex), to the PAS. Localisation of active Atg1 and PtdIns(3) kinase on the PAS results in PtdIns(3)P formation and recruitment of the PtdIns(3)P-binding Atg18-Atg2 complex (Obara et al., 2008). The function of this complex is unclear, but it is thought to be required, along with the Atg1 kinase complex, for Atg9 trafficking between the PAS and Atg9 reservoir. Atg9 is the only transmembrane protein that is essential for autophagy (Noda et al., 2000). Its function is currently unclear, but it is known to cycle between the PAS and Atg9 reservoir and so may be shuttling lipids or protein factors. The Atg12–5-16 complex is recruited subsequently to, or concurrently with, Atg18-Atg2 recruitment. The Atg12–5 conjugate acts as an E3-like enzyme to enhance the activity of the Atg8 lipidation machinery, therefore promoting Atg8 conjugation to phosphatidylethanolamine (PE) at the PAS. The exact function of lipidated Atg8 is

unknown, but is thought to be required for autophagosome membrane expansion and fusion (Nakatogawa et al., 2007).

The aim of my PhD is to characterise the function of WIPI2, a mammalian autophagy protein. I will discuss the mammalian core autophagy machinery below, referring to yeast proteins where their functions or characteristics shed more light on the possible functions of their mammalian homologous.

1.3 Molecular machinery

1.3.1 Upstream inhibitor and initiation complexes

Autophagy occurs at a basal rate in all cells to ensure cellular homeostasis and is also a key catabolic mechanism for the provision of essential intermediate metabolites during starvation. As such, it is extensively activated in periods of cellular stress such as amino acid, glucose or growth factor starvation, hypoxia, and low ATP levels. As well as being efficiently and rapidly switched on, autophagy must be effectively inhibited (to basal levels) to ensure against inappropriate intracellular digestion during non-starved conditions. As autophagy plays such a central role in response to nutrient starvation, it should not be surprising that the process is inhibited by mechanistic target of rapamycin complex 1 (mTORC1), which reflects the nutrient status of the cell, and activated by adenosine monophosphate-activated protein kinase (AMPK), which reflects the energy status of the cell. Active mTORC1 inhibits autophagy by inhibitory phosphorylation of the ULK complex, whereas AMPK activates autophagy through ULK and Beclin1 phosphorylation.

mTORC1 is a serine/threonine kinase that acts as a nexus point, integrating nutrient and stress signals and controlling cell growth through processes including transcription and autophagy. mTORC1, like mTORC2, is a multisubunit complex which contains the serine/threonine protein kinase mTOR. mTORC1 and mTORC2 are regulated by growth factors, however mTORC1 also integrates signals from oxygen and amino acid supply, cellular stress and energy levels (Laplante and Sabatini, 2012). mTORC1 is active under normoxic conditions in the presence of nutrients and growth factors, and is inactivated by the removal of nutrients or growth factors, or under

hypoxic conditions. mTORC1 activity requires substrate recognition via Raptor (Nojima et al., 2003). mTORC1 activation is controlled through two branches: Rheb and the Rag GTPases. All upstream signalling inputs, with the noticeable exception of amino acid availability, signal through control of Rheb activity. Rheb is a small GTPase that is controlled by its GTPase activating protein (GAP), a complex consisting of heterodimeric TSC1/TSC2, and TDC1D17. Upstream inputs influence mTORC1 activity by controlling TSC1/TSC2 activity, for example growth factors activate mTORC1 by phosphorylation and inactivation of TSC1/TSC2 by Akt. Active Rheb is essential for mTORC1 activation (Alers et al., 2012). Amino acid availability regulation of mTORC1 activation is achieved through the vacuolar H^+-ATPase (V-ATPase) – Ragulator – Rag GTPase system, which controls mTORC1 proximity to lysosome-localised Rheb (Sancak et al., 2008, Sancak et al., 2010, Zoncu et al., 2011, Bar-Peled et al., 2012). The Rag GTPases are heterodimers of RagA/B and Rag C/D, which directly bind Raptor when the Rag GTPase is active (Rag A/B are GTP loaded) (Sancak et al., 2008). The Ragulator complex, which constitutively binds Rag GTPases, activates Rag GTPases when amino acids are present. The Ragulator is the GTPase exchange factor (GEF) for the Rag GTPases and is responsible for their lysosomal localisation (Sancak et al., 2010, Bar-Peled et al., 2012). The Ragulator is active in the presence of amino acids, but not after amino acid starvation. The mechanism of amino acid-dependent activation of the Ragulator complex is not fully understood, but involves V-ATPase (Zoncu et al., 2011). V-ATPase senses intra-lysosomal amino acid content and relays this signal to Ragulator though a change in the V-ATPase - Ragulator interaction (Bar-Peled et al., 2012). In the presence of amino acids, Ragulator activates the Rag GTPases, enabling binding to Raptor and mTORC1 recruitment to the lysosome surface, where Rheb is localised. In this manner, mTORC1 activity is controlled by two factors: active Rheb on the lysosome surface and mTORC1 localisation to the lysosome through amino acid-dependent recruitment by the Rag GTPases (Figure 1.2).

AMPK is a key energy sensor in the cell and acts as a metabolic checkpoint by downregulating anabolic pathways while simultaneously upregulating metabolic pathways during periods of low cellular ATP levels. AMPK is a heterotrimeric complex and its activation requires phosphorylation within its catalytic α subunit by upstream kinases (Alers et al., 2012). Further modulation of AMPK activity is achieved through

AMP, ADP or ATP binding to its ɣ-subunit (Cheung et al., 2000, Xiao et al., 2011). AMP, ADP and ATP compete for binding of the ɣ-subunit and bind with different affinities: AMP/ADP bind the ɣ-subunit of AMPK more strongly than ATP does. During high AMP/ADP:ATP ratios, indicative of low intracellular energy, AMP and ADP outcompete ATP for AMPK binding and protect activated AMPK from dephosphorylation and subsequent inhibition. In addition, AMP binding allosterically further activates active AMPK. In cells with a high energy level, ATP will be abundant and the AMP/ADT:ATP ratio will low. Therefore, ATP will outcompete AMP or ADP for AMPK binding, removing protection from dephosphorylation and the allosteric activation by AMP, and so reducing AMPK activity.

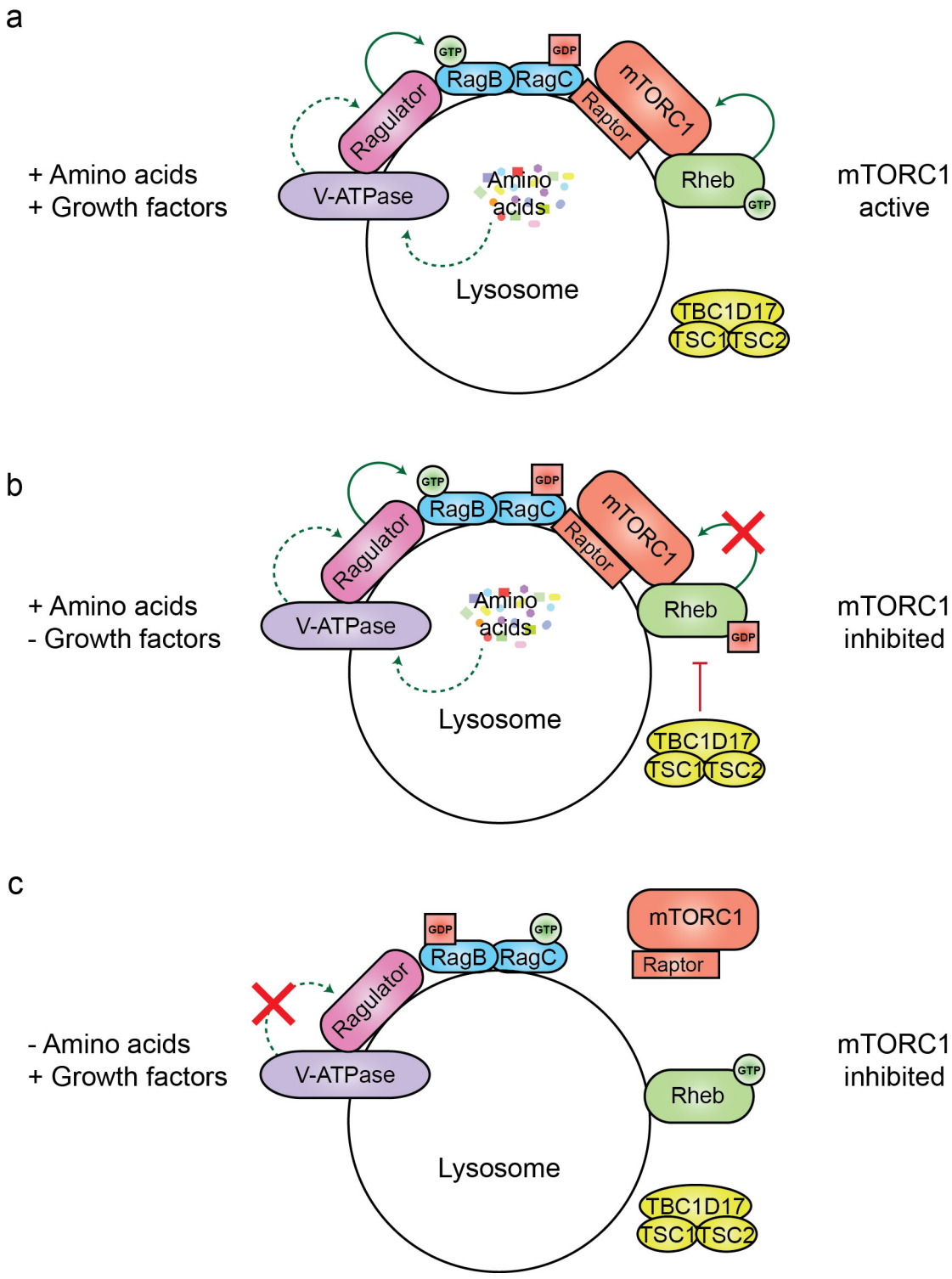

Figure 1.2 mTORC1 activity control

mTORC1 activation requires both active Rheb and Rag GTPase. **(a)** mTORC1 is active in the presence of amino acids and growth factors. Amino acids activate the Ragulator complex, through an unknown mechanism involving the V-ATPase, which subsequently leads to nucleotide exchange and activation on the Rag GTPases. Active Rag GTPases bind Raptor and recruit mTORC1 to the lysosome surface. Growth factor presence inhibits Rheb GAP TSC1/TSC2 complex, therefore activating Rheb and

subsequently mTORC1 on the lysosome. **(b)** mTORC1 is inactive in the presence of amino acids and absence of growth factors. Amino acids activate the Rag GTPases through the Ragulator complex and V-ATPase. Growth factor starvation activates the Rheb GAP TSC1/TSC2, subsequently inhibiting Rheb and inhibiting Rheb-mediated activation of mTORC1. **(c)** mTORC1 is inactive in the presence of growth factors but absence of amino acids. The inhibitory GAP activity of the TSC1/TSC2 complex is removed by growth factor presence, resulting in Rheb activation. However, mTORC1 is not on the lysosome as the Rag GTPases are not active and so cannot bind Raptor. Ragulator complex activation requires amino-acid dependent action of V-ATPase.

1.3.2 ULK kinase complex

S. cerevisiae Atg1 is a serine/threonine kinase that forms a starvation dependent complex with Atg13, and Atg17-Atg29-Atg31 (Kamada et al., 2000, Cao et al., 2009). Hypophosphorylated Atg13 directly binds Atg1 and Atg17, resulting in Atg1 kinase activation and complex localisation to the PAS through the Atg17-Atg29-Atg31 complex (Kamada et al., 2000, Kabeya et al., 2005, Suzuki et al., 2007, Kawamata et al., 2008). When active, TORC1 directly phosphorylates Atg13, reducing its affinity for both Atg1 and Atg17 (Kamada et al., 2010). Consequently, active TORC1 inhibits Atg1 kinase and autophagy progression.

There are five mammalian Atg1 homologues: Unc-51 like kinase (ULK) 1/2/3/4 and STK36, and of these ULK1 and ULK2 are closely related to the *Caenorhabditis elegans* Atg1 homologue UNC51 (Chan et al., 2007, Hara et al., 2008). ULK1 and 2 are serine/threonine kinases that have been shown to be required for autophagy and are thought to have at least partially redundant functions; ULK1 or ULK2 knockout MEFs show only a mild autophagy defect, while double knock out ($ULK1^{-/-}$ and $ULK2^{-/-}$) MEFs show no starvation-induced autophagy (McAlpine et al., 2013). Of the two proteins, ULK1 is the better characterised.

ULK1/2 forms a complex with mammalian homologues of Atg13 (Atg13) and Atg17 (FIP200) along with Atg101, a protein not present in *S. cerevisiae* (Hara et al., 2008, Chan et al., 2009, Jung et al., 2009, Hosokawa et al., 2009b). ULK1 directly binds Atg13, which further binds FIP200 and Atg101 directly. The resulting ULK1/2 complex translocates to the phagophore formation site under starvation conditions. FIP200 is the most upstream protein in the autophagy cascade and is required for targeting downstream core autophagy machinery to the phagophore (Itakura and

Mizushima, 2010). In contrast to the *S. cerevisiae* Atg1 complex, the ULK1/2 complex is formed in both in both fed and starved conditions. Instead, the ULK complex displays a nutrient-dependent interaction with mTORC1: Raptor directly binds ULK1 in fed conditions, resulting in mTORC1-mediated phosphorylation of ULK1/2 and Atg13, and subsequently ULK1/2 kinase inhibition (Figure 1.3) (Hosokawa et al., 2009a). During nutrient deprivation, mTORC1 dissociates from ULK1/2, leading to ULK1/2 kinase activation, ULK1 autophosphorylation, direct phosphorylation of Atg13 and FIP200 by ULK1 and autophagy initiation through the phosphorylation of downstream targets (Jung et al., 2009, Chan et al., 2009). In addition to phosphorylation of members of the ULK1 complex, ULK1 also directly phosphorylates and inactivates mTORC1 itself (Figure 1.3) (Dunlop et al., 2011). Active ULK1 phosphorylates Raptor on multiple sites, causing a decrease in mTORC1 activity probably as a result of a reduced substrate binding by Raptor, thereby providing a positive feedback loop for efficient autophagy activation upon starvation.

ULK1 activity is further controlled by AMPK. AMPK binds to and directly phosphorylates ULK1, resulting in ULK1 kinase activation and autophagy initiation in conditions in which AMPK is active, such as low intracellular ATP levels (Figure 1.3) (Egan et al., 2011, Kim et al., 2011a). This AMPK-phosphorylation and activation of ULK1 provides the second mechanism to two-pronged pathway for autophagy activation by AMPK in conditions of low ATP levels; as well as directly activating ULK1, AMPK also phosphorylates Raptor and inhibits mTORC1 activity (Alers et al., 2012). As described above, mTORC1 inactivation results in a loss of its inhibitory phosphorylation of ULK1/2 and Atg13 and therefore autophagy activation. AMPK binding to ULK1 is regulated by mTORC1: active mTORC1 phosphorylates ULK1 within the region shown to bind AMPK, therefore disrupting binding (Kim et al., 2011a).

The role of ULK1 in starvation-induced autophagy was first characterised seven years ago and although not fully understood, a clearer picture of mechanisms regulating its activity is emerging. However, how this kinase complex leads to autophagosome biogenesis is still not well understood. The number of ULK1/2 kinase targets identified is low, although it is known that ULK1 activates the Beclin1 PtdIns(3)P kinase complex

through direct phosphorylation while yeast Atg1 activates Atg9 through direct phosphorylation (see Chapter 1.3.3 and 1.3.6, respectively).

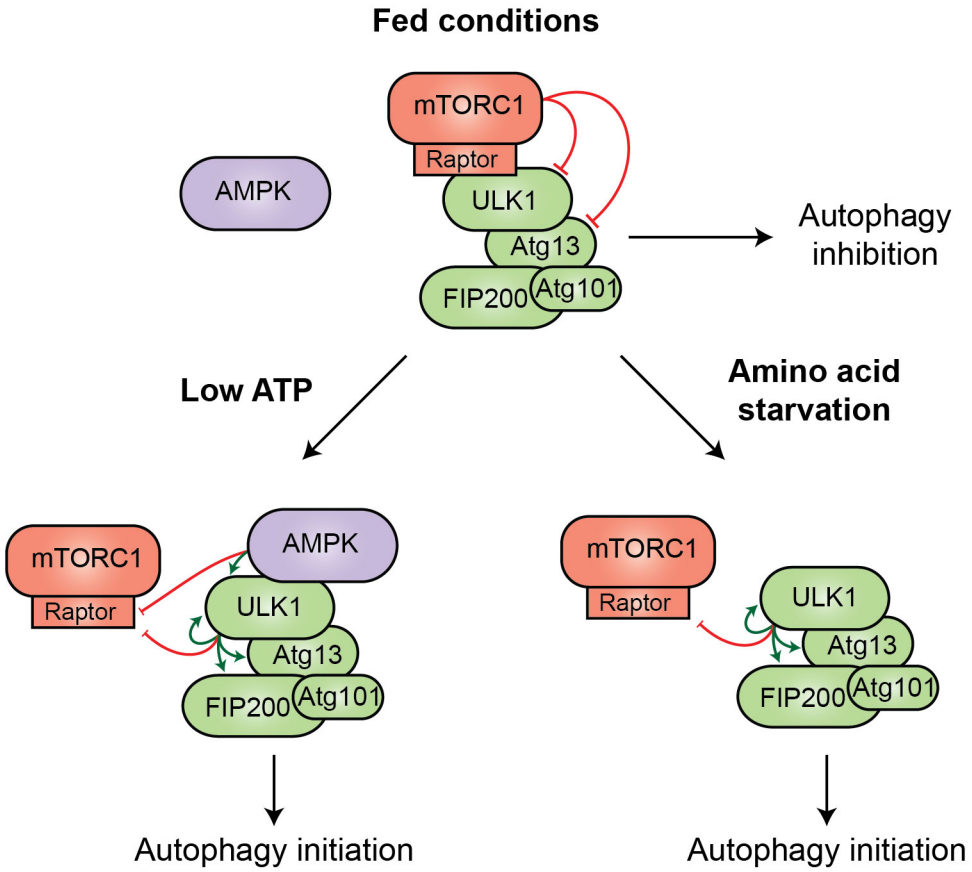

Figure 1.3 Control of ULK1 activity by mTORC1 and AMPK

The ULK kinase complex is held in an inhibited state by active mTORC1 which binds ULK and phosphorylates both ULK and Atg13. Amino acid starvation results in mTORC1 inhibition through upstream signalling cascades (Figure 1.2) and ULK phosphorylation of Raptor. Active ULK undergoes autophosphorylation and phosphorylates Atg13 and FIP200, resulting in activation of the ULK complex. During glucose starvation, AMPK phosphorylates Raptor, inhibiting mTORC1, while also phosphorylating and activating ULK. Red and green lines indicate inhibitory and activating phosphorylation, respectively.

1.3.3 PtdIns(3)P kinase complexes

PtdIns(3)P production on the PAS in yeast, or omegasome in mammalian cells, is required for recruitment of all autophagy proteins downstream of the PtdIns(3) kinase complex. Additionally, omegasome-localised PtdIns(3)P production is also required for stabilising the ULK kinase complex (Karanasios et al., 2013b). The functions of

PtdIns(3)P in autophagosome formation are not yet fully understood, but downstream PtdIns(3)P binding proteins have been identified and characterised to some extent (see Chapter 1.3.4). Very little PtdIns(3)P is found on the endoplasmic reticulum (ER) during normal cell growth conditions and the localised production of the ER-localised PtdIns(3)P pool in mammalian autophagy is a result of an autophagy-specific PtdIns(3) kinase.

PtdIns(3) kinases phosphorylate phosphatidylinositol on the 3' position of the inositol ring. There are three classes of PtdIns(3) kinases: class I produces PtdIns(3,4)P_2, PtdIns(3,4,5)P_3 and a small amount of PtdIns(3)P. Primarily acting at the plasma membrane, this class is involved in receptor-mediated signalling. Class II PtdIns(3) kinases produce PtdIns(3)P and PtsIn(3,5)P_2, however their functions are poorly understood. Class III PtdIns(3) kinase produces PtdIns(3)P only and is implicated in intracellular trafficking at multiple stages including endosome function, retrograde traffic from endosome to Golgi, multivesicular body (MVB) formation and autophagy (Foster et al., 2003). Unlike class I and II kinases, all eukaryotes have a single Class III PtdIns(3) kinase, the Vps34 PtdIns(3)P kinase (Foster et al., 2003). Yeast have two class III PtdIns(3)P kinase complexes formed of a core kinase complex of Vps34, Vps15 and Atg6 along with either Atg14 (complex I) or Vps38 (complex II). Complex I is required for PtdIns(3)P production for autophagy and complex II for the vacuolar sorting (Vps) pathway.

Mammalian cells have at least two Vps34 complexes, both of which contain the Atg6 homologue Beclin1, the first autophagy protein to be identified in mammals, and mammalian Vps15 (formerly p150) (Liang et al., 1999, Panaretou et al., 1997). Both Beclin1 and Vps15 directly bind Vps34 and are needed for PtdIns(3) kinase activity (Liang et al., 2006, Yan et al., 2009). Vps15 myristoylation at its N-terminus is thought to be involved in membrane targeting of the Vps34-Vps15 complex (Panaretou et al., 1997). Beclin1 promotes the formation of the Vps34-Vps15 core complex and interacts with cofactors, including UVRAG, Atg14L, Ambra1, NRBF2 and Bif-1, to modulate of the activity of the Vps34 kinase and regulate of Vps34 activity or function (Liang et al., 2006, Matsunaga et al., 2009, Fimia et al., 2007, Lu et al., 2014, Takahashi et al., 2007).

Mammalian Atg14 (Atg14L) shows weak homology to yeast Atg14 and is required for Vps34 PtdIns(3)P kinase activity in autophagy (Figure 1.4a) (Zhong et al.,

2009, Kim et al., 2013, Russell et al., 2013). Atg14L and Beclin1 directly interact via their coiled coil domains and this interaction is required for Atg14L interaction with the Vps34-Vps15 complex, although additional direct binding to the Vps34-Vps15 complex by Atg14L1 has not been excluded (Matsunaga et al., 2010). Atg14L localises, with the Vps34 kinase complex, to the omegasome during starvation (Matsunaga et al., 2010). Although omegasome localisation of Atg14L is starvation-dependent, Atg14L is constitutively ER localised, independent of Vps34 activity or Beclin1 binding (Itakura et al., 2008, Matsunaga et al., 2010). Through its interaction with Beclin1, Atg14L is responsible for the ER-targeting of the Vps34 kinase complex and subsequent ER-localised PtdIns(3)P during starvation-induced autophagy. Atg14L contains two signals for ER localisation: N-terminal cysteine repeats and a C-terminal BATS (BARKOR/Atg14L autophagosome targeting sequence) (Matsunaga et al., 2010, Fan et al., 2011). Although critical for Vps34 targeting to the ER and subsequent autophagy, ER recruitment via Atg14L cannot explain the trigger for autophagy as Atg14L localisation to the ER does not change with nutritional status of the cell, and Atg14L localisation to puncta representing omegasomes, but not the ER, is disrupted in ULK1 kinase inhibited cells (Matsunaga et al., 2010).

In contrast to Atg14L, the function of the Beclin1 interacting protein UVRAG is widely debated. UVRAG was identified as a Beclin1 interacting protein, whose direct interaction with Beclin1 is mediated through a coiled coil interaction between the two proteins (Liang et al., 2006). Atg14L and UVRAG form distinct Vps34-Vps15-Beclin1 complexes, possibly through a mutually exclusive binding to the same region of the Beclin1 coiled coil domain (Matsunaga et al., 2009). UVRAG is localised, with Vps34, to Rab9 containing endosomes involved in retrograde trafficking to the Golgi, and to a lesser extent on Rab5 and Rab7 positive endosomes, early endosomes and late endosomes, respectively. UVRAG colocalisation with autophagosomes has been observed, however this was found using transiently overexpressed proteins and has not been repeated in subsequent studies (Liang et al., 2006, Itakura et al., 2008, Matsunaga et al., 2009). Similarly, different groups have seen different effects of UVRAG overexpression and knockdown on autophagy. However, there is a consensus on the effect of UVRAG knockdown on endocytic degradation: UVRAG is required for the degradation of epidermal growth factor receptor (EGFR) (Matsunaga et al., 2009, Jiang

et al., 2014, Liang et al., 2008). UVRAG has weak homology with yeast Vps38 (Itakura et al., 2008). This and its possibly indirect role in autophagy suggest that UVRAG may be involved in endocytic sorting to the lysosome rather than in autophagic degradation (Figure 1.4b).

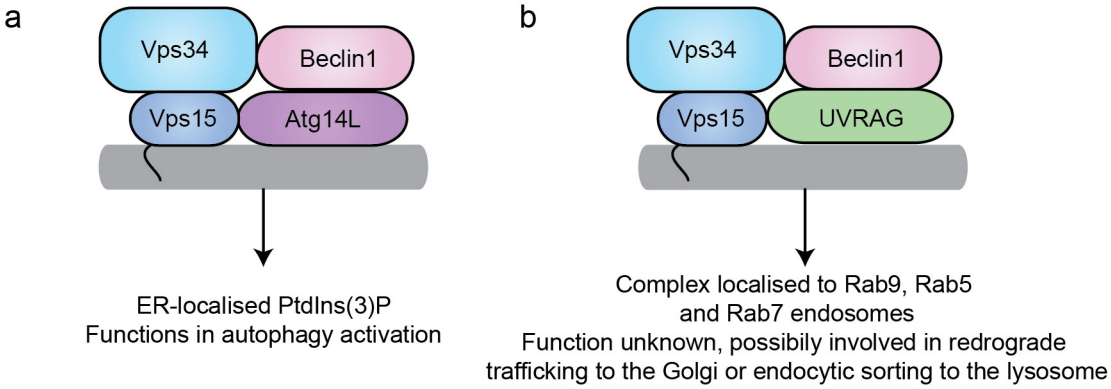

Figure 1.4 The Atg14L- and UVRAG-containing Vps34 PtdIns(3)P kinase complexes
Beclin1-Vps34-Vps15 core complexe can bind **(a)** Atg14L, forming complex I which is needed for omegasome-localised PtdIns(3)P production and therefore autophagy, and **(b)** UVRAG, forming complex II, the function of which is not clear, but is needed for proper EGFR degradation possibly as a result of involvement of complex II in retrograde trafficking or endocytic sorting to the lysosome.

Rubicon binds to UVRAG and Rab7 in a mutually exclusive manner (Sun et al., 2010). Active Rab7-GTP binds Rubicon and releases UVRAG to interact with the vacuolar/lysosomal homotypic fusion and vacuole protein sorting (HOPS) tethering complex (Figure 1.5) (Sun et al., 2010, Tabata et al., 2010, Liang et al., 2008). Until earlier this year it was thought that autophagosome-localised UVRAG binds HOPS and mediates autophagosome – lysosome fusion after release from inhibitory interaction with Rubicon by active Rab7 (Liang et al., 2008). However, identification of the interaction between Syntaxin (Stx) 17, a component of the SNARE complex required for autophagosome – lysosome fusion (Itakura et al., 2012), and HOPS showed that the Stx17-HOPS interaction is required for autophagosome maturation, but that UVRAG is not present in this complex and is not directly required for autophagosome formation or maturation (Jiang et al., 2014). Instead, HOPS and UVRAG, unlike Stx17, are both required for endocytic degradation (Liang et al., 2008, Jiang et al., 2014). This may be due to a direct requirement for the UVRAG-HOPS complex in late endosome – lysosome fusion or as a result of improper hydrolase delivery to the lysosome due to

impaired retrograde trafficking. Support for a role in late endosome – lysosome fusion includes the presence of UVRAG and Rubicon on Rab7-posisitve late endosomes and the negative effect of Rubicon on endosomal maturation (Sun et al., 2010). The function of Rab7-GTP in removing Rubicon-mediated inhibition of UVRAG-HOPS interaction could provide a mechanism for controlling late endosome – lysosome fusion (Sun et al., 2010). Similarly, UVRAG is present on Rab9 positive endosomes, which represent retrograde traffic to the Golgi apparatus, and may therefore be a true mammalian homologue of Vps38 (Itakura et al., 2008). Involvement of UVRAG at either step of the endocytic degradation pathway may result in an indirect effect of UVRAG function on autolysosome degradation due to its function impacting delivery of hydrolases to the lysosome (Jiang et al., 2014). The involvement of the Vps34 PtdIns(3)P kinase in UVRAG-dependent trafficking events is not known, although Bif-1, a UVRAG interacting protein, and Rab7-GTP have been shown to increase the activity of the Beclin1-containing Vps34 PtdIns(3)P kinase during starvation (Takahashi et al., 2007, Tabata et al., 2010). Interestingly, the activity of the UVRAG-containing Vps34 PtdIns(3)P kinase complex increases during starvation (Kim et al., 2013, Russell et al., 2013), suggesting that, even if its function in autophagy is indirect, the UVRAG Vsp34 kinase complex must be active for autophagy.

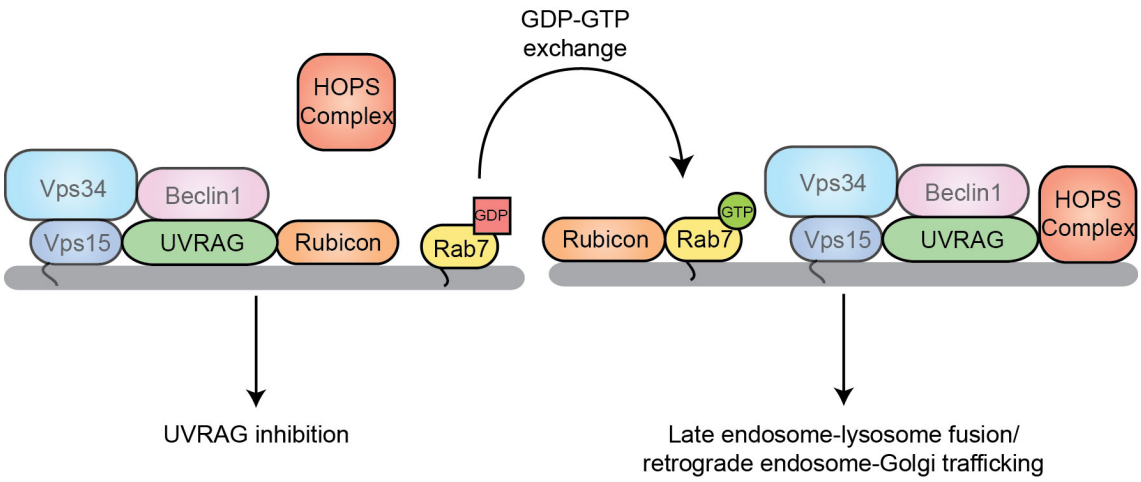

Figure 1.5 UVRAG involvement in endocytic trafficking

UVRAG interaction with the HOPS complex is inhibited by Rubicon, therefore inhibiting UVRAG function. Rab7-GTP releases this inhibition by binding Rubicon and allowing UVRAG-HOPS interaction and downstream functions. The requirement for the core Vps34 complex (Vps34, Vps15 and Beclin1) in this UVRAG function is yet to be studied.

As described above, different Beclin1 interacting proteins can change and modulate the function of the Vps34 PtdIns(3) kinase complex. The activity of Vps34 PtdIns(3)P kinase complexes are very tightly regulated. In starvation (amino acid and glucose) the activity of bulk Vps34 PtdIns(3)P kinase decreases, however that of Atg14L or UVRAG containing complexes increases (Russell et al., 2013, Kim et al., 2013). Although regulation of the autophagy-specific (Atg14L containing) complex is not fully understood, at least three mechanisms of starvation-induced Vps34 PtdIns(3) kinase activation have been identified:

1) During starvation, active ULK1 (and ULK2) kinase complex directly phosphorylates the N-terminus of Beclin1, resulting in increased Vps34 complex activity (Figure 1.6a) (Russell et al., 2013). This ULK1-mediated phosphorylation of Beclin1 is conserved in *C. elegans* but not *S. cerevisiae* and requires Atg14L, which acts as an adaptor. Although ULK1 kinase activity is required for localisation of the Beclin1 complex to forming autophagosomes (Matsunaga et al., 2010), Beclin1 phosphorylation by ULK1 is not the signal required for this localisation; the Beclin1 complex must be omegasome-localised for Atg14L to mediate the ULK1-Beclin1 interaction and enable subsequent phosphorylation. Therefore, ULK1, or its downstream targets, acts both upstream and downstream of Vps34 localisation and, perhaps, the colocalisation of the Vps34 complex and ULK1 kinase complex at the omegasome acts as a coincidence detector for autophagosome progression.

2) Ambra1 is a highly conserved WD-40 protein that directly binds Beclin1 and is required for autophagy (Fimia et al., 2007). Ambra1 interacts with microtubules in a nutrient-dependent manner. During starvation, ULK1 phosphorylation of Ambra1 results in Ambra1 dissociation from dynein intermediate chain (DIC) and subsequent translocation to the ER (Figure 1.6b) (Di Bartolomeo et al., 2010). Although Ambra1 tethers the Vps34 complex away from the ER, Ambra1 depletion results in a loss of Beclin1 translocation to the ER in both fed and starved conditions and so it appears to be required for ER localisation of the Vps34 complex in a manner more complex and active than simply tethering and restraining the complex during non-autophagy conditions. It will be interesting to see what, if any, the interplay between Ambra1 and

Atg14L is in determining the omegasome-localisation of the Vps34 PtdIns(3) kinase complex during autophagy.

3) Glucose starvation alone results in an increase of Atg14L- or UVRAG-associated Vps34, but a general decrease in bulk Vps34 activity. Glucose starvation results in an increase in AMP/ADP:ATP ratio and subsequently leads to AMPK activation. AMPK directly phosphorylates Vps34 and Beclin1 (Figure 1.6c) (Kim et al., 2013). Beclin1 phosphorylation increases the activity of the Vps34 complex and therefore is required for autophagy. Atg14L binding to Beclin1, but not ER localisation, is required for AMPK-mediated Beclin1 phosphorylation, suggesting that Atg14L is again acting as an adaptor between a kinase and its target Beclin1. AMPK phosphorylation of Vps34 results in a glucose starvation-dependent reduction in Atg14L1- and UVRAG-free Vps34 complexes (the functions of these complexes have not been described). Vps34 phosphorylation has no effect on autophagy, and is in fact inhibited by Atg14L presence in the complex, but is needed for cell survival during glucose starvation.

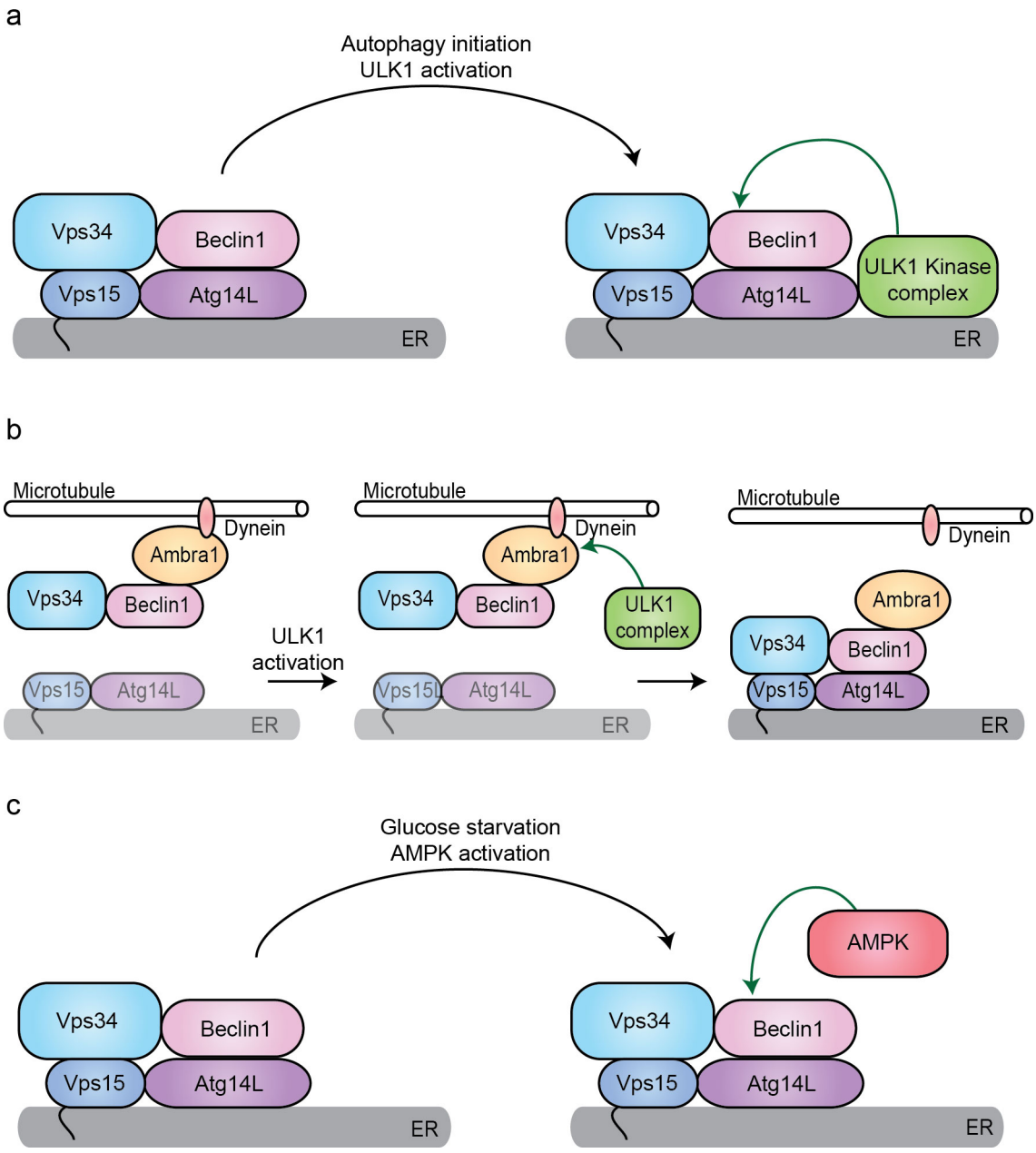

Figure 1.6 Control of Atg14L-containing Vps34 PtdIns(3) kinase complex activity

(a) Active ULK1 kinase complex binds Atg14L and activates the Vps34 PtdIns(3)P kinase by phosphorylating Beclin1. **(b)** During fed conditions, Ambra1 is associated with Vps34 and Beclin1 on microtubules through an interaction with Dynein. During starvation, active ULK1 phosphorylates Ambra1, inhibiting its interaction with Dynein and allowing translocation of the Ambra1-Beclin1-Vps34 complex to the ER. The localisation of Vps15 and Atg14L during this Ambra1-mediated relocalisation has not been published, but Atg14L is constitutively on the ER, and Vps15 is myristoylated so both proteins are shown docked to the ER membrane in all conditions. **(c)** Active AMPK phosphorylates Beclin1, leading to Vps34 PtdIns(3) kinase activation.

1.3.4 PtdIns(3)P binding proteins

As described above, PtdIns(3)P production at the site of forming autophagosomes is essential for starvation-induced autophagy. The role that this phosphoinositide plays is not well understood but the general consensus is that it acts to recruit downstream proteins. A number of PtdIns(3)P binding proteins involved in autophagy have been identified, but their functions and mechanisms of action are currently unclear. These proteins include the β-propellers that bind phosphoinositides (PROPPIN) family, and double FYVE domain-containing protein 1 (DFCP1) in mammals.

1.3.4.1 DFCP1

DFCP1 contains both an ER-targeting domain and two PtdIns(3)P binding FYVE domains (Axe et al., 2008). Autophagy activation leads to DFCP1 localisation to the pool of ER-localised PtdIns(3)P produced by the Atg14L-containing Vps34 PtdIns(3) kinase complex (Matsunaga et al., 2010, Axe et al., 2008). These DFCP1 labelled structures are termed omegasomes and are PtdIns(3)P-enriched platforms from which autophagosome biogenesis is nucleated (Axe et al., 2008). Omegasomes are dynamic, initially forming as small punctate domains, which expand into ring-shaped structures before collapsing into small punctate domains again. Coinciding with omegasome expansion and collapse, LC3- and Atg5-positive phagophores form within the centre of the omegasome before expanding and exiting the omegasome. Once exited, the forming autophagosome matures and becomes acidified. DFCP1 function is currently unknown; DFCP1 depletion has no effect on autophagy and it is likely to play a non-essential function in autophagy because there is no known yeast homologue. However, DFCP1 overexpression results in autophagosome inhibition, possibly by sequestering omegasome-localised PtdIns(3)P from other PtdIns(3)P-binding proteins (Axe et al., 2008).

1.3.4.2 The PROPPIN family

The PROPPIN family of WD-40 motif-containing proteins are conserved between yeast and mammals and bind PtdIns(3)P and PtdIns(3,5)P_2 through the atypical phosphoinositide binding FRRG motif. There are three PROPPINs identified in *S. cerevisiae* (Atg18, Atg21 and Hsv2) and *S. pombe* (Atg18a, b and c), two in *C. elegans* (Atg18 and Epg-6) and four in mammalian cells (WIPI1, 2, 3 and 4). Crystallisation of the Atg18 homologue Hsv2 from *Kluyveromyces marxianus* has revealed that PROPPINs form seven-bladed β-propellers with a non-Velcro propeller closure (Krick et al., 2012, Baskaran et al., 2012, Watanabe et al., 2012). The conserved FRRG motif forms two PtdIns(3)P binding sites in blades 5 and 6 of the β-propeller (Figure 1.7). Protein attachment to membranes is enhanced by a hydrophobic loop positioned in blade 6 (Krick et al., 2012, Baskaran et al., 2012). WD-40 domains are the most common protein-protein interaction domains in the eukaryotic genome (Xu and Min, 2011), and as such it is likely that the function of the PROPPIN family will be to mediate protein-protein and protein-lipid interactions. The PROPPINs are positioned on the membrane so that they lie with their side touching and their faces of the β-propeller perpendicular to the membrane (Figure 1.7). Most protein interactions with WD-40 proteins are mediated by the loops between the β-sheets within each blade of the β-propeller. Therefore, this orientation ideally positions the loops of blades not involved in membrane binding for protein interactions when the PROPPIN is membrane bound.

S. cerevisiae Atg18 is essential for autophagy and the Cvt pathway (Barth et al., 2001), Atg21 functions in autophagy and the Cvt pathway but is only essential for the Cvt pathway (Stromhaug et al., 2004, Meiling-Wesse et al., 2004), and poorly characterised Hsv2 (Ygr223c) is known to function in micronucleophagy (Krick et al., 2008). Atg18 and Atg21 have non-redundant functions. Atg21 acts before vesicle closure and its loss reduces Atg8 lipidation, and recruitment of Atg8 and Atg5 to the PAS during the Cvt pathway and starvation-induced autophagy (Stromhaug et al., 2004, Nair et al., 2010, Meiling-Wesse et al., 2004). PtdIns(3)P binding by Atg21 is essential for its function in the Cvt pathway (Krick et al., 2006, Nair et al., 2010), but is dispensable for autophagy (Nair et al., 2010). To date, the function of Atg21 is unknown and Atg18 is the only identified Atg21 binding partner (Nair et al., 2010),

although this interaction is disputed (Meiling-Wesse et al., 2004). Further work to identify binding partners will shed light on the function of this protein.

A number of Atg18 binding proteins have been identified, including Atg2, Vac7 and Vac14. Atg18 binds Atg2 through the loops between β-sheets in blade two, which is on the opposite side of the protein to the membrane binding FRRG motif and membrane insertion loop in blades 5 and 6 (Watanabe et al., 2012, Rieter et al., 2013). The Atg18-Atg2 complex is essential for autophagy and has been implicated in Atg9 trafficking from the PAS and protection of Atg8-PE from premature Atg4-mediated deconjugation (Nair et al., 2010). PAS localisation of Atg18 is dependent on both PtdIns(3)P and Atg2 binding (Obara et al., 2008, Rieter et al., 2013), suggesting that Atg18 recruitment is tightly controlled by this cooperative mechanism. However, the function of Atg2 is not just to ensure Atg18 PAS localisation; Atg18 localised to the PAS cannot compensate for Atg2 loss (Kobayashi et al., 2012). The requirement of Atg18 for Atg2-PAS localisation is controversial, with reports of Atg18 loss both reducing (Obara et al., 2008) and having no effect on localisation of Atg2 to the PAS (Rieter et al., 2013). It may be that these differences are due to variations in the sensitivities of the techniques used and that Atg18 loss has a partial effect on Atg2 localisation. Consistently, Atg2 targeted to the PAS can only partially rescue autophagy in *Atg18Δ* strains (Kobayashi et al., 2012), indicating that Atg18 is involved in mediating Atg2 localisation and in additional autophagy functions. Loss of either Atg18 or Atg2 results in increased Atg8 lipidation and increased Atg8 and Atg16 PAS-localisation in fed and starved conditions, suggesting that the complex functions in dissociation of these proteins from the PAS.

As well as its localisation to the PAS, Atg18 is found on endosomes and vacuoles (Obara et al., 2008). Vacuole localisation is dependent on PtdIns(3,5)P_2 binding and the presence of the vacuole-localised Atg18 binding partner Vac7. Atg18 is required for proper vacuole morphology through modulation of PtdIns(3,5)P_2 production. Atg18 recruitment to the vacuole surface through PtdIns(3,5)P_2 and Vac7 binding may result in Vac7 sequestration from and therefore inhibition of the PtdIns(3)P 5-kinase Fab1 (Efe et al., 2007). Interestingly, in *Pichia pastoris* (a methylotrophic yeast) Atg18 binding to PtdIns$(3,5)_2$ and subsequent regulation of vacuolar morphology is regulated by Atg18 phosphorylation (Tamura et al., 2013). Phosphorylation within the loop between blades 6 and 7 of Atg18 reduces the affinity of Atg18 for

PtdIns(3,5)P_2 and subsequently reduces binding to the vacuolar membrane. This phosphorylation is the only reported post-translational modification mediating control of PROPPIN phosphatidylinositol binding and although it is not required for macroautophagy, phosphoregulation of Atg18 is required for optimal micropexophagy. Conservation of the *Pichia pastoris* Atg18 phosphorylation site in higher eukaryotes, including in human WIPI1, suggests other PROPPIN proteins may be regulated in a similar manner (Tamura et al., 2013).

Unlike in *S. cerevisiae*, all three of *S. pombe* PROPPINs are required for autophagy (Sun et al., 2013). In a similar manner to Atg18 and Atg2 deletion in *S. cerevisiae*, Atg18b and c deletions accumulate Atg8 puncta. However, Atg18a deletions and Atg18a-FTTG mutants (which cannot bind PtdIns(3)P) have no Atg8 puncta. Interestingly, Atg18a interacts with Atg5 and it is probable that Atg18a acts as a platform to mediate the PtdIns(3)P-dependent recruitment of the Atg12–5-16 complex, although this remains to be shown.

Mammalian cells have four PROPPIN proteins: the WD repeat domain phosphoinositide-interacting (WIPI) proteins WIPI1, 2, 3 and 4. WIPI1 and WIPI2 are evolutionarily more closely related to Atg18 than WIPI3 and WIPI4 are (Polson et al., 2010), however it remains to be determined which of the proteins are functionally conserved. All four isoforms have a 7-bladed β-propeller and a conserved PtdIns(3)P binding domain and membrane insertion loop (Figure 1.8 a). WIPI2 is required for autophagy, functioning downstream of the Atg14L-containing Vps34 PtdIns(3)P kinase complex, but upstream of LC3 lipidation. Similarly to DFCP1, WIPI2 forms punctate and ring-shaped structures after starvation. WIPI2 puncta colocalise with DFCP1 and Atg16L1, but not with acidified autophagosomes, and WIPI2 rings are often intertwined with or very closely associated with DFCP1 rings (Polson et al., 2010). WIPI2 has six isoforms, WIPI2a, b, c, d, δ and e (Figure 1.8 b). Of these, the localisation of WIPI2a-d starvation-induced puncta has been analysed. WIPI2b and d form starvation-induced puncta, where as WIPI2a and c do not (Mauthe et al., 2011). This difference in localisation can be assigned to the presence of an 18 amino-acid insert between β-sheets one and two of the first blade of WIPI2a and c (Figure 1.8b and 1.9); presence of the insert renders the protein unable to form puncta, suggesting that this insert may be inhibiting an interaction critical to puncta formation or disrupting proper protein folding.

WIPI1 is not as widely expressed as WIPI2 and its function is not well established (Polson et al., 2010, Mauthe et al., 2011), although it is known to function downstream of the Atg14L PtdIns(3) kinase complex but upstream of the Atg5 and Atg7 pathways (Itakura and Mizushima, 2010, Mauthe et al., 2011). Overexpression of WIPI1 displaces WIPI2 from forming autophagosomes, presumably by competing with WIPI2 for PtdIns(3)P binding, resulting in autophagy inhibition (Polson et al., 2010). This demonstrates that WIPI1 and WIPI2 have non-redundant functions in autophagy.

The function of WIPI3 in autophagy is not known, however WIPI4 is thought to act in conjunction with Atg2 (Velikkakath et al., 2012). There are two Atg2 homologues in mammalian cells with redundant functions: Atg2a and Atg2b (Velikkakath et al., 2012). Depletion of both of these results in the formation of LC3-positive, unclosed autophagosomes and increased LC3 lipidation (Velikkakath et al., 2012). Similarly, WIPI4 knockdown blocks autophagosome exit from the omegasome, resulting in enlarged DFCP1 rings with LC3-positive phagophores at their centre (Lu et al., 2011). The accumulation of LC3 at phagophores and LC3 lipidation in WIPI4 and Atg2 knockdowns is similar to *atg18Δ* and *Atg2Δ* strains in *S. cerevisiae*, suggesting that although not evolutionarily closely related, WIPI4 may be functionally related to Atg18. *C. elegans* has one WIPI1/WIPI2-like protein, Atg18, and one WIPI3/WIPI4 protein. The *C. elegans* WIPI4 homologue EPG-6 directly binds Atg2 and functions downstream of LGG-1 (LC3 homologue) lipidation, possibly during autophagosome closure (Lu et al., 2011). The EPG-6-Atg2 complex is required for Atg9 distribution, again suggesting that WIPI4 homologues have similar functions to Atg18. The function of Atg18 in *C. elegans* is unknown, but it is thought to act before EPG-6 (Lu et al., 2011).

The functions of the PROPPIN family during autophagy are poorly understood. It is probable that the functions of these proteins will be in the formation of protein-protein interactions and the anchoring of subsequent complexes to membranes in a phosphatidylinositol-dependent manner. Identification of interacting partners will shed light on the function of this family of core autophagy proteins.

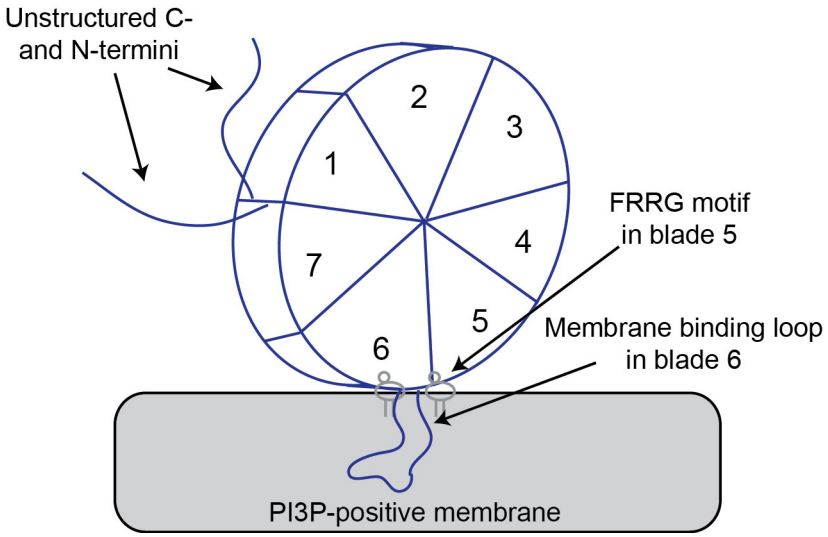

Figure 1.7 Model of PROPPIN structure

The PROPPIN proteins form 7-bladed β-propellers with an FRRG motif in blade 5 that forms two PtdIns(3)P binding pockets on blades 5 and 6, and a hydrophobic membrane insertion loop in blade 6 (Krick et al., 2012, Baskaran et al., 2012, Watanabe et al., 2012).

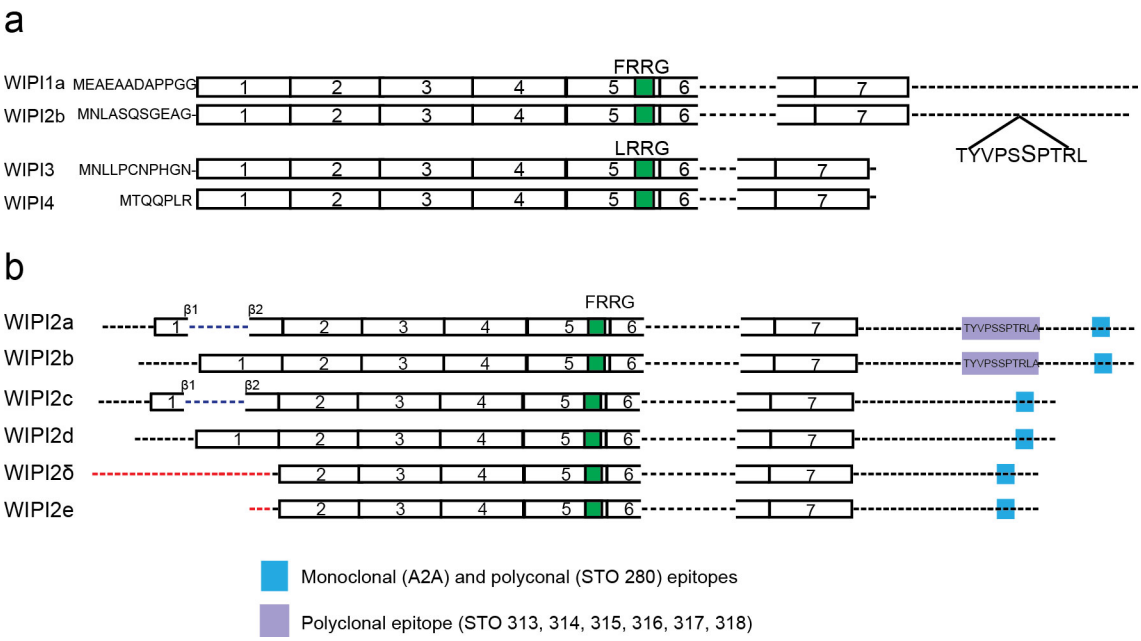

Figure 1.8 Schematic of human WIPI and WIPI2 proteins

(a) WIPI1-4 have a well conserved FRRG/LRRG PtdIns(3)P-binding motif in blade 5 (shown in green) of the 7-blade WD-40 repeat. All four homologues also have a hydrophobic membrane insertion loop in blade 6 (shown by dashes). WIPI1 and WIPI2 have extended C-termini compared to WIPI3 and WIPI4. **(b)** There are six WIPI2 isoforms. WIPI2a, b, c and d have a seven-blade structure, whereas WIPI2δ and e are missing the first blade. All sequence represented by black dashes or boxes are identical. WIPI2a and c have an 18 amino acid insert between β-sheets 1 and 2 of the first blade of the β-propeller. WIPI2a and b have an 11 amino insert in their C-terminus. WIPI2δ and e have different N-termini to WIPI2a, b, c and d. Blue box represents the epitope used for production of the monoclonal antibody A2A and polyclonal antibody STO 280, while the purple box represents the epitope used for production of antibodies STO 313-318 (Chapter 5.2)

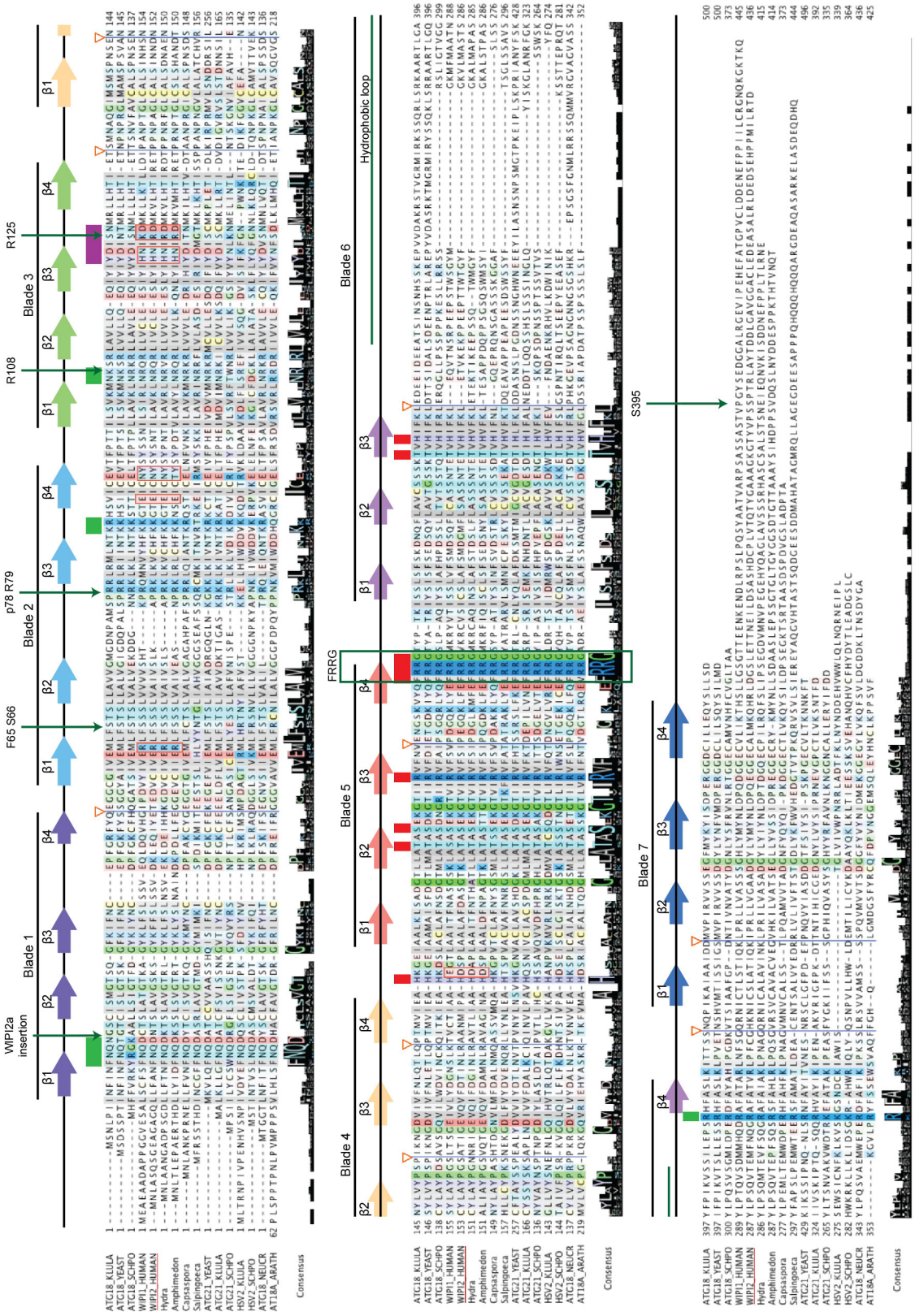

Figure 1.9 Alignment of human WIPI2 and homologues

Comparison of ATG18_KULA, *Kluyveromyces lactis* Atg18; ATG18_YEAST, *Saccharomyces cerevisiae* Atg18; ATG18_SCHPO *Schizosaccharomyces pombe*

ATG18a; WIPI1_HUMAN, WIPI1a ; WIPI2_HUMAN, WIPI2b; Hydra, *Hydra magnipapillata* Atg18; Amphime don, *Amphimedon queenslandica* Atg18, non-bilaterians from the Great Barrier; Capsaspora ,*Capsaspora owczarzaki* Atg18, unicellular animal; Salpingoeca, *Salpingoeca rosetta* Atg18, unicellular animal Choanoflagellate; ATG21_YEAST, *Saccharomyces cerevisiae* Atg21; ATG21_KLULA, *K. lactis* Atg21; ATG21_SCHPO, *S. pombe* Atg21 (Atg18b); HSV2_KLULA *K. lactis* Hsv1; HSV2_SCHPO *S. pombe* Hsv2 (Atg18c); ATG18_NEUCR, *Neurospora crassa* Atg18*,* fungi; ATG18_ARATH, *Arabidopsis thaliana* Atg18*,* plant. The alignment was generated using Jalview. Sequences and sequence numbering are from Uniprot. Scale numbering is from WIPI2b. Normalized consensus histogram is shown below alignment indicating % conservation. Residues in each column are coloured by function and intensity proportional to conservation above 20%. Coloured bars above a position indicate a highly conserved solvent-exposed loop, green; PtdIns(3)P-binding residue, red. A purple bar indicates where there are animal-specific substitutions. Inverted triangles are positions where non-conserved insertions were hidden to reduce the size of the figure. Positions of residues required for Atg2 binding by Atg18 (F65 S66, P78 R79) are numbered according to WIPI2b. Atg16L1 binding residues are R108 and R125 (Chapter 3). The location of the WPII2a loop insertion and the possible WIPI2 phosphorylation site (S295) (Chapter 5) are labelled. The conserved RFFG motif is boxed, the hydrophobic loop is labelled, and the β-sheets and β-propeller blades are numbered. Analysis, alignment and figure provided by Michael Wilson.

1.3.5 Ubiquitin-like conjugation systems

There are two ubiquitin-like conjugation systems, conserved from yeast to man, that are essential for autophagosome formation. The Atg12 conjugation system results in the formation of the Atg12–5 conjugate, while the Atg8 (LC3/GABARAP) conjugation systems results in Atg8 conjugation to the lipid phosphatidylethanolamine (PE). A large proportion of the core autophagy machinery is involved in these systems, and the functions and the resultant mechanisms of the two ubiquitin-like conjugation pathways are well conserved. Although Atg12 and Atg8 (and their mammalian counterparts) have no clear sequence homology to ubiquitin, structural analyses show that they contain a ubiquitin fold, and so are termed ‘ubiquitin-like proteins’ (Ubl).

1.3.5.1 The Atg12 conjugation system

Atg12 is covalently bound to Atg5 through the sequential action of two proteins, Atg7 and Atg10 (Figure 1.10 a). Atg7, an E1-like enzyme, activates the C-terminal glycine of

Atg12 by binding it via the catalytic cysteine of Atg7 in an ATP-dependent manner, forming a thioester bond (Mizushima et al., 1998). Atg7 then catalyses the transfer of Atg12 to the E2-like enzyme, Atg10, by binding Atg10 and promoting Atg12 transfer to the active site of Atg10. Atg10, without the action of an E3-like enzyme, subsequently binds Atg5 and catalyses the covalent linkage between the C-terminal glycine of Atg12 and an internal lysine within Atg5 (Mizushima et al., 1998). No free (monomeric) Atg5 or Atg12 is detected in cells, meaning that it likely that Atg12 and Atg5 are constitutively conjugated. The sequence of events for Atg12 conjugation is very similar between yeast and mammalian proteins.

Once formed, the Atg12–5 conjugate forms a complex with Atg16L1 (Atg16 in yeast) as a consequence of Atg5-Atg16L1 binding (Mizushima et al., 2003). Atg16L1 homodimerises though its coiled coil domain, forming an Atg12–5-16L1 complex with a 2:2:2 stoichiometry. This complex is also formed through Atg16 homodimerisation in yeast, although yeast Atg16 lacks the C-terminal WD-40 domain present in higher eukaryotic Atg16 homologues. The Atg12–5-16(L1) complex acts as an E3-like enzyme in the conjugation of Atg8/LC3 to PE by bringing activated Ubl protein LC3 (in conjugation with Atg3) into close proximity to the target substrate (phosphatidylethanolamine, PE) through an Atg12-Atg3 interaction (Figure 1.11) (Fujita et al., 2008). Atg12–5 is able to catalyse LC3–PE conjugation *in vitro*, however the mechanism for this catalysis is not well understood (Sakoh-Nakatogawa et al., 2013, Noda et al., 2013).

1.3.5.2 The Atg8 conjugation system

There is one Atg8 protein in yeast, whereas in higher eukaryotes and mammalian cells the family has diverged and contains at least eight Atg8 family members, which can be split into two subfamilies: GATE-16/GABARAP and LC3. Unless specified otherwise, 'LC3' will refer to all mammalian Atg8 family members. The conjugation pathway for each of these proteins is thought to be the same and conserved between yeast and humans.

Unlike Atg12, LC3 must be C-terminally cleaved by Atg4 before activation by the E1-like enzyme, Atg7 (Figure 1.10 b). Again, *S. cerevisiae* has one Atg4 cysteine

protease, whereas higher eukaryotes have multiple Atg4 homologues, with four (Atg4A, B, C and D) in humans (Marino et al., 2003). The differential functions of these human homologues are not completely understood, but it is thought that they have different specificities for different Atg8 family members. Atg4-mediated cleavage exposes a C-terminal glycine. Once processed by Atg4, LC3 is termed LC3-I and is present in the cytosol.

Processed LC3 is then bound and activated by Atg7, the same E1-like enzyme that activates Atg12, in an ATP-dependent manner. As during Atg12 activation, Atg7 forms a thioester bond between the C-terminal glycine of LC3 and the Atg7 active site, and binds to the E2-like enzyme Atg3 to catalyse the transfer of the C-terminal LC3 glycine to the active site of Atg3 (Kabeya et al., 2000, Ichimura et al., 2000). Atg3 binds Atg12, resulting in recruitment of Atg3–LC3 to the membrane and the formation of an amide bond between the C-terminal lysine of LC3 and PE (Figure 1.11). LC3 conjugated to PE is termed LC3-II.

LC3-II decorates both the inside and outside of the forming autophagosome. External LC3 is cleaved from the autophagosome surface by the Atg4 proteases. The functions for this cleavage of LC3 after autophagosome closure is not properly understood, but a study in *S. cerevisiae* using mutant Atg8ΔR, which does not need initial activating cleavage by Atg4, in an *atg4Δ* strain has shown that Atg8 deconjugation is required for autophagosome formation and expansion, and may serve as a signal for Atg14 release from the PAS (Nair et al., 2012).

The functions of Atg8 proteins are unclear. LC3 is thought to be required for phagophore expansion, while GATE-16/GABARAP is required for autophagosome closure (Weidberg et al., 2010). Furthermore, Atg8 has been shown to mediate hemi-fusion of liposomes *in vitro*, although this finding may represent a technical artefact (Nakatogawa et al., 2007, Nair et al., 2012). Atg8 proteins act in the recruitment of specific cargo for autophagic digestion; yeast Atg8 binds Atg32 (an outer mitochondrial membrane-spanning protein) and this interaction is required for mitophagy in yeast. Similarly, numerous mammalian LC3-binding proteins have been identified, such as p62 and NDP52 that act as cargo adaptors in during xenophagy (Chapter 1.6). These Atg8- and LC3-binding proteins interact with Atg8 or LC3 as a result of a consensus-binding motif: Atg8-interacting motifs (AIMs) in yeast or LC3-interacting regions

(LIRs) in mammals. In mammals, phosphorylation of these motifs regulates recruitment of cargo and adaptors to forming autophagosomes, therefore providing targeted degradation of autophagy substrates. Recent findings that some core autophagic machinery also have AIM/LIR motifs has raised the possibility that Atg8/LC3 lipidation may serve to provide a positive feedback mechanism whereby lipidated Atg8/LC3 can recruit upstream complexes, reinitiating further Atg8/LC3 lipidation and membrane expansion.

Because LC3 on the inner surface of autophagosomes is not removed during maturation, LC3 is widely used as an autophagy readout. Lipidated LC3 is termed LC3-II and migrates more rapidly than LC3-I by SDS-PAGE and so the two forms of LC3 can be visualised and quantified by western blot. Furthermore, LC3-positive vesicles can be detected by staining and immunofluorescence or electron microscopy and is frequently used for visualisation of autophagosomes. As LC3 is present on autophagosome membrane from formation to degradation in the lysosome, LC3 can be used as a marker for all stages of autophagy. GFP-LC3 is frequently used for visualising phagophores and autophagosomes, but the acidic environment of autolysosomes quenches the GFP signal. RFP-GFP-LC3 can be used to visualise autolysosomes and distinguish between immature and mature autophagosomes: LC3-positive vehicles appear yellow when they are not acidified (immature autophagosomes) and become red once autophagosomes fuse with the lysosome (mature autophagosomes).

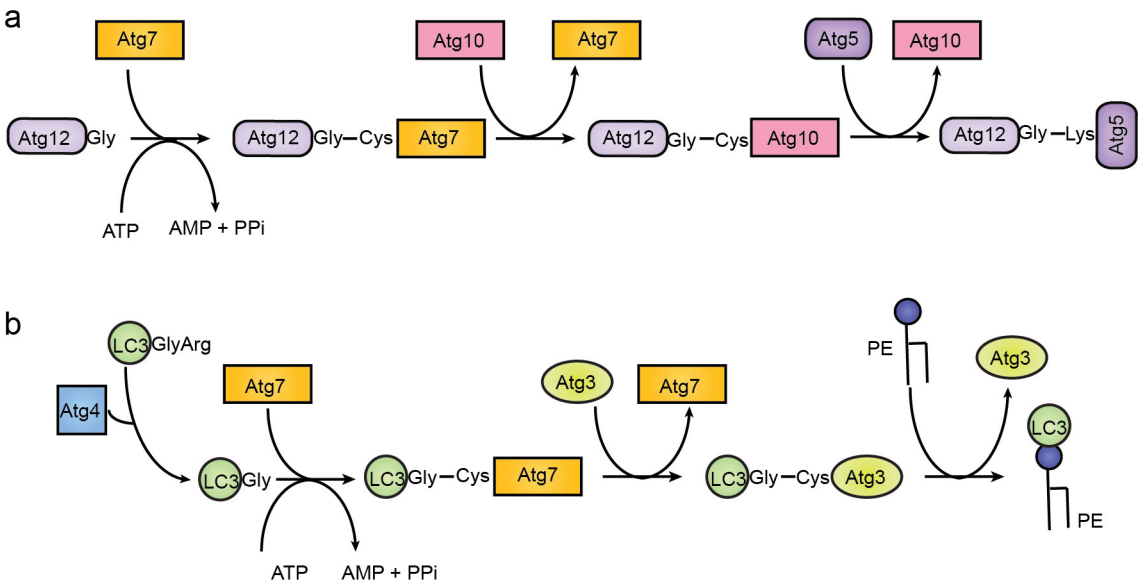

Figure 1.10 Ubiquitin-like conjugation systems

(a) Atg12–5 conjugation is catalysed by the E1-like protein Atg7 and the E2-like protein Atg10. **(b)** LC3 is activated by C-terminal cleavage mediated by Atg4. Atg7 and Atg3 then act as E1-like and E2-like proteins, respectively, in the conjugation of LC3 to PE.

1.3.5.3 Atg16L1 binding partners

As described above, the Atg12 –5-16L1 complex acts as in E3-like enzyme in LC3 lipidation (Fujita et al., 2008). Atg12–5-16L1 localises to the phagophore, but not on closed autophagosomes (Mizushima et al., 2003). Therefore, Atg12–5-16L1 staining can be used to identify the phagophore, but not mature autophagosomes. Molecular dissection of the complex has revealed that Atg16L1 is responsible for membrane localisation, through its central coiled coil domain containing region, and therefore determines the site of Atg3–LC3 recruitment and subsequently LC3 lipidation (Figure 1.11) (Fujita et al., 2008). Atg16L1 recruitment to the phagophore depends on PtdIns(3)P production at the omegasome, however no intrinsic membrane or PtdIns(3)P-binding has been found in Atg16L1 (or Atg12 and Atg5) and there is no known binding partner of Atg16L1 that can explain this PtdIns(3)P-dependent recruitment. Similarly in yeast, Atg16 localisation depends on PtdIns(3)P presence at the PAS and there is currently no explanation for this, although Atg5 has been shown to bind liposomes in an *in vitro* reconstitution experiment (Romanov et al., 2012). Recently, a global screen for autophagy proteins in *S. pombe* has shown that Atg5 can

bind Atg18a (Chapter 1.3.4.2) (Sun et al., 2013). This interaction may provide the mechanism for PtdIns(3)P-dependent recruitment in this system, however the molecular mechanism of PtdIns(3)P-dependent recruitment of the Atg12–5-16L1 complex is a long standing question within the autophagy field.

Atg5 binds the N-terminal region of Atg16L1. Besides Atg5, a number of Atg16L1 binding proteins have been identified. These include, Rab33B, FIP200 and ubiquitin (Fukuda and Itoh, 2008, Nishimura et al., 2013, Gammoh et al., 2013, Fujita et al., 2013). Atg16L1 can be split into three regions: the N-terminal Atg5 binding domain, the middle region which contains the coiled coil domain required for homodimerisation and the C-terminal WD-40 domain (Figure 1.12). Atg16L1 directly binds active Rab33B through the coiled coil domain of Atg16L1 (Fukuda and Itoh, 2008). Rab33B is a Golgi-localised Rab protein that is required for Golgi – ER retrograde trafficking. Overexpressed Rab33B is able to recruit Atg16L1 to the Golgi during fed conditions (Fukuda and Itoh, 2008). During starvation conditions or upon expression of GTP-locked Rab33B mutants, Rab33B and Atg16L1 colocalise in puncta. This suggests that Rab33B may be involved in determining Atg16L1 localisation. Both Rab33B and its GAP, OATL1, have been shown to be required for proper autophagy flux (Itoh et al., 2011). Overexpression of either protein results in an increase in LC3 lipidation and delayed autophagosome fusion. As well as inactivating Rab33B, OATL1 directly binds LC3, GABARAP and GATE-16 through a LIR domain (Itoh et al., 2011). Both the GAP activity and LIR motif of OATL1 are required for proper autophagy. However, it is unclear whether Rab33B and OATL1 function directly in this process. Instead, perturbation of their action in retrograde trafficking may indirectly affect autophagosome degradation, as may be true of UVRAG. Consistent with this, GATE-16 and GABARAP function in intra-Golgi transport and ER-Golgi transport, respectively (Sagiv et al., 2000, Nakamura et al., 2008). It is conceivable that OATL1-LC3 and Rab33B-mediated Golgi localisation of the Atg12–5-16L1 complex may be required in some manner for intracellular membrane trafficking, rather than for autophagosome formation (Itoh et al., 2011).

Atg16L1 directly binds FIP200 and ubiquitin through its coiled coil and WD-40 domains, respectively, and these interactions are thought to be involved, at least in part, in recruiting the Atg12–5-16L1 complex during starvation- and pathogen-induced

autophagy (Nishimura et al., 2013, Gammoh et al., 2013, Fujita et al., 2013). The minimal FIP200 binding domain (FBD) has been mapped to Atg16L1 230-246 (Figure 1.12). However, the three studies detailing the FIP200-Atg16L1 interaction use different deletion mutants of FIP200 and so have subtly different results. Atg16L1 deletion mutants of 230-300 or 229-242 cannot rescue starvation induced autophagy in Atg16L1$^{\Delta/\Delta}$ MEFs (which contain Atg16L1 with a deleted coiled coil domain resulting in total autophagy inhibition) (Nishimura et al., 2013, Gammoh et al., 2013), whereas Atg16L1 with amino acids 239-242 mutated to alanine can rescue autophagy unless combined with a mutant of Atg16L1 unable to bind ubiquitin (Fujita et al., 2013) Similarly, ubiquitin binding has been shown to be required for starvation-induced autophagy only when FIP200 binding is disrupted. Finally, Atg16L1 1-230 that cannot bind FIP200 can rescue autophagy in Atg16L1$^{\Delta/\Delta}$ MEF cells. This, combined with the inability of FIP200 or ubiquitin-mediated recruitment to explain the PtdIns(3)P binding dependence of Atg16L1 recruitment, suggests that an additional interaction may also be responsible for Atg16L1 recruitment.

Mammalian cells contain two isoforms of *S. cerevisiae* Atg16, Atg16L1 and Atg16L2. As described above, Atg16L1 is essential for autophagy. However, despite sharing the same domain structure as Atg16L1, forming homodimers with itself, heterodimers with Atg16L1 and binding the Atg12–5 conjugate through an N-terminal interaction with Atg5, Atg16L2 is not functional in starvation-induced autophagy (Ishibashi et al., 2011). Like Atg16L1, ectopic localisation of the N-terminal Atg16L2 Atg5-interacting domain can act as an E3-like enzyme, with Atg12–5, and promote plasma membrane-localised LC3 conjugation. However, the coiled coil domain of Atg16L2 cannot bind the phagophore membrane (Ishibashi et al., 2011). The region of Atg16L1 through which the protein binds the phagophore membrane has been mapped to amino acids 229-242, a region poorly conserved in Atg16L2. This region is responsible for binding FIP200, making this protein an ideal candidate for Atg16L1 recruitment (Nishimura et al., 2013, Gammoh et al., 2013, Fujita et al., 2013).

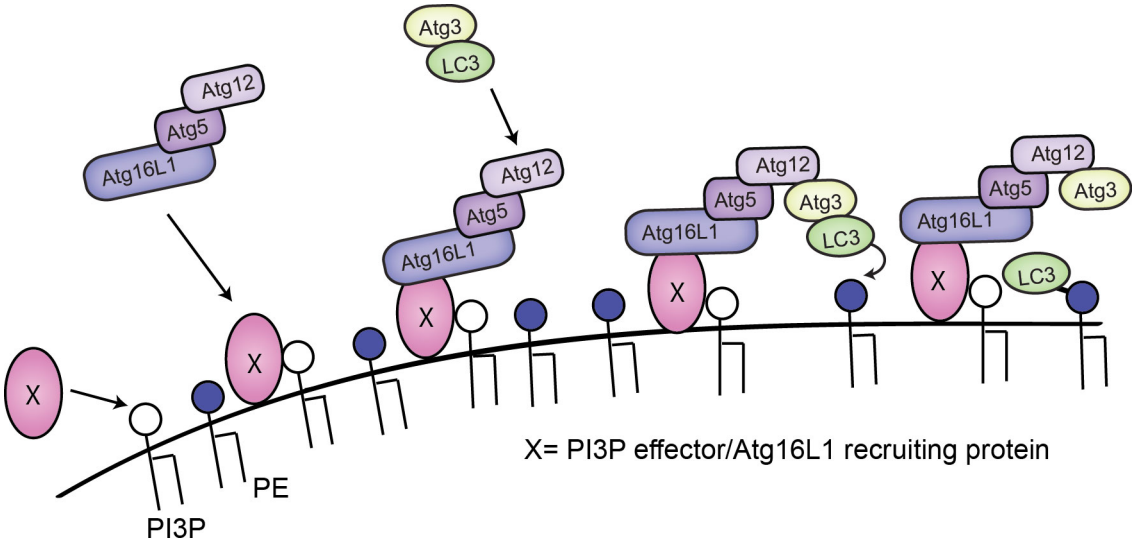

Figure 1.11 The Atg12–5-16L1 complex acts as an E3-like complex

The Atg12–5-16L1 complex is recruited to PtdIns(3)P positive autophagosome membranes through an unknown mechanism, possibly through an unidentified PtdIns(3)P-binding protein. The Atg12–5-16L1 complex subsequently recruits Atg3–LC3, and catalyses LC3 lipidation. The Atg12–5-16L1 complex is present in a 2:2:2 stoichiometry due to Atg16L1 homodimerisation (not shown in figure).

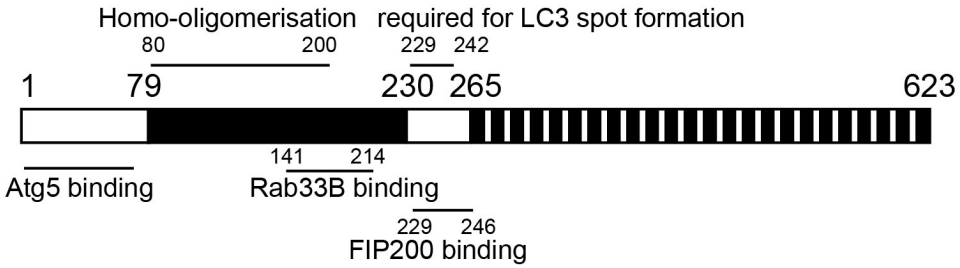

Figure 1.12 Schematic of Atg16L1

Atg16L1 binds Atg5 through its N-terminus (white box), forms homodimers and binds Rab33B through its coiled coil-domain (black box) and binds ubiquitin through its WD-40 motif (striped box). FIP200 binding and the region required for LC3 spot formation have been mapped to a region between the coiled coil domain and WD-40 motif.

1.3.6 mAtg9

Atg9 is the only conserved transmembrane protein within the core set of autophagy proteins that is required for autophagy (Young et al., 2006). Yeast Atg9 and its mammalian homologue (mAtg9) have six transmembrane domains with cytosol exposed N- and C- termini. While the transmembrane domains of Atg9 and mAtg9 are conserved, the N- and C-termini are not (Orsi et al., 2012). As the only membrane

spanning protein of the core autophagy proteins, it is widely thought that mAtg9 may be acting to deliver membrane or protein components essential for autophagosome formation, however the function of mAtg9 remains elusive. mAtg9 colocalises with the trans Golgi network (TGN), recycling and late endosomes, and to a small degree early endosomes (Orsi et al., 2012, Young et al., 2006). Both recycling endosomes and Golgi have been implicated in the search for the source of the autophagosome membrane (see Chapter 1.4) and it is possible that mAtg9 is shuttling membrane or protein between these organelles and the forming autophagosome. Additionally, Atg9 is required for the PAS localisation of Atg2, Atg8, Atg14 and Atg18 in yeast (Suzuki et al., 2007). Consistent with this, direct phosphorylation of Atg9 by Atg1 is required for Atg18 recruitment and subsequent progression of autophagy (Papinski et al., 2014). It is unclear if mAtg9 similarly acts in autophagy machinery recruitment; autophagosome formation is reduced in Atg9 KO MEFs, however loss of mAtg9 does not affect the composition of formed autophagosomes (Orsi et al., 2012).

Mammalian and yeast Atg9 cycle between the site of autophagosome formation (the omegasome and PAS, respectively) during starvation. Yeast Atg9 is localised within an Atg9 reservoir that is composed of bundles of vesicles and tubules (Mari et al., 2010). Upon nutrient withdrawal, the Atg9 reservoir translocates to the PAS in a manner dependent on its interaction with Atg17 (FIP200 homologue) and Atg1 (Sekito et al., 2009). Recycling of Atg9 from the PAS requires the Atg18-Atg2 complex (Reggiori et al., 2004). Similarly, mAtg9 is found in a mainly juxtanuclear localisation on clusters of tubules and vesicles (corresponding to the yeast Atg9 reservoir), which colocalise with markers of the trans Golgi network (TGN), early, late and recycling endosomes during fed conditions (Orsi et al., 2012, Young et al., 2006). Nutrient starvation results in mAtg9 dispersion to a peripheral localisation, where it is found in close proximity to forming autophagosomes (Orsi et al., 2012). mAtg9 shuttles between these compartments, but does not become a stable component of the autophagosome. Instead, autophagosomes and mAtg9 vesicles come into contact via ‘kiss-and-run’ interactions (Orsi et al., 2012). The mechanism of mAtg9 trafficking between its juxtanuclear localisation and forming autophagosomes is well conserved. As in yeast, mAtg9 dispersion after starvation requires ULK1 and PtdIns(3)P production, while its recycling depends on the Atg18 homologue WIPI2 (Young et al., 2006, Orsi et al.,

2012). As well as the core autophagy machinery, other proteins are thought to be involved in mAtg9 trafficking. Bif-1, a curvature-driving protein that can bind UVRAG (see Chapter 1.3.4) is required for Golgi tubulation and mAtg9 dispersion from the TGN after starvation (Takahashi et al., 2011).

mAtg9 dispersion upon starvation is required for autophagy and control of its trafficking may provide mechanisms through which autophagy can be modulated in response to specific stimuli, as may be the case through the p38 MAP kinase pathway (Webber and Tooze, 2010). p38-interacting protein (p38IP) interacts with the C-terminus of mAtg9 and is required for mAtg9 starvation-induced trafficking. The interaction between p38IP and mAtg9 is negatively regulated by active p38 (a mitogen-activated protein kinase, MAPK), and so inactivation of the p38 MAP kinase pathway leads to increased autophagy (Webber and Tooze, 2010).

Atg9 plays a key role in autophagy: *atg9Δ* mutant *S. cerevisiae* are incapable of forming autophagosomes, while mAtg9 is required during early neonatal starvation in mice – a period for which survival depends on autophagy – and Atg9 KO MEFs display a reduced autophagy response (Saitoh et al., 2009). Further characterisation of Atg9 interacting partners, be they protein or lipid, will shed further light on the function and regulation of this protein.

1.3.7 Summary of mammalian autophagy proteins

Table 1.1 Summary of mammalian autophagy proteins

Mammalian Atg protein	Function	Yeast homologue	References
ULK1/2	Serine/threonine kinase	Atg1	(Chan et al., 2007)
Atg2a, b	Binds WIPI4	Atg2	(Velikkakath et al., 2012)
Atg3	E2-like protein involved in conjugation of Atg8 proteins to PE	Atg3	(Tanida et al., 2002)
Atg4A, B, C and D	Activation of Atg8 proteins for conjugation to PE, and cleavage of Atg8-PE	Atg4	(Marino et al., 2003)
Atg5	Conjugated to Atg12 and acts as an E3-like protein in Atg8-PE conjugation	Atg5	(Mizushima et al., 2001)
Beclin1	Core component of the Vps34-	Atg6	(Liang et al., 1999)

	Vps15 PtdIns(3) kinase complex		
Atg7	Acts as an E1-like protein in Atg12–5 and Atg8–PE conjugation cascades	Atg7	(Tanida et al., 2001)
LC3	Conjugated to PE. Possibly involved in phagophore elongation	Atg8	(Kabeya et al., 2004, Weidberg et al., 2010)
GATE16/ GABARAP	Conjugated to PE. Possibly involved in autophagosome closure	Atg8	(Kabeya et al., 2004, Weidberg et al., 2010)
mAtg9	Transmembrane protein	Atg9	(Young et al., 2006)
Atg10	Acts as an E2-like protein in Atg12–5 conjugation	Atg10	(Mizushima et al., 1998)
Atg12	Conjugated to Atg5 and acts as an E3-like protein in Atg8-PE conjugation	Atg12	(Mizushima et al., 1998)
Atg13	Core component of the ULK kinase complex	Atg13	(Chan et al., 2009)
Atg14L	Autophagy-specific component of the Vps34-Vps15 PtdIns(3) kinase complex	Atg14	(Sun et al., 2008)
Atg16L1	Forms a complex with Atg12–5 and acts as an E3-like protein in Atg8-PE conjugation	Atg16	(Mizushima et al., 2003)
FIP200	Core component of the ULK kinase complex	Atg17	(Hara et al., 2008)
WIPI1/2/3/4	Binds PtdInd(3)P	Atg18 Atg21 Hsv2	(Proikas-Cezanne et al., 2004, Polson et al., 2010, Velikkakath et al., 2012)

1.4 Autophagosome membrane biogenesis

Autophagy initiation results in the formation of numerous autophagosomes, indicating a concerted effort in *de novo* lipid synthesis and membrane mobilisation. The debate over the source of the autophagosome membrane has been running for decades and has still not reached a final conclusion. Advances in knowledge of the mammalian autophagy pathway and in detection of forming autophagosomes by electron and fluorescence microscopy have advanced understanding the position in the cell where autophagosomes form and the source of the expanding membrane. The current consensus is that the majority of autophagosomes are formed from omegasomes on the

ER and at sites of ER and mitochondria contact. The discovery of DFCP1 led to the description of omegasomes as PtdIns(3)P-enriched subdomains of the ER from where the phagophore and forming autophagosomes emanate (Axe et al., 2008). The ULK1 and Atg14L positive Vps34 complexes both localise to the omegasome (Karanasios et al., 2013b, Matsunaga et al., 2010). Together with the identification of phagophores cradled between two ER cisternae (probably the omegasome) (Hayashi-Nishino et al., 2009, Yla-Anttila et al., 2009), this strongly suggests that the ER is the site at which autophagosomes originate from. More recently, autophagosome formation at ER and mitochondria contact sites has been described (Hamasaki et al., 2013). Physical contact between the ER and mitochondria are important for processes such as calcium signalling and lipid transfer between the ER and mitochondria (Lamb et al., 2013). Core autophagy proteins such as Atg5 and Atg14L are found at these sites and disruption of contact sites impairs autophagosome formation. The *de novo* formation of the phagophore membrane is supported by the fact that the ER is the main site for lipid synthesis in the cell and that the ER and mitochondria contact sites contain specific lipid synthesis enzymes in both mammals and yeast (van Meer et al., 2008). However, *de novo* lipid synthesis for phagophore expansion remains to be demonstrated.

Although the ER is the only organelle shown to act as a source for autophagosomes by electron microscopy, membrane contribution to growing and maturing autophagosomes from additional organelles, including the ERGIC, mAtg9-associated TGN and endosomes and the plasma membrane, has been demonstrated indirectly. mAtg9 resides on the tubular vesicular clusters that colocalise with the TGN, recycling and endosome compartments during fed conditions and disperse from the TGN localisation to endosomal positions during starvation (Orsi et al., 2012). mAtg9 is required for autophagy and mAtg9 vesicles transiently contact growing autophagosomes. Although its function is not known, it may be involved in shuttling protein or lipids between compartments which is it associated with (the TGN, recycling and early endosomes) and growing autophagosomes. The ER-Golgi intermediate compartment (ERGIC) is required for autophagosome formation and purified ERGIC is able to support LC3 lipidation (Ge et al., 2013), suggesting this compartment may act as a membrane source. Evidence for the involvement of the plasma membrane as a membrane source for autophagosome formation comes from the identification of

Clathrin heavy chain and AP-2 as Atg16L1 interactors (Ravikumar et al., 2010). Atg16L1 vesicles are formed as a result of Clathrin-mediated endocytosis and these vesicles undergo VAMP7, syntain7- and syntaxin8-dependent homotypic fusion before becoming LC3-positive (Moreau et al., 2011). It has been proposed that these Atg16L1- and LC3-positive vesicles represent phagophores.

The membrane reorganisation and lipid synthesis required during autophagy could well involve both de novo lipid synthesis and membrane delivery from additional compartments by vesicle trafficking. Vesicle transport would allow for the delivery of additional proteins to the autophagosome, which may provide an explanation for the acidification of autophagosomes without fusion with an acidic compartment (Dunn, 1990, Axe et al., 2008).

1.5 Autophagy in health and disease

Basal autophagy is required for turning over old and damaged long-lived proteins and organelles. Therefore, autophagy is required for protection against a number of diseases resulting from deregulated protein and organelle turnover and has been implicated in a number of pathologies including cancer, neurodegenerative diseases and diabetes (Jiang and Mizushima, 2014, Quan et al., 2012).

A number of core autophagy proteins have been implicated in suppression of tumorigenesis. Monoallelic deletion of Beclin1 results in increased sporadic tumours (Aita et al., 1999). Concurrently, Beclin1 is commonly deleted in breast, ovarian and prostate cancer. Re-expression of Beclin1 restores autophagy in the MCF7 breast cancer cell lines, leading to a reduction in proliferation and inhibition of tumorigenesis of these cells (Liang et al., 1999). The expression of autophagy proteins Atg5 and WIPI1 are also altered in human cancers (Liu et al., 2013, Proikas-Cezanne et al., 2004). Autophagy clears damaged and long-lived proteins and organelles and it is widely accepted that this action protects against reactive oxygen species (ROS) and proteotoxicity, which can contribute to cancer development (White, 2012). Impaired autophagy therefore lessens protection against these factors, increasing the incidence of tumour formation. In addition to impaired autophagy resulting in increased ROS through dysfunctional mitophagy, in cells with impaired autophagy the pro-survival

antioxidant-defence pathway is switched on (White, 2012). p62 binds and sequesters KEAP1 from its binding partner NRF2, therefore releasing NRF2 from inhibition by KEAP1 and allowing the transcription factor NRF2 to translocate to the nucleus and activate antioxidant-defence genes (White, 2012). Transcriptional control by NRF2 is tightly controlled through modification of KEAP1 or p62 transcriptional control in normal cells. However, p62 accumulation in autophagy defective cells means that antioxidant-defence genes are constitutively switched on and tumorigenesis is promoted (White, 2012). Therefore, autophagy can act as a tumour suppressive mechanism and impaired autophagy can promote oncogenic actions of other proteins, such as NRF2.

Conversely, autophagy can promote survival of stressed cancer cells. Cancer cells in hypoxic environments within tumours show high levels of autophagy and inhibition of autophagy in these cells promotes cancer cell death. The mechanisms by which autophagy supports tumour survival are not fully understood and are likely to differ between different cancer types and tumour environments (White, 2012). As well as promoting tumour cell survival, autophagy is upregulated and promotes cell survival during metastasis (White, 2012). Therefore, autophagy functions in both preventing cancer initiation, and supporting cancer cell survival and metastasis.

Sporadic mutations in the WIPI4 gene results in severely reduced WIPI4 protein expression and leads to the development of static encephalopathy of children with neurodegeneration in adulthood (SENDA) (Saitsu et al., 2013). SENDA is a severe neurological disorder that causes early-onset spastic paraplegia and mental retardation. Later in life, in their early 30's, patients experience sudden on-set Parkinson's and dystonia (Jiang and Mizushima, 2014). Cells from patients with WIPI4 mutations show impaired autophagy, with impaired LC flux and increased formation of LC3 and Atg9 positive autophagosomes, probably representing unclosed autophagosomes (Saitsu et al., 2013). Why the effects of these WIPI4 mutations are only manifested in the brain is unclear, but may reflect cell type differences, perhaps long-lived neurons are particularly vulnerable to autophagy loss.

A point mutation in Atg16L1 resulting in a threonine to alanine substitution at position 300 is strongly associated with Crohn's disease. Crohn's disease is a major inflammatory bowel disease, a long-term pathology that causes inflammation of the digestive system. Atg16L1 T300A is more susceptible to caspase-3-mediated

degradation than wild type Atg16L1. Caspase-3 is activated by conditions including metabolic and nutrient stress and pathogen infection. In cells with Atg16L1 T300A mutants, caspase-3 activation results in impaired basal autophagy due to Atg16L1 T300A cleavage, which subsequently causes sustained cellular stress, resulting in inflammation and Crohn's disease progression (Murthy et al., 2014). This illustrates how basal autophagy is essential to cellular homeostasis and the effect disruption of this can have at the organism level.

1.6 Xenophagy

Xenophagy is the selective degradation of intracellular pathogens by autophagy. As for other forms of selective autophagy, this process involves identification of the pathogen by cargo receptors and the core autophagy machinery for subsequent autophagosome formation. Invading bacteria that are targeted for degradation are identified by the infected cell and subsequently marked in some form for recognition by cargo receptors. These 'eat-me' signals include ubiquitination, diacylglycerol (DAG) and exposed glycans from damaged membranes. There are a number of known cargo receptors for bacterial autophagy and these are p62, nuclear domain 10 protein 52 (NDP52), neighbour of BRCA1 gene 1 (NBR1), optineurin (OPTN) and galectin-8. Ubiquitination is probably the best understood mechanism of bacterial targeting, but whether this is ubiquitination of a host or bacterial proteins is unknown. NDP52, p62 and OPTN recognise ubiquitin through their various ubiquitin-binding domains and bind LC3 though LIR motifs. These cargo receptors are not redundant, and they display ubiquitin-linkage and Atg8 homologue preferences, therefore allowing additional layers of regulation and control of this process (Gomes and Dikic, 2014). DAG, a lipid second messenger, is localised to the *Salmonella* containing vesicle (SCV) through an unknown mechanism and subsequently may drive autophagy initiation via the JNK-pathway. During infection of cells, damage of endosomes is often caused, exposing glycans. Galectin-8 binds exposed glycans and through a direct interaction recruits NDP52 (Thurston et al., 2012). NDP52 then binds ubiquitinated protein in the vicinity of the bacteria and leads to bacterial sequestration through its interaction with LC3.

Furthermore, NDP52 can bind TANK binding kinase 1 (TBK1) (Thurston et al., 2009), which phosphorylates OPTN and increases its affinity for LC3 (Wild et al., 2011).

Intracellular bacteria grow and replicate either in the cytosol or in membrane-bound compartments. *Shigella* and *Listeria* are examples of cytosolic bacteria, whereas *Salmonella* resides and replicates in specialised vesicles. Intracellular bacteria have evolved a number of mechanisms in order to avoid degradation by either the endocytic or autophagic pathways. *Salmonella* inhibit SCV targeting to the lysosome though an unknown mechanism, while cytosolic bacteria *Shigella* avoid detection by the autophagy machinery by mechanisms such as expression of virulence factors that outcompete Atg5-Tecpr1 (Tectonin β-propeller repeat-containing protein) for VirG binding, therefore avoiding targeting to the autophagosome (Gomes and Dikic, 2014). However, a subpopulation of bacteria is recognised and targeted for degradation by xenophagy. *Salmonella* is used extensively to study xenophagy, both at the whole organism level and in cellular systems.

Salmonella invade non-phagocytic cells through injection of virulence factors via their type three-secretion systems (TTSS) to induce plasma membrane ruffling and subsequent uptake into a vesicle (Gorvel and Meresse, 2001). The SCV very quickly becomes decorated with early and recycling endosome markers, probably through direct fusion with these compartments (Gorvel and Meresse, 2001, Finlay and Brumell, 2000). Within one hour the SCV is uncoupled from the endocytic pathway and is labelled by late endosome and lysosome markers, including the LAMP proteins, through an unknown mechanism requiring Rab7 but not involving lysosome fusion (Finlay and Brumell, 2000). Although *Salmonella* has evolved mechanisms to avoid eventual targeting to the lysosome, some SCVs are damaged by the TTSS and the *Salmonella* become exposed to the cytosol and/or the cell detects exposed glycans. This results in ubiquitination and detection by cargo receptors, culminating in *Salmonella* degradation through xenophagy (Birmingham et al., 2006).

Xenophagy requires the core autophagy machinery. Deletion or depletion of these proteins results in hyperproliferation of Salmonella, culminating in cell or organism death (Jia et al., 2009, Birmingham et al., 2006). Xenophagy activity in infected cells peaks after one hour, before returning to very low basal levels (Birmingham et al., 2006, Tattoli et al., 2012). *Salmonella*-induced membrane damage

causes amino acid depletion from the cells though an unknown mechanism, leading to mTORC1 inhibition and autophagy activation (Tattoli et al., 2012). mTORC1 activation is restored by amino acid recovery after one hour. Again, this occurs through a poorly understood *Salmonella*-driven mechanism. Bacterial autophagy occurs at PtdIns(3)P enriched domains of the ER, in which DFCP1, Atg14L and LC3 surround the SCV (Huang et al., 2011).

The functions of the core autophagy machinery in xenophagy are currently not well understood. Under wild type conditions, autophagic sequestration of the SCV results in a double membrane-bound autophagosome surrounding the single SCV membrane enclosing the *Salmonella.* As expected, the Atg12–5-16L1 complex and the E1- and E2-like enzymes are required for LC3 targeting to the SCV (Kageyama et al., 2011). However, SCVs in Atg7 KO cells are surrounded by a double membrane, which is thought to be unclosed, showing that LC3 is not required for expansion of the phagophore around the SCV. These cells are defective in autophagy and *Salmonella* replication is not restricted (Kageyama et al., 2011). The requirement for mAtg9, functional ULK1 kinase complex, and the Atg14L PtdIns(3) kinase complex is not clear. mAtg9 and FIP200 knockout cells have *Salmonella*-targeted LC3. However, this LC3 is targeted, and presumably lipidated, directly to the SCV membrane, as there is no double phagophore present. These LC3-lipidated SCVs seem not to be functional for autophagy-mediated *Salmonella* degradation, as Atg9 or FIP200 KO results in increased *Salmonella* infection (Kageyama et al., 2011). Additionally, the role of PtdIns(3)P in LC3 recruitment to the SCV is not understood. A number of groups have reported that LC3 recruitment is reduced, although not inhibited by PtdIns(3)P-loss (Huang et al., 2011, Birmingham et al., 2006), while others have reported that PtdIns(3)P is dispensable (Kageyama et al., 2011). Unlike in starvation-induced autophagy, LC3 recruitment appears not to be absolutely dependent on PtdIns(3)P production, and instead PtdIns(3)P deficiency may manifest itself as a subtle defect in LC3 recruitment. Similarly, the requirement for FIP200 in LC3 recruitment is more complex than in starvation-induced autophagy. FIP200 and ubiquitin both directly bind Atg16L1. FIP200 and ubiquitin binding of Atg16L1, along with some other currently unidentified Atg16L1 binding protein, are required for LC3 recruitment to the SCV (Fujita et al., 2013). The requirement for FIP200 and ubiquitin binding of Atg16L1 seems to be

redundant in xenophagy. Indeed, it appears as though recruitment of the Atg12–5-16L1 complex is more complicated than in starvation-induced autophagy, perhaps reflecting the more complex nature of xenophagy. Evolution of Atg16L1 in higher eukaryotes may reflect these complex and redundant mechanisms as yeast Atg16 do not contain the WD-40 domain shown to be required for ubiquitin binding (Fujita et al., 2013). Atg16L1 binding to ubiquitin may facilitate LC3 recruitment directly to the SCV, without the requirement for a double membrane phagophore. This interaction is similar to Atg5 binding to VirG – a *Shigella* virulence protein – which is required for xenophagy of *Shigella* (Ogawa et al., 2011). It is probable that there are other members of the core autophagy machinery that similarly mediate interactions with target bacteria.

1.7 Aims and objectives

Since the identification of the first mammalian autophagy protein in the late 1990s there has been rapid progress in the identification of other autophagy proteins and dissection of their molecular functions. It has become clear that autophagy is highly regulated and involves the concerted and sequential action of core autophagy proteins. Although a lot of progress has been made, there are still a number of unanswered questions regarding the core autophagy machinery. In this study I aimed to address the outstanding questions of what the functions of mAtg9 and WIPI2 are. mAtg9 is the only transmembrane protein required for autophagy and so mechanistic understanding of its function may shed light on the membrane dynamics involved in autophagosome formation. WIPI2 is WD-40 domain-containing, PtdIns(3)P-binding protein required for autophagy. PtdIns(3)P production is absolutely essential for autophagy and is required for recruitment of core autophagy proteins, including those involved in LC3 lipidation, to the forming autophagosome. There is currently no link between PtdIns(3)P production and recruitment of downstream proteins. As a WD-40 domain protein, WIPI2 may act as a platform to recruit downstream core autophagy proteins in a PtdIns(3)P-dependent manner. A fuller understanding of autophagy may open new avenues for therapeutic manipulation of this process.

Chapter 2. Materials & Methods

2.1 Cell Biology

2.1.1 Cell culture

Cell culture flasks, dishes and plates were obtained from Corning, and Dulbecco's Modified Eagle Medium (DMEM) and fetal bovine serum (FCS) from Sigma. Earle's Balanced Salt Solution (EBSS) (5.56 mM D-glucose, 123.08 mM NaCl, 5.37 mM KCl, 1.82 mM $CaCl_2$, 0.81 mM $MgSO_4$, 0.99 mM Na_2HPO_4, 13.10 mM $NaHCO_3$), trypsin (0.25% trypsin in Tris Saline) and versene (0.02% (w/v) EDTA in PBSA) were produced by Cell Services at the LRI.

HeLa, HEK293A and HEK293A derivatives were maintained in DMEM supplemented with 10% FCS and 4.8 mM L-glutamine under humidified conditions at 37 ºC in 10% CO_2. Stably expressing GFP-LC3 HEK293A line (2GL9 cells) is as previously described (Chan et al., 2009) and is not maintained under selection. GFP-WIPI2b stably expressing HEK293A cell line was produced by Hannah Polson (Dooley et al., 2014) and this cell line is maintained under 400 μg/mL geneticin (Life Technologies). MEF cell lines were maintained in DMEM supplemented with 20% FCS and 4.8 mM L-glutamine under humidified conditions at 37 ºC in 10% CO_2. $FIP200^{-/-}$ and matched wild type immortalized MEF cell lines were a kind gift from Jun-Lin Guan (Gan et al., 2006), $Atg16^{\Delta/\Delta}$ and matched immortalized MEF cell lines were kind gift from Shizuo Akira (Saitoh et al., 2008), (Kuma et al., 2004)and $TSC2^{-/-}$ and matched immortalized MEF cell lines were a kind gift frim Ivan Gout (Zhang et al., 2003).

Cells were grown until 80-90% confluent and were passaged by washing once in versene before incubation in 0.08% trypsin to detach cells. For maintenance, detached cells were diluted 1:10 (HEK and HeLa cell lines) or 1:5 (MEF cell lines). Cells were used until a passage number of 25, after which they were discarded. If used for transfection, MEF cell lines were used for a maximum of 5 passages after recovery from frozen, after which the transfection efficiency became too low. Cells were frozen in 90% FCS, 10% DMSO. Generally, trypsinised cells from a confluent T-150 flask were centrifuged (1000 rpm, 4 minutes, room temperature) and resuspended in 10 mL of

90:10 FCS:DMSO mixture. Aliquots of 1 mL were frozen. When defrosting, these aliquots were resuspended into T-75 flasks for HEK and HeLa cell lines, or T-25 flasks for MEF cells lines.

Where indicated as 'fed' or 'starved', cells are incubated in fresh DMEM or EBSS, respectively, for two hours (unless otherwise stated) after washing twice with the relevant medium (DMEM or EBSS). Where indicated, cells were treated with 100 nM Bafilomycin A1 (Calbiochem), or 100 nM wortmannin (Calbiochem) for the duration of the starvation treatment. To reduce detachment of HEK293A cells and derivative cell lines, poly-D-lysine (Sigma, USA) was used to coat the wells of 6-, 12- and 24-well plates when cells were cultured in these vessels. Poly-D-lysine coating was not required for HeLa or MEF cell lines in any dish or plates, or for HEK293A and derivatives in dishes.

2.1.2 Transfection

All siRNA was used at a final concentration of 50 nM.

2.1.2.1 Oligofectamine transfection

Oligofectamine (Life Technologies) was used for siRNA transfection of HEK293A and HeLa cell lines. The following is for transfection in a 6 cm plate, and bigger or smaller transfections were scaled according to dish surface area ratios. 4.5 X 10^5 cells were plated the day before oligofectamine transfection so that on they day of transfection ('hit 1') they would be approximately 40% confluent. Solution A: 6 µL of Oligofectamine was added to 34 µL of OptiMem (a reduced serum cell culture medium, Life Technologies). Solution B: 5 µL of siRNA at a stock concentration of 20 µM was added to 360 µL of Opitmem. Solutions A and B were incubated separately for 10 minutes at room temperature before mixing together and incubating a further 20 minutes at room temperature. All mixtures were tapped after they were made up to ensure proper mixing, and briefly spun down after mixing to ensure that liquid was not in the lid of containers. The A and B mix was added to cells which had had DMEM medium replaced with 3600 µL OptiMem, resulting in a final volume of 2 mL optiMem-oliofectamine-siRNA mix. Cells were incubated in this mix at 37 ºC for 4-6 hours.

2.1.2.2 Lipofectamine transfection

Lipofectamine2000 (Life Technologies) was used for siRNA and plasmid transfections of HEK293A and HeLa cell lines that are above 70% confluent. Lipofectamine2000 is toxic to cells below this confluency. Cells were plated to be 80% confluent on the day of transfection. For transfection of plasmid DNA for immunoprecipitation of overexpressed proteins, 10 cm plates were seeded with 4 X 10^6 HEK293A (or derivative) cells the day before Lipofectamine2000 transfection. Cell numbers for smaller dish sizes were scaled according to plate surface area ratios. Generally, Lipofectmaine2000 was used for transfection of cells treated with Oligofectamine the previous day, for a two-hit siRNA protocol (see below). The following was the reaction mixture for transfecting a 6 cm dish. Mixes for differently sized dishes were scaled according to surface area ratios. Mix 'A' was formed of 6 μL of Lipofectamine2000 in 1 mL OptiMem. Mix 'B' is formed of 5 μL siRNA (stock of 20 μM) and/or 1 μg of plasmid DNA in 500 μL of Optimem. Mixes A and B were incubated separately at room temperature for 10 minutes before mixing and further incubating for 30 minutes at room temperature. All mixtures were tapped after they were made up to ensure proper mixing, and briefly spun down after mixing to ensure lipid was not in the lid of containers. Cells were incubated in the AB mixture, after aspirating the DMEM they were grown in, for at least 6 hours (but not longer than 8 hours) before replacing the mix with fresh DMEM.

2.1.2.3 Two-hit knockdown

Day one: plate cells for correct confluency for Oligofectamine treatment the following day.
Day two: Oligofectamine transfection of siRNA.
Day three: Lipofectamine2000 transfection of siRNA. If rescuing the knockdown, then at this stage siRNA resistant plasmid DNA is also transfected with the siRNA.

Day four: re-plate cells from dishes (normally 6 cm) into 12- and 24-well plates for western blot and immunoflourescence assays. These plates were poly-D-lysine coated if HEK293A, or derivative, cell lines were used.
Day five: Autophagy assays: starvation/drug treatments 72 hours after initial knockdown.

2.1.2.4 JetPRIMEtransfection

JetPRIME (PolyPlus Transfection) was used for transfection of MEF cell lines that were at least 70% confluent. Note that jetPRIME is toxic to cells below this confluency. The mix of transfection agent and DNA concentration was optimised for the lowest toxicity with the highest expression. For transfection in a 24-well plate, 2.4 X 10^4 MEF cells were plated per well the day prior for transfection. For a single well of a 24-well plate: 0.5 μg of plasmid DNA was diluted into 75 μL of jetPRIME buffer. The mixture was vortexed for 10 s and spun down. 1 μL of jetPRIME was added to the buffer-DNA mixture, and the resulting mixture was vortexed for a further 10 s before being spun down and incubated for 10 minutes at room temperature. The jetPrime mixture was added dropwise to cells in 0.5 mL of DMEM. Cells were incubated for 4 hours in the DMEM-jetPRIME mix before the medium was replaced with fresh DMEM. For different well or plate sizes, both the number of cells seeded and the transfection mixes were scaled up according to surface area ratios of the plates: twice the volume of jetPRIME mix (jetPRIME, DNA and buffer) and twice the number of cells were used for transfection in a 12-well plate.

2.1.2.5 siRNA duplexes

siRNA was reconstituted in 1X siRNA buffer (Thermo Scientific) (60 mM KCl, 6 mM HEPES pH 7.5, 0.2 mM $MgCl_2$).

Table 2.1 siRNA used in this thesis

Target gene	siRNA	Target sequence	Supplier
(RISC-free control)	D-001220-0	N/A	Dharmacon
Atg2a	J-026591-17	AGUUGGAGGUGGCGGGACA	Dharmacon
Atg2a	J-026591-18	CGUAAUGAGCACAGGCGAU	Dharmacon
Atg2a	J-026591-19	GCAAGGAGGUCUACGAGAG	Dharmacon
Atg2a	J-026591-20	CCAACAAUGUGGUACACGU	Dharmacon
Atg2b	J-016822-18	GUAAAGAAAUGCCUCGAAA	Dharmacon
Atg2b	J-016822-19	GAACUUACGUUACCAAAUA	Dharmacon
Atg2b	J-016822-20	CAAUAGAGCAGUACCGGAA	Dharmacon
Atg2b	J-016822-22	CCAUGUGUCUAGUGGAGUA	Dharmacon
FIP200	J-021117-05	GGAGUGGGCUGGUGCUUUA	Dharmacon
FIP200	J-021117-06	AAACUACGAUUGACACUAA	Dharmacon
FIP200	J-021117-07	GCAAAGAAAUUAGGGAAUC	Dharmacon
FIP200	J-021117-08	UAAACUUGACGGACUAAUA	Dharmacon
ULK1	D-005049-04	UGUAGGUGUUUAAGAAUUG	Dharmacon
WIPI2	J-020521-09	CGACAGUCCUUUAGCGGCA	Dharmacon
WIPI2	J-020521-12	GGACCGGGUACUUCGGGAA	Dharmacon
WIPI2	Hs_WIPI2_4	CTCGCTAGCCACAATTCAGAA	Qiagen

2.1.3 *Salmonella* growth

Salmonella typhimurium SL 1344 was a kind gift from David Holden. All *Salmonella* work was carried out under a laminar flow hood in a containment level 2 facility. A scraping of *Salmonella* was removed from the -80 ºC DMSO stock (see Chapter 2.3.9) using a pipette tip and was incubated in 3 mL of LB (1% Bacto-Tryptone (w/v), 0.5% yeast extract, 1.7 M NaCl, LRI), shaking overnight in a 37 ºC water bath. To control for other bacterial contamination, 3 mL of LB with no *Salmonella* was prepared and incubated at the same time. The following morning, assuming that the 3 mL of control LB was clear, 90 µL of the overnight *Salmonella* culture was added to 3 mL of pre-warmed LB. This culture was incubated, shaking at 37 ºC in a water bath, until the bacteria reached mid-log growth (OD_{600} 2-2.5). The optical density (OD) was measured by diluting the *Salmonella* culture 1:10 (100 µL in 900 µL of LB). An OD of 0.2-0.25 corresponds to 2-2.5 when this dilution is accounted for. LB was used as the blank and the absorbance at 600 nm was read using a spectrometer. From the OD_{600}, the number of Salmonella per mL was estimated (OD X 10^9 per mL).

2.1.4 *Salmonella* infection

Salmonella was used to infect HeLa or MEF cells in 24 well plates. HeLa cells were treated with siRNA as described in Chapter 2.1.2.3, and re-plated on day 4 at a cell density of 7 X 10^4 cells per well of a 24-well plate for *Salmonella* infection the following day. MEF cells were plated into 24-well plates and transfected the day before *Salmonella* infection as described in Chapter 2.1.2.4. *Salmonella* infection was carried out at a multiplicity of infection (MOI) of 100 for infection of HeLa cells and 50 for MEF cells. The volume of *Salmonella* culture at mid-log phase (see Chapter 2.1.3 above) needed for achieving this MOI was calculated using the OD_{600} reading and an estimation of the cell number. I estimated that there were 1 X 10^5 HeLa cells per well (as 7 X 10^4 were plated per well the evening before infection) and roughly 3.5 X 10^4 MEF cells per well (2.4 X 10^4) plated the previous day. To calculate the volume of *Salmonella* culture (in mL) that was required for each well, the MOI was multiplied by the estimated number of cells and then divided by the number of bacteria per mL. LB-*Salmonella* mix was added to each well by diluting it into 1 mL of DMEM and adding this to the cells (after removing existing DMEM from the well). Plates were then spun at 2000 rpm at room temperature for 10 minutes in a plate-carrying centrifuge with swing-out arms before incubation at 37 ºC under humidified conditions with 10% CO_2. Cells were then washed once in PBSA before addition of 1mL DMEM with 50 μg/mL gentamicin (Sigma) and incubation at 37 ºC for a further hour. This constitutes infection for 1 hour. After infection, plates were put on ice and cells were washed twice with PBSA before fixing as usual for immunofluorescence (see Chapter 2.2.10) or cell lysis for colony counting.

For colony counting, cells were lysed using 0.1% Triton X-100 in PBSA. After aspiration of PBSA from washing, 150 μL of lysis buffer was added to each well. Lysis buffer was pipetted up and down and the pipette tip was use to scrape across the well surface to maximise cell lysis. Once lysed, 100 μL of lysis buffer was added to 900 μL of LB in an Eppendorf tube and placed on ice (tube 1). Two further 1:10 serial dilutions were made by adding 100 μL from tube 1 into 900 μL of LB (forming tube 2), and subsequently diluting 100 μL from tube 2 into 900 μL of LB (forming tube 3). All tubes

were incubated on ice until all wells had been lysed and serial dilutions made. 100 µL of each LB-cell lysate mix was then spread on LB plates and incubated at 37 ºC over night. The following day colonies were counted from plates containing 30-300 colonies. This assay assumes that each colony formed represents a single colony forming unit (c.u.f.), i.e. a living *Salmonella* bacterium. Colony counting was performed in triplicate for each condition of *Salmonella* infection (e.g. RF and WIPI2 KD).

For wortmannin treatment during *Salmonella* infection, wortmannin was added to medium at a final concentration of 100 nM for 15 minutes prior to infection and for the duration of infection.

2.2 Biochemistry

2.2.1 Antibodies

Table 2.2 Primary antibodies

Antigen	Species	Antibody	Supplier	Dilution	Notes
Actin	Rabbit	ab8227	Abcam	WB 1:2000	
Atg5	Rabbit		CosmoBio	WB 1:200	
Atg9	Rabbit	STO218	CRUK	WB 1:1000* IP:1:200*	
Atg9	Hamster	14F2		WB 1:1000	
Atg16	Rabbit	STO285	CRUK	IF 1:250* WB 1:250*	IF: digitonin permeabilize
Atg16	Rabbit		CosmoBio	IF 1:400 WB 1:1000	IF: digitonin permeabilize
Atg16	Mouse	1F12	MBL	IF 1:400 WB 1:1000	IF: digitonin permeabilize
Calreticulin	Chicken		Abcam	IF 1:200	
EEA1	Mouse	BD		WB 1:2500	
FIP200	Rabbit		Bethyl Labs	WB 1:2000	Incubate overnight
FLAG	Rabbit		Sigma		
FLAG	Mouse	M2	Sigma	IF 1:4000	Reduced background with preclearing
GFP	Rabbit		Abcam	WB 1:5000	
HA	Mouse	HA.11	Covance	WB 1:1000	

LAMP1	Mouse	CD107A	BD	IF 1:400	
LC3B	Rabbit	ab48394	Abcam	IF 1:2500 WB 1:2500	Methanol fix for IF
RFP (mCherry)	Rabbit		MBL	WB 1:1000	
Myc	Mouse	9E10	CRUK	WB 1:500 IP: 1:200	
p62 C-terminus	Guinea Pig	GP62-C	Progen	IF 1:300	
p62	Mouse		BD	WB 1:500	Incubate overnight
Stx13	Rabbit		Synaptic systems	WB 1:1000	
TfR	Mouse		Invitrogen	WB 1:500	
Ubiquitin	Mouse	FK2	MBL	IF 1:200	
ULK1	Rabbit	STO250	CRUK	WB 1:100	
WIPI2	Rabbit	STO280	CRUK	IF 1:400* WB 1:250	Use whole serum for western blot
WIPI2	Mouse	2A2	Dundee Cell Products	IF 1:4000 WB 1:1000 IP: 1:200	

*, affinity purified antibody

Table 2.3 Secondary antibodies

Antigen	Conjugated to	Supplier	Dilution
Rabbit IgG	HRP	GE Healthcare	WB 1:4000
Mouse IgG	HRP	GE Healthcare	WB 1:4000
Hamster IgG	HRP	GE Healthcare	WB 1:4000
Rabbit IgG	Alexa Fluor 488	Life Technologies	IF 1:1000
Rabbit IgG	Alexa Fluor 555	Life Technologies	IF 1:1000
Rabbit IgG	Alexa Fluor 647	Life Technologies	IF 1:1000
Mouse IgG	Alexa Fluor 488	Life Technologies	IF 1:1000
Mouse IgG	Alexa Fluor 555	Life Technologies	IF 1:1000
Mouse IgG	Alexa Fluor 647	Life Technologies	IF 1:1000
Guinea pig IgG	Alexa Fluor 555	Life Technologies	IF 1:1000
Chicken IgG	Alexa Fluor 488	Life Technologies	1:1000

2.2.2 Cell lysis for western blot

For cell lysis before immunoprecipitation see Chapter 2.2.5. For analysis of knockdown, expression, LC3 lipidation or p62 degradation, cells were lysed in 1% Triton TNTE (1% Triton X-100, 20 mM Tris HCl pH 7.5, 150 mM NaCl, 5 mM EDTA) supplemented with 1X complete protease inhibitor cocktail (Roche) on ice. 100 µL of lysis buffer was used for a single well of a 12-well plate, and volumes were adjusted for other sized plates or dishes based on their relative surface area. Cells were incubated, on ice, in the lysis buffer for approximately 3 minutes before scraping the cells off with a pipette tip and repeated washing of the wells with the lysis buffer. The lysis buffer from each well was then transferred to a clean Eppendorf tube and spun at maximum speed (13 000 rpm) for 15 minutes to pellet the nuclei. The clarified lysate was transferred to clean Eppendorf tubes and 5X SDS sample buffer (15% SDS (w/v), 213.5 mM Tris-HCl pH 6.8, 50% glycerol (w/v), 16% β-mercaptoethanol, bromophenol blue) was added to a final concentration of 1X. Samples were heated at 65 ºC for 10 minutes before loading onto SDS-PAGE gels for electrophoresis and protein transfer (see below).

When required, Bio-Rad protein assay dye solution (Bio-Rad) was used to determine protein concentration to correct for uneven loading. Serial dilutions of an IgG standard (Bio-rad) in lysis buffer were made up to 800 µL with dH_2O and added to 200 µL of dye solution for the production of a standard curve. The protein content of samples was determined by making up small volume of the sample to 800 µL with water, as for the standard IgG, and adding 200 µL of dye solution. Both the protein sample mixes and the standard mixes were vortexed and incubated at room temperature for 15-60 minutes before measuring the absorbance at 595 nm using a spectrometer.

2.2.3 SDS-PAGE and protein transfer

SDS-PAGE was performed using NuPAGE 4-12% Bis-Tris precast mini or midi protein gels (Life Technologies). Gels were run at 200 V in MOPS (Life technologies, 20 X stock: 50 mM MOPS, 50 mM Tris Base, 0.1% SDS, 1 mM EDTA, pH 7.7) or MES (Life technologies, 20 X stock: 50 mM MES, 50 mM Tris Base, 0.1% SDS, 1 mM

EDTA, pH 7.3) until the dye front reached the bottom of the gel (the time taken was approximately 40 minutes - 1 hour depending on the size of the gel). MES was generally used for the running buffer, apart from for crosslinking experiments in Chapter 3.2.

Proteins were transferred to PDVF (polyvinylidene fluoride) membrane (Millipore) using wet transfer. PDVF membrane was pre-wet in methanol before rinsing in transfer buffer (0.2% methanol, 150 mM glycine, 20 mM tris base). Thick blot paper (Sigma) and transfer sponges were also pre-wet in transfer buffer. Proteins were transferred onto the membrane at 27. V for 1 hour 30 min. Protein transfer to the membrane was visualised using Ponceau S solution (Sigma) – the membrane was incubated in the stain for ≥ 10 minutes while rocking at room temperature. Excess stain was removed by repeated washing in water. After scanning the Ponceau-stained membrane, the stain was removed by repeated washing in PBSA.

2.2.4 Western blotting and detection

The following incubation periods are all at room temperature (unless otherwise specified) and on a rocker. If dry, PDVF membranes were re-wet in methanol and rinsed in PBSA. Membranes were incubated in in 5% powder milk (w/v) (Marvel) 0.1% PBSA-tween (PBST) for one hour for blocking. Following blocking, membranes were incubated in primary antibodies diluted as indicated in Table 2.2 in 5% milk (w/v) 0.1% PBST for one hour, unless indicated otherwise in Table 2.2. Where noted that an antibody was used overnight, this incubation was at 4 ºC. After incubation in primary antibody, the membrane was washed once quickly in 0.1% PBST, once for 10 minutes in PBST and twice for 5 minutes. Membrane were then incubated in HRP-conjugated secondary antibodies (see Table 2.3) for 40 minutes - 1 hour in 5% milk 0.1% PBST before washing in 0.1% PBST as for washing after primary antibody incubation, but with an additional two 5 minute washes (total of four 5 minute washes). Following washing, membranes were transferred to a glass plate and covered in ECL (Amersham, GE healthcare) for 2 minutes before exposing to film (Amersham Hyperfilm ECL, GE healthcare). Exposure times varied between western blots. For validation of phosphospecific antibodies, the above protocol was followed apart from: western blots

were blocked in 5% BSA (w/v) dissolved in 0.1% TBS-tween (TBST), washed in 0.1%TBST and primary and secondary antibodies were diluted in 1% BSA in 0.1% TBST.

For re-probing the same membrane, membranes were incubated in Restore Western Blot Stripping Buffer (Thermo Scientific) for 15 minutes while rocking at room temperature. Membranes were subsequently washed in 1% PBST once quickly and four times for 5 minutes before blocking in 5% milk 0.1% PBST for 40 minutes and then continuing with primary and secondary antibody incubations and washes as above.

2.2.5 Immunoprecipitation

For immunoprecipitation of endogenous protein, cells were grown to 80-100% confluency in 10 cm dishes and for immunoprecipitation of overexpressed protein, cells were transfected as described in Chapter 2.1.2.2 and were used for immunoprecipitation the following day. Cells were washed twice in PBSA (7 mL per wash) and then scraped in 1 mL of ice-cold lysis buffer supplemented with 1X complete protease inhibitor (Roche) and incubated for 10 minutes on ice for cell lysis. CHAPS (50 mM Tris HCl pH 7.5, 150 mM NaCl, 1 mM EDTA, 1% CHAPS (w/v)) was used for lysis and washing of endogenous Atg9 immunoprecipitation (not crosslinked). RIPA buffer (150 mM NaCl, 1% NP-40, 0.5% sodium deoxycholate, 0.1% SDS, 50 mM Trs HCl pH 7.5) was used for cell lysis and bead washing of crosslinked Atg9 before mass spectrometry analysis. 0.3% Triton X-100 TNTE (20 mM Tris HCl pH 7.5, 150 mM NaCl, 0.3% Triton X-100, 5 mM EDTA) was used for cell lysis and bead washing for immunoprecipitation of myc-tagged proteins. 1% Triton X-100 (20 mM Tris HCl pH 7.5, 150 mM NaCl, 1% Triton X-100, 5 mM EDTA) was used for cell lysis and bead washing of DSP-crosslinked proteins. NP-40 based buffers were used for cell lysis and washing for GFP-Trap and FLAG IP (see below). Once lysed, cells were spun at 13 000 rpm for 15 minutes at 4 ºCto pellet the nuclei.

This following protocol is for immunoprecipitation of endogenous Atg9, endogenous WIPI2 (but not co-immunoprecipitation with Atg16L1), and myc-tagged proteins. For each immunoprecipitation, 40 µL of protein A bead slurry (for rabbit antibodies), or protein G bead slurry (for mouse antibodies) (both Sigma) was washed

three times in 1 mL of PBSA and once in relevant lysis buffer in a 1.5 mL Eppendorf tube. The beads were subsequently resuspended in 100 µL of lysis butter and incubated with the relevant antibody for ten minutes on ice, followed by washing once in 1 mL of lysis buffer before the clarified cell lysate was added. Immunoprecipitation mixes were rotated for one hour at 4 ºC and were subsequently washed three times in 1 mL of relevant wash buffer. After removal of the final wash, beads were resuspended in 50 µL of 2 X SDS sample buffer before visualisation by western blot.

For immunoprecipitation of endogenous WIPI2 after DSP-treatment (see Chapter 2.2.8) and cell lysis, the clarified lysate for each immunoprecipitation was incubated with WIPI2 monoclonal antibody by rotating overnight at 4 ºC. Subsequently, washed protein G beads (washed as described above) were added to the lysate-antibody mix and the immunoprecipitation mixture rotated at 4 ºC for 2 hours. Beads were washed four times in 1 mL 1% Triton X-100 TNTE and the beads resuspended in 50 µL of 2X SDS sample buffer with 50 mM dithiothreitol (DTT) and boiled at 100 ºC for 10 minutes to cleave the crosslinker.

For RFP-, GFP-Trap and FLAG immunoprecipitation, cells from a confluent 10 cm dish were washed as described above and then scraped in 1 mL of cold PBSA, the cells were pelleted (1000 rpm at 4 ºC in a bench top centrifuge) and the PBSA removed from the cell pellet. The pellet of cells was subsequently lysed in 400 µL of GFP-Trap lysis buffer (10 mM Tris HCl pH 7.5, 150 mM NaCl, 0.5 mM EDTA, 0.5% NP-40) on ice for 15 minutes and spun at 13 000 rpm at 4 ºC to pellet nuclei. The clarified lysate was added to 500 µL of GFP-Trap dilution buffer (10 mM Tris HCl pH 7.5, 150 mM NaCl, 0.5 mM EDTA). RFP- and GFP-Trap immunoprecipitations were pre-cleared with blocked agarose beads (Chromtek). 20 µL of blocked agarose bead slurry was used for each RFP- or GFP-Trap, washed once in 1 mL PBSA and resuspended in 100 µL GFP-Trap dilution buffer before being added to the cell lysate. RFP- and GFP-Traps were precleared for 40 minutes, rotating at 4 ºC. 40 µL of supernatant from the pre-clear was used as ‘start’ sample and the remaining was added to RFP- or GFP-Trap beads (both ChromTek). 15 µL of Trap beads were used for each immunoprecipitation and were washed and resuspended in dilution buffer as for the blocked agarose beads. RFP- or GFP-tagged proteins were immunoprecipitated with the relevant Trap beads for one hour while by rotating at 4 ºC. FLAG M2 Affinity Gel (Sigma) was used for

immunoprecipitation of FLAG-tagged proteins. 20 μL agarose slurry was used per immunoprecipitation. The slurry was washed in the same manner as for Trap beads before adding to the FLAG-tagged cell lysates (with no preclear) and rotating at 4 ºC for one hour. RFP, GFP, and FLAG immunoprecipitations were all washed three times in 1 mL of GFP-Trap lysis buffer before adding 50 μL of 2 X SDS buffer and heating at 65 ºC for 10 minutes.

2.2.6 Immunoprecipitation from mixed lysates

In my hands, expression of tagged proteins could be very variable after co-transfection. Therefore, in experiments involving co-immunoprecipitation of overexpressed proteins, proteins were overexpressed in different cell populations before mixing cell lysates to try and even out protein expression. Briefly, cells were lysed as detailed for GPF-Trap (Chapter 2.2.5) and clarified lysate was produced. The clarified lysates from cells expressing tagged proteins were then used for pre-clearing with blocked agarose beads (see GFP-Trap details in Chapter 2.2.5) and 40 μL of 'start' sample was taken. Pre-cleared cell lysates were then mixed with those from cells expressing different proteins, and immunoprecipitation was performed from these mixtures. 'Start' samples were not mixed. See below for more detail.

2.2.6.1 FLAG-Atg16L1 and FLAG-Atg16L2 co-immunoprecipitation with GFP-tagged proteins

Plasmids coding for GFP, GFP-WIPI1a, GFP-WIPI2b, FLAG-Atg16L1 and FLAG-Atg16L2 were separately transfected in 10 cm plates (see Chapter 2.1.2.2). Cell washing and production of clarified lysates, preclearing and removal of 'start' sample before mixing lysates was performed as detailed above and in Chapter 2.2.5. GFP, GFP-WIPI1a and GFP-WIPI2b containing cell lysates were individually split evenly into two new Eppendorf tubes (on ice). One of each of the GFP-tagged protein lysates was then mixed with a third of the FLAG-tagged Atg16L1 and Atg16L2 containing cell lysate. GFP-Trap was performed form these mixtures as normal.

2.2.6.2 Fine mapping of Atg16L1 binding sites using point mutants

A total of 11 FLAG-tagged Atg16L1 and Atg16L2 constructs were used to test for co-immunoprecipitation with GFP-WIPI2b or endogenous FIP200. A 10 cm plate was used for transfection with each FLAG-tagged Atg16 construct (see Chapter 2.1.2.2) along with 4 X 10 cm plates of HEK293A cells stably expressing GFP-WIPI2b. Following cell lysis, production of clarified cell lysates and removal of 'start' samples (before mixing samples), cell lysates expressing FLAG-tagged proteins were split into two. Half of this sample was used for immunoprecipitation using FLAG Affinity Gel (Sigma) (see Chapter 2.2.5) to test for endogenous FIP200 co-immunoprecipitation. The other half of the FLAG-tagged lysates were each mixed with cell lysate from cells stably expressing GFP-WIPI2b. This lysate had been pooled from the 4 X 10 cm plates, before being split into 11 equal parts for mixing with the 11 FLAG-tagged lysates. In summary, cell lysate from roughly a third of a 10 cm plate of HEK293A cells stably expressing GFP-WIPI2b was mixed with cell lysate from a half of a 10 cm plate of HEK293A cells transiently over expressing FLAG-tagged Atg16 proteins.

2.2.6.3 Charge-change rescue experiment

In this experiment, four FLAG-tagged Atg16L1 constructs were mixed with four GFP-tagged WIPI2b constructs in all possible permutations (Figure 3.25a). A single 10 cm plate was transiently transfected with each construct. Following cell lysis, production of clarified cell lysates and 'start' removal (before mixing), these lysates were split into quarters and each quarter was mixed with a different quarter of cell lysates containing over expressed protein with the corresponding tag (i.e. a quarter of GFP-tagged WIPI2 containing cell lysate would be mixed with a quarter of FLAG-tagged Atg16L1 containing cell lysate). The mixes were then used for GFP-Trap as usual.

2.2.7 *In vitro* translation coupled with immunoprecipitation

Immunoprecipitation of GFP- or myc-tagged proteins followed by co-immunoprecipitation of *in vitro* translated Atg16L1 constructs was used to demonstrate

interactions. Immunoprecipitation and GFP-Trap were performed as described above.

TNT Quick Couple Transcription/Translation Systems (Promega) was used for *in vitro* translation of the T7 promoter-controlled constructs indicated in figures. 40 µL of TNT master mix was used with 0.5 µg of plasmid DNA, and 2 µL of ^{35}S-methonine (PerkinElmer) at 10mCi/mL in a final volume of 50 µL. The reaction was incubated while shaking at 30 ºC for 90 minutes.

A 10 cm plate of HEK203A cells was used for GFP-Trap or immunoprecipitation (see above) and the final products (after final washes) of immunoprecipitation were resuspended in 500 µL of wash buffer (GFP-Trap lysis buffer). 20 µL of *in vitro* translation product was added to the 500 µL of immunoprecipitation and the resulting mixture was rotated at 4 ºC for one hour. The beads were subsequently washed three times in wash buffer and the beads resuspended in 2X SDS sample buffer and the products analysed by SDS-PAGE followed by autoradiography and western blot.

2.2.8 Crosslinking

Dithiobis[succinimidyl propionate]/ Lomant's reagent (DPS) (ProteoChem), Bis[2-(succinimidooxycarbonyloxy)ethyl]sulfone (BSOCOES) (ProteoChem) and Disuccinimidlk suberate (DSS) (ProteoChem) are all amine-reactive, cell permeable crosslinkers that were used according to manufacturer's instructions. Plates of cells were washed on ice with PBSA twice before crosslinking. Protease inhibitors were not used during crosslinking of whole cells. When first dissolving crosslinkers, DMSO over a molecular sieve (anhydrous/'dry' DMSO) was used.

BSOCOES was dissolved in dry dimethyl sulfoxide (DMSO) (Sigma) to obtain a stock solution of 20 mM concentration immediately before use. This stock solution was diluted in PBSA to give a total volume of 6 mL. Final concentrations of BSOCOES that were used are as indicated in figures. The 6 mL of crosslinker was directly added to HEK293A cells in 10 cm dishes. After incubation on ice for 30 minutes, cells were washed in 1 M Tris HCl, pH 7.5, to quench the crosslinker. Cells were then washed in PBSA and lysed as usual for western blot.

DSS crosslinker was similarly made up to 20 mM in dry DMSO immediately before use. This stock solution was then diluted in PBSA to obtain a final solution of 2 mM. Incubation time for crosslinking was optimised using HEK293A cells in 6 cm plates, with 2 mL of DSS solution added to each plate. Crosslinking was quenched by adding Tris HCl pH 7.5 to a final concentration of 100 mM and incubating for 15 minutes. For DSS treatment before Atg9 immunoprecipitation, 4 X 15 cm plates of HEK293A cells were treated with DSS (15 mL per plate) and incubated on ice for 1 hour before quenching and cell lysis and Atg9 immunoprecipitation.

DSP was made up to an initial concentration of 10 mM using dry DMSO immediately before use before further dilution in PBSA to the concentrations indicated in figures and figure legends. HEK293A cells from a 10 cm plate were scraped into 1.5 mL Eppendorf tubes using 1 mL of ice cold PBSA and spun down (1000 rpm, 4 ºC, 2 minutes) to pellet the cells. The cells were resuspended in 1 mL of PBSA-DSP mix and incubated on ice for 30 minutes. The tubes were flicked occasionally to resuspend cells. Crosslinking was quenched by adding 1 M Tris HCl pH 7.5 to a final concentration of 20 mM and incubating on ice for a further 15 minutes. Cells were then spun down and lysed as usual.

2.2.9 Mass spectrometry

DSS crosslinking followed by endogenous Atg9 immunoprecipitation was used for mass spectrometry. Final washes of Atg9 immunoprecipitates were carried out in sterile conditions (under a laminar-flow hood) and SDS-PAGE was performed using a clean gel tank and sterile MOPS running buffer. SDS-PAGE gel was run as usual, until the dye front exited the gel, and the gel was stained using GelCode Blue Stain Reagent (Thermo Scientific), a colloidal Coomassie based dye. Lanes were cut into 1 mm slices for tryptic digest and mass spectrometry analysis. Each 1 mm slice was placed in a single well of a 96 well plate, covered in sterile water and transported to the LRI Mass Spectrometry facility. Digest and analysis was done by the LRI mass spectrometry facility.

2.2.10 Immunofluorescence labelling and confocal microscopy

HEK293A, HeLa and MEF cells were plated onto glass coverslips (LRI) in 12- or 24-well plates (these were coated in poly-D-lysine for HEK293A cells) for immunofluorescence (IF). For IF after Salmonella infection, cells were plated at densities described in Chapter 2.1.4. Otherwise, for IF after siRNA treatment, HEK293A cells were plated at 1.4 X 10^5 cells per well of a 12-well plate, and 7 X 10^4 cells per well of a 24-well plate the day before fixing. MEF cells were plates at a density of 8 X 10^4 cells per well of a 12-well plate.

Cells on coverslips were washed twice in PBSA while incubated on ice. All subsequent steps and solutions are at room temperature, unless otherwise stated. Cells were fixed in 3% paraformaldehyde (agar scientific) in PBS supplemented with 0.01 mM $MgCl_2$ and 0.01 mM $CaCl_2$ for twenty minutes. Typically, cells were then washed twice in PBSA before permeabilization with room temperature methanol for five minutes. For Atg16L1 staining, cells fixed with PFA were permeabilized using digitonin (50 μg/mL) for 5 minutes at room temperature. Following permeabilization, cells were washed twice with PBSA and then blocked for one hour in 5% BSA fraction V (Roche) in PBSA. Primary antibodies were diluted as indicated in Table 2.2 in 1% BSA in PBSA. Coverslips were inverted onto 100 μL drops of primary antibody mix and incubated in a humidified container for 1 hour. Coverslips were washed once in 1% BSA in PBSA before being inverted onto drops of 100 μL in secondary antibody, diluted as indicated in Table 2.3, in 1% BSA. Cells were incubated with secondary antibody for between 40 minutes and 1 hour. If used, Hoechst (Sigma) was added with the secondary antibody at 1:200. Finally, coverslips were washed once in 1% BSA, twice in PBSA and once in water before mounting onto glass microscope slides (Thermo Scientific) with 5 μL of Mowiol 4-88 (CalBiochem).

Confocal images were taken with a Zeiss Axioplan 2 LSM710 laser-scanning microscope with a 63X, 1.4, oil-immersion objective or a 40X, 1.3, oil-immersion objective (Carl Zeiss MicroImaging, Inc). Generally, a 40X objective was used for capturing images for LC3 or WIPI2 puncta counting, while a 63X objective was used for imaging Salmonella. Confocal images were taken with a slice thickness of 0.7 μm (normally for spot counting) or 1 μm (Salmonella images). Laser setting were kept

constant for imaging each condition of an experiment. Images were processed using Zen 2009 software.

2.2.11 ELISA

96-well MaxiSorp Immuno Plates (Nunc) protein-binding plates were used for ELISA. Plates were coated by diluting peptide to the final concentrations indicated in figures or figure legends in a final volume of 50 µL of Binding Buffer (0.1 M $NaHCO_3$, 0.2 M Na_2CO_3, 0.2 M $NaHCO_3$). Plates containing peptide in Binding Buffer were covered and incubated overnight at 4 ºC. After incubation, unbound peptide was washed from wells by washing three times with 0.1% Tween in Tris-buffered saline (TBS). Between washes, fluid was removed from plates by flicking well and patting dry on paper towel. Wells were subsequently filled with 150 µL Blocking Buffer (TBS/0.1% Tween, 1% BSA fraction V (Roche)) and incubated at room temperature for 1 hour. Plates were flicked well and patted dry on paper towels to remove Blocking Buffer. Subsequently, primary antibody was diluted in Blocking Buffer at the concentrations described in figures and 100 µL of diluted primary antibody was added to each well. Primary antibody was incubated for 1 hour and wells were then washed three times in TBS/0.1% Tween. Secondary antibody was diluted 1:4000 in Blocking Buffer and added to wells for 1 hour at room temperature. Wells were washed four times in TBS/0.1% Tween before 75 µL of ELISA substrate, *o*-phenylenediamine dihydrochloride (OPD) (Sigma), was added per well. The reaction was stopped after 10 minutes by adding 50 µL of 2 M HCl per well. ELISA plates were read at 490 nm using a SpectraMax Plus absorbance micro plate reader (Spectramax Plus (Molecular Devises)). When performing peptide competition, competing peptide(s) were added at a final concentration of 1 µg/mL to primary antibody solutions and incubated at room temperature, rocking, for 10 minutes before adding the primary antibody-peptide mix to the ELISA plate.

2.3 Molecular biology

2.3.1 PCR

Polymerase chain reaction (PCR) was typically performed using KOD hot start DNA polymerase (Novagen).

PCR mix:

10X Buffer for KOD Hot Start DNA Polymerase	5 µL
25 mM $MgSO_4$	3 µL
dNTPs (2 mM each)	5 µL
Forward primer (10 µM)	1.5 µL
Reverse primer (10 µM)	1.5 µL
Template plasmid	10 ng
KOD Hot Start Polymerase	1 µL
AccuPrime	5 µL
Nuclease-free water	to 50 µL

Components (apart from DNA, primers (Sigma) and AccuPrime (Life Technologies)) are from the KOD Hot Start Kit (Novagen).

PCR cycle:

Segment	Cycles	Temperature (ºC)	Time
1	1	95	2 min
2	30	95	20 sec
		55	10 sec
		65	25 s/kb
3	1	4	∞

PCR products were purified using DNA agarose gel electrophoresis (Chapter 2.3.2) if there were multiple PCR products, or using QIAquick PCR purification Kit (Qiagen) (spin column purification) according to the manufacturer's instructions. When spin column purifying, PCR products were eluted in 30 µL elution buffer (EB) (Qiagen).

2.3.2 DNA agarose gel electrophoresis

0.8% agarose (Invitrogen) was dissolved in 1 X Tris-acetate-EDTA (TAE) buffer (LRI) by heating using a microwave. One drop of 0.625 mg/mL ethidium bromide (Amresco) was added per 50-100 mL of molten agarose and the mixture was chilled slightly in water before pouring into a holder with well comb to set. DNA was added to 5X loading buffer (Qiagen) and loaded into wells. Hyperladder I (Bioline) was used as a size standard. DNA bands were imaged using a UV irradiator (GeneFlash, SynGene BioImaging). If required, DNA bands were excised using a clean sample, while visualising using a UV lamp, and purified using QIAquick Gel Extraction Kit (Qiagen) according to the manufacturer's instructions. DNA was eluted from the column using 30 µL EB (Qiagen) and incubating at room temperature for 2 minutes before eluting.

2.3.3 Restriction enzyme digestion

DNA in the form of plasmids and PCR products were digested using the relevant restriction enzymes from New England Biolabs (NEB) according to the manufacturer's instructions.

Generally, the following mix was used:

DNA	1 µg
10X NEBuffer	5 µL
100X BSA (if required)	0.5 µL
Restriction enzyme	10 units
Nuclease-free water	to 50 µL

Reactions were incubated for at least an hour at the optimum temperature. If double digestions were required, the best compromise was chosen in terms of NEBuffer. If no suitable buffer were available or if the incubation temperatures were different, serial digestions were performed with DNA purification between each digest. Double digestions were used to prevent re-ligation of the vector, with no insert, during DNA ligation.

2.3.4 DNA phosphatase treatment

To prevent religation of the vector, cut vector was treated with DNA calf intestinal phosphatase (CIP) (NEB) after restriction digestion. 10 units of CIP was added to the restriction digestion and incubated for 37 ºC for 1 hour.

2.3.5 Ligation

DNA fragments were ligated typically using T4 DNA Ligase (NEB) according to the manufacturer's instructions.

Ligation mix:

10X T4 DNA Ligase Buffer	2 µL
Vector DNA (3 kb)	50 ng
Insert DNA (1 kb)	50 ng
T4 DNA Ligase	1 µL
Nuclease-free water	to 20 µL

Ligations were usually incubated at 16 ºC overnight. A vector to insert ratio of 1:3 is shown above. If ligations were unsuccessful with a 1:3 ratio and a higher insert ration was tried, or if vector and insert sizes differed from those shown above, DNA amounts were calculated using an online calculator (NEBioCalculator). Total DNA concentration was kept below 10 ng/µL

2.3.6 Site directed mutagenesis

For site directed mutagenesis (SDM) QuickChange Multi Site-Directed Kit (Agilent Technologies) was used according to the manufacture's instructions, with very minor adjustments. Briefly, primers were designed to incorporate single or multiple base pair changes (see Table 2.4). These primers were used for production of circular PCR products using an enzyme mix containing high fidelity PfuTurbo DNA polymerase and

nick-sealing 'components'. See below for PCR mix and cycle. Following PCR, the original plasmid template was degraded by incubation Dpn I, and the resulting mix was used to transform XL10-GOLD ultracompetent cells (see Chapter 2.3.7). Colonies formed were used for miniprep production, verified by sequencing and then used for maxiprep production.

PCR mix:
Note, a half or a third of the recommended volumes work well. Half reactions are shown below.

10X QuickChange Multi reaction buffer	1.25 µL
Quick Solution	0.25 µL
Template DNA	25 ng
Mutagenic primer	50 ng
dNTP	0.5 µg
QuickChange Multi enzyme blend	0.5 µL
dH_2O to 12.5 µL	

PCR cycle:

Segment	Cycles	Temperature (ºC)	Time
1	1	95	1 min
2	30	95	1 min
		55	1 min
		65	2 min/kb
3	1	4	∞

2.3.7 Bacterial transformation

Chemically competent DH5α *E. coli* (Life Technologies), stored at -80 ºC, was defrosted on ice. 50 µL of DH5α was used per transformation. DNA was incubated with the bacteria for 30 minutes on ice. For transformation of ligation products, 10 µl of ligation mixture was added to the bacteria, and for transformation of plasmid DNA, 0.5 µg of DNA was added to the bacteria. Following incubation on ice, the bacteria were heat shocked at 42 ºC for 40 seconds before incubating on ice for 1 minute. 200 µL of SOC (2% trypton (w/v), 0.5% yeast extract (w/v), 10.0 mM NaCl, 2.7 mM KCl, 21.0

mM $MgCl_2$, 20.8 mM $MgSO_4$, 20 mM D-glucose, LRI) was added to the bacteria and the bacteria were recovered by incubating at 37 ºC in a shaking incubator for 1 hour. Bacteria were plated onto LB-agar plates (1% Bacto-Tryptone (w/v), 0.5% yeast extract, 1.7 M NaCl, 1.5% agar, LRI) containing the appropriate antibiotic (either ampicillin or kanamycin) at 50 μg/μL. For transformation of ligation products, the full 250 μL of bacteria-SOC mixture was plated, whereas 50 μL of plasmid transformation was plated. Bacteria were incubated overnight at 37 ºC to allow formation of colonies.

XL10-Gold Ultracompetent Cells (Agilent) were used for transformation of SDM products. The procedure for these bacteria is the same as for DH5α, apart from that 25 μL, rather than 50 μL, can be used per transformation and 1 μL of β-Mercaptoethanol is mixed into chilled bacteria by tapping, and the mixture incubated on ice for ten minutes before addition of DNA. 3 μL of SDM product was used for each transformation. Bacteria on plates were incubated for at least 16 hours to allow visible colonies to form.

2.3.8 Preparation of plasmid DNA

Colonies from bacterial plates were picked and used in 5 mL LB (1% Bacto-Tryptone (w/v), 0.5% yeast extract, 1.7 M NaCl, LRI) plus relevant antibiotics at a concentration of 50 μg/μL for miniprep plasmid DNA production. These cultures were grown in a shaking incubator at 37 ºC for at least 8 hours. Bacteria were pelleted at 4000 rpm for 20 minutes at 4 ºC and the supernatant discarded. When a large number of minipreps were being processed the miniprep service at the LRI equipment park was used. For small numbers of minipreps, Qiaprep Miniprep Kit (Qiagen) was used according to the manufacturer's instructions. DNA was eluted in 50 μL EB buffer.

For production of larger quantities of sequence-verified plasmids, maxipreps were performed. Bacterial colonies were picked from transformation plates or from DMSO or glycerol stocks and were added to 250 mL of LB medium with added antibiotic and incubated for 24 hours while shaking at 37 ºC. Bacterial pellets were pelleted at 4000 rpm for 20 minutes at 4 ºC and the supernatant discarded. Qiagen Plasmid Maxi Kit was then used according to the manufacturer's instructions for purification of plasmid DNA. After precipitation and washing, DNA was redissolved in

500 µL TE (Tris-EDTA) buffer. The concentration of DNA was subsequently measured using a spectrophotometer (NanoDrop, Thermo Scientific) and the DNA made up to 1 µL/µL with TE. Aliquots were stored at -20 ºC for long-term storage, or at 4 ºC if the aliquot was in regular use.

2.3.9 DMSO stock production

DMSO stocks of *E. coli* DH5α expressing plasmids and *Salmonella typhimurium* SL 1344 were stored at -80 ºC and were used for starter cultures. 900 µL of cultures (either 1 mL of a maxi prep culture for *E. coli*, or aliquots of 1 mL from a 20 mL culture from an overnight incubation of *salmonella*) were mixed with 100 µL of DMSO in a cryovial (Corning) for freezing and storage at -80 ºC.

2.3.10 Primers

All primers were purchased from Sigma.

Table 2.4 Primers used in this thesis

Primer name	Sequence	Used for
HA-Atg16-1-Forward	ATTCTAGAATGTACCCATACGATGTTCCAGATTACGCTCTGTCGTCGGGCCTGCGCGCCG	HA-Atg16L1 1-207
Atg16-207-Reverse	ctGGATCCtcatgcattgaggcgat	HA-Atg16L1 1-207
Atg16L1 mus 1-207 SDM	CAATCGCCTCAATGCATagGAGAATGAGAAGGAC	Stop codon at 208
Atg16L1 1-230 SDM	GAAGCAGCAAAGGAATagCCTCTACCTGTTGAAC	Stop codon at 231
Atg16L1 1-242 SDM	GATGACATTGAAGTCtagATTGTGGATGAGACC	Stop codon at 243
Atg16L1 mus E208R	CCAATCGCCTCAATGCAAGGAATGAGAAGGACTCC	Atg16L1 E208R
Atg16L1 mus D212R	GCAGAGAATGAGAAGcgcTCCAGGAGGCGTCAAGC	Atg16L1 D212R
Atg16L1 mus E226R	CTGCAGAAGGAGCTTGCAagaGCAGCAAAGGAACCTCTAC	Atg16L1 E226R
Atg16L1 mus E230R	GAGCTTGCAGAAGCAGCAAAGagaCCTCTACCTGTTGAAC	Atg16L1 E230R
Atg16L1 mus E235R	CAAAGGAACCTCTACCTGTTagaCAGGATGATGACATTGAAG	Atg16L1 E235R
Atg16L1 mus D237R	CCTCTACCTGTTGAACAGcgtGATGACATTGAAGTCATTG	Atg16L1 E237R
Atg16L1 mus D238R	CTACCTGTTGAACAGGATcgtGACATTGAAGTCATTGTGG	Atg16L1 D238R
Atg16L1 mus D239R	CCTGTTGAACAGGATGATcgcATTGAAGTCATTGTGGATG	Atg16L1 D239R
Atg16L1 mus E241R	GAACAGGATGATGACATTcgtGTCATTGTGGATGAGACC	Atg16L1 E241R
Atg16L1 mus E246R	CATTGAAGTCATTGTGGATaggACCTCAGACCACACAGAAG	Atg16L1 E246R
Atg16L1 mus D249R	CATTGTGGATGAGACCTCAcgcCACACAGAAGAGACCTCTC	Atg16L1 D249R
Atg16L1 mus E253R	GACCTCAGACCACACAGAAcggAGCCTCTCCCGTCCGAGCTG	Atg16L1 E253R
Atg16L1 mus E226R E230R	GAGCTTGCAagaGCAGCAAAGagaCCTCTACCTGTTGAAC	Atg16L1 E226R E230R
Atg16L1 mus D237R D239R	CCTGTTGAACAGcgtGATcgcATTGAAGTCATTGTGGATG	Atg16L1 D237R D239R
WIPI2 mut RR	GGACAAAAACTCTTTGAGTTTACGACAGGAGTAAAGAGGTGCGTG	WIPI2 FTTG
WIPI1-STOP-mut	ACAGCTTGCTTGGCTCAtaaACAACAGAAGAGAATAAAG	WIPI1ΔCT
WIPI2-STOP-mut	CACCGGCTGGACGGCAGTtaaGAAACGACCAATGAGATC	WIPI2ΔCT
WIPI2b-R108E	GCTGTGAAGCTCAACgagCAGAGGCTGATAGTATG	WIPI2b R108E
WIPI2b-R125E	CATCCACAACATTgagGACATGAAGGTGCTGC	WIPI2b R125E
WIPI2b-R125K	CATCCACAACATTaagGACATGAAGGTGCTGC	WIPI2b R125K
WIPI2a-E26K	CAACCAGGACAACACACAaaaGTGAAAGGGGGCATCAAG	WIPI2a E26K
WIPI2a-R31E-L35E	GAAAGGGCATCAgaaGCAGCTGGTgaaGGCCG	WIPI2a R31E L35E
WIPI2a-R31E-L35E R	CGGCCttcACCAGCTGCttcTGATGCCCCTTTC	WIPI2a R31E L35E
WIPI2bsiRES-SDM-2 (Step 1)	GTGGGTGCCGCCGACGGGTATCTTTACATGTACAAC	Producing WIPI2 siRES to Quiagen #3)
WIPI2bsiRES-SDM-1-corrected (Step 2)	GTGGGTGCCGCCGATGGTTATCTTTACATGTACAAC	Producing WIPI2 siRES to Quiagen #3)
WIPI2-CAAX-R-TRUE	TCGGGCAAGCTTTCACATAATTACACACTTTGTCTTTGACTTCTTTTTTCTTTTTTACCATCTTTTCTAGAGTC	WIPI2b-CAAX
WIPI2-CAAX-F-TRUE	GACGAGCTCGGGCCCACCATGAACCTGGCGAGCCAGAGCGGG	WIPI2-CAAX
HA-WIPI2CAAX-forward	ATGAATTCACCATGTACCCATACGATGTTCCAGATTACGCTAACCTGGCGAGCCAGAGCGGG	Producing HA-WIPI2-CAAX
Reverse-WIPI2CAAX	AACTTAAGCTTTCACATAATTACAC	Subcloning WIPI2-CAAX into mCherry vector
mCherry-WIPI2CAAX-forward	ATCTCGAGGGAACCTGGCGAGCCAGAGCGGG	Subcloning WIPI2-CAAX into mCherry vector
cherry-WIPI2-correction	CGAGGGAACCTGGCGAGCCAGAGCGGGAGGCC	Correcting frame shift in mCherry-WIPI2-CAAX
dCAAX SDM	CCATGATTCTTCGGACTGACtgaAGAAAAGATGGTAAAAAGAAG	Production of WIPI2ΔCAAX
WIPI2b-phosphomutantSDMd/e	GGTACTTACGTGCCTGAAGACCCAACGAGACTTGCC	WIPI2 S394E S3945E
WIPI2b-phosphomutantSDM-ala	GGTACTTACGTGCCTGCAGCCCCAACGAGACTTGCC	WIPI2 S394A S3945A
WIPI2b-singlephosmutSDM-e	GGTACTTACGTGCCTTCAGACCCAACGAGACTTGCC	WIPI2 S3945E

2.3.11 Plasmids

Table 2.5 Plasmids used in this thesis

Name	Insert	Vector	Resistance	Source
pEGFP-C1	GFP	pEGFP-C1	Kanamycin	Clontech
GFP-WIPI2b	WIPI2b	pEGFP-C1	Kanamycin	H. Polson
GFP-WIPI1a	WIPI1a	pEGFP-C1	Kanamycin	T. Proikas-Cezanne
GFP-WIPI2a	WIPI2a	pEGFP-C1	Kanamycin	M. Clague
GFP-Rab33B	Rab33B	pEGFP-C2	Kanamycin	F. Barr
pcDNA3.1(-)		pcDNA3.1(-)	Ampicillin	
GFP-Atg16L1	Atg16L1	pEGFP-C1	Kanamycin	T. Yoshimori
HA-Atg16L1 (mus) 1-207	Atg16L1 1-207	pcDNA3.1(-)	Ampicillin	H Dooley
pRK5mycApg5	Atg5	pRK5	Ampicillin	A Tolkovsky
myc-WIPI1a	WIPI1a	pCMVTag3	Kanamycin	T. Proikas-Cezanne
myc-WIPI2b	WIPI2b	pCMVTag3	Kanamycin	H. Polson
pMRXires-puro-Atg16L WT	Atg16L-WT (human)	pMX-IRES-GFP (GFP removed)	Ampicillin	T. Yoshimori
pMRXires-puro-Atg16L delta CCD	Atg16L Δ69-213 (human)	pMX-IRES-GFP (GFP removed)	Ampicillin	T. Yoshimori
pMRXires-puro-Atg16L delta WD	Atg16L 1-249 (human)	pMX-IRES-GFP (GFP removed)	Ampicillin	T. Yoshimori
pcDNA3.1-Flag Atg16L WT	Atg16L1 WT (Mus)	pcDNA3.1	Ampicillin	T Yoshimori
pcDNA3.1-Flag Atg16L ΔN	Atg16L1 79-623	pcDNA3.1	Ampicillin	T. Yoshimori
pcDNA3.1-Flag Atg16L ΔC	Atg16L1 1-265	pcDNA3.1	Ampicillin	T. Yoshimori
pcDNA3.1-Flag Atg16L1 1-242	Atg16L1 1-242	pcDNA3.1	Ampicillin	H. Dooley
pcDNA3.1-Flag Atg16L1 1-230	Atg16L1 1-230	pcDNA3.1	Ampicillin	H. Dooley
pcDNA3.1-Flag Atg16L1 1-207	Atg16L1 1-207	pcDNA3.1	Ampicillin	H. Dooley
Flag-Atg16L2	Atg16L2	pcDNA3.1	Ampicillin	M. Fukuda
Flag-Atg16L1 E208R	Atg16L1 E241R (mus)	pcDNA3.1	Ampicillin	H. Dooley
Flag-Atg16L1 D212R	Atg16L1 D212R (mus)	pcDNA3.1	Ampicillin	H. Dooley
Flag-Atg16L1	Atg16L1	pcDNA3.1	Ampicillin	H. Dooley

E226R	E226R (mus)			
Flag-Atg16L1 E230R	Atg16L1 E230R (mus)	pcDNA3.1	Ampicillin	H. Dooley
Flag-Atg16L1 E235R	Atg16L1 E235R (mus)	pcDNA3.1	Ampicillin	H. Dooley
Flag-Atg16L1 D237R	Atg16L1 D237R (mus)	pcDNA3.1	Ampicillin	H. Dooley
Flag-Atg16L1 D238R	Atg16L1 D238R (mus)	pcDNA3.1	Ampicillin	H. Dooley
Flag-Atg16L1 D239R	Atg16L1 D239R (mus)	pcDNA3.1	Ampicillin	H. Dooley
Flag-Atg16L1 E241R	Atg16L1 E241R (mus)	pcDNA3.1	Ampicillin	H. Dooley
Flag-Atg16L1 E246R	Atg16L1 E246R (mus)	pcDNA3.1	Ampicillin	H. Dooley
Flag-Atg16L1 D249R	Atg16L1 D249R (mus)	pcDNA3.1	Ampicillin	H. Dooley
Flag-Atg16L1 E253R	Atg16L1 E253R (mus)	pcDNA3.1	Ampicillin	H. Dooley
Flag-Atg16L1 E226R E230R	Atg16L1 E226R E230R (mus)	pcDNA3.1	Ampicillin	H. Dooley
Flag-Atg16L1 D237R D239R	Atg16L1 D237R D239R (mus)	pcDNA3.1	Ampicillin	H. Dooley
pEGFP-WIPI2b delta CT	WIPI2b 1-360	pEGFP-C1	Kanamycin	H. Polson
pEGFP-WIPI1a delta CT	WIPI1a 1-362	pEGFP-C1	Kanamycin	H. Polson
GFP-WIPI2b FRRG siRES Qiagen #3	WIPI2b FTTG siRES	pEGFP-C1	Kanamycin	H. Dooley
pEGFP-WIPI2b R108E	WIPI2b R108E	pEGFP-C1	Kanamycin	H. Dooley
pEGFP-WIPI2b R125E	WIPI2b R108E	pEGFP-C1	Kanamycin	H. Dooley
pEGFP-WIPI2b R108E R125E	WIPI2b R108E R125E	pEGFP-C1	Kanamycin	H. Dooley
pEGFP-WIPI2b R125K	WIPI2b R125K	pEGFP-C1	Kanamycin	H. Dooley
pEGFP-WIPI2a E26K	WIPI2a E26R	pEGFP-C1	Kanamycin	H. Dooley
pEGFP-WIPI2a R31E L35E	WIPI2a R31E L35E	pEGFP-C1	Kanamycin	H. Dooley
pEGFP-WIPI2b siRES Qiagen #3	WIPI2b siRES	pEGFP-C1	Kanamycin	H. Dooley
pEGFP-WIPI2b R108E R125E	WIPI2b R108E R125E siRES	pEGFP-C1	Kanamycin	H. Dooley

siRES Qiagen #3				
GFP-WIPI2b R108E R125E FRRG siRES Qiagen #3	WIPI2b R108E R125E FTTG siRES	pEGFP-C1	Kanamycin	H. Dooley
myc-DFCP1	DFCP1		Ampicillin	N. Ktistakis
pcDNA3.1(-) mCherry	mCherry	pcDNA3.1	Ampicillin	H. Jefferies
mCherry-WIPI2b-CAAX RR	mCherry-WIPI2b-CAAX FTTG	pcDNA3.1	Ampicillin	H. Dooley
mCherry-WIPI2b-RR	WIPI2b FTTG	pcDNA3.1	Ampicillin	H. Dooley
mCherry-WIPI2b-CAAX RR R108E R125E	WIPI2b-CAAX FTTG R108E R125E	pcDNA3.1	Ampicillin	H. Dooley
HA-WIPI2b-CAAX RR	WIPI2b-CAAX FTTG	pcDNA3.1	Ampicillin	H. Dooley
GFP-LC3	LC3	pEGFP-C1	Kanamycin	T. Yoshimori
GFP-WIPI2b S395A	WIPI2b S395A	pEGFP-C1	Kanamycin	H. Dooley
GFP-WIPI2b S395E	WIPI2b S395E	pEGFP-C1	Kanamycin	H. Dooley
GFP-WIPI2b S394A S395A	WIPI2b S394A S395A	pEGFP-C1	Kanamycin	H. Dooley
GFP-WIPI2b S394E S395E	WIPI2b S394E S395E	pEGFP-C1	Kanamycin	H. Dooley

2.3.12 Sequencing

Sequencing was carried out using BigDye Terminator v3.1 (BDT) (LRI) sequencing reactions.

Reaction mix:

8 µL BDT

3.2 pMol Sequencing primer

150 ng DNA

Made up to 10 µL in dH_2O

PCR cycle:

Segment	Cycles	Temperature (°C)	Time
1	1	96	3 min
2	25	96	10 sec
		50	5 sec
		60	4 min
3	1	4	∞

Sequencing reactions were cleaned up using the DyeEx 2.0 Spin Kit (Qiagen) according to the manufacture's instructions. Cleaned reactions were dried using a vacuum centrifuge for 20 minutes. Sequencing was performed using capillary sequencing on an Applied Biosystems 3730Xl DNA analyser by LRI sequencing services. DNA sequences were analysed and aligned using ApE (Universal) and MegAlign (DNASTAR) software.

2.4 Analysis

2.4.1 Imaris image software

LC3 and WIPI2 puncta were quantified using Imaris X64 software. Thresholds for detection limits (size and intensity of puncta) were set manually by comparing puncta detection in starved (+ Bafilomycin) vs fed cells. The same set-up was used for each condition of an experiment. Cells were counted manually. LC3 and p62-positive Salmonella were quantified using Imaris-assisted manually counting: detection limits were set using Imaris, and identified LC3- or p62-positive Salmonella were manually counted.

2.4.2 Image J densitometry

ImageJ (National Institute of Health) was used for quantification of western blots by measuring the density of film exposure.

2.4.3 Statistical analysis

Statistical analysis was performed using Prism6 (GraphPad software) as indicated in figure legends. Asterisk(s) indicate significance: *, $p \leq 0.05$, **, $p \leq 0.01$, ***, $p \leq 0.001$, ****, $p \leq 0.0001$. Data shown is the mean of the indicated number of experiments. Error bars are standard error of the mean.

Chapter 3. Validation of Atg16L1 as a WIPI2b binding partner and mapping the Atg16L1-WIPI2b interaction

3.1 Introduction and aim

3.1.1 Introduction

Both the function of PtdIns(3)P at the omegasome and the function of mAtg9 remain outstanding questions in our understanding of autophagy. PtdIns(3)P production is essential for both mammalian and yeast autophagy, however the molecular mechanisms underpinning this requirement are not known. It is probable that in both yeast and mammalian cells PtdIns(3)P acts, at least in part, to recruit PtdIns(3)P binding proteins. In *S. cerevisiae*, PAS-localised PtdIns(3)P recruits the Atg18-Atg2 complex through PtdIns(3)P binding protein Atg18, and this complex subsequently exerts an essential function (Obara et al., 2008). The functions that Atg18 and Atg2 exert at the PAS are not fully understood. The complex is required for Atg9 recycling from the PAS (Reggiori et al., 2004), and has been implicated in other roles such as protection of Atg8-PE from premature cleavage by Atg4 (Nair et al., 2010). Atg2 can be localised to the PAS via a FYVE domain, and this Atg2-FYVE protein partially rescues autophagy in *atg18Δ* cells (Kobayashi et al., 2012). Thus, one of the molecular functions of Atg18 is the PtdIns(3)P-dependent localisation of Atg2 at the PAS. In a similar manner, the molecular requirement for PtdIns(3)P in mammalian autophagy may be explained by the recruitment of a omegasome-localised PtdIns(3)P binding protein which subsequently exerts an essential function.

Atg18 is a WD-40 domain-containing protein. WD-40 domains frequently function as protein-protein interaction platforms (Xu and Min, 2011). In light of this, it is possible that the function of the mammalian Atg18 homologues, WIPI (WD-40 repeat containing proteins that interact with phosphoinositides) proteins, is similarly to act as protein interaction platforms to recruit proteins to the phagophore in a PtdIns(3)P-dependent manner. WIPI1 and WIPI2 both localise to the omegasome during amino acid starvation in a PtdIns(3)P dependent manner and are thought to exert a function,

which is currently not known (Proikas-Cezanne et al., 2004, Polson et al., 2010). Hannah Polson, a previous Postdoctoral researcher in the lab, performed a mass spectrometry-based screen to find WIPI1a and WIPI2b interactors. Hannah established and used HEK293A GFP, GFP-WIPI1a and GFP-WIPI2b stable cell lines for GFP-Trap immunoprecipitation before mass spectrometry analysis of proteins co-immunoprecipitated with the GFP-tagged proteins. Hannah used GFP-WIPI2b rather than GFP-WIPI2a as she observed that WIPI2a does not form puncta during starvation, whereas WIPI2b does (Dooley et al., 2014), an observation that has been repeated by another lab (Mauthe et al., 2011). A separate set of interactors was pulled down with both WIPI1a and WIPI2b. Notably, GFP-WIPI1a interacted with a number of coatomer (COP) proteins; whereas GFP-WIPI2b interacted with the Atg12–5-16L1 complex. Hannah validated these interactors using co-immunoprecipitation of GFP-tagged WIPI (Figure 3.1 c). Hannah further validation between the Atg12–5-16L1 complex and GFP-WIPI2b using immunofluorescence. She found that GFP-WIPI2b puncta, but not GFP alone or GFP-WIPI1a, colocalised with Atg16L1 puncta (Figure 3.1 d, e and f).

Yeast and mammalian Atg9 proteins have six transmembrane domains, and in both Atg9 is the only known transmembrane protein that is required for autophagy. However, the function of this protein remains elusive. The origin of the autophagosome membrane is an area of high interest and it is thought that there are multiple sources of membrane including ER (Axe et al., 2008), recycling endosomes (Longatti et al., 2012), Golgi (Geng et al., 2010, Ohashi and Munro, 2010, van der Vaart et al., 2010), mitochondria (Hamasaki et al., 2013), and plasma membrane (Ravikumar et al., 2010). The current consensus is that Atg9 may function to supply membrane to the growing autophagosome and, although this has not been directly shown, mAtg9 has been shown to partly localise to a number of possible autophagosome membrane sources including the trans-Golgi network (Young et al., 2006), recycling endosomes (Orsi et al., 2012) and plasma membrane (Puri et al., 2013). If mAtg9 is responsible for membrane supply, then the targeting and trafficking of this protein must be highly controlled and regulated. mAtg9 traffics between a juxtanuclear localisation in starvation conditions and peripheral localisation during amino acid starvation and this movement is controlled by ULK1 (Young et al., 2006), WIPI2 (Orsi et al., 2012) and through Atg9 interaction with p38IP (Webber and Tooze, 2010). Additionally, mAtg9 may be involved in other

protein-protein interactions which are unrelated to membrane trafficking but which may help elucidate the function. Andrea Orsi, a previous Postdoctoral researcher in the lab, used HEK293A cells transiently overexpressing HA-Atg9 for a mass spectrometry screen for mAtg9 interacting partners. He identified Transferrin receptor and Syntaxin 13, among others, as potential mAtg9 interacting partners (Orsi et al., 2012).

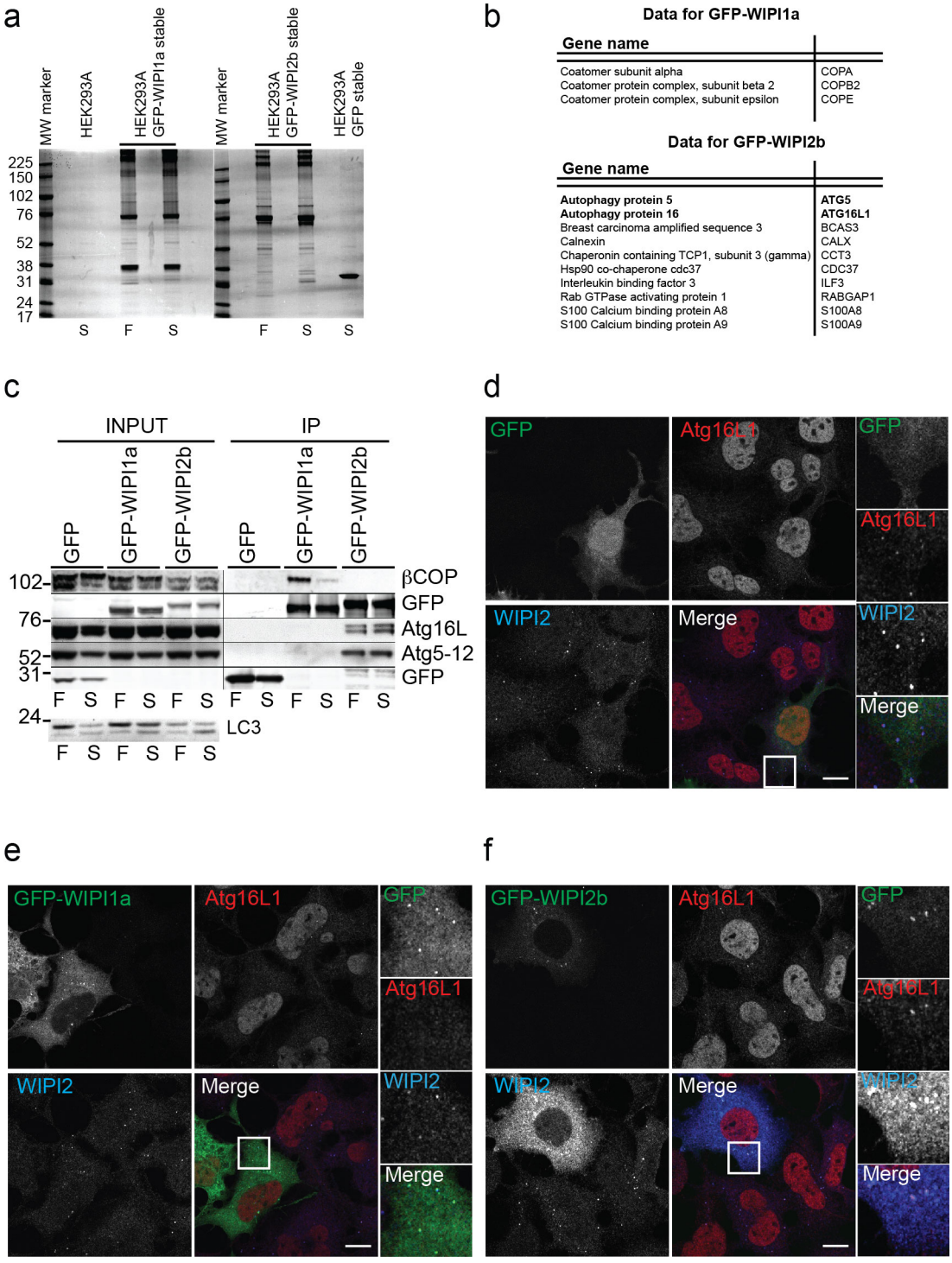

Figure 3.1 Mass spectroscopy screen for and validation of WIPI1 and WIPI2 interactors

(a) HEK293A cell lines stably expressing GFP, GFP-WIPI1a or GFP-WIPI2b were treated in full medium (F) or starved in EBSS (S) for two hours before being used for GFP-TRAP. Colloidal Coomassie stained SDS-PAGE gel of purified protein complexes is shown. **(b)** A list of identified GFP-WIPI1a and GFP-WIPI2b interacting proteins. Proteins found in GFP or untransfected HEK293A control cell lines were removed from these lists. **(e-f)** HEK293A cells stably expressing GFP **(d)**, GFP-WIPI1a **(e)** or GFP-WIPI2b **(f)** were starved for two hours before being fixed and analysed by confocal

microscopy using antibodies against endogenous WIPI2 and Atg16L1 as indicated. Scale bars are 10 μm. Molecular weights are in kDa. Data and Figure provided by Hannah Polson

3.1.2 Aim

In order to further characterise the functions of both mAtg9 and WIPI2, I began by trying a crosslinking-mass spectrometry based approach in order to find novel interacting partners. I began by using a crosslinker-based approach in order to identify interactions that may have been missed in previous interaction screens due to their transient or weak nature. In addition to this, I continued work begun by Hannah Polson and Andrea Orsi on WIPI2 and Atg9, respectively.

Cell-permeable crosslinkers provide a method by which protein-protein interactions can be stabilised in intact cells to allow for detection of transient or weak interacting partners. In addition, identification of peptides that covalently attached to WIPI2 or mAtg9 via the crosslinker would help identify the interaction sites on both the binding partners and the protein of interest (mAtg9 or WIPI2) and so allow a low-resolution model of the interaction to be formed. There are a wide variety of cell-permeable crosslinkers that are commercially available, and these include general and site-specific crosslinkers. As my aim was to identify novel interactors, we had no specific site of interest that we wanted to target by using site-specific crosslinkers and so I chose to use amine-reactive crosslinkers. The detection of crosslinked peptides in the mass spectrum is challenging as they make up a small proportion of the total peptides detected. Using deuterated crosslinkers can make crosslinked peptides easier to identify. By using a 1:1 ratio of non-deuterated and deuterated crosslinker, any mass spectrum peaks that are a result of two peptides attached by the crosslinker should be a specific molecular weight apart from an identical set of peaks (the molecular weight difference dictated by the difference in molecular weights of the deuterated and non-deuterated crosslinkers). This very specific pattern of molecular weight difference has been previously used to successfully identify crosslinked peptides (Ihling et al., 2006). My experiment plan was to crosslink intact cells with the amine-reactive crosslinker DSS and its deuterated partner DSS-d4, immunoprecipitate mAtg9 or WIPI2 to enrich for their interactors, followed by mass spectrometry analysis (Figure 3.2)

The Atg12–5-16L1 complex localises to the phagophore in a PtdIns(3)P dependent manner (Fujita et al., 2008). However, none of the three complex members (Atg5, Atg12 and Atg16L1) process any known PtdIns(3)P binding. Furthermore, there is no known binding partner of the Atg12–5-16L1 complex with PtdIns(3)P binding ability. From Hannah Polson's previous work, the Atg12–5-16L1 complex was the interactor that had the most direct link with autophagy, and was the most exciting when the results were viewed with the aim of finding the function of either WIPI1a or WIPI2b in autophagy, as WIPI2b may be the PtdIns(3)P binding protein through which the Atg12–5-16L1 complex is recruited. I therefore chose to concentrate on validating and mapping the possible interaction between WIPI2b and the Atg12–5-16L1 complex, alongside performing a crosslinking-mass spectrometry screen for additional WIPI2b and mAtg9 interactors. To validate and map the WIPI2-Atg12–5-16L1 interaction, I used a number of approaches, including endogenous co-immunoprecipitation, site directed mutagenesis and protein truncation to map the interaction, and a charge swapping approach to show a direct binding between WIPI2b and Atg16L1. During my work in mapping the interaction between Atg16L1 and WIPI2b, the work showing that FIP200 binds Atg16L1 was published (Gammoh et al., 2013, Nishimura et al., 2013, Fujita et al., 2013). I therefore mapped the region of Atg16L1 that interacts with FIP200.

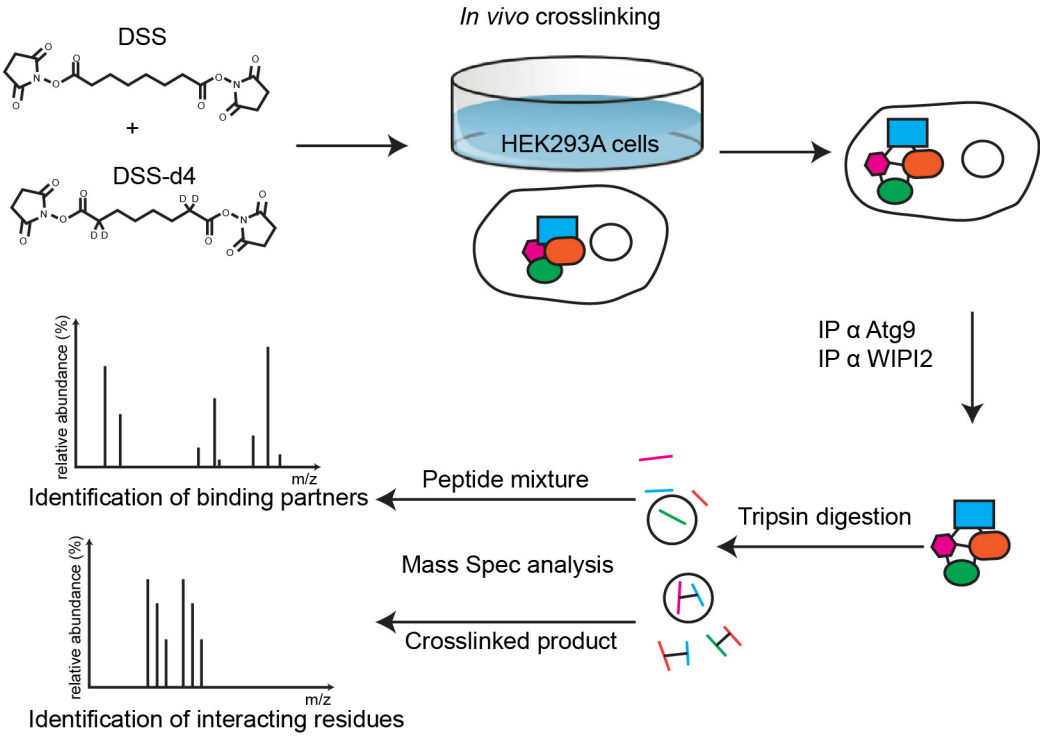

Figure 3.2 Crosslinking - mass spectrometry experiment schematic

Figure adapted from (Sinz, 2010). Crosslinkers DSS and deuterated analogue DSS-d4 would be added to HEK293A cells in a 1:1 ratio before WIPI2 or mAtg9 immunoprecipitation followed by mass spectroscopy analysis for identification of binding partners and interacting regions.

3.2 Crosslinking – mass spectrometry

3.2.1 Crosslinking optimisation

I optimised mAtg9 and WIPI2 crosslinking with an amine-specific crosslinker, BSOCOES. BSOCOES has a spacer length of 13.0 Å, is base cleavable, has been used in the lab before (Otto et al., 2010), and has the same amine-reactive group as DSS. HEK293A cells were treated with either full medium (Fed) or EBSS (Starved) for two hours before being treated with BSOCOES between 0.5 and 2 mM, or with DMSO as a control for 30 minutes before SDS-PAGE and western blot analysis (Figure 3.3). EEA1 forms a dimer (Callaghan et al., 1999) and was used as a positive control. Both EEA1 and mAtg9 showed a shift in molecular weight with BSOCOES treatment at all concentrations in both fed and starved conditions. These molecular weight shifts appeared to be discrete, suggestive of distinct protein complexes. In addition, the

molecular weight shifts seen with mAtg9 in fed and starved conditions appear to differ, suggesting that the mAtg9 complexes may change between fed and starved conditions. A smear of WIPI2 was consistently seen after treatment with crosslinker with no distinct changes in molecular weight and the majority of the WIPI2 signal was still present as a major band at around 49 kDa, representing monomeric WIPI2, even with treatment of 2 mM BSOCOES, and with UV-activated crosslinkers tried (data not shown). The reasons for this are unclear. The antibodies used for western blotting pick up all of the WIPI2 isoforms and a number of isoforms, including isoforms WIPI2a and WIPI2c, do not form starvation-induced puncta (Mauthe et al., 2011). Additionally, a large proportion of WIPI2 protein is cytosolic, while a smaller portion of the protein binds the membrane in a wortmannin-independent manner (Polson et al., 2010). It may be that WIPI2 forms isoform-specific complexes, and that these complexes make up the smear upon crosslinking, while some isoforms remain monomeric. To clarify this, crosslinking would have to be performed on cells expressing tagged isoforms of WIPI2. I continued crosslinking optimisation by focusing on mAtg9.

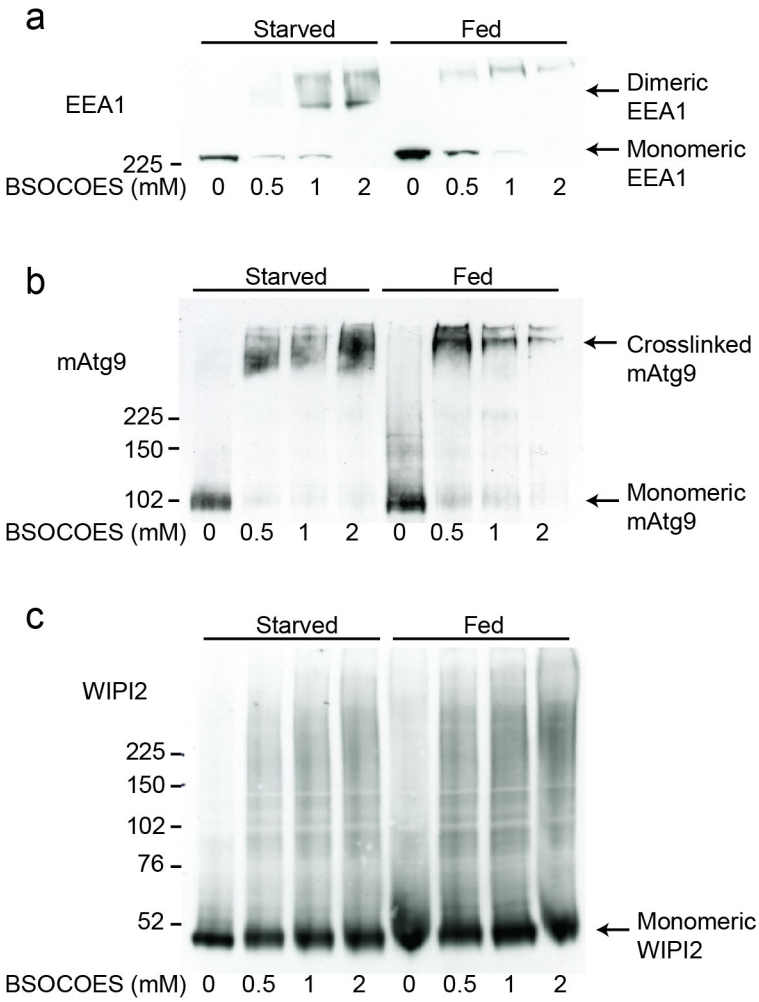

Figure 3.3 BSOCOES optimisation

HEK293A cells were treated with full medium (Fed) or starvation medium (Starved) for two hours before treatment with the indicated concentration of BSOCOES for 30 minutes. Cells were then lysed in 0.3% triton X-100 TNTE and used for western blot with antibodies against EEA1 **(a)**, mAtg9 **(b)** or WIPI2 **(c)**. Molecular weights are in kDa.

3.2.2 Deuterated crosslinking and mAtg9 immunoprecipitation

DSS and BSOCOES crosslinkers have the same amine-reactive groups. BSOCOES effectively crosslinked mAtg9 at all three concentrations tried (0.5, 1.0, 2.0 mM). In order to minimise the time for which the cells were treated with crosslinker, I used 2 mM DSS and tried varying the time of cell incubation with crosslinker (Figure 3.4 a and b). The most effective crosslinking (as judged by appearance of higher molecular weight EEA1) was at 1 hour crosslinking with 2 mM DSS.

Following time optimisation, I ensured that I could effectively immunoprecipitate mAtg9 from crosslinked cell lysates. HEK293A cells were treated with 2 mM DSS on ice for 1 hour before cell lysis in RIPA buffer and mAtg9 immunoprecipitation. RIPA buffer contains the ionic detergents SDS and NP-40 and is therefore more denaturing than milder lysis buffers such as TNTE. I decided to use RIPA in order to try and increase the proportion of crosslinked interactions detected during mass spectroscopy by minimising non-crosslinked interactions between mAtg9 and its interactors. I had previously optimised mAtg9 immunoprecipitation in RIPA buffer (data not shown). mAtg9 was effectively immunoprecipitated from DSS-treated samples (Figure 3.4 c). The mAtg9 band at its monomeric molecular weight of 95 kDa can be faintly seen in the input and beads alone unbound lane with no DSS treatment. This band is not present in the input after DSS treatment, and a higher molecular weight band at a molecular weight of 225 kDa appears and is effectively immunoprecipitated, suggesting that both crosslinking and immunoprecipitation worked. The ladder of higher molecular weight bands seen after immunoprecipitation of mAtg9 (in both DMSO and DSS treated samples) have been seen previously by Jemma Webber (a previous PhD student in the lab) following endogenous mAtg9 immunoprecipitation. It is not clear whether they are SDS-resistant complexes of mAtg9 or background bands from the rabbit anti-Atg9 antibody used for immunoprecipitation that are cross-reacting with the hamster anti-Atg9 used for western blot.

To ensure that I could immunoprecipitate enough mAtg9 to be detected by mass spectrometry, I scaled-up the endogenous immunoprecipitation of mAtg9 from one 10 cm plate per immunoprecipitation, to four 15 cm plates and found that with this number of HEK392A cells, a band that could be mAtg9 can be seen at the correct molecular weight for monomeric mAtg9 by colloidal Coomassie staining (data not shown). Following this, I performed a large-scale crosslinking and immunoprecipitation experiment in which I used four 15 cm plates treated with negative control DMSO, and four 15 cm plates treated with a 1:1 ratio of DSS and DSS-d4 at a total concentration of 2 mM for 1 hour on ice. The cells were subsequently lysed using RIPA buffer and immunoprecipitated with rabbit anti-mAtg9 antibody. The products of immunoprecipitation were run on an SDS-PAGE gel and stained with colloidal Coomassie stain. The immunoprecipitation product from the DMSO-treated control

showed a band at the correct molecular weight along with banding above this weight, and the crosslinked-treated immunoprecipitation showed a reduced band at the correct size for monomeric mAg9, a reduced banding above this size and an increase in the high molecular weigh complexes at the top of the colloidal Coomassie-stained gel (data not shown). The samples were analysed by Mark Skehel and colleagues at the LRI mass spectrometry facility at the Clare Hall laboratories. Unfortunately, they were unable to detect any mass spectra peaks that corresponded to deuterated and non-deuterated crosslinked peptides, either because the spectrum was too complex to analyse or because the peptides were below the detection threshold. At this stage other areas of my work were showing more promise and so this area of my project was stopped.

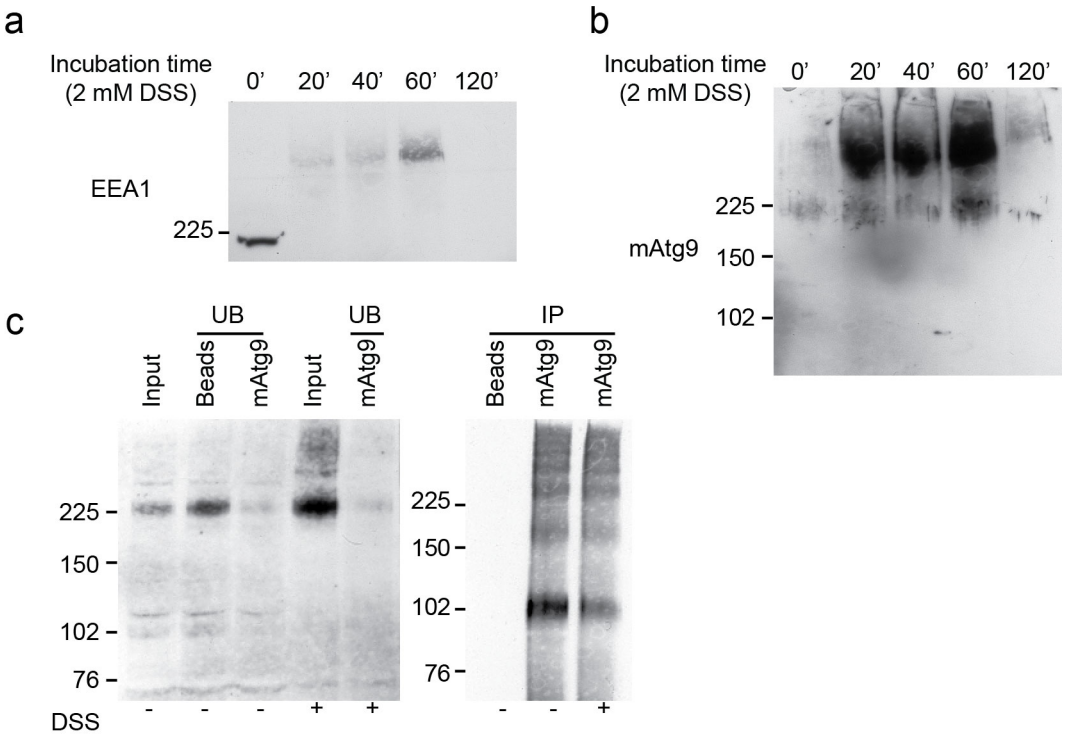

Figure 3.4 DSS optimisation and mAtg9 immunoprecipitation following crosslinking

(a,b) HEK293A cells were treated with 2 mM DSS for the indicated time before western blotting analysis with **(a)** anti-EEA1 and **(b)** anti-mAtg9 antibodies. **(c)** HEK293A cells were treated with either DMSO as a negative control or 2 mM DSS for one hour before cell lysis in RIPA buffer and mAtg9 immunoprecipitation and western blot analysis. Molecular weights are in kDa. EEA1 and mAtg9 monomers and higher molecular weigh complexes are as indicated in Figure 3.3

3.3 mAtg9 interactor validation

Andrea Orsi found transferrin receptor (TfR) and Syntaxin 13 (Stx13) in his mass spectrometry screen for mAtg9 interactors using HA-mAtg9 transiently transfected HEK293A cells. TfR is a carrier for transferrin (which binds free iron) and is removed from the plasma membrane by clathrin-mediated endocytosis into early endosomes, before being sorted in recycling endosomes and recycled to the plasma membrane (van Dam and Stoorvogel, 2002). Syntaxin 13 is a Q-SNARE required for recycling of internalised proteins, including TfR, to the plasma membrane and is localised on early and recycling endosomes (Prekeris et al., 1998). mAtg9 binding to, or colocalising in the same compartment as, TfR and Stx13 would suggest that mAtg9 is at least partially localised to the recycling endosome. I used endogenous immunoprecipitation of mAtg9 to try and validate Andrea Orsi's data suggesting that mAtg9 interacts with TfR and Stx13. I found that TfR, but not Stx13, co-immunoprecipitated with endogenous mAtg9 after cell lysis using CHAPS buffer (Figure 3.5 a and b). CHAPs lysis buffer was used as it results in efficient Atg9 immunoprecipitation (Jemma Webber, thesis). CHAPS is a non-denaturing lysis buffer and so it is possible that the mAtg9-TfR interaction is not direct and may instead be the result of mAtg9 and TfR interacting through another protein or their colocalisation within a lipid raft. This result supports other data suggesting that mAtg9 is localised in the Atg9 compartment, as in yeast, which are thought to be tubular-vesicular clusters which traffic through other membrane compartments, including early and recycling endosomes (Mari et al., 2010, Orsi et al., 2012).

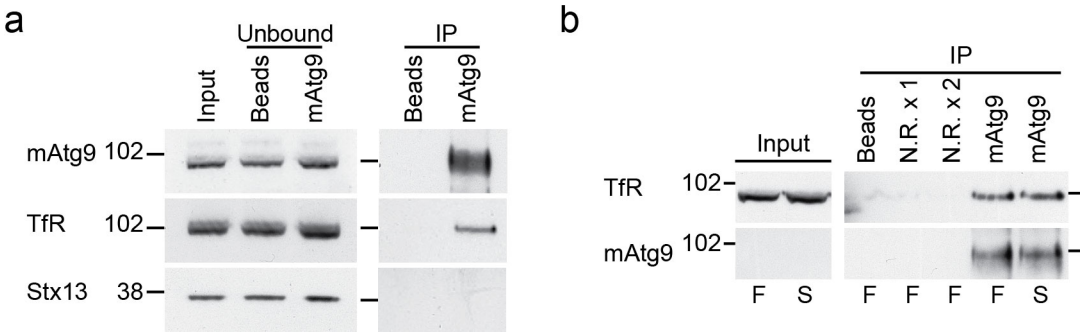

Figure 3.5 Atg9 co-immunoprecipitates TfR, but not Stx13

(a) HEK293A cells were lysed with CHAPS lysis buffer before immunoprecipitation with anti-mAtg9 antibodies, or beads alone control before western blot analysis. **(b)** Cells lysed as for **(a)** and immunoprecipitated with anti-mAtg9 antibody or controls beads alone, and non-relevant antibody (N.R.) (WIPI1 polyclonal antibody) at 1X or 2X the concentration of mAtg9 antibody before western blot analysis.

3.4 Validation of the Atg16L1-WIPI2b interaction

3.4.1 Validation of the interaction between the Atg12–5-16L1 complex and WIPI2b using GFP-tagged proteins

The main approach to interactor validation is usually endogenous co-immunoprecipitation of the complex. However, co-immunoprecipitation of the Atg12–5-16L1 complex with WIPI2 had proven difficult and had not been achieved in attempts made previously by Hannah Polson before she left the lab. I therefore began my approach to validating the interaction by repeating some of Hannah's work done using GFP-tagged proteins. As expected, GFP-Trap of transiently over expressed GFP-WIPI2b co-immunoprecipitated endogenous Atg16L1 in both fed and starved conditions, whereas GFP-Trap of transiently over expressed GFP (control) did not (Figure 3.6 a). Similarly, endogenous Atg16L1 co-immunoprecipitated with GFP (or CFP)-tagged proteins from cells transiently transfected with WIPI2b or known interactors Atg5 and Rab33B, but not with WIPI2a or WIPI1a (Figure 3.6 b). WIPI2a is an isoform of WIPI2 that differs from WIPI2b by an 18 amino acid insert in blade 1 of the 7-bladed β propeller of WIPI2 (Figure 1.8b). This insertion renders WIPI2a both unable to bind Atg16L1 (Figure 3.6 b) and unable to form puncta upon autophagy initiation (Dooley et al., 2014, Mauthe et al., 2011).

In Hannah Polson's validation of WIPI2b interaction with the Atg12–5-16L1 complex, she established that the interaction was likely to be mediated through Atg16L1 by co-immunoprecipitating FLAG-Atg16L1 ΔN (which can not bind the Atg5–12 conjugate) through GFP-WIPI2b (Figure 3.11). Therefore, I tried to validate the interaction between WIPI2b and the Atg12–5-16L1 complex by overexpressing GFP-Atg16L1 and using GFP-Trap to look for co-immunoprecipitated endogenous WIPI2 (Figure 3.7). While positive control FIP200 came down with GFP-Atg16L1, WIPI2 did not.

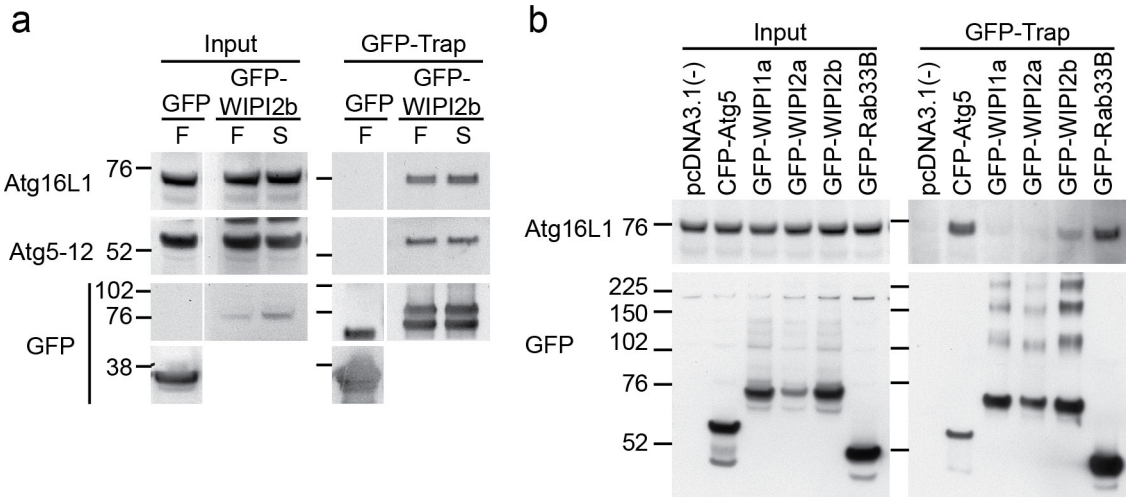

Figure 3.6 GFP-WIPI2 co-immunoprecipitates the Atg12–5-16L1 complex

(a) HEK293A cells transiently transfected with either GFP or GFP-WIPI2b were treated with full medium (F) or EBSS (S) for two hours as indicated before cell lysis and GFP-Trap. Protein complexes were analysed by western blot. **(b)** HEK293A cells were transiently transfected with the indicated constructs before cell lysis and GFP-Trap. Protein complexes were analysed by western blot. All molecular weights are shown in kDa.

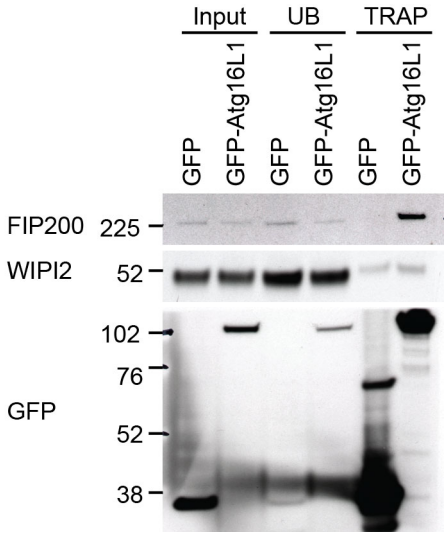

Figure 3.7 GFP Trap of GFP-Atg16L1

Cell lysates from HEK293A cells transiently overexpressing GFP or GFP-Atg16L1 were used for GFP-Trap followed by western blot using the indicated antibodies. Molecular weights are shown in kDa.

3.4.2 Validation of the interaction between the Atg12–5-16L1 complex and WIPI2b using myc-WIPI2b

At this stage in my project I was unable to co-immunoprecipitate endogenous Atg12–5-16L1 with endogenous WIPI2b and as the only way in which I could demonstrate the WIPI2-Atg16L1interaction was though GFP-Trap of GFP-WIPI2b, I was concerned that the interaction could be an artefact of the GFP-WIPI2b construct. I therefore tried to co-immunoprecipitate *in vitro* translated, [^{35}S] methionine-labelled HA-Atg16L1 with myc-tagged WIPI2b. Hannah Polson mapped the WIPI2b-Atg16L1 interaction to the coiled coil domain of Atg16L1 (Figure 3.11) and so I used Atg16L1 FL and HA-Atg16L1 1-207 to try to begin mapping the WIPI2 binding site more finely. Although myc-Atg5 co-immunoprecipitated *in vitro* translated Atg16L1 FL and HA-Atg16L1 1-207, myc-WIPI2b did not co-immunoprecipitate Atg16L1 (Figure 3.8a). However, co-immunoprecipitation of *in vitro* translated Atg16L1 FL, but not 1-207, with GFP-Trap of GFP-WIPI2b worked (Figure 3.8b). This result suggests that the interaction observed between GFP-WIPI2b and Atg16L1 is not an artefact and further suggests that WIPI2b binds between 207 and 265 of Atg16L1.The western blot of the myc-immunoprecipitation, performed before mixing the myc-immunoprecipitation beads with the *in vitro* translated Atg16L1, showed a large amount of myc-tagged protein in

the unbound lysates (Figure 3.8a), whereas the GFP-Trap completely cleared GFP-WIPI from the unbound (Figure 3.8b). By running the myc-IP and GFP-Trap alongside each other and using an anti-WIPI2 antibody for western blot, the efficiencies of transfection and immunoprecipitation can be directly compared (Figure 3.8c). While the expression levels of myc-WIPI2b and GFP-WIPI2b were similar (input lanes), the myc-immunoprecipitation was very inefficient compared to GFP-Trap. This may provide an explanation as to why co-immunoprecipitation of Atg16L1 with myc-WIPI2b had not worked so far. The inefficiency of the myc-immunoprecipitation may have been due to the myc-WIPI constructs having a single myc-tag; multiple myc-tags may have improved the efficiency of the immunoprecipitation.

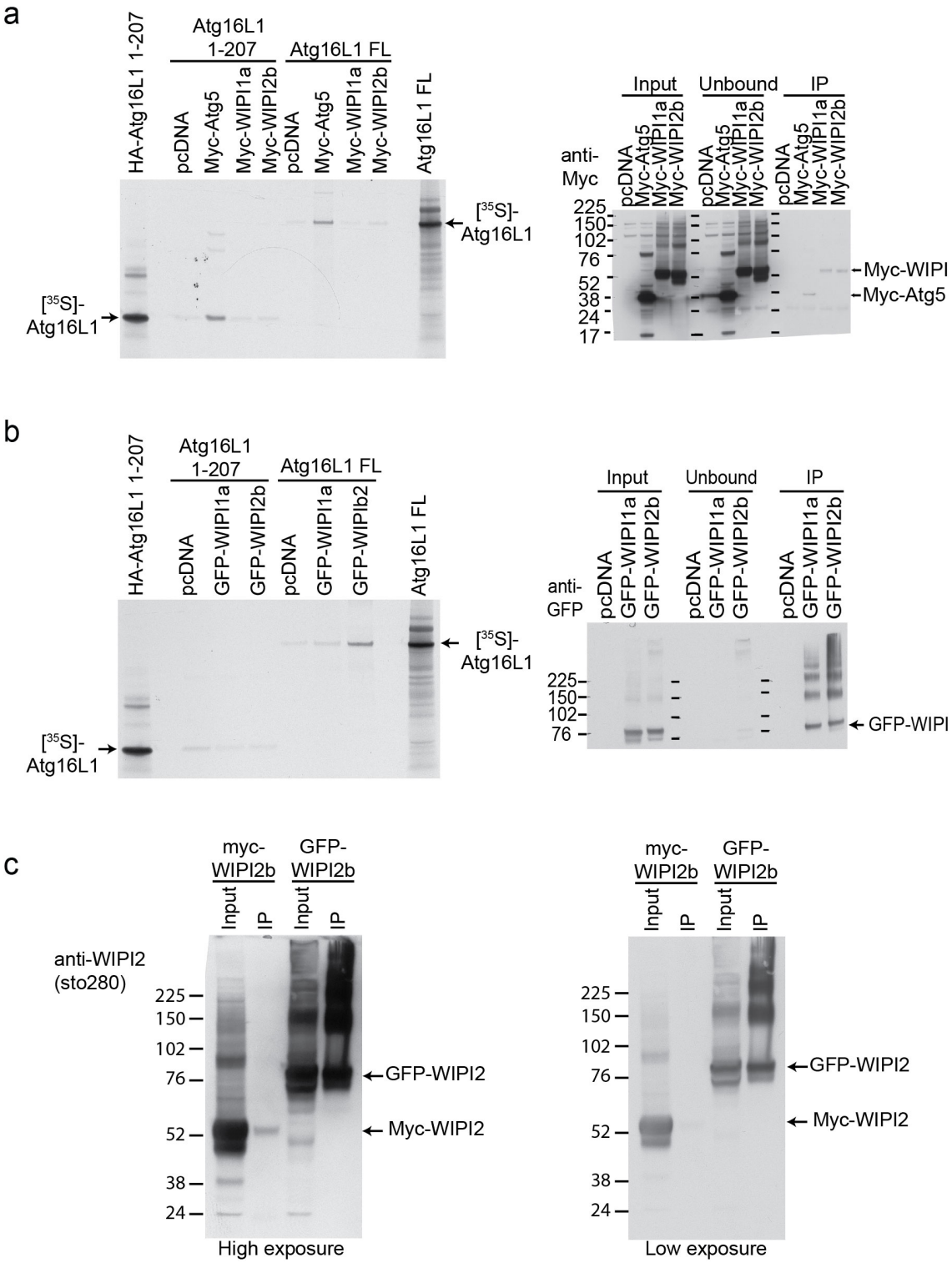

Figure 3.8 Comparison of myc- and GFP-tagged WIPI2b immunoprecipitation

(a) Cell lysates from HEK293A cells transiently transfected with pcDNA3.1(-) control, myc-tagged Atg5, WIPI1a or WIPI2b were used for immunoprecipitation with anti-myc antibodies. Immunoprecipitated product was mixed with *in vitro* translated [^{35}S] methionine labelled HA-Atg16L1 1-207 or full length Atg16L1, and the co-immunoprecipitated radiolabelled protein was visualised using autoradiography (left

hand panel). Right hand panel shows western blot of myc-IP. **(b)** As for **(a)** but using cell lysates from HEK293A cells transiently transfected with pcDNA3.1(-) control, GFP-WIPI1a or GFP-WIPI2b for GFP-Trap. Right hand panel shows western blot of GFP-Trap. **(c)** comparison of the efficiency of immuoprecipitation of myc- and GFP-WIPI2b using anti-myc antibodies and GFP-Trap, respectively. Immunoprecipitated tagged WIPI2b was visualised by immunoblotting using anti-WIPI2 antibody. Molecular weights are in kDa.

3.4.3 Validation of the endogenous interaction between the Atg12–5-16L1 complex and WIPI2b using crosslinking

The difficulty of co-immunoprecipitating the Atg12 5-16L1 complex with endogenous WIPI2b is suggestive of a weak or transient Atg16L1-WIPI2 interaction. If so, this would be similar to the Atg16L1-FIP200 interaction, which can only be co-immunoprecipitated using endogenous proteins when the interaction is stabilised either in Atg3 KO MEFs, where the phagophore is stalled before LC3 lipidation, or using the amine-reactive crosslinker DSP (Nishimura et al., 2013, Gammoh et al., 2013). I investigated whether DSP could stabilise any interaction between the Atg12–5-16L1 complex and WIPI2b sufficiently to enable co-immunoprecipitation by treating HEK 293A cells with DSP at either 0.5 or 1.0 mM for 30 minutes before cell lysis and subsequent immunoprecipitation using antibodies against WIPI2 (Figure 3.9). Treating the cells with either 0.5 or 1.0 mM DSP resulted in co-immunoprecipitation of the Atg12–5-16L1 complex with WIPI2.

After successfully co-immunoprecipitating the Atg12–5-16L1 complex through WIPI2, I tried to perform the reverse co-immunoprecipitation through endogenous Atg16L1 (Figure 3.10). Attempts to do this were unsuccessful, even though endogenous Atg16L1 was effectively depleted from the unbound lysate. WIPI2 runs at approximately 49 kDa, and so the signal is often obscured by signal from the heavy chain (even when different species of antibody are used for immunoprecipitation and western blotting as in Figure 3.10). Given more time I would readdress this issue by crosslinking the Atg16L1 antibody to beads prior to immunoprecipitation as it may be possible that WIPI2 signal is obscured by the heavy chain in Figure 3.10.

As described in 3.4.1, the interaction between GFP-WIPI2b and the Atg12–5-16L1 complex is not starvation-dependent. To confirm that this is also the case with the

interaction between endogenous proteins, I compared co-immunoprecipitation between fed and starved HEK 293A cells and saw no change in interaction with a change in starvation state (data not shown). This result is consistent with data using GFP-WIPI2b (Figure 3.6), and is also similar to the Atg16L1-FIP200 interaction, which is starvation independent (Nishimura et al., 2013).

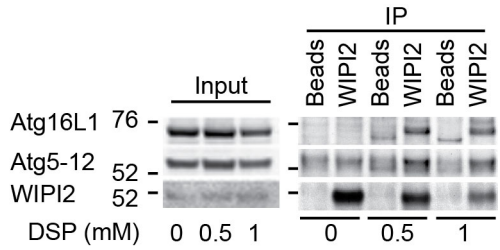

Figure 3.9 Endogenous co-immunoprecipitation of WIPI2 and Atg12-5-16L1

HEK293A cells were treated with DSP crosslinker at the indicated concentrations, before being lysed and used for WIPI2 immunoprecipitation followed by SDS-PAGE and western blot analysis. Molecular weight is in kDa.

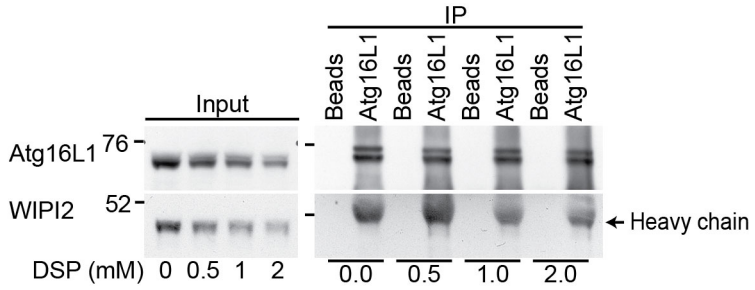

Figure 3.10 Endogenous immunoprecipitation of Atg16L1

HEK293A cells were treated with DSP crosslinker at the indicated concentrations, before being lysed and used for Atg16L1 immunoprecipitation followed by SDS-PAGE and western blot analysis. Molecular weight is in kDa.

3.5 Mapping the WIPI2b binding site on Atg16L1

3.5.1 Atg16L1 is the member of the Atg12–5-16L1 complex that is responsible for interacting with WIPI2b

Previous work has shown that Atg16L1 is the member of the Atg12–5-16L1 complex through which the whole complex is recruited to the forming autophagosome membrane (Fujita et al., 2008). Specifically, the region of Atg16L1 that contains the coiled coil

domain, the region encompassing amino acids 79-265, is the region that is thought to mediate membrane localisation (Fujita et al., 2008) (see Chapter 1.3.5.3). Hannah Polson used fragments of Atg16L1 in her initial validation experiments to determine whether the interaction between the Atg12–5-16L1 complex and WIPI2b is mediated through Atg5–12 or Atg16L1. She transiently overexpressed FLAG-tagged Atg16L1 constructs in stably expressing GFP-WIPI2b HEK 293A cells before utilising GFP-Trap to look for co-immunoprecipitation of FLAG-Atg16L1 with GFP-WIPI2b (Figure 3.11 a and b). Deletion of the N- or C-terminus of Atg16L1 had no effect on binding to WIPI2b (Figure 3.11a). The interaction between Atg16L1 and the Atg5–12 conjugate is mediated by Atg5 and the N-terminal domain of Atg16L1 and so Atg16L1 ΔN does not bind the Atg5–12 conjugate. Therefore, the interaction between FLAG-Atg16L1 ΔN and GFP-WIPI2b demonstrates that the Atg5–12 conjugate is not needed for the interaction between Atg16L1 and WIPI2b, indicating that the interaction with WIPI2b is mediated by Atg16L1. In addition, deletion of either the N- or C-terminus of Atg16L1 had no effect on WIPI2b binding, showing that the Atg16L1-WIPI2b interaction must be mediated through the middle region of Atg16L1: amino acids 79-265. These results were supported by results that Hannah obtained when using transient overexpression of untagged human Atg16L1 in the GFP-WIPI2b stable cell line. She found that Atg16L1 full length and ΔWD were co-immunoprecipitated with GFP-WIPI2b. However, deletion of the coiled coil domain (amino acids 69-213) rendered Atg16L1 unable to bind WIPI2b (Figure 3.11b).

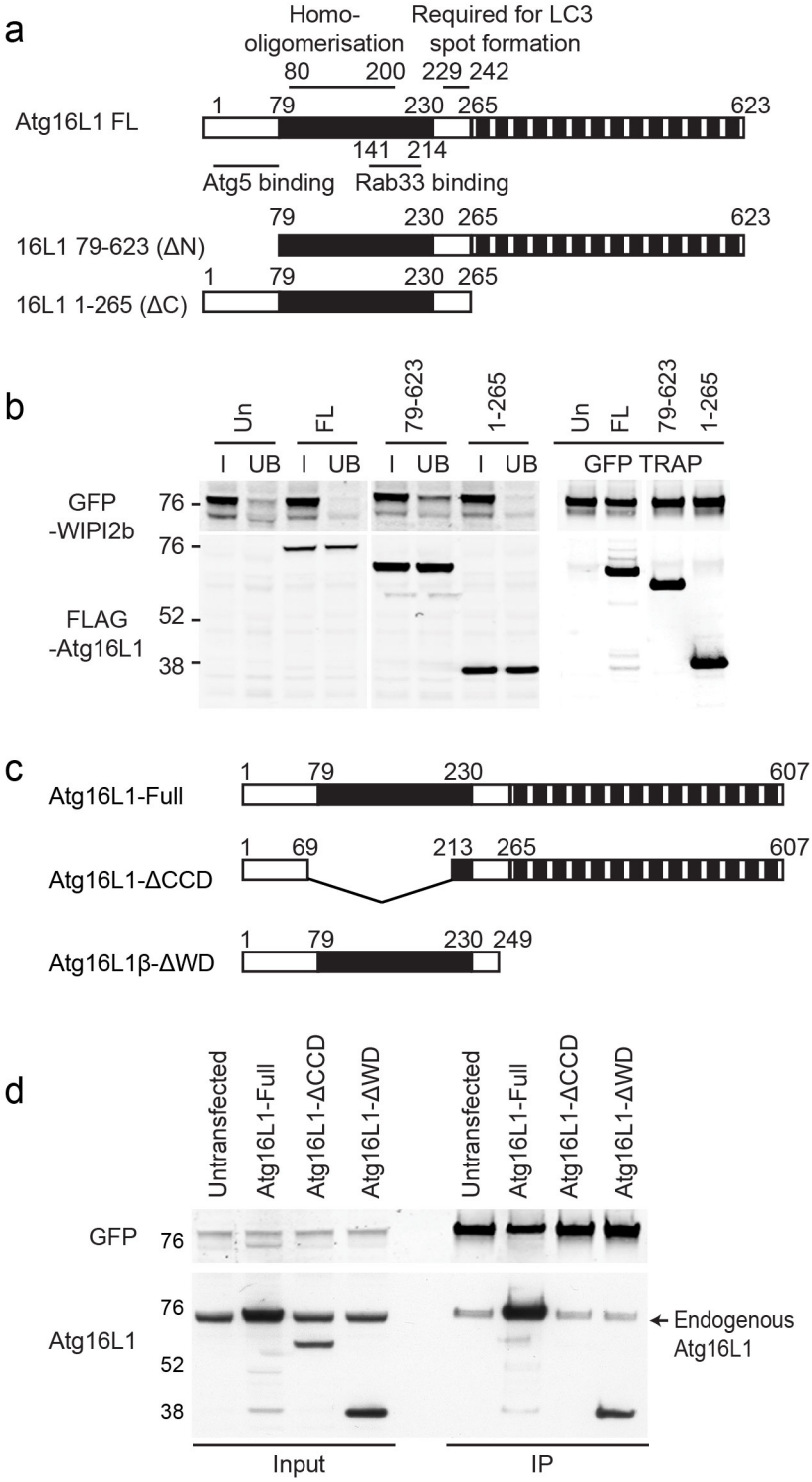

Figure 3.11 WIPI2b binds Atg16L1 between amino acids 79 and 265

(a) Schematic of mouse Atg16L1 constructs used. White N-terminal box represents the Atg5 binding domain. Black box represents the coiled-coil domain of Atg16L1. Stripped box represents the WD-40 domain. Adapted from (Fujita et al., 2008). **(b)** Untransfected (Un), full length (FL), 79-623 or 1-265 FLAG-tagged Atg16L1 constructs were transiently transfected in HEK293A cells stably expressing GFP-WIPI2b before being used for GFP-Trap. Tags were visualised by immuoblot. **(c)**

Schematic of human Atg16L1 constructs sued. Boxes as for **(a)**. Adapted from (Fujita et al., 2009). **(d)** Untransfected, full length, ΔCCD and ΔWD Atg16L1 were transiently transfected into HEK293A cells stably expressing GFP-WIPI2b and the cell lysates were used GFP-Trap. Protein complexes were visualised by immunoblot using the indicated antibodies. Molecular weights are in kDa. **(b)** and **(d)**: data and panels provided by Hannah Polson.

3.5.2 The WIPI2b binding site on Atg16L1 is located between amino acids 207-230

As the interaction between Atg16L1 and WIPI2b seems to be mediated by a region contained within 207-265 of Atg16L1 (Figures 3.8 and 3.11), I used site directed mutagenesis to produce a series of C-terminal truncations of FLAG-Atg16L1 to further map the interaction site on Atg16L1 (Figure 3.12 a). The truncations at amino acids 242 and 230 were chosen in light of data published on Atg16L2 (Ishibashi et al., 2011). This study showed that Atg16L2, a homologue of Atg16L1, can form an Atg12–5-16L2 complex but cannot function in autophagy due to its inability to bind the phagophore membrane. The authors postulated that amino acids 229-242 of Atg16L1 are the residues that are required for Atg16L1 localisation to membrane, possibly through binding either directly to the phagophore membrane or an unidentified phagophore-localised protein. Our working model is that WIPI2b may be the membrane-localised protein that is binding Atg16L1 and subsequently recruiting the Atg12–5-16L1 complex to the site of autophagosome formation. If this is true then loss of amino acids 229-242 may result in loss of WIPI2b binding. Atg16L1 forms homodimers through its coiled coil domain (Fukuda and Itoh, 2008). I was concerned that when overexpressed in HEK 293A cells the C-terminal deletions would form heterodimers with endogenous Atg16L1, which would then able to bind to WIPI2b. In an attempt to minimise this, I used *in vitro* translation using [^{35}S] methionine to express radioactive FLAG-Atg16L1 truncations in a cell-free system before mixing with GFP (negative control), CFP-Atg5 (positive control), GFP-WIPI2b or GFP-WIPI1a attached to GFP-Trap beads (Figure 3.12 b and c). Atg16L1 1-265 was co-immunoprecipitated with GFP-WIPI2b and CFP-Atg5, as expected, but not GFP or GFP-WIPI1a, as is seen with full length FLAG-Atg16L1 (Figures 3.1 c and 3.6 b). The same result was seen for Atg16L1 1-242. Atg16L1 1-230 bound GFP and CFP-Atg5 as expected, but I repeatedly saw an increase

in binding of this truncation to GFP-WIPI2b and GFP-WIPI1a when compared to binding seen for Atg16L1 1-265 or 1-242. Truncation of Atg16L1 at amino acid 207 abolished binding to either GFP-WIPI1a or GFP-WIPI2b, but not to CFP-Atg5. These results suggest that the binding site for WIPI2b on Atg16L1 is located between amino acids 207 and 230, and that the truncation at amino acid 230 may reveal some conformation-sensitive binding site that enables an increased binding of Atg16L1 to both WIPI1a and WIPI2b. From these results, it appears that wild-type binding to WIPI2b is conferred by amino acids 207-242.

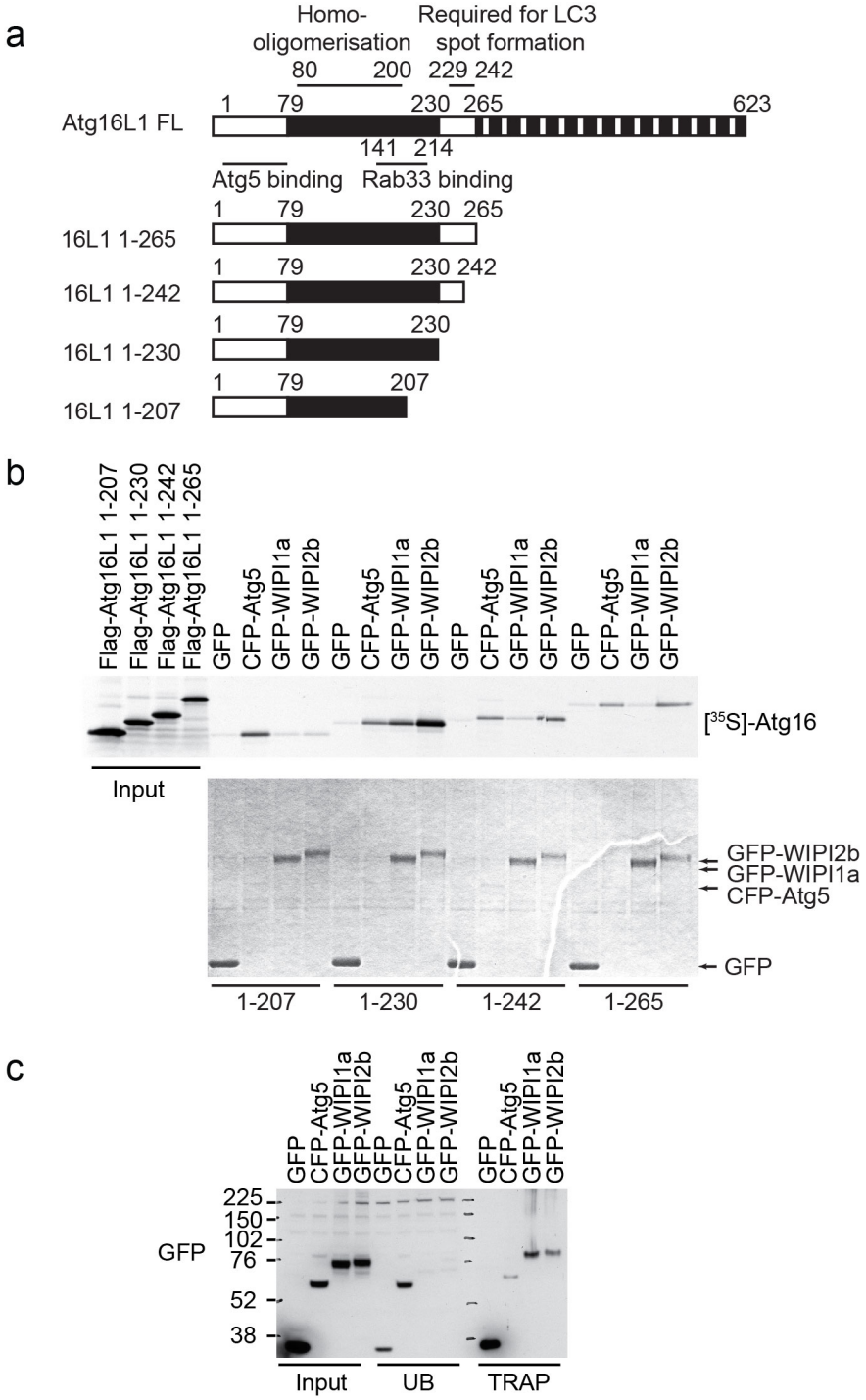

Figure 3.12 WIPI2b binds Atg16L1 between amino acids 207 and 230

(a) Schematic of mouse Atg16L1 constructs used. White N-terminal box represents the Atg5 binding domain. Black box represents the coiled-coil domain of Atg16L1. Stripped box represents the WD-40 domain. Adapted from (Fujita et al., 2008). **(b)** HEK293A cells transiently expressing controls GFP, CFP-Atg5, GFP-WIPI1a or GFP-WIPI2b were used for GFP-Trap, the products of which were mixed with the indicated *in vitro* translated [^{35}S] methionine-labelled FLAG-Atg16L1 before protein complexes were resolved by SDS-PAGE and visualised by autoradiography (upper panel). Lower

panel is colloidal Coomassie-stained gel. **(c)** Western-blot of GFP-Traps used for **(b)**. Molecular weights are in kDa.

3.5.3 WIPI2b does not bind Atg16L2

Amino acids 207-242 encompass the region 229-242, which was identified as being important for Atg16L1 puncta formation following amino acid starvation and which is not conserved in Atg16L2, possibly rendering Atg16L2 unable to bind to the phagophore membrane or a membrane localised protein (Ishibashi et al., 2011). It therefore follows that if WIPI2b is the protein that localises Atg16L1 to the phagophore, Atg16L2 will not bind WIPI2b. GFP-Trap of Flag-Atg16L2 shows that this is the case (Figure 3.13). GFP-WIPI1a binding to Atg16L1 seems to be variable. When over expressed Atg16L1 is used, GFP-Trap of GFP-WIPI1a co-immunoprecipitates Atg16L1 to a greater extent than the GFP control does. However, when only GFP-WIPI1a is overexpressed, GFP-trap of GFP-WIPI1a does not co-immunoprecipitate endogenous Atg16L1 to a greater degree than the GFP control. It may be that the WIPI1a-Atg16L1 interaction is much weaker than that of WIPI2b-Atg16L1, and so the WIPI1a-Atg16L1 interaction is only detected when both proteins are overexpressed.

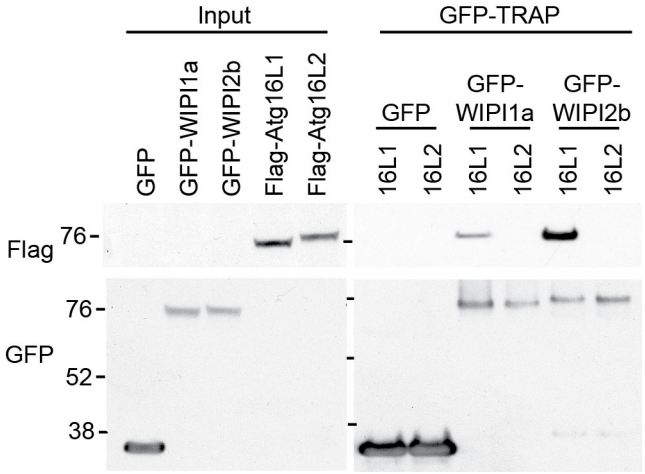

Figure 3.13 GFP-WIPI2b does not bind Atg16L2

Cell lysates from HEK293A cells transiently overexpressing GFP, GFP-WIPI1a or GFP-WIPI2b were mixed with cell lysates from FLAG-Atg16L1 or FLAG-Atg16L2 transiently expressing cells and used for GFP-Trap. Immuoprecipitated protein complexes were visualised using western blot. Molecular weights are in kDa.

3.5.4 Atg16L1 E226 and E230 are required for WIPI2b binding

WIPI2b does not bind Atg16L2 and the binding region for WIPI2b on Atg16L1 is between 207 and 242. Therefore, alignment of Atg16L1 and Atg16L2 in this region may provide some indication of the residues that are important for WIPI2b binding. In collaboration with Dr Michael Wilson at the Babraham Institute, Cambridge, UK, we identified from the alignment of Atg16L1 and Atg16L2 between amino acids 207 and 242 of Atg16L1 that this stretch of Atg16L1 is much more acidic than that of Atg16L2 (Figure 3.14). To determine whether or not these acidic residues in Atg16L1 are important for interaction with WIPI2b, I point mutated each of the non-conserved acid residues to arginine to mimic the charge on Atg16L2 (Figure 3.14). GFP-Trap of GFP-WIPI2b shows that mutation of either Atg16L1 E226 or E230 significantly reduces FLAG-Atg16L1 interaction with GFP-WIPI2b (Figure 3.15 a and b). This result suggests that these sites are critical for WIPI2b binding and explains why FLAG-Atg16L1 1-207 cannot bind WIPI2b, and may also explain why FLAG-Atg16L1 1-230 shows an increased binding to both WIPI1a and WIPI2b. Truncation just after E230 may mean that the WIPI binding site is sterically unhindered, as the Atg16L1 protein C-terminal to this is removed, and so the WIPI binding site may be able to form a complex with either WIPI1a or WIPI2b more readily.

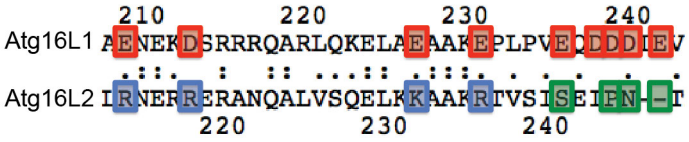

Figure 3.14 Alignment of Atg16L1 and Atg16L2 between amino acids 207 and 265

Alignment between Atg16L1 and Atg16L2 in the WIPI2b binding region of Atg16L1. Non-conserved acidic residues on Atg16L1 are coloured red. Basic residues on Atg16L2 are blue, and non-charged residues are green.

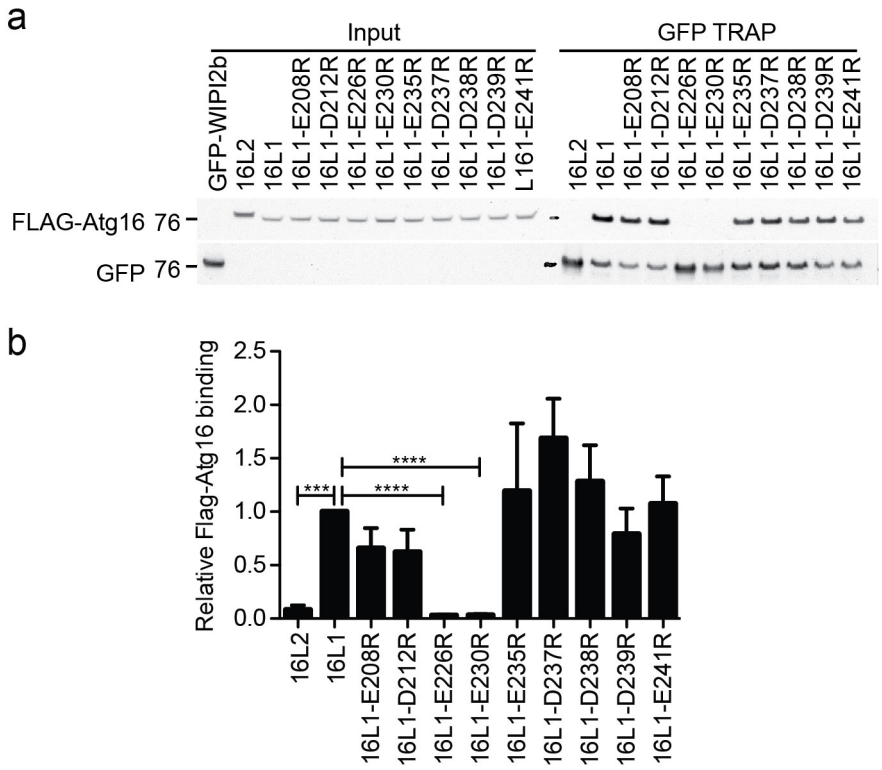

Figure 3.15 WIPI2b binds amino acids E226 and E230 of Atg16L1

(a) Cell lysate from HEK293A cells transiently overexpressing GFP-WIPI2b was mixed with cell lysates from HEK293A cells overexpressing the indicated FLAG-tagged Atg16L1 and Atg16L2 constructs before being used for GFP-Trap. Protein complexes were visualised by western blot. Molecular weights are in kDa. **(b)** Statistical analysis of **(a)**. The SEM for four independent experiments is shown. Statistical analysis was performed by Student's t test. ***, $p \leq 0.001$, ****, $p \leq 0.0001$.

3.5.5 Atg16L1 D237, D238, D239 and E241 are required for FIP200 binding

At this stage of characterising the Atg16L1-WIPI2b interaction, two separate studies showing that FIP200 binds Atg16L1 and that this interaction is required for Atg12–5-16L1 complex recruitment to the forming autophagosome were published (Nishimura et al., 2013, Gammoh et al., 2013). These papers demonstrated that the FIP200 binding domain (FBD) is between amino acids 230 and 300 of Atg16L1 (Nishimura et al., 2013) or amino acids 229 and 242 (Gammoh et al., 2013). From these data, the minimal region required for FIP200 binding can be assumed to be 230-242. This region includes amino acid E230 of Atg16L1 that is required for WIPI2b binding (Figure 3.15). FIP200 binds Atg16L1 directly (Nishimura et al., 2013, Gammoh et al., 2013) and so the overlap of the WIPI2b and FIP200 binding sites on Atg16L1 raises the possibility that

FIP200 mediates the interaction between WIPI2b and Atg16L1, or that FIP200 and WIPI2b binding sites are mutually exclusive. To establish if the binding sites of WIPI2b and FIP200 overlap, I investigated the effect of the Atg16L1 point mutants (Figure 3.14) on FIP200 binding (Figure 3.16 a and b). I found that mutation of Atg16L1 D237, D238, D239 or D241 to arginine significantly reduced the binding of endogenous FIP200 to FLAG-Atg16L1, and that E235R reproducibly reduced binding although this effect was not significant. Results shown in Figures 3.15 and 3.16 demonstrate that WIPI2b and FIP200 have independent binding sites. The charge change mutations that affect WIPI2b binding have no significant effect on FIP200 binding, and vice versa. Note, FIP200 did not bind FLAG-Atg16L2 as expected from previous work (Gammoh et al., 2013).

Following this fine mapping of the FIP200 interaction site, a third paper was published detailing the Atg16L1-FIP200 interaction (Fujita et al., 2013). This paper mapped the interaction using alanine scanning in sets of five amino acids in a yeast two-hybrid experiment, therefore mapping the interaction site more finely than previous papers to between Atg16L1 239-246. In light of results from this paper, I extended the region over which I mutated acidic residues that are not conserved on Atg16L2. I used FLAG-tagged Atg16L1 E246R and Atg16L1 D249R to determine whether endogenous FIP200 can bind these charge changed mutants (Figure 3.17). I found that FIP200 co-immunoprecipitation with FLAG-Atg16L1 mutants was recovered to near wild type levels for E246R and D249R when compared to D235 and D237. This is similar to published results, although I did not find that mutants at Atg16L1 E246 or D249 had an effect, which I was expecting in light of previous work (Fujita et al., 2013). The reason for this difference could be either because of the difference between yeast two hybrid and co-immunoprecipitation using over expressed Atg16L1 or because of the difference in mutations: previous work by Fujita *et al.* used five adjacent alanine mutations, whereas I used single charge changed mutations.

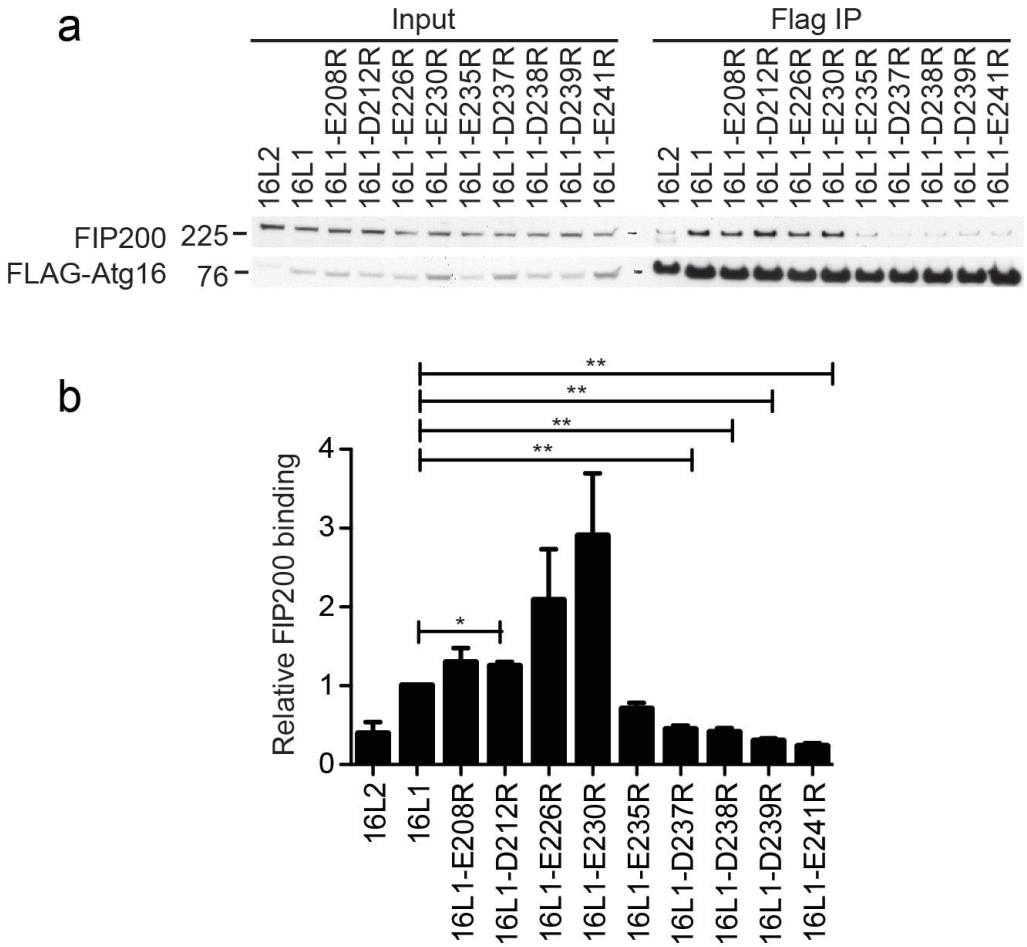

Figure 3.16 FIP200 binds amino acids D237, D238, D239 and E241 of Atg16L1

(a) Cell lysates from HEK293A cells overexpressing the indicated FLAG-tagged Atg16L1 and Atg16L2 constructs were used for FLAG immunoprecipitation with FLAG M2 agarose beads. Protein complexes were visualised by western blot. **(b)** Statistical analysis of **(a)**. The SEM for three independent experiments is shown. Statistical analysis was performed by Student's t test. *, $p \leq 0.05$. **, $p \leq 0.01$. Molecular weight is shown in kDa.

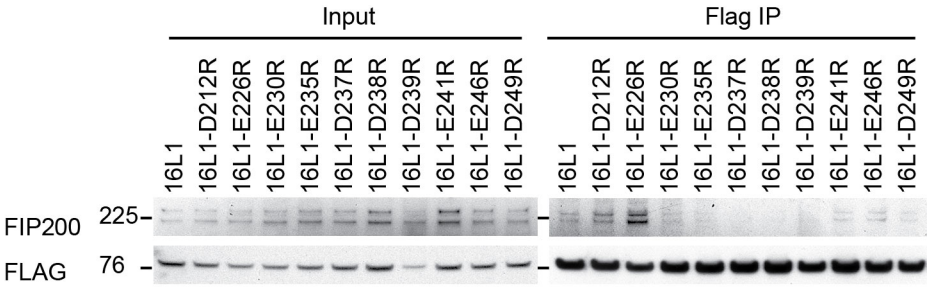

Figure 3.17 Atg16L1 E246R and D249R do not affect FIP200 binding

HEK293A cells transiently overexpressing the indicated FLAG-Atg16L1 constructs were used for FLAG immunoprecipitation using FLAG M2 agarose beads. Protein complexes were visualised using western blot. Molecular weight is shown in kDa.

3.5.6 WIPI2b and FIP200 bind separate sites on and bind independently to Atg16L1

Fine mapping of the WIPI2b and FIP200 binding sites on Atg16L1 show that the acidic residues required for the interactions do not overlap. However, the footprint of the proteins at the binding sites may be larger than the size of the sites suggested by the fine mapping experiments. This leads to the possibility that there may be some form of regulation of Atg16L1 binding between WIPI2b and FIP200, which result in cooperative or mutually exclusive binding.

In order to determine if there is cooperation or mutual exclusion between WIPI2b and FIP200 binding to Atg16L1, I used double charge change point mutants of Atg16L1. Results in Chapters 3.5.4 and 3.5.5 strongly suggest that there is no requirement for WIPI2b binding to allow FIP200 binding to Atg16L1, or vice versa, as mutations that significantly reduced either WIPI2b or FIP200 binding had no significant effect on Atg16L1 interaction. However, to make sure that the point mutants used completely abolish binding to Atg16L1, I used double charge change point mutants: FLAG-Atg16L1 E226R E230R (ERER) to disrupt WIPI2b binding and FLAG-Atg16L1 D237R D239R (DRDR) to disrupt FIP200 binding, before looking for co-immunoprecipitation of FIP200 and WIPI2b respectively (Figure 3.18). Abolition of WIPI2b binding had no effect on FIP200 binding, and vice versa in this system. Interestingly, endogenous FIP200 was co-immunoprecipitated through FLAG-Atg16L1 WT when using GFP-Trap for GFP-WIPI2b immunoprecipitation, showing that a trimeric complex of FIP200-Atg16L1-WIPI2b can be formed when both Atg16L1 and WIPI2b overexpressed. Endogenous co-immunoprecipitation of Atg16L1 with WIPI2 from FIP200 knockout MEFs shows that WIPI2 and Atg16L1 interact in the absence of FIP200 (Figure 3.19 a). There was a general trend, seen in all three experiments, for a greater amount of Atg16L1 to be co-immunoprecipitated with WIPI2 from FIP200 KO MEFs compared the to co-immunoprecipitation seen from the FIP200 wild type MEFs. However, this trend was not significant (Figure 3.19 b). Together, these result show that FIP200 binding to Atg16L1 is not required for WIPI2b to bind Atg16L1, and vice versa, and that WIPI2b and FIP200 are able to bind Atg16L1 at the same time.

The binding sites on Atg16L1, as mapped by charge change point mutations (Figures 3. 15 and 3.16) place the WIPI2b and FIP200 binding sites on either side of a

four amino acid stretch that includes two prolines (Figure 3.14). Modelling of the region 207- 265 of Atg16L1 by Michael Wilson predicts that the WIPI2b and FIP200 binding sites lie on either side of this proline-induced loop that separates the sites (Figure 3.20). It is possible that the separation of the sites by this loop would allow for both proteins to bind either independently or together.

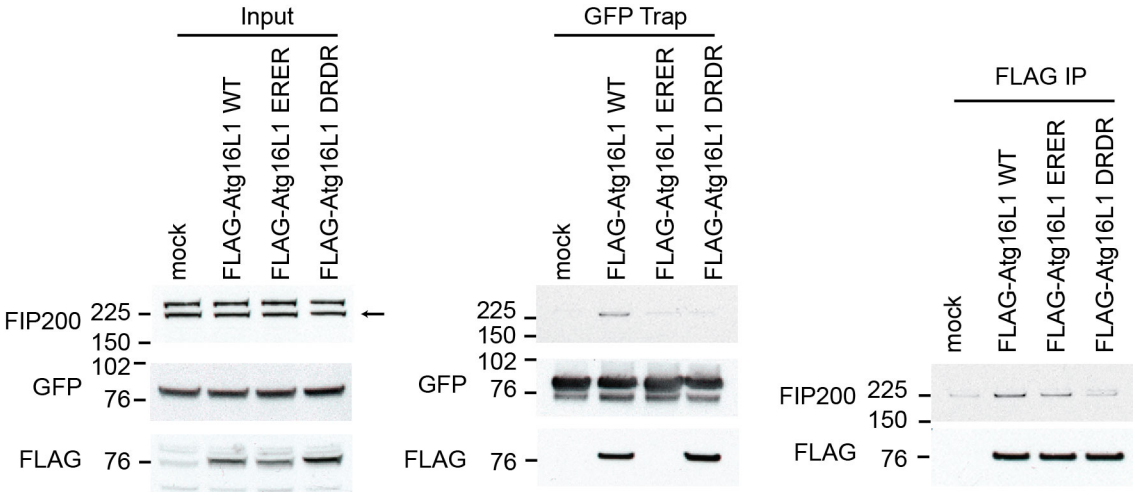

Figure 3.18 Atg16L1 mutants unable to bind WIPI2b can bind FIP200, and vice versa

HEK293A cells stably expressing GFP-WIPI2b were transiently transfected with mock transfection, Atg16L1 WT, E226R E230R (ERER), or D237R D239R (DRDR) were used for GFP-Trap or FLAG-immunoprecipitation using FLAG M2 agarose beads. Protein complexes were visualised by western blot using the indicated antibodies. Molecular weights are in kDa.

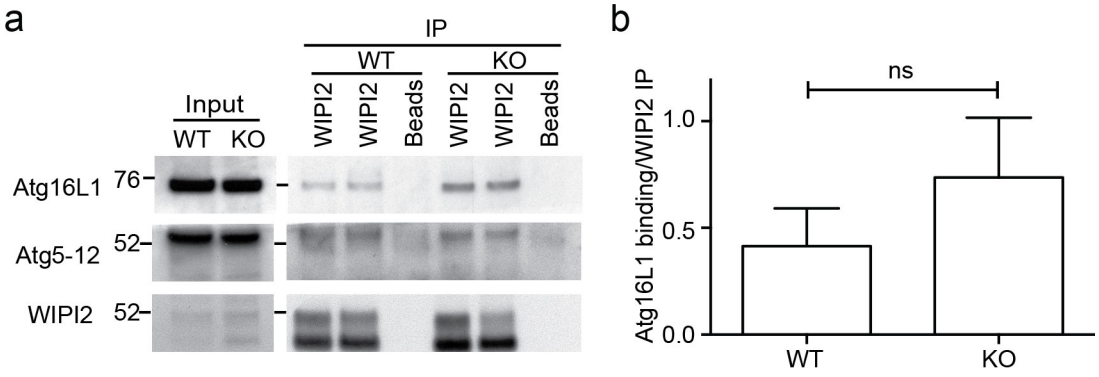

Figure 3.19 Atg16L1-WIPI2 co-immunoprecipitation in FIP200 KO MEFs

(a) FIP200 wild type (WT) and knock out (KO) MEF cells were treated with 0.5 mM DSP crosslinker for 30 minutes before cell lysis and immunoprecipitation with anti-WIPI2 antibodies and protein complex analysis by western blot. **(b)** Statistical analysis of **(a)**. The SEM for three independent experiments is shown. Results were analysed by Student's t-test, ns, not significant. Molecular weights are in kDa.

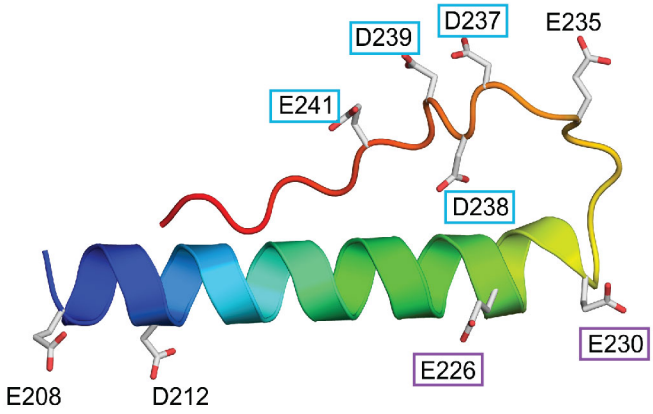

Figure 3.20 Structural model of Atg16L1 207-265

Structural model of the region of Atg16L1 (207-246) that interacts with WIPI2b and FIP200. Residues required for FIP200 or WIPI2b binding are labelled in blue and purple, respectively. Modelling and figure provided by Michael Wilson.

3.6 Mapping the Atg16L1 binding site on WIPI2b

3.6.1 WIPI2b binds Atg16L1 through its WD-40 domain

The mammalian WIPI proteins, along with their yeast homologues, are members of the PROPPIN (β-propellers that bind polyphosphoinositides) family. These proteins contain WD-40 domains, which form β-propellers. WD-40 domains are one of the most abundant protein motifs in the eukaryotic genome and are involved in protein-protein or protein-DNA interactions (Xu and Min, 2011). In light of this, it is highly probable that WIPI2b binds Atg16L1 through a region on its β-propeller, rather than through its C-terminal extension. Hannah Poslon previously showed that deletion of the C-terminus of WIPI2b did not disrupt Atg16L1 binding (data not shown). To confirm this, I used a C-terminal deletion of GFP-WIPI2b (WIPI2b ΔCT) to test for an effect on Atg16L1 binding. I used GFP and GFP-WIPI2b as negative and positive controls respectively, and at the same time tested for Atg16L1 binding by GFP-tagged WIPI2a, WIPI1a, and WIPI1a ΔCT (Figure 3.21). GFP-WIPI2b bound as expected. GFP-WIPI2b ΔCT retained the ability to bind Atg16L1, demonstrating that the interaction is not mediated by the C-terminus. Surprisingly, the interaction with Atg16L1 was significantly

increased by deletion of the C-terminus of WIPI2b and similarly, deletion of the C-terminus of WIPI1a conferred Atg16L1 binding ability to a significantly higher degree than full length GFP-WIPI1a. The C-termini of WIPI1 and WIPI2 are relatively different when compared to the WD-40 domain of the proteins (Figure 1.9) and this, along with differences within their β-propellers, may be a possible explanation for the different binding partners of WIPI1 and WIPI2.

The WIPI2-Atg16L1 interaction is not affected by starvation (Figures 3.1 and 3.6) and Hannah Polson previously showed that WIPI2 with a mutated PtdIns(3)P binding domain (FTTG) also had an unaltered Atg16L1 binding ability (data not shown). I also found that GFP-WIPI2b FTTG showed no significant difference in Atg16L1 binding (Figure 3.22 a and b). These results suggest that the binding site for Atg16L1 is not altered by WIPI2 binding PtdIns(3)P. GFP-WIPI2a or GFP-WIPI1a did not co-immunoprecipitate endogenous Atg16L1 (Figure 3.21 and 3.22). WIPI2a is identical to WIPI2b except for an 18 amino acid insertion between sheets β1 and β2 of the first blade of the 7-bladed β-propeller (Figure 1.8). This insertion renders WIPI2a both unable to bind Atg16L1 (Figure 3.21 a and 3.22) and unable to form puncta upon autophagy initiation (Dooley et al., 2014, Mauthe et al., 2011). Because WIPI2b can bind Atg16L1 during fed conditions, a condition in which WIPI2b does not make puncta, it is unlikely that it is the inability of WIPI2a to form spots that makes this protein unable to interact with Atg16L1, and therefore it is possible that the insertion in WIPI2a is directly obstructing the Atg16L1 binding site on WIPI2.

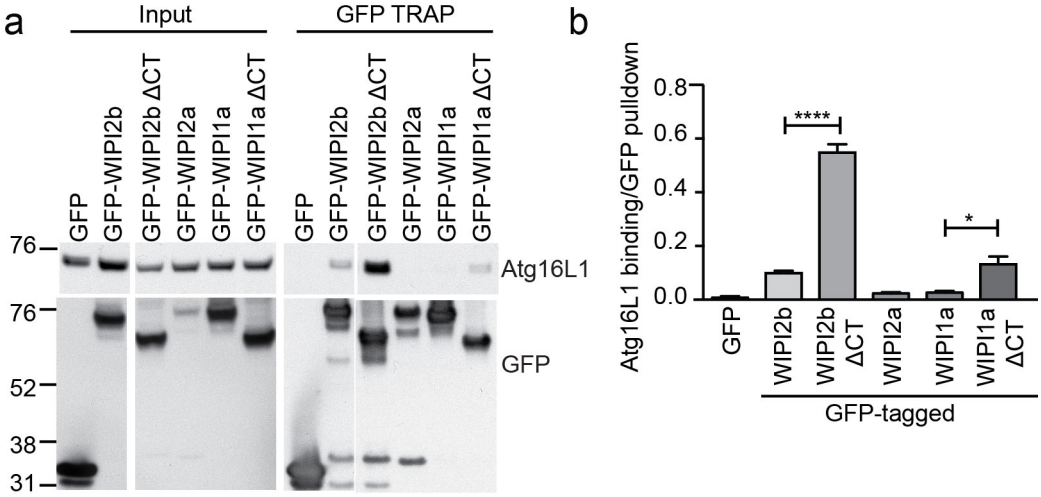

Figure 3.21 WIPI C-terminal deletion increases Atg16L1 binding

(a) HEK293A cells were transiently transfected with the indicated GFP-tagged constructs before cell lysis and GFP-Trap. Protein complexes were visualised using western blot. **(b)** Statistical analysis of **(a)**. SEM from two independent experiments, statistical analysis was performed by one-way ANOVA with Tukey post-test. *, $p \leq 0.05$. ****, $p \leq 0.0001$. Molecular weight is in kDa.

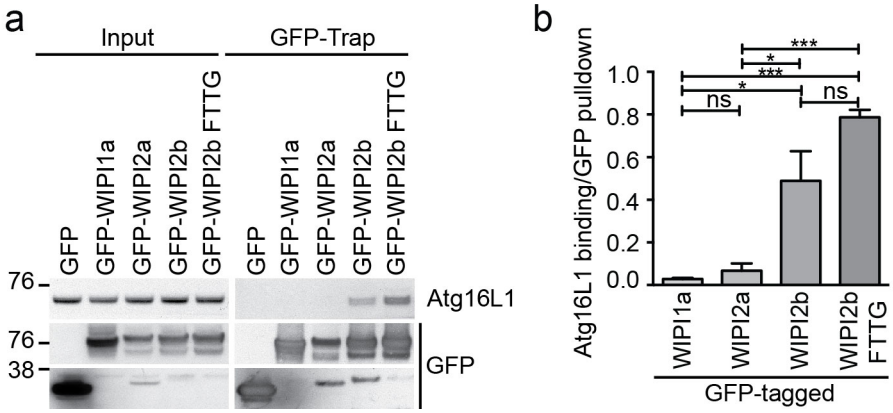

Figure 3.22 WIPI2b FTTG binds Atg16L1

(a) HEK293A cells were transiently transfected with the indicated GFP-tagged constructs before cell lysis and GFP-Trap. Protein complexes were visualised using western blot. **(b)** Statistical analysis of **(a)**. SEM from three independent experiments, statistical analysis was performed by one-way ANOVA with Tukey post-test. *, $p \leq 0.05$. ***, $p \leq 0.001$. Molecular weight is in kDa.

3.6.2 WIPI2b binds Atg16L1 through a basically charged cleft

The crystal structure of Hsv2, a *K. lactis* yeast PROPPIN protein in the same family as Atg18, has been published by three independent groups (Krick et al., 2012, Baskaran et

al., 2012, Watanabe et al., 2012). These papers showed that the PROPPIN proteins form seven-bladed β-propellers with an open-Velcro topology and two PtdIns(3)P binding sites formed from the non-canonical PtdIns(3)P binding motif, FRRG. Michael Wilson used a crystal structure of Hsv2 to build a model of WIPI2b (Figure 3.23). He found that there is a basically charged, solute-exposed cleft between blades 1 and 2 of the β-propeller. This cleft is proximal to the site at which WIPI2a has an 18 amino acid insertion (between β-sheets 1 and 2 of the first blade of the propeller, coloured yellow in Figure 3.23) and so may be obscured in WIPI2a. In addition, this cleft is positioned opposite the PtdIns(3)P binding motif and hydrophobic membrane insertion loop, meaning that the cleft is suitably positioned for binding Atg16L1 when WIPI2 is bound to the membrane. This region of Atg18 is known to bind Atg2 (Watanabe et al., 2012). Michael proposed that this cleft would be ideal for binding the acidic stretch of Atg16L1 on which the WIPI2b binding site is located and he identified two solute-exposed arginines (R108 and R125) within this cleft. I cloned point mutants of GFP-WIPI2b, changing the arginine residues to glutamic acid, and making both single and double point charge-change mutants. I overexpressed these point mutants and used GFP-Trap to test for binding to *in vitro* translated and endogenous Atg16L1 (Figure 3.24). I found that mutation of either of the residues disrupted Atg16L1 binding and that mutation of both residues abolished binding to both *in vitro* translated Atg16L1 and the endogenous Atg12–5-16L1 complex (Figure 3.24 a and b). These results suggest that the Atg16L1-WIPI2b interaction is mediated between an acidic stretch on Atg16L1 and a basically charged cleft on WIPI2b.

Arginines 108 and 125 in WIPI2b are partially conserved in WIPI1a, with a lysine at the position equivalent to 125 (Figure 1.9). I used site directed mutagenesis to produce a R125K point mutant of GFP-WIPI2b to test for any change in Atg16L1 binding. I found that the arginine to lysine mutation had no effect on Atg16L1 binding (Figure 3.24 a and b) and so this cannot explain the difference between WIPI1a and WIPI2b in Atg16L1 binding ability.

In order to test whether the 18 amino acid insert in WIPI2a in blade 1 is positioned so that the Atg16L1 binding site on WIPI2 is obscured in this isoform, I used site directed mutagenesis to try to dislodge the loop. The insertion contains a number of acidic residues and also a number of hydrophobic residues, any of which may mediate

binding to the basically charged cleft between blades 2 and 3. I used site directed mutagenesis to produce GFP-WIPI2a point mutants E26K and R21E L35E to try and introduce a repulsion between the residues in the loop and the basically charged cleft. Neither of these mutations had any affect on Atg16L1 binding (Figure 3.24 a and b) and so I can not confirm whether or not the loop is positioned over the Atg16L1-binding cleft between blades 1 and 2 of WIPI2.

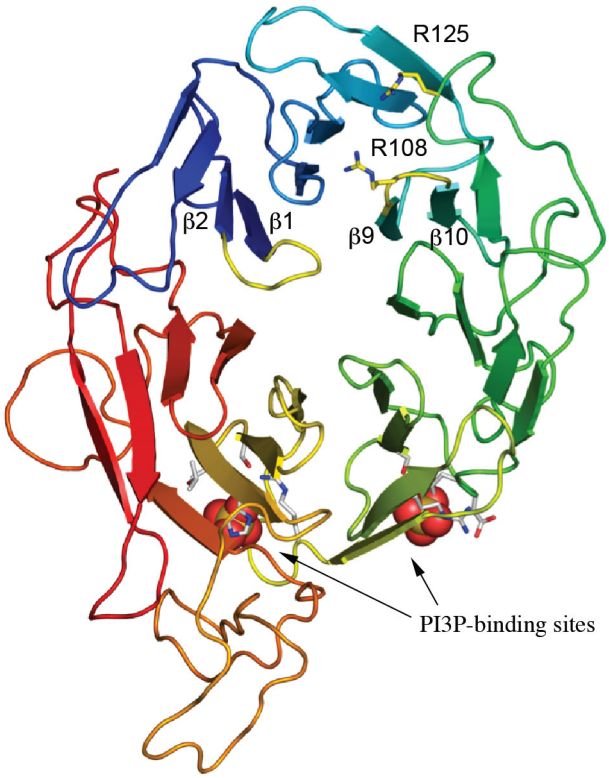

Figure 3.23 Model of WIPI2b

Model for human WIPI2b (14-377) based on the X-ray structure of *Kluyvelomyces marxianus* Hsv2 homologue ((Watanabe et al., 2012);3vu4.pdb) made with the iterative threading assembly refinement (I-TAASER;(Roy et al., 2010)). The cartoon is coloured from the N-terminus with blue to red gradient. The β1-β2 and β9-β10 loops are coloured yellow, R108 and R125 are shown as sticks. Residues that bind PtdIns(3)P and sulfates bound in 3vu4.pdb are shown as sticks and sphere representations, respectively. Modelling done and figure provided by Michael Wilson.

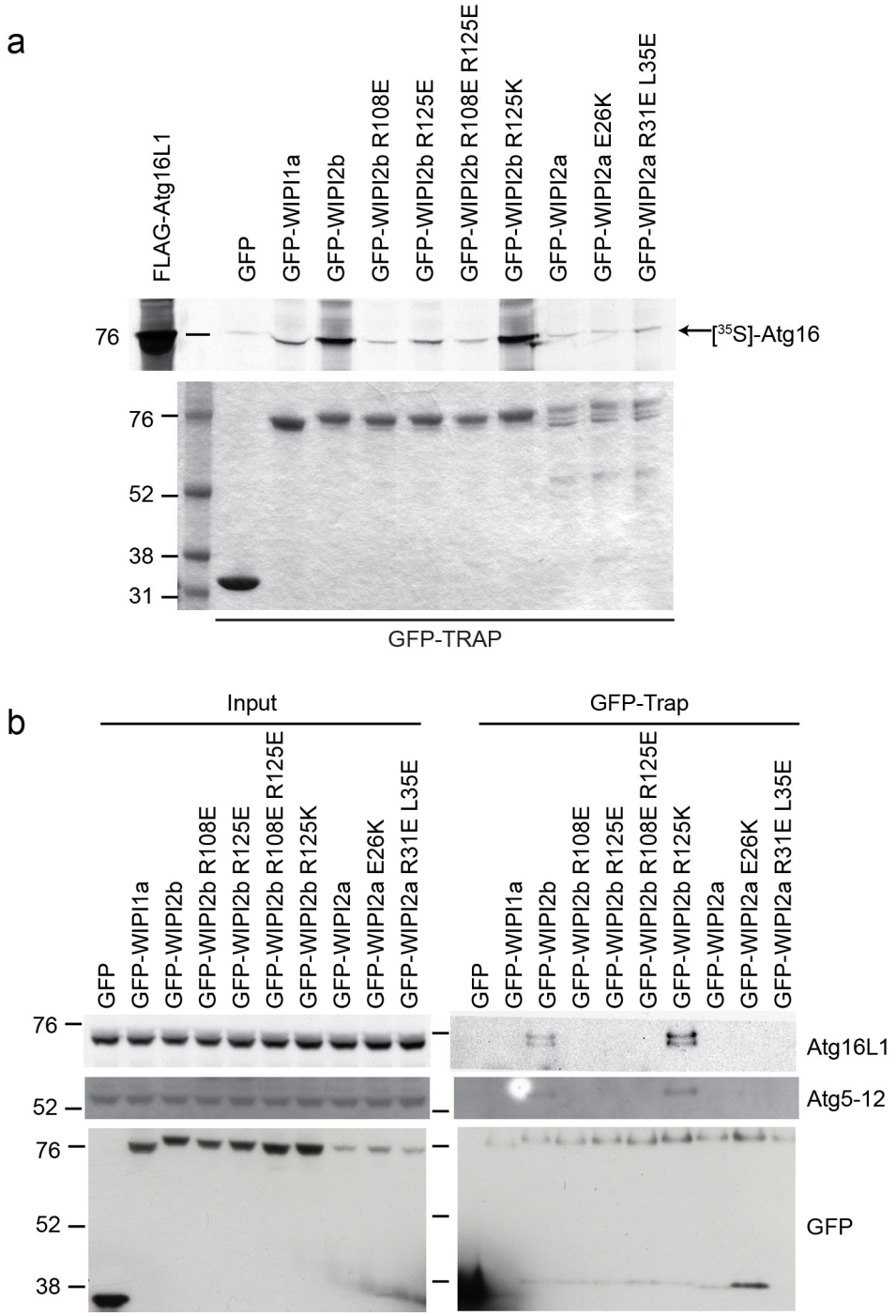

Figure 3.24 Mutation of WIPI2b R108E or R125E reduces Atg16L1 binding

HEK293A cells were transiently transfected with the indicated GFP constructs. **(a)** Transfected cell lysates were used for GFP-Trap before being mixed with *in vitro* translated [^{35}S] methionine-labelled FLAG-Atg16L1. The resulting protein complexes were visualised using autoradiography. **(b)** GFP-Traps products from cells transfected as for **(a)** were probed for endogenous Atg16L1 and Atg5–12 as indicated.

3.7 Atg16L1 and WIPI2b bind directly

In order to determine whether the interaction between the acidic stretch on Atg16L1 and the basic cleft on WIPI2b is direct, I performed a charge change experiment using the WIPI2b and Atg16L1 point mutants. If the interactions between any of the residues that have been implicated in the WIPI2b-Atg16L1 interaction are direct, I expected to see the charge change mutants of these sites co-immunoprecipitate. I used cell lysates from cells overexpressing GFP-WIPI2b WT, R108E, R125E and R108E R125E, and FLAG-Atg16L1 WT, E226R, E130R and E226R E230R and mixed the cell lysates in all possible permutations before performing a GFP-Trap assay (Figure 3.25 a and b). The WIPI2b-Atg16L1 interaction is significantly restored when the GFP-WIPI2b R108E mutant is mixed with FLAG-Atg16L1 E230R when compared to the interaction between GFP-WIPI2b R108E and FLAG-Atg16L1 WT (Figure 3.25b and c). This result strongly suggests that residues arginine-108 on WIPI2b and glutamic acid-230 on Atg16L1 are directly interacting. A proposed model of the WIPI2b-Atg16L1 interaction was constructed by Michael Wilson based on these results is shown in Figure 3.26.

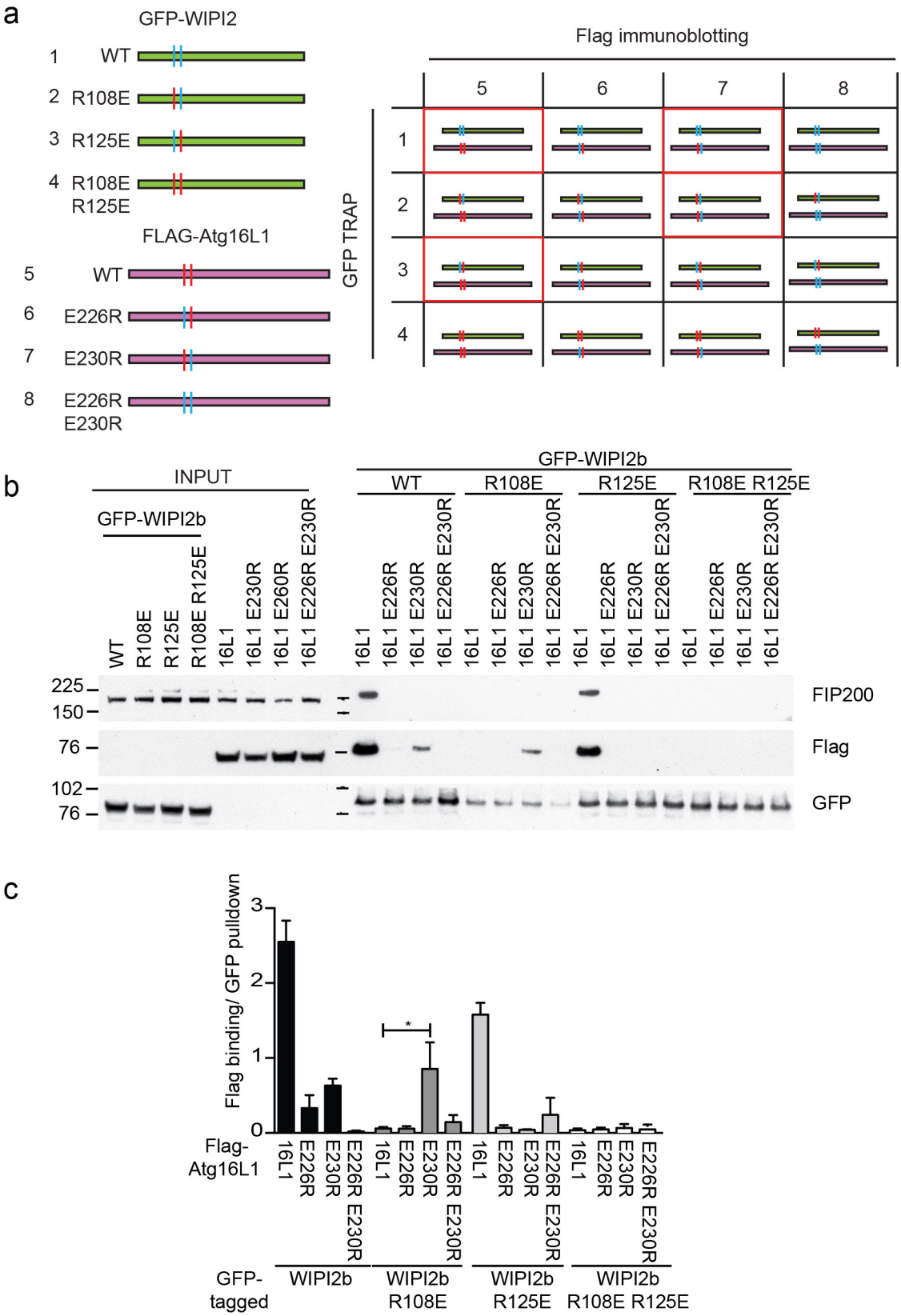

Figure 3.25 WIPI2b and Atg16L1 bind directly through WIPI2b R108 and Atg16 E230

Cell lysates from HEK293A cells transiently transfected with GFP-WIPI2b WT, R108E, R125E and R108E R125E were mixed in all possible permutations with FLAG-

Atg16L1 WT, E226R, E230R and E226R E230R before GFP-Trap of resulting protein complexes. **(a**) Schematic showing permutations of cell lysate mixes. Red boxes indicate combinations which resulted in co-immunoprecipitation of indicated GFP-WIPI2b and FLAG-Atg16L1 proteins. **(b)** Western blot analysis of protein complexes with indicated antibodies. **(c)** Statistical analysis of **(b)**. The SEM for three independent experiments is shown. Statistical analysis was performed by one-way ANOVA with Tukey post-test. *, $p \leq 0.05$. Molecular weight markers are shown in kDa.

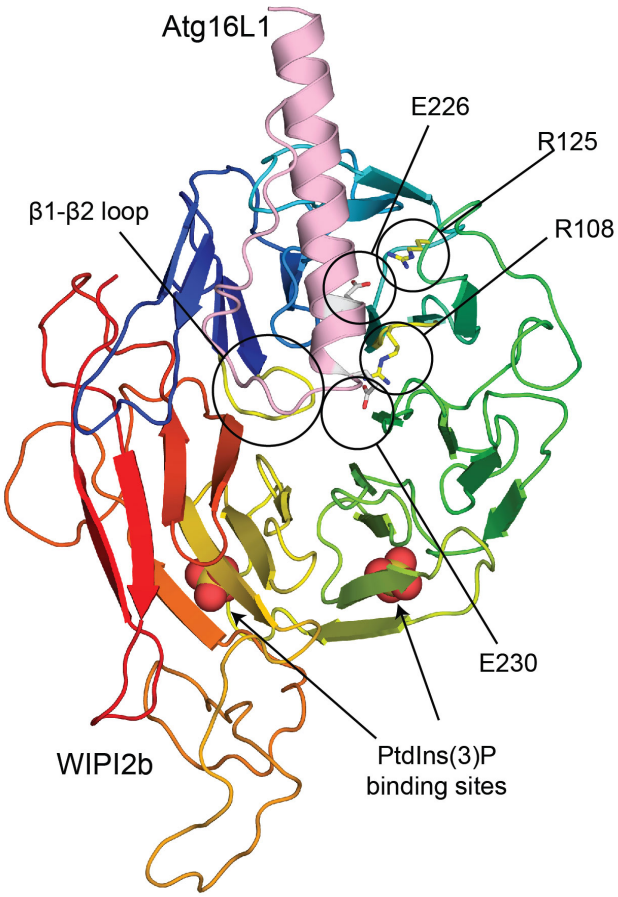

Figure 3.26 Model of Atg16L1 docked to WIPI2b

Model of Atg16L1 (207-265) (pink) docked onto WIPI2b (14-377) (rainbow). WIPI2b was modelled using 3vu4.pdb (Watanabe et al., 2012) and Atg16L1 was modelled *ab initio* using I-TASSER (Roy et al., 2010). Both models were initially docked using ZDOCK for rigid-body protein-protein docking (Pierce et al., 2011), constrained by requiring E226 and E230 of Atg16L1, R108 and R125 of WIPI2b to be in the binding site. The top scoring docked model was then refined using RosettaDock (Lyskov and Gray, 2008) for local docking optimization. In the docking model shown, E230 interacts with R108. Modelling done and figure provided from Michael Wilson.

3.8 Discussion

In this chapter I have shown that WIPI2b and Atg16L1 bind directly, and have identified some of the residues required for this interaction.

WIPI1a and WIPI2a cannot bind Atg16L1 to the same extent as WIPI2b. The 18 amino acid insertion in WIPI2a is likely to be somehow disrupting Atg16L1 binding. The amino acids required for binding Atg16L1 in WIPI2b (R108 and R125) are well conserved in WIPI1a and, unlike for WIPI2a, there are no amino acid insertions that are likely to be blocking the interaction. Therefore, the difference in binding ability can not be explained by poor conservation of residues so far identified as important for Atg16L1 binding and so must be due to some other feature of WIPI1a. I have seen that the C-terminus of WIPI1a is somehow disrupting Atg16L1 binding. The C-terminus of WIPI2b contains a potential phosphorylation site (Hsu et al., 2011), and therefore may provide a mechanism of regulating the Atg16L1 interaction. This is investigated further in Chapter 5.

The region of Atg16L1 that binds WIPI2 is adjacent to the FIP200 binding region on Atg16L1. The close proximity of the two binding sites suggests that there may be some form of cross talk or regulation in the binding of FIP200 and WIPI2b. However, I have not seen any evidence of this – mutants of Atg16L1 unable to bind WIPI2b can still bind FIP200 and vice versa. Also, when using overexpressed proteins, a trimeric complex of WIPI2b-Atg16L1-FIP200 can exist. Investigation into any cross talk or regulation would require further work. It appears that in order to bind WIPI2b, Atg16L1 must be a homodimer. Figure 3.11d shows that human Atg16L1 ΔCCD, which lacks amino acids 69-213, cannot bind WIPI2b. This construct is unable to form homodimers (Fukuda and Itoh, 2008) but does contain residues E226 and E230, which are required for WIPI2b binding. In contrast, FIP200 is able to bind to Atg16L1 mutants that do not form homodimers (Nishimura et al., 2013). It is possible that the Atg16L1 interaction with WIPI2b is weaker than that with FIP200 and the interaction stabilised when a dimer of Atg16L1 binds to two WIPI2b proteins. If this is true, then it would be interesting to investigate whether the inability of WIPI2b to bind monomeric Atg16L1 provides any function or regulation during autophagy.

FIP200 has been shown to be responsible for recruiting the Atg16L1 complex to forming autophagosomes (Nishimura et al., 2013, Gammoh et al., 2013). Interestingly, the Atg16L1 constructs lacking FIP200 binding ability used for rescue of autophagy in Atg16L1$^{\Delta/\Delta}$ MEFs in these papers lacked Atg16L1 amino acid 230 and so will have disrupted WIPI2b binding. Therefore, lack of autophagy rescue seen when using these mutants in these experiments could be, at least partially, attributable to loss of WIPI2b interaction. Intriguingly, in the study by Nishimura *et al.*, an Atg16L1 1-230 construct was used to rescue autophagy in Atg16L1$^{\Delta/\Delta}$ MEFs. The authors found that although unable to bind FIP200, this construct was able to rescue LC3 lipidation, p62 degradation, LC3 and Atg16L1 spot formation and GFP-LC3 lysosomal degradation to the same extent as full length Atg16L1 (Nishimura et al., 2013). If WIPI2b is capable of recruiting the Atg12–5-16L1 complex to the phagophore, then these results can be explained in terms of the Atg16L1-WIPI2b interaction.

Chapter 4. WIPI2b recruits the Atg12–5-16L1 complex to the phagophore

4.1 Introduction and aim

4.1.1 Introduction

The recruitment of the Atg12–5-16L1 complex is dependent on production of PtdIns(3)P at the forming autophagosome (Itakura and Mizushima, 2010). However, there is currently no explanation for this observation; there has been no observed PtdIns(3)P-binding ability of the Atg12–5-16L1 complex and there is no known phagophore-localised PtdIns(3)P binding protein that binds the complex. As described in Chapter 3, I have shown that WIPI2b binds Atg16L1. Our working model is that WIPI2b recruits the Atg12–5-16L1 complex in a PtdIns(3)P-dependent manner to the site of LC3 lipidation. Previous work on WIPI2b by Hannah Polson has shown that WIPI2 acts as an early autophagy protein, required for and functioning upstream of LC3 lipidation (Polson et al., 2010). Hannah's previous findings are consistent with WIPI2 acting to recruit the Atg12–5-16L1 complex during starvation-induced autophagy. This function has been ascribed to FIP200 (Nishimura et al., 2013, Gammoh et al., 2013) and also to FIP200- and ubiquitin-Atg16L1 acting in a redundant manner in recruiting the Atg12–5-16L1 complex (Fujita et al., 2013). As described in Chapter 3.8, previous studies do not exclude the possibility that WIPI2 may be functioning in this role either in parallel with or instead of FIP200.

The recruitment of LC3 to the growing autophagosome is dependent on Atg12–5-16L1 in both canonical and bacterial autophagy (Itakura and Mizushima, 2010, Fujita et al., 2013). However, the mechanism of Atg12–5-16L1 complex recruitment to the membrane appears to be more complex during xenophagy than starvation-induced autophagy (Fujita et al., 2013). Atg16L1 recruitment to *Salmonella* and latex beads involves FIP200 and ubiquitin binding by Atg16L1, and there may be additional recruitment mechanisms (Fujita et al., 2013). It is possible that the WD repeat on the C-terminus of Atg16L1, absent in yeast, may have evolved to provide additional recruitment mechanisms of Atg16L1 to allow for more complex autophagy in mammalian cells (Fujita et al., 2013). The requirement for WIPI2b during xenophagy

has not been studied and the requirement for PtdIns(3)P in this process is an area under debate (Huang et al., 2011, Kageyama et al., 2011).

4.1.2 Aim

Following from mapping the Atg16L1-WIPI2b interaction, my aim was to determine the function of this interaction. I investigated this by using point mutants of WIPI2b unable to bind Atg16L1 and Atg16L1 mutants unable to bind FIP200 or WIPI2b. Ectopic localisation of WIPI2b to the plasma membrane was used to investigate whether WIPI2b is able to recruit Atg16L1 to a membrane and xenophagy was used to determine how well conserved the requirement for WIPI2b is in other forms of autophagy.

4.2 WIPI2 functions upstream of Atg16L1 and LC3 lipidation

4.2.1 WIPI2 knockdown decreases LC3 lipidation and LC3 spot formation during starvation

WIPI2 acts in early autophagy and is required for LC3 lipidation and puncta formation in starvation-induced autophagy, as shown by using WIPI2 siRNA knockdown(Polson et al., 2010). Hannah used WIPI2 siRNA #9 from Dharmacon, and noted on several occassions that ULK1 was depleted in WIPI2 knockdown cells (unpublished data and personal comunication). I used WIPI2 knockdown with the Dharmacon #9 and #12 siRNAs to deplete WIPI2 protein and look at ULK1 levels. As Hannah had previously seen, I saw that Dharmacon #12 depleted WIPI2 less efficiently than #9 and did not reduce ULK1 levels, but that #9 very effectively reduced WIPI2 levels and also caused ULK1 depletion (Figure 4.1a). In order to establish whether was is an off-target result, I used an siRNA from Qiagen (#3) to determine whether ULK1 depletion is also seen using siRNA with a different target sequence. I found that this siRNA efficiently depeleted WIPI2, but also caused a slight decrease in ULK1 levels (Figure 4.1b). From this I concluded that ULK1 decrease upon WIPI2 knockdown is unlikely to be an off-target effect and instead may be a real effect of WIPI2 depletion. As I was concentrating

on characterising the funciton of the Atg16L1-WIPI2 interaction, I did not pursue the reasons behind this decrease in ULK1 levels, which may be transcriptional or due to destabilisation of ULK1 upon WIPI2 depletion as seen with Atg16L1 depletion (Nishimura et al., 2013).

I generally saw a better WIPI2 knockdown using the Qiagen siRNA, and so I used this for subsequent experiments. As Hannah had performed previous knockdown experiments using the Dharmacon duplex, I ensured that I could reproduce her results using the Qiagen siRNA. I found that WIPI2 knockdown led to a reproducible decrease in starvtion-induced LC3 lipidation (Figure 4.2a and b) and a significant decrease in starvation-induced LC3 puncta formation (Figure 4.3a and b) as expected.

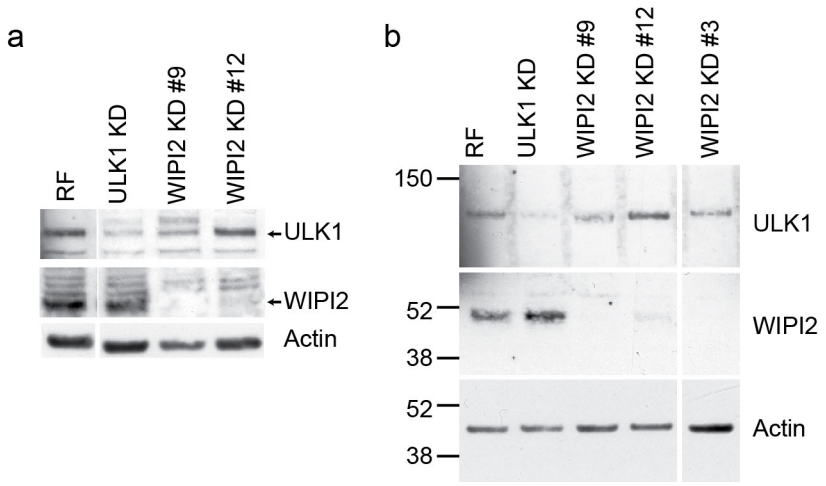

Figure 4.1 ULK1 depletion in cells depleted of WIPI2

(a and **b)** HEK293A cells were treated with the indicated siRNA for 72 hours before cell lysis and western blot analysis. Molecular weight markers are in kDa.

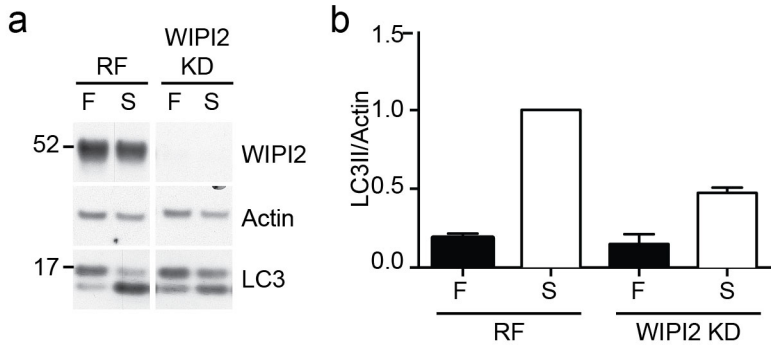

Figure 4.2 WIPI2 knockdown reduces starvation induced LC3 lipidation

(a) HEK293A cells treated with RISC-free (RF) or WIPI2 siRNA for 72 hours were treated with full medium (F) or starvation medium (S) for two hours before western blot analysis. Molecular weights are in kDa. **(b)** Statistical analysis of **(a)**. The SEM for four independent experiments is shown. The difference between RISC-free starved and WIPI2 knockdown starved is not significant in this set of experiments, but is reproducible.

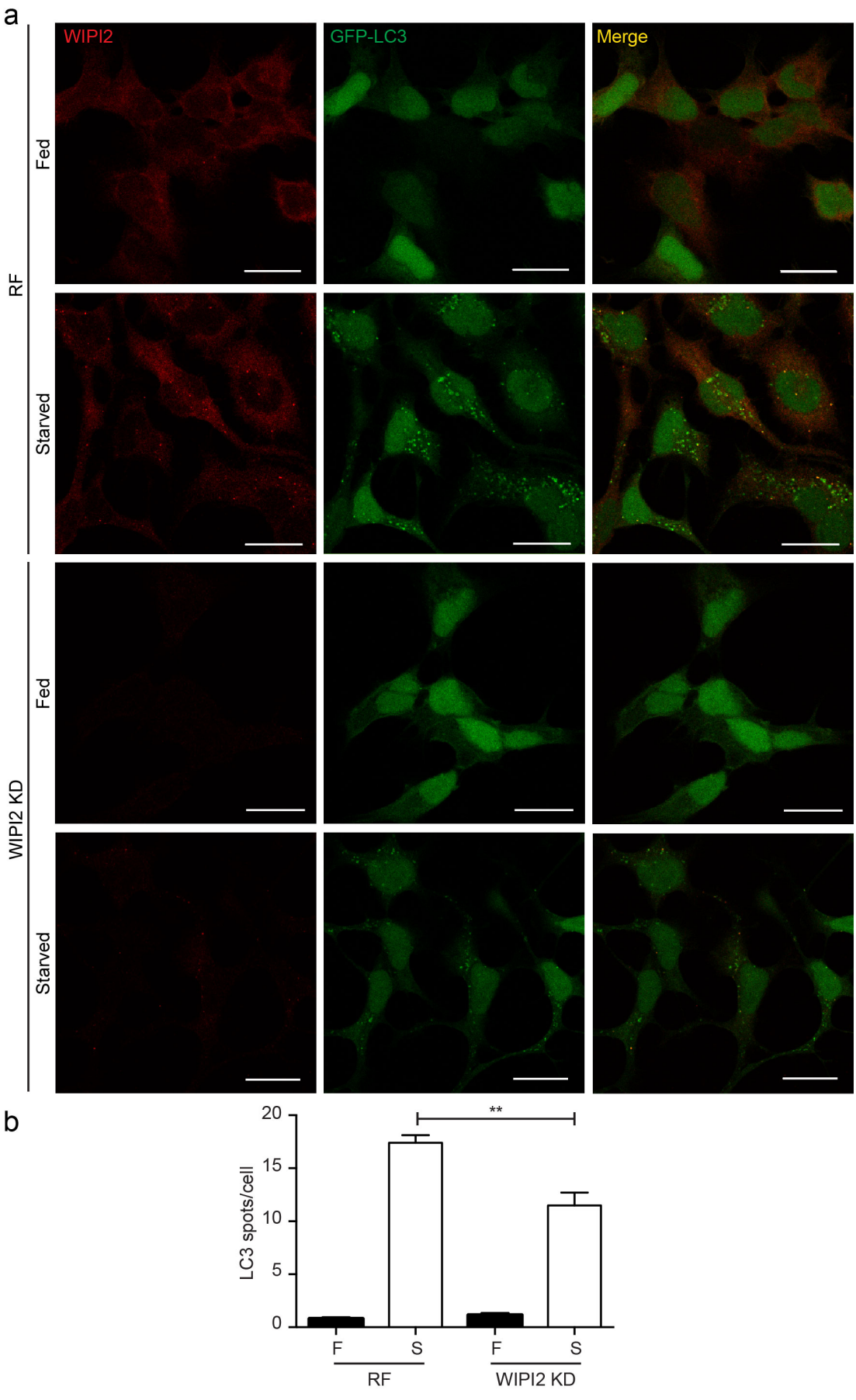
a
WIPI2
GFP-LC3
Merge
RF
Fed
Starved
WIPI2 KD
Fed
Starved
b
LC3 spots/cell
20
15
10
5
0
**
F
S
F
S
RF
WIPI2 KD

Figure 4.3 WIPI2 knockdown reduces starvation-induced GFP-LC3 puncta

(a) 2GL9 cells treated with RISC-free (RF) control or WIPI2 siRNA for 72 hours were treated with full medium (Fed) or starvation medium (Starved) for two hours before fixing and staining for confocal analysis. Scale bars are 20 μm. **(b)** Statistical analysis of the number of LC3 spots from **(a)**. The SEM for three independent experiments is shown. Statistical analysis was performed using student's t-test. **, $p \leq 0.01$.

4.2.2 Atg16L1$^{\Delta/\Delta}$ MEFs form WIPI2 puncta in fed and starved conditions

If WIPI2 acts to recruit the Atg12–5-16L1 complex through binding Atg16L1, then WIPI2 would function upstream of Atg16L1. To test this, I looked for WIPI2 puncta formation in Atg16L1$^{\Delta/\Delta}$ MEFs. Atg16L1$^{\Delta/\Delta}$ MEFs are non-functional in autophagy: they do not produce LC3-II, Atg12–5 or LC3 puncta, and p62 and long-lived protein degradation is severely impaired (Saitoh et al., 2008). Atg16L1$^{\Delta/\Delta}$ MEFs are not complete knockout cells, but contain Atg16L1 with a deleted coiled coil domain (amino acids 69-213) (Saitoh et al., 2008). This Atg16L1$^{\Delta/\Delta}$ protein is non functional for autophagy, stalling autophagosome formation before LC3 lipidation. If WIPI2 acts upstream of Atg16L1 then WIPI2 puncta would be formed in these MEFs, both in fed and starved conditions, on PtdIns(3)P positive stalled omegasome as seen with HA-WIPI1a and GFP-DFCP1 in Atg5 KO MEFs (Itakura and Mizushima, 2010). I found that WIPI2 puncta were formed in Atg16L1$^{\Delta/\Delta}$ MEFs in both fed and starved condition (Figure 4.4 a and b). This result and previous work on WIPI2 (Polson et al., 2010) shows that WIPI2 functions downstream of PtdIns(3)P formation and upstream of Atg16L1, therefore supporting the model of PtdIns(3)P-dependent WIPI2b recruitment of the Atg12–5-16L1 complex. The number of WIPI2 starvation-induced puncta in Atg16L1$^{\Delta/\Delta}$ MEFs is significantly fewer than in WT MEFs. I have not investigated the reason for this, but it may be due to the decrease in the protein levels of the ULK1 kinase complex in Atg16L1$^{\Delta/\Delta}$ MEFs (Nishimura et al., 2013).

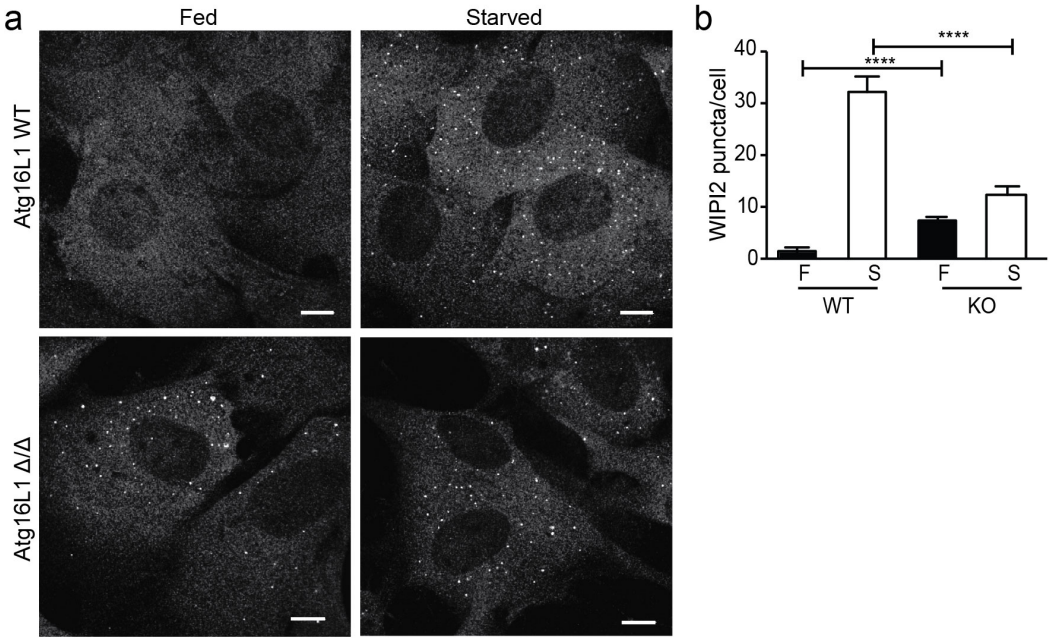

Figure 4.4 Atg16L1$^{\Delta/\Delta}$ MEFs form WIPI2 puncta

(a) Atg16L1 WT and $^{\Delta/\Delta}$ MEFs were treated with full medium (Fed) or starvation medium (Starved) for two hours before being fix, stained for WIPI2 and visualised by confocal microscopy. Scale bars are 10 μm. **(b)** Statistical analysis of **(a)**. The SEM for three independent experiments is shown. Statistical analysis performed using unpaired student's t-test. ****, $p \leq 0.0001$.

4.3 Atg16L1 binding by WIPI2b is required for WIPI2b function in autophagy

I used WIPI2b rescue experiments in order to determine whether WIPI2b interaction with Atg16L1 is required for WIPI2 function in autophagy. HEK293A cells were treated with either RISC-free or WIPI2 siRNA before expression of either GFP as a negative control, or siRNA resistant GFP-WIPI2b or GFP-WIPI2b R108E R125E (RERE) (Atg16L1 binding mutant) before analysing starvation-induced autophagy in these cells by LC3 shift assay. I was surprised to find that LC3 lipidation was significantly inhibited in WIPI2 siRNA treated cells which were transiently expressing GFP-WIPI2b RERE (Figure 4.5a and b). Although not significant, there was a general trend in GFP-WIPI2b overexpressing cells towards an increase in LC3 lipidation in both RISC-free and WIPI2 siRNA treated cells, suggesting that WIPI2 overexpression may be able to drive autophagy to some extent.

I postulated that WIPI2b-RERE may have an inhibitory effect in WIPI2 depleted cells because overexpressed GFP-WIPI2b RERE may be able to successfully out-compete residual endogenous WIPI2 for PtdIns(3)P binding and therefore blocking Atg12–5-16L1 recruitment and subsequent LC3 lipidation. To test this, I expressed a PtdIns(3)P binding mutant of WIPI2b that was unable to bind Atg16L1 (GFP-WIPI2b FTTG RERE). If GFP-WIPI2b RERE inhibits autophagy by blocking PtdIns(3)P sites on the forming autophagosome then a PtdIns(3)P binding mutant of this protein should have no inhibitory effect on autophagy. Consistently, I found that GFP-WIPI2b FTTG RERE had no inhibitory effect on autophagy as measured by LC3 lipidation or p62 degradation (Figure 4.6a, b and c), whereas GFP-WIPI2b RERE did. The effects of GFP-WIPI2b RERE overexpression on autophagy inhibition were most apparent when looking at p62 degradation. p62 is an autophagy-specific substrate (Bjorkoy et al., 2005) and a cargo adaptor in the degradation of ubiquitinated proteins and organelles (Kim et al., 2008). In cells overexpressing the Atg16L1 binding mutant, p62 was significantly increased compared to expressing GFP alone (significance not indicated on graph) or other GFP-WIPI2b constructs (Figure 4.6c). However, expression of the Atg16L1 binding mutant which could not bind PtdIns(3)P (GFP-WIPI2b FTTG RERE) did not significantly accumulate p62. These results were supported by LC3 spot formation assays carried out by Minoo Razi. HEK293A cells transiently overexpressing GFP-WIPI2b RERE after WIPI2 depletion showed significantly fewer endogenous LC3 spots compared to GFP-WIPI2 WT and FTTG RERE cells (Figure 4.6d and e).

GFP-WIPI2b formed starvation-induced puncta as expected. These puncta were not formed in cells expressing WIPI2b unable to bind PtdIns(3)P: either GFP-WIPI2b FTTG or GFP-WIPI2b FTTG RERE (Figure 4.6 d and f). GFP-WIPI2b RERE formed large, LC3-negative ring shaped structures (Figure 4.6e and 4.7) and Minoo found that they colocalised with myc-DFCP1 and p62. Although the degradation of p62 requires interaction with LC3 through the LIR of p62 (Pankiv et al., 2007), p62 localisation to the site of autophagosome formation does not require p62 binding to LC3 and instead requires p62 self-oligomerisation through its PB1 domain (Itakura and Mizushima, 2011). Therefore, the GFP-WIPI2 RERE structures are likely to be omegasomes. This is supported by correlative light and electron microscopy (CLEM) samples of GFP-WIPI2b samples analysed by Minoo (Dooley et al., 2014).

These experiments show that WIPI2b that is unable to bind Atg16L1 blocks autophagosome maturation and LC3 lipidation in WIPI2 depleted cells. Furthermore, this inhibition is dependent on the ability of WIPI2b RERE to localise to omegasomes through PtdIns(3)P binding. Together these data demonstrate that WIPI2b must be able to bind both PtdIns(3)P and Atg16L1 in order to function in autophagy. Additionally, GFP-WIPI2b RERE can form puncta, showing that Atg16L1-WIPI2b binding is not required for PtdIns(3)P-dependent WIPI2b recruitment to the forming autophagosome. This can also be concluded by WIPI2 puncta formation in $Atg16^{\Delta/\Delta}$ MEFs (Figure 4.4). In conjunction with results showing that the GFP-WIPI2 FTTG mutant interaction with Atg16L1 is unaltered compared to wild type GFP-WIPI2b (Figure 3.22), it seems likely that the interactions of WIPI2 with PtdIns(3)P and Atg16L1 operate independently. However, this raises the question of why WIPI2a can neither bind PtdIns(3)P nor make starvation-induced puncta? The 18 amino acid insertion between β-sheets 1 and 2 in the first blade of the WD-40 domain of WIPI2a is the only feature that distinguishes it from puncta-forming and Atg16L1-binding WIPI2b. The localisation of the 18 amino acid insert adjacent to the Atg16L1 binding domain and opposite the PtdIns(3)P binding sites suggests that the insertion affects Atg16L1, but not PtdIns(3)P-binding. However, perhaps this insert destabilises the protein or protein folding. Consistent with this, GFP-WIPI2a does not express as well as GFP-WIPI2b even though they have the same vector backbone.

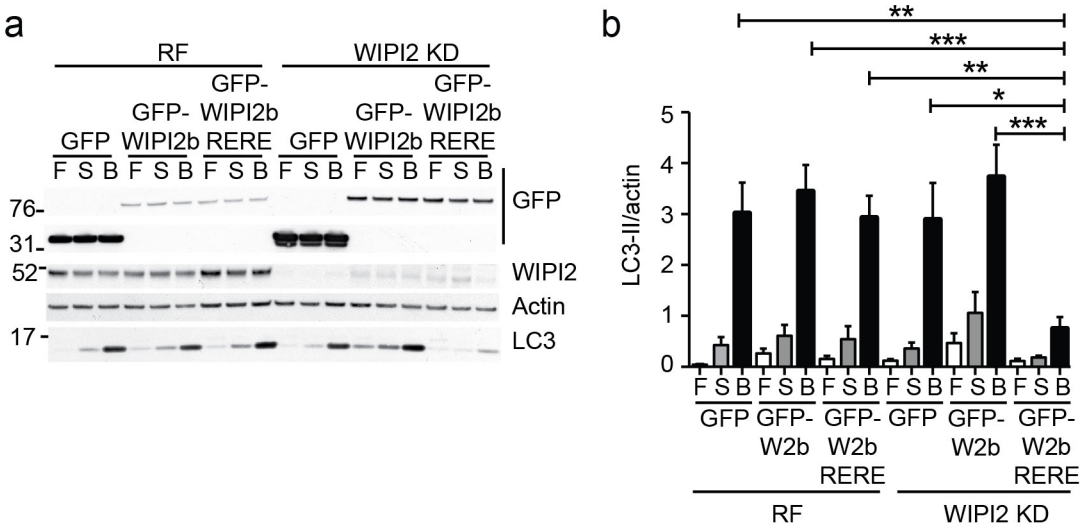

Figure 4.5 GFP-WIPI2b RERE inhibits LC3 lipidation in WIPI2 knockdown cells

HEK293A cells were treated with either RISC-free (RF) or WIPI2 siRNA for 72 hours and transiently transfected with the indicated GFP-tagged constructs for 48 hours before being treated with full medium (F), starvation medium (S) or starvation medium and Bafilomycin A (B) for two hours. **(a)** Cells were lysed and LC3 lipidation was analysed by western blot. Molecular weight markers are in kDa. **(b)** Statistical analysis of **(a)**. SEM for three independent experiments is shown. Statistical analysis performed by one-way ANOVA with Tukey post-test. *, $p \leq 0.05$; **, $p \leq 0.01$; ***, $p \leq 0.001$.

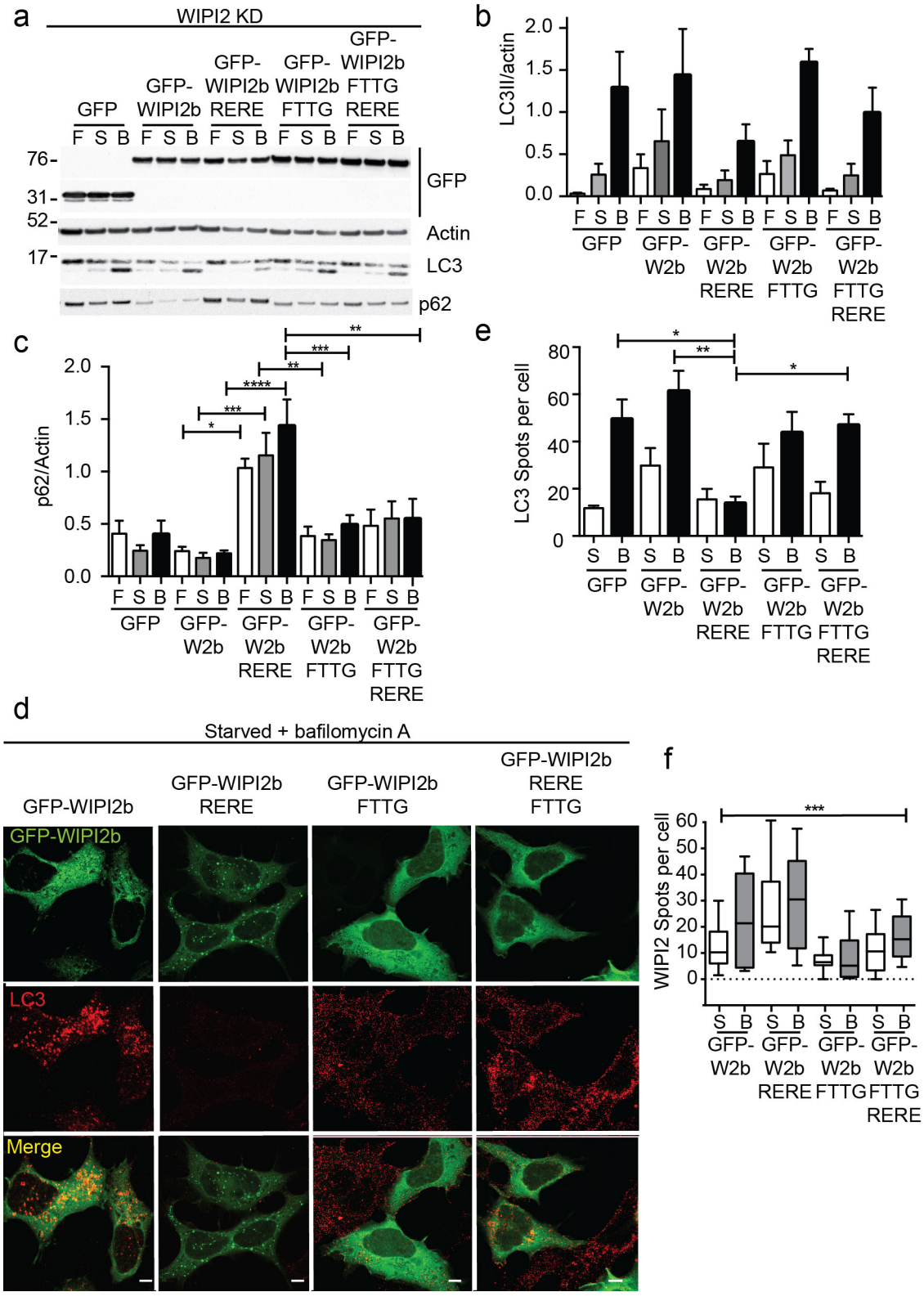

Figure 4.6 WIPI2 unable to bind Atg16L1 and PtdIns(3)P does not act as a dominant negative inhibitor of autophagy

(a) HEK293A cells were treated with WIPI2 siRNA for 72 hours and the indicated siRNA resistant contracts were overexpressed for 48 hours before the cells were treated with full medium (F), starvation medium (S) or starvation medium with Bafilomycin A (B) for two hours. Cells were lysed and analysed for LC3 lipidation and p62 degradation by western blot. Molecular weight markers are in kDa. **(b)** Statistical analysis of LC3 lipidation from **(a)**. The SEM for two independent experiments is shown. **(c)** Statistical analysis of p62 degradation from **(a)**. The SEM for four independent experiments is shown. Statistical analysis was performed by one-way ANOVA with Tukey post-test. **(d)** Cells were siRNA treated and transfected as for **(a)** before being treated with starvation medium or starvation medium with Bafilomycin A for two hours. Cells were fixed and analysed by confocal microscopy. Starvation plus Bafilomycin A is shown. Scale bars are 10 μm. **(e)** Statistical analysis of LC3 puncta formation from **(d)**. The SEM for three independent experiments is shown. Statistical analysis was performed by one-way ANOVA with Dunn's post-test. **(f)** Statistical analysis of GFP-WIPI2b puncta formation from **(d)**. The SEM from 10 cells per condition is shown. Statistical analysis was performed by one-way ANOVA. ***, $p \leq 0.001$. Experiments in **(d)**, **(e)** and **(f)** were performed by Minoo Razi. *, $p \leq 0.05$; **, $p \leq 0.01$; ***, $p \leq 0.001$; ****, $p \leq 0.0001$.

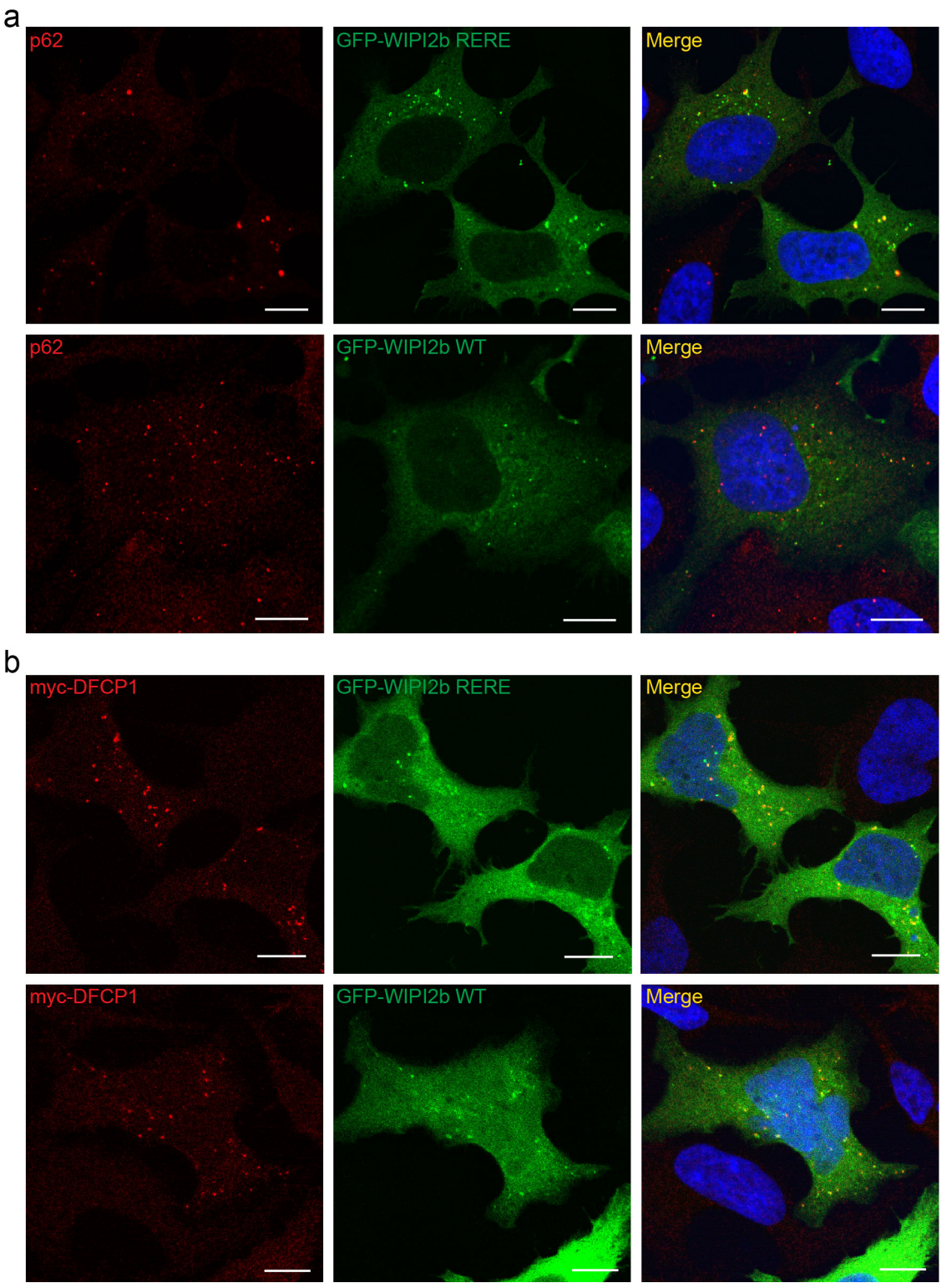

Figure 4.7 GFP-WIPI2 RERE colocalises with p62 and DFCP1

(a) HEK293A cells were treated with WIPI2 siRNA for 72 hours and the indicated siRNA resistant constructs were overexpressed for 48 hours. The cells were starved for two hours followed by fixation and staining with antibodies against endogenous p62 for confocal microscopy analysis. **(b)** Cells treated with siRNA and GFP-constructs as in **(a)** were co-transfected with myc-DFPC1 for 48 hours before fixation and staining with

an antibody against myc for confocal microscopy analysis. Scale bars are 10 μm. Experiment performed by Minoo Razi.

4.4 WIPI2b localisation to a membrane is sufficient to drive LC3 lipidation

4.4.1 WIPI2b-CAAX localises to the plasma membrane

Data in Chapter 4.3 show that the Atg16L1-WIPI2b interaction is required for autophagy. This supports my hypothesis that WIPI2b is the PtdIns(3)P effector that recruits the Atg12–5-16L1 complex. However, my results so far do not directly demonstrate the ability of WIPI2 to recruit the Atg12–5-16L1 complex. In order to determine whether or not WIPI2b can specify the site of Atg12–5-16L1 recruitment, I used WIPI2b-CAAX constructs to ectopically localise WIPI2b to the plasma membrane. The plasma membrane contains phosphatidylethanolamine and ectopic localisation of Atg16L1 to the plasma membrane via a CAAX motif has been used to demonstrate the ability of Atg16L1 to recruit the Atg12–5 conjugate and drive LC3 lipidation (Fujita et al., 2008). If WIPI2b localisation to a membrane is sufficient to recruit the Atg12–5-16L1 complex (through binding to Atg16L1) to that membrane, then WIPI2b ectopic localisation to the plasma membrane will result in Atg12–5-16L1 recruitment to the plasma membrane and subsequently lead to Atg3-LC3 recruitment and LC3 lipidation (Figure 4.8a). As CAAX localisation to the plasma membrane is independent of the usual autophagy stimuli (mTORC1 inactivation and PtdIns(3) kinase activation), LC3 lipidation should be increased in cells overexpressing WIPI2b-CAAX constructs independently of these signalling inputs.

kRAS is targeted to the plasma membrane by its C-terminus, which contains two signals: the CAAX motif (where C is cysteine, A is any aliphatic amino acid, and X is any amino acid) and a polybasic stretch of amino acids (Wright and Philips, 2006). The C-terminal CAAX motif undergoes a series of posttranslational modifications that result in the C-terminus of the protein becoming hydrophobic and suitable for interaction with the membrane (Figure 4.8b). I cloned the kRAS CAAX sequence (Fujita et al., 2008) onto the C-terminus of WIPI2b (Figure 4.8b) for this series of experiments. The WIPI2b constructs that I cloned are all FTTG mutants to ensure that they are not able to function

in canonical autophagy. mCherry-WIPI2b-CAAX localises to the plasma membrane as expected (Figure 4.9).

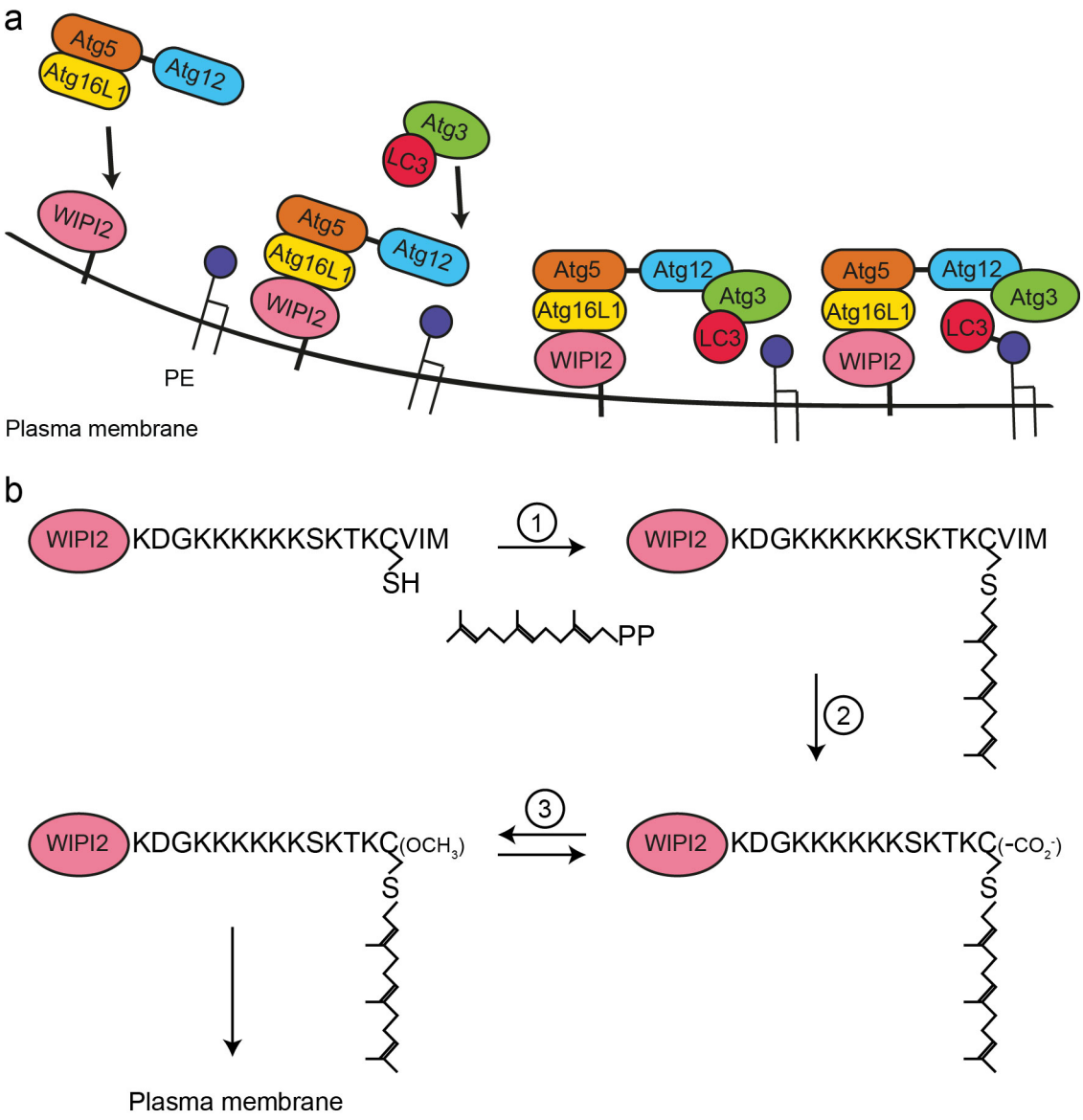

Figure 4.8 WIPI2b targeting to the plasma membrane

(a) Schematic of expected sequential recruitment of autophagy proteins to the plasma membrane after WIPI2b plasma membrane localisation. **(b)** Schematic of WIPI2b-CAAX posttranslational modification. Adapted from (Wright and Philips, 2006). Step 1: addition of a 15 carbon farnesyl isoprenoid catalysed by FTase (farnesyltransferase). Step 2: cleavage of the three amino acids C-terminal to the cysteine by Rce1 (Ras-converting enzyme 1). Step 3: Methyl esterification of the carboxyl group of cysteine, catalysed by Icmt (isoprenylcysteine carboxyl methyltransferase).

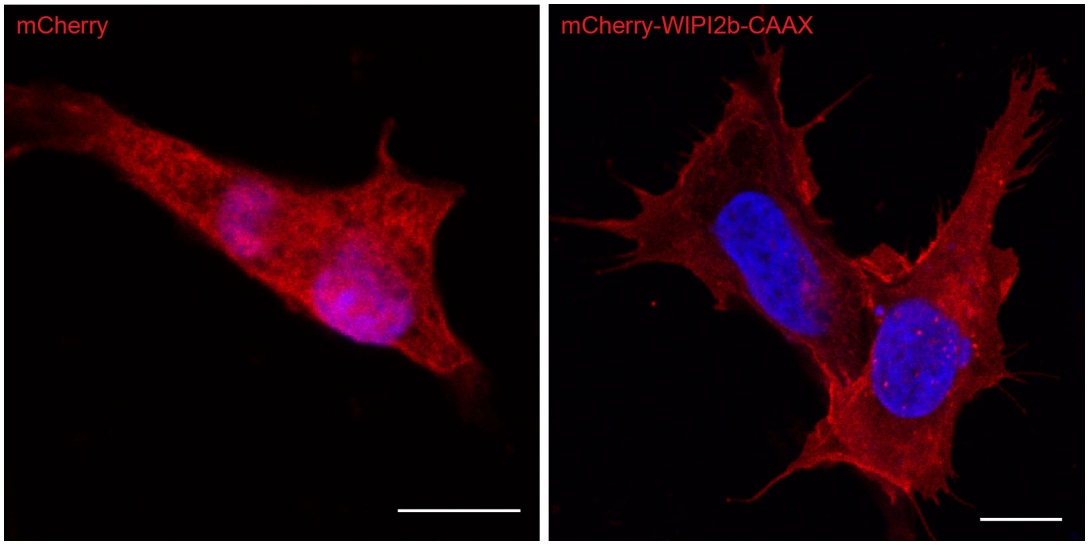

Figure 4.9 mCherry-WIPI2b-CAAX localises to the plasma membrane

HEK293A cells (2GL9) were transiently transfected with mCherry or mCherry-WIPI2b-CAAX 48 hours before fixation for confocal microscopy analysis. Hoechst was used to stain nuclei. Scale bars are 10 μm.

4.4.2 WIPI2b-CAAX drives LC3 lipidation and LC3 plasma membrane-localisation dependent on Atg16L1 binding, but independently of mTORC1 inactivation or PtdIns(3)P production

In order to test whether plasma membrane-localised WIPI2b can lead to Atg12–5-16L1 complex recruitment and subsequent LC3 lipidation, I assayed LC3 lipidation in cells transiently overexpressing mCherry-WIPI2b-CAAX constructs. If WIPI2b directly recruits the Atg12–5-16L1 complex, then an increase in LC3 lipidation should be seen in all conditions, including during fed conditions (active mTORC1) and wortmannin treatment (inactive Vps34 PtdIns(3) kinase complex). mCherry-WIPI2b-CAAX expression resulted in a significant increase in LC3 lipidation in both fed and wortmannin treated cells (Figure 4.10a and b) when compared to cells expressing mCherry-WIPI2b with no C-terminal CAAX motif. This increase in LC3 lipidation was lost by using mCherry-WIPI2b-RERE-CAAX mutants unable to bind Atg16L1 (Figure 4.10a, b and c). All mCherry-WIPI2b-CAAX constructs used were plasma membrane localised and the overexpression of mCherry-WIPI2b-CAAX, but not mCherry-WIPI2b-RERE-CAAX, resulted in plasma membrane-localised LC3 (Figure 4.11, experiment performed by Minoo Razi). Together, these result demonstrate that plasma

membrane-localised WIPI2b can recruit LC3 and the LC3 conjugation machinery (the Atg12–5-16L1 complex and Atg3–LC3 conjugate) through binding Atg16L1. Once WIPI2b is membrane localised, the recruitment of Atg16L1 by WIPI2b is independent of upstream signals including mTORC1 inactivation and PtdIns(3)P binding.

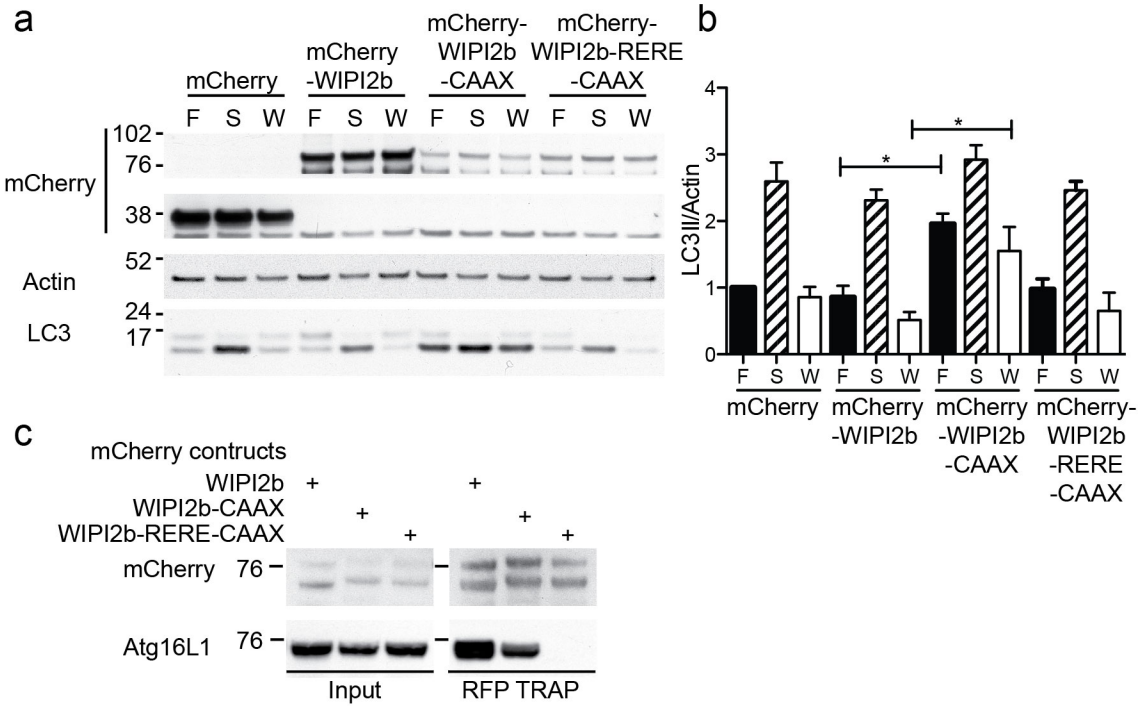

Figure 4.10 WIPI2b-CAAX promotes LC3 lipidation in fed and wortmannin-treated conditions

(a) HEK293A cells were transiently transfected with the indicated mCherry constructs before being treated with full medium (F), starvation medium (S) or starvation medium with wortmannin (W) for two hours. LC3 lipidation was assayed by western blot. **(b)** statistical analysis of **(a)**. The SEM for three independent experiments is shown. Statistical analysis was performed by one-way ANOVA with Tukey's post test. *, $p \leq 0.05$. **(c)** Cell lysates from HEK293A cells transiently transfected with the indicated mCherry constructs were used for RFP-Trap. Immunoprecipitated protein complexes were analysed by western blot. Note, all WIPI2b constructs are FTTG mutants. Molecular weight markers are shown in kDa.

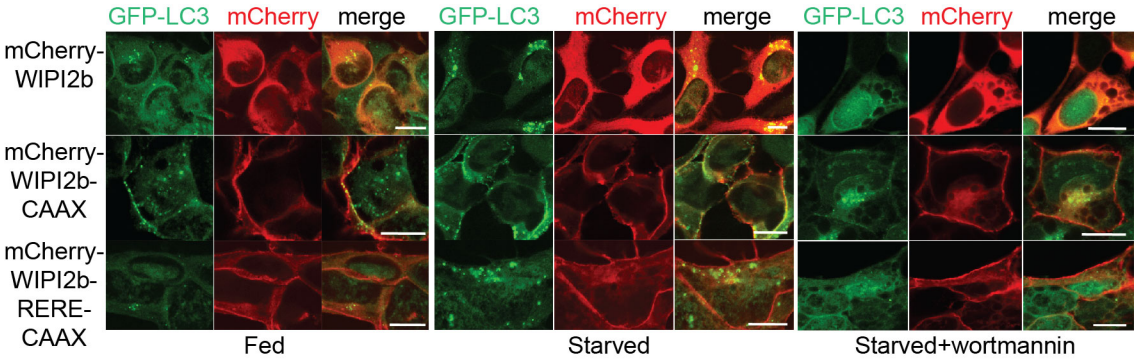

Figure 4.11 WIPI2b-CAAX colocalises with GFP-LC3 on the plasma membrane

GFP-LC3 stably expressing cells were transiently transfected with the indicated mCherry constructs. Cells were treated in full medium (fed), starvation medium (starved) or starvation medium with wortmannin (starved+wortmannin) for two hours before confocal microscopy analysis. Scale bars are 10 μm. Experiment was performed and figure provided by Minoo Razi.

4.4.3 WIPI2b-CAAX promoted LC3 lipidation is independent of FIP200

Atg16L1 binds FIP200 and this interaction is thought to be required for Atg12–5-16L1 recruitment to the forming autophagosome (Nishimura et al., 2013, Gammoh et al., 2013). My results so far have shown that WIPI2b is able to recruit the Atg12–5-16L1 complex to a membrane. Although I have shown that, once WIPI2b is membrane localised, this recruitment is independent of upstream signalling such as mTORC1 and PtdIns(3)P production, the dependence on the presence of FIP200 is not known. In order to test this I used RISC-free control siRNA or siRNA to knockdown Atg16L1 or FIP200 before transiently transfecting the cells with HA-WIPI2b-CAAX (FTTG mutant). I have shown (Figure 4.10 and 4.11) that WIPI2b-CAAX driven LC3 lipidation is dependent on Atg16L1 binding, and so Atg16L1 knockdown was used as a positive control for depleting a protein required for WIPI2-CAAX driven LC3 lipidation. RISC-free siRNA was used as a negative control. I found that FIP200 knockdown had no effect on WIPI2b-CAAX driven LC3 lipidation, in contrast to Atg16L1 knockdown where LC3 lipidation was lost in fed and wortmannin treated condition (Figure 4.12), showing that WIPI2b-CAAX mediated recruitment of the LC3 lipidation machinery does not require FIP200.

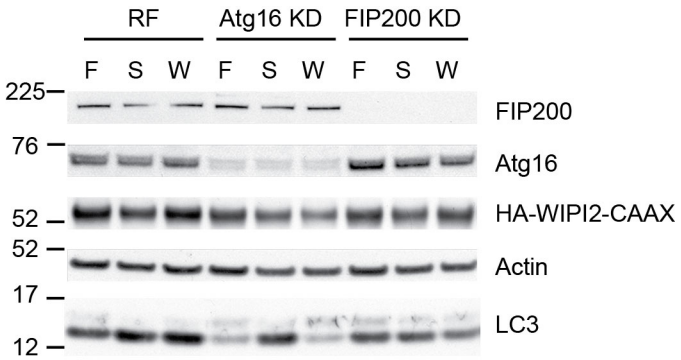

Figure 4.12 WIP2-CAAX driven LC3 lipidation is independent of FIP200

HEK293A cells were treated with RISC-free, Atg16L1 or FIP200 siRNA for 72 hours before transient transfection with HA-WIPI2b-CAAX for 48 hours. Cells were treated with full medium (F), starvation medium (S) or starvation medium and wortmannin (W) for two hours before western blot analysis. Molecular weight markers are in kDa.

4.5 WIPI2b, but not FIP200, binding is required for Atg16L1 rescue of Atg16L1$^{\Delta/\Delta}$ MEFs

The binding sites for WIPI2b and FIP200 on Atg16L1 are very close (Chapter 3.5). Although I have not detected any interdependence or exclusivity in binding, it is possible that WIPI2b and FIP200 function together in autophagy. To further test the requirements for Atg16L1 interaction with WIPI2b and FIP200 in starvation-induced autophagy, I used point mutants of Atg16L1 that can bind WIPI2b but not FIP200 (Atg16L1 D237R D239 R, DRDR), and vice versa (Atg16L1 E226R E230R, ERER) (Figure 3.18), to rescue autophagy in Atg16L1$^{\Delta/\Delta}$ MEF cells.

Transient transfection of Atg16L1$^{\Delta/\Delta}$ MEFs with FLAG-Atg16L1 WT or FIP200-binding deficient FLAG-Atg16L1 DRDR resulted in a significant restoration of LC3 lipidation. In contrast, transfection with WIPI2b-binding mutant FLAG-Atg16L1 ERER did not significantly restore LC3 lipidation compared to mock transfection (Figure 4.13a and b). Similarly, the number of LC3 puncta formed during starvation was significantly fewer in Atg16L1$^{\Delta/\Delta}$ MEFs rescued with FLAG-Atg16L1 ERER than with Atg16L1 WT. However, there was no significant difference between rescue with FLAG-Atg16L1 WT and DRDR (Figure 4.14a and b). These results demonstrate that Atg16L1 must be able to bind WIPI2b in order function in autophagy and that binding to FIP200 is not required.

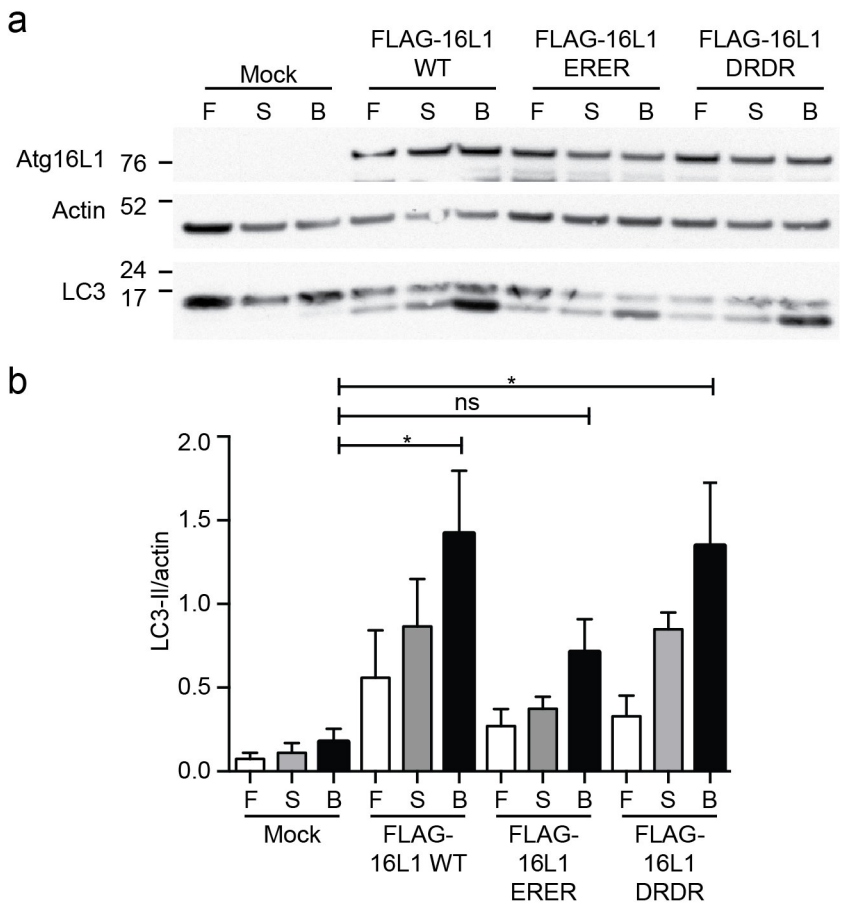

Figure 4.13 Atg16L1 unable to bind WIPI2b cannot rescue LC3 lipidation

(a) Atg16L1$^{\Delta/\Delta}$ MEFs were transiently transfected with the indicated constructs before being treated with full medium (F), starvation medium (S) or starvation medium with Bafilomycin A (B) for two hours. LC3 lipidation was analysed by western blot. Molecular weight markers are in kDa. **(b)** Statistical analysis of **(a)**. The SEM for three independent experiments is shown. Statistical analysis was performed by one-way ANOVA with Tukey's post hoc test. *, $p \leq 0.05$.

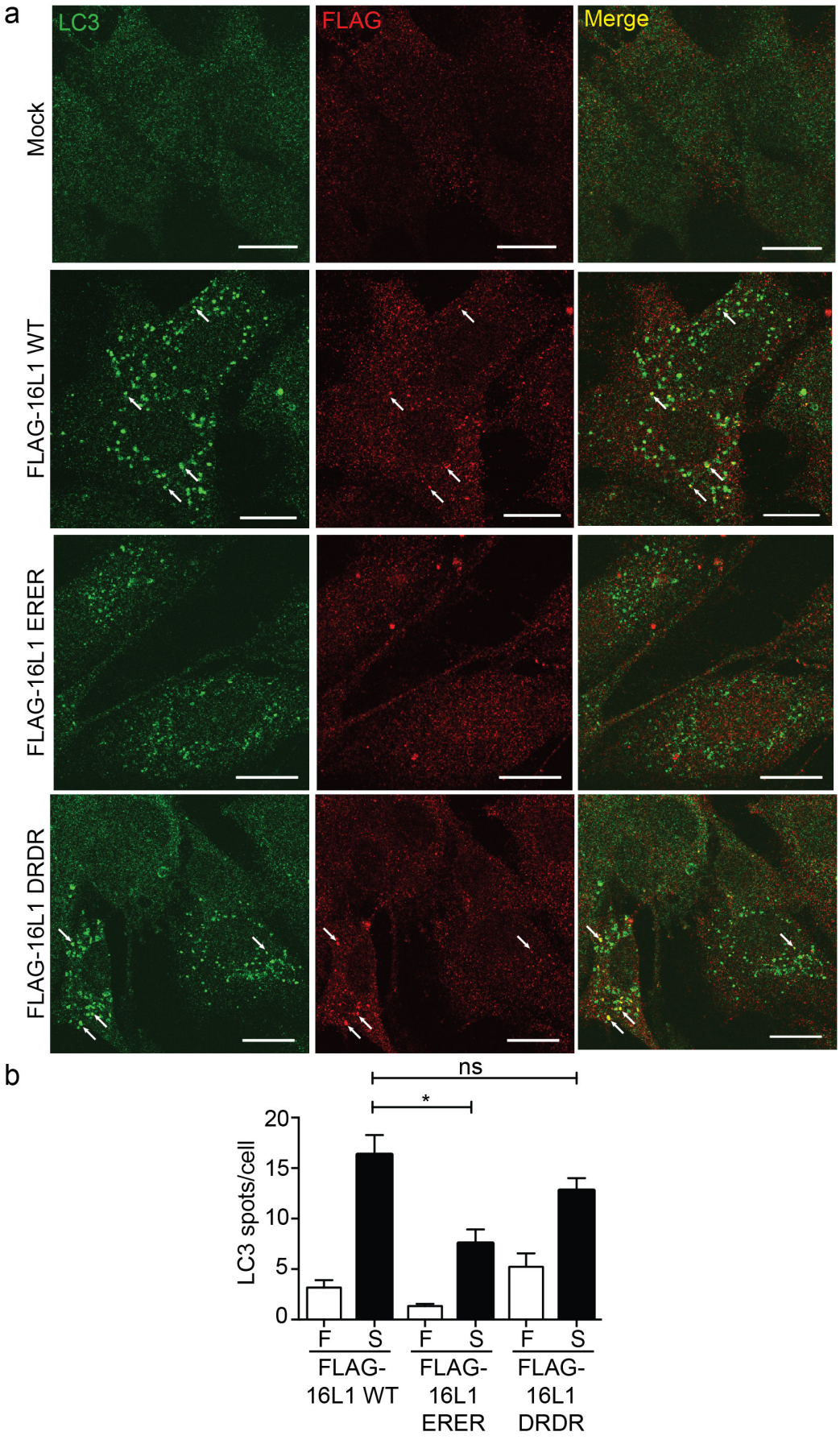
a
LC3
FLAG
Merge
Mock
FLAG-16L1 WT
FLAG-16L1 ERER
FLAG-16L1 DRDR
b
ns
*
LC3 spots/cell
20
15
10
5
0
F
S
FLAG-16L1 WT
FLAG-16L1 ERER
FLAG-16L1 DRDR

Figure 4.14 Atg16L1 unable to bind WIPI2b cannot rescue LC3 puncta formation
(a) Atg16L1$^{\Delta/\Delta}$ MEFs were transiently transfected with the indicated constructs before being treated with full (F) or starvation (S) medium for two hours. Cells were fixed and stained with the indicated antibodies. LC3 puncta formation was analysed by confocal microscopy. Starved cells are shown. Scale bars are 20 μm. **(b)** Statistical analysis of **(a)**. The SEM for three independent experiments is shown. Statistical analysis was performed by one-way ANOVA with Dunn post test. *, $p \leq 0.05$.

4.6 Atg16L1-WIPI2b interaction is required for xenophagy

4.6.1 WIPI2 colocalises with LC3 on the SCV

Salmonella enterica serovar Typhimurium invades non-phagocytic cells using a type three secretion system (TTSS) and enters the cell enclosed in a vacuole, termed the salmonella containing vacuole (SCV). During the first few hours of *Salmonella* infection, the SCV matures from a vacuole containing early endosome markers, to one which is decorated with late endosomal markers such as LAMP-1 (Gorvel and Meresse, 2001). Autophagy limits the replication of *Salmonella* both in whole organisms and cell models (Birmingham et al., 2006, Jia et al., 2009) and it is thought that the host cell initiates autophagy-mediated degradation of *Salmonella*, a process named xenophagy, in response to damage to the SCV by the TTSS (Birmingham et al., 2006). Although the exact signals of this damage are not well understood (Gomes and Dikic, 2014), we know that damage results in ubiquitination of host and/or bacterial proteins (Birmingham et al., 2006), leading to recruitment of cargo-receptors such as p62 (Zheng et al., 2009) and xenophagy at PtdIns(3)P-enriched domains on the ER (Huang et al., 2011).

Xenophagy requires the use of the canonical autophagy machinery to produce a double-membraned vesicle around the SCV. However, the mechanistic details are less well understood than for macroautophagy. A recent study has shown that formation of the double-membraned phagophore surrounding the SCV requires the function of the ULK1 kinase complex and mAtg9 (Kageyama et al., 2011). The same study found that in situations where the phagophore does not form, LC3 can be recruited to the SCV independently of the ULK1 kinase complex, mAtg9 and the Vps34 PtdIns(3) kinase complex, and that this recruitment is dependent on the LC3 lipidation machinery (Atg7, Atg3 and the Atg12–5-16L1 complex). Kageyama, *et al*., reported no change in LC3

localisation to the *Salmonella* (likely the SCV surface) after wortmannin treatment, which is in contrast to a different study that showed that wortmannin treatment significantly reduces LC3 recruitment to *Salmonella* (Huang et al., 2011). It appears that xenophagy may be a more complex process than macroautophagy and that multiple mechanisms may be in place for recruiting the Atg12–5-16L1 complex. FIP200 and ubiquitin have recently been shown to bind Atg16L1 and this could subsequently lead to LC3 recruitment (Fujita et al., 2013). It is possible that the membrane of the SCV itself may provide a platform that allows for LC3 recruitment, via the Atg12–5-16L1 complex, through an unknown mechanism in situations, such as wortmannin treatments and FIP200, ULK1, Atg14L or mAtg9 knockout MEFs, where phagophore formation has been disrupted, but that this is not the wild type scenario (Kageyama et al., 2011).

Although Beclin1 is needed for autophagy-mediated limitation of *Salmonella* growth (Sun et al., 2008, Jia et al., 2009), the role of PtdIns(3)P binding proteins in xenophagy have not yet been investigated. Ubiquitin, p62 and WIPI2 colocalise together around *Salmonella* as expected (Figure 4.15a), showing that WIPI2 localises to ubiquitin-labelled *Salmonella*. As p62 and ubiquitin colocalised on damaged SCVs as expected, I used p62 as a marker for ubiquitinated SCVs because the guinea pig anti-p62 that we use in the lab allowed me more flexibility when triple labelling for immunofluorescence. I found that WIPI2 colocalises with LAMP1 and p62, and so WIPI2 is either localised to, or on a membrane surrounding, the SCV (Figure 4.15b). Xenophagy occurs at omegasomes on the ER (Huang et al., 2011). I found WIPI2- and p62-labelled *Salmonella* on SCVs localised to the ER (Figure 4.15 c). Therefore, WIPI2-labelled SCVs localise to regions of the ER that may represent omegasome, although co-localisation with DFCP1 would be needed to confirm this. Combined, these results show that WIPI2 localises to damaged SCVs and can be found on the ER, which is thought to be the site of bacterial autophagy.

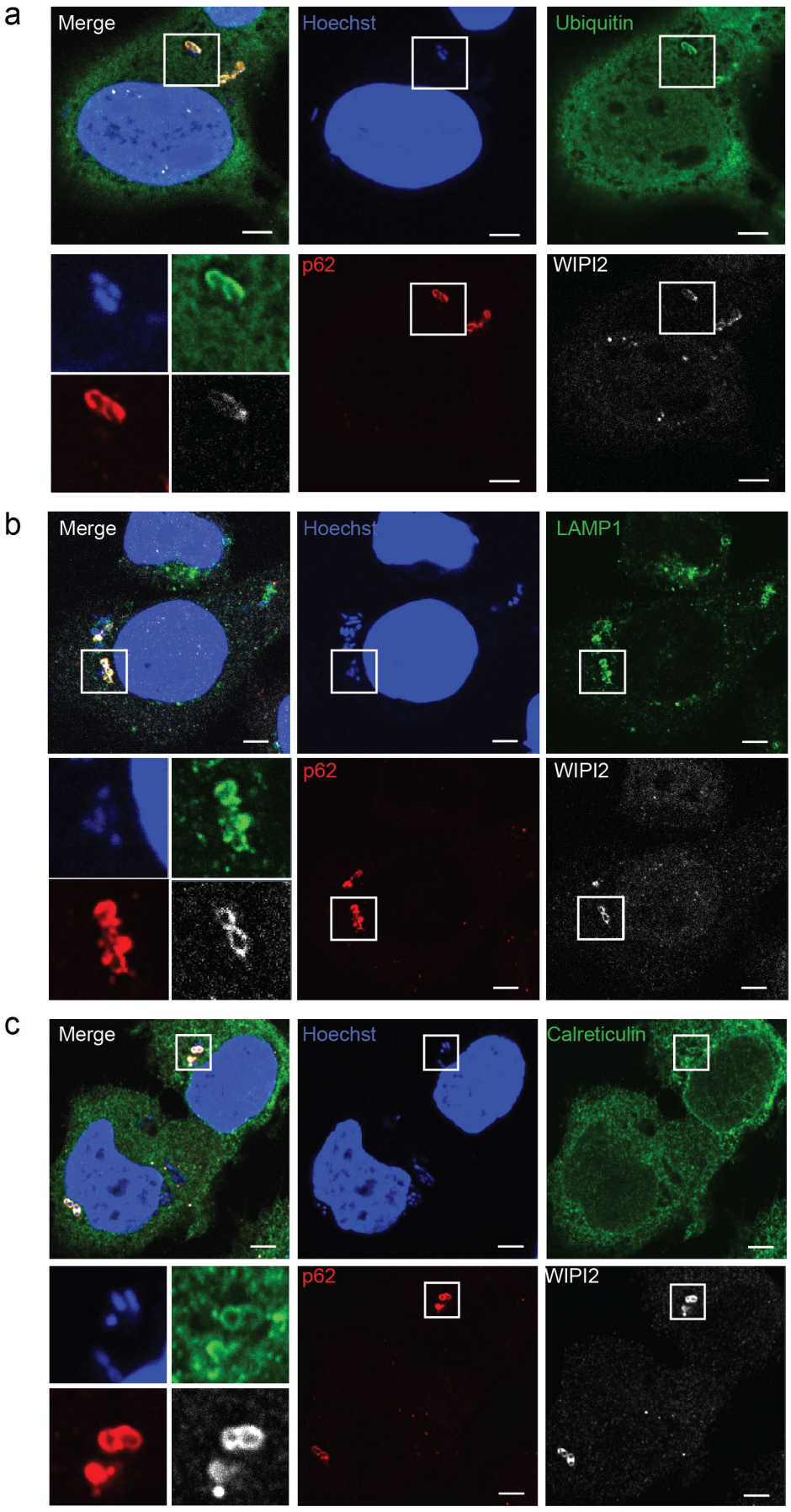
a
Merge
Hoechst
Ubiquitin
p62
WIPI2
b
Merge
Hoechst
LAMP1
p62
WIPI2
c
Merge
Hoechst
Calreticulin
p62
WIPI2

Figure 4.15 WIPI2 colocalises with damaged SCVs on the ER

HeLa cells were infected with Salmonella with an MOI of 100 for one hour before fixing and labelling for immunofluorescence with Hoechst dye, anti-p62, anti-WIPI2 and **(a)** anti-ubiquitin **(b)** anti-LAMP1 and **(c)** anti-calreticulin. Scale bars are 5 μL.

4.6.2 WIPI2 is needed for xenophagy

As WIPI2 is found on damaged SCVs and is needed for macroautophagy, I asked if it is similarly required for xenophagy by depleting WIPI2 from HeLa cells and assaying the effect on bacterial proliferation and on LC3 recruitment to the SCV. Xenophagy reduces the number of *Salmonella* in the cell and so autophagy inhibition results in an increased number of *Salmonella* in each infected cell (Birmingham et al., 2006). Colony count assays can be used to estimate the number of live *Salmonella* in cells after infection. Colony count assays are performed by lysing the cells after infection, making serial dilutions of the cell lysates and plating the cell lysate on LB plates. Each live *Salmonella* will form a colony and so after an overnight incubation the number of colonies per plate represents the number *Salmonella* from that set of cells. WIPI2 knockdown resulted in an increased number of colonies compared to a RISC-free control (Figure 4.16a), showing that WIPI2 is required for bacterial autophagy. Similarly to starvation-induced autophagy, WIPI2 is required for LC3 recruitment to the SCV; LC3 recruitment is significantly impaired in WIPI2 depleted cells (Figure 4.16b and c). Note that WIPI2 and LC3 colocalise on the damaged SCV. These results show that WIPI2 is required for autophagy-mediated degradation of cytosol-exposed *Salmonella*, and this is likely to be as a result of impaired LC3 recruitment.

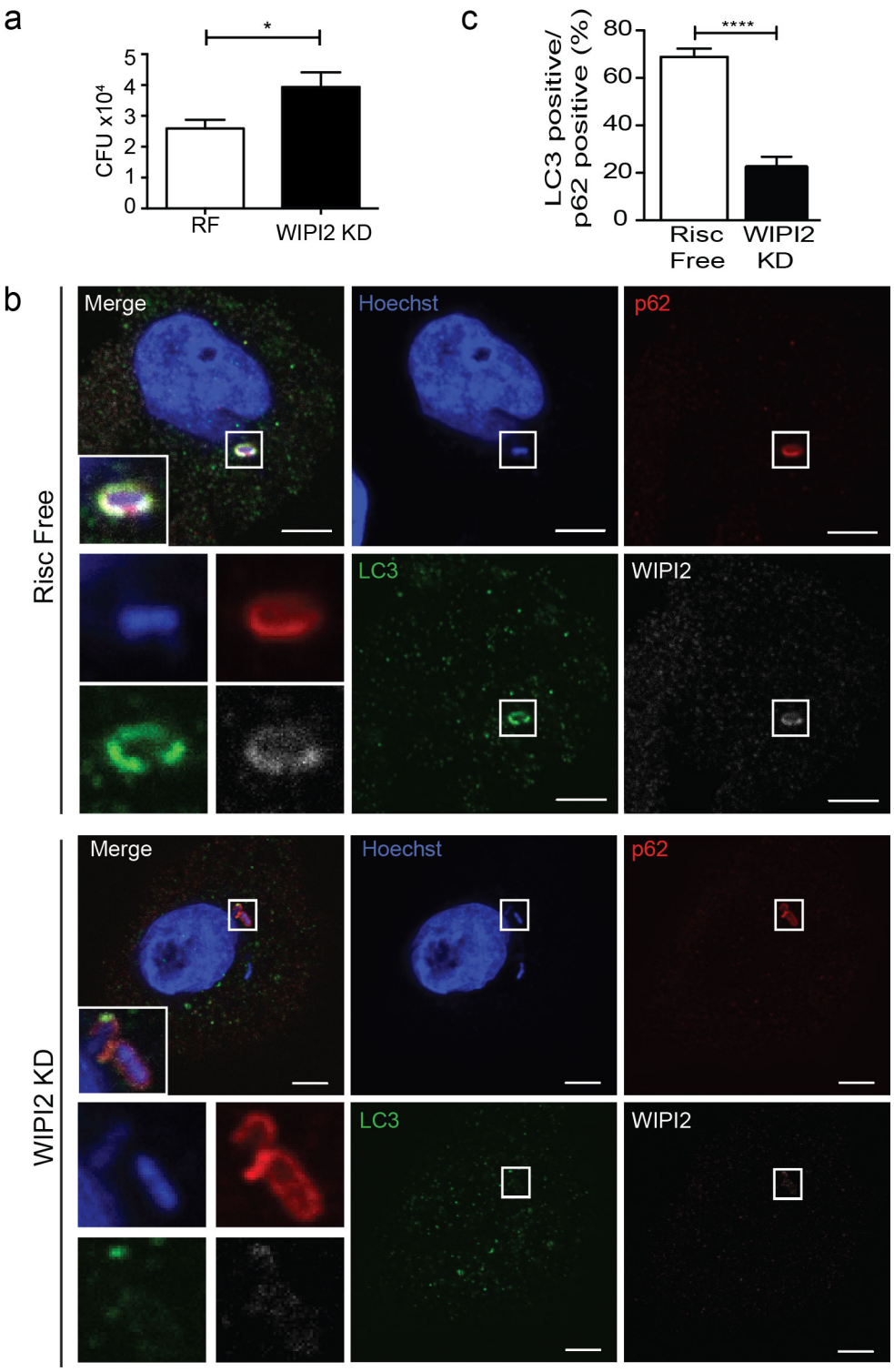

Figure 4.16 WIPI2 knockdown reduces xenophagy and LC3 recruitment to the SCV

(a) HeLa cells were treated with either RISC-free (control) or WIPI2 siRNA for 72 hours before infection with *Salmonella* at an MOI of 100 for one hour. Infected cells were lysed serial dilutions were plated on LB plates. The LB plates were incubated over night and the number of colony forming units (CFUs) were counted. The SEM for three independent experiments in triplicate is shown. Statistical analysis performed using

unpaired student's t-test. *, $p \leq 0.05$ **(b)** HeLa cells were treated with siRNA and infected as in **(a)**. Cells were then lysed and stained with the indicated antibodies for confocal microscopy analysis. Scale bars are 5 μm. **(c)** Statistical analysis of **(b)**. The SEM for three independent experiments is shown. Statistical analysis performed using unpaired student's t-test. ****, $p \leq 0.0001$.

4.6.3 Atg16L1-WIPI2b binding is required for LC3 localisation to the SCV

A number of factors are thought to be required for Atg16L1 recruitment to the SCV (Fujita et al., 2013), therefore I used rescue of Atg16L1$^{\Delta/\Delta}$ MEFs to determine whether the interaction with WIPI2b is an addition mechanism of Atg16L1 recruitment. Atg16L1$^{\Delta/\Delta}$ MEFs rescued with FLAG-Atg16L1 WIPI2b binding mutant (ERER) showed significantly less LC3-positive p62-labelled bacteria than cells rescued with wild type Atg16L1 (Figure 4.17a and b). In contrast, there was no significant difference in LC3 recruitment between Atg16L1 WT and FIP200 binding mutant (DRDR), demonstrating that Atg16L1 must be able to bind WIPI2b to allow for Atg12–5-16L1 recruitment and subsequent LC3 targeting during xenophagy.

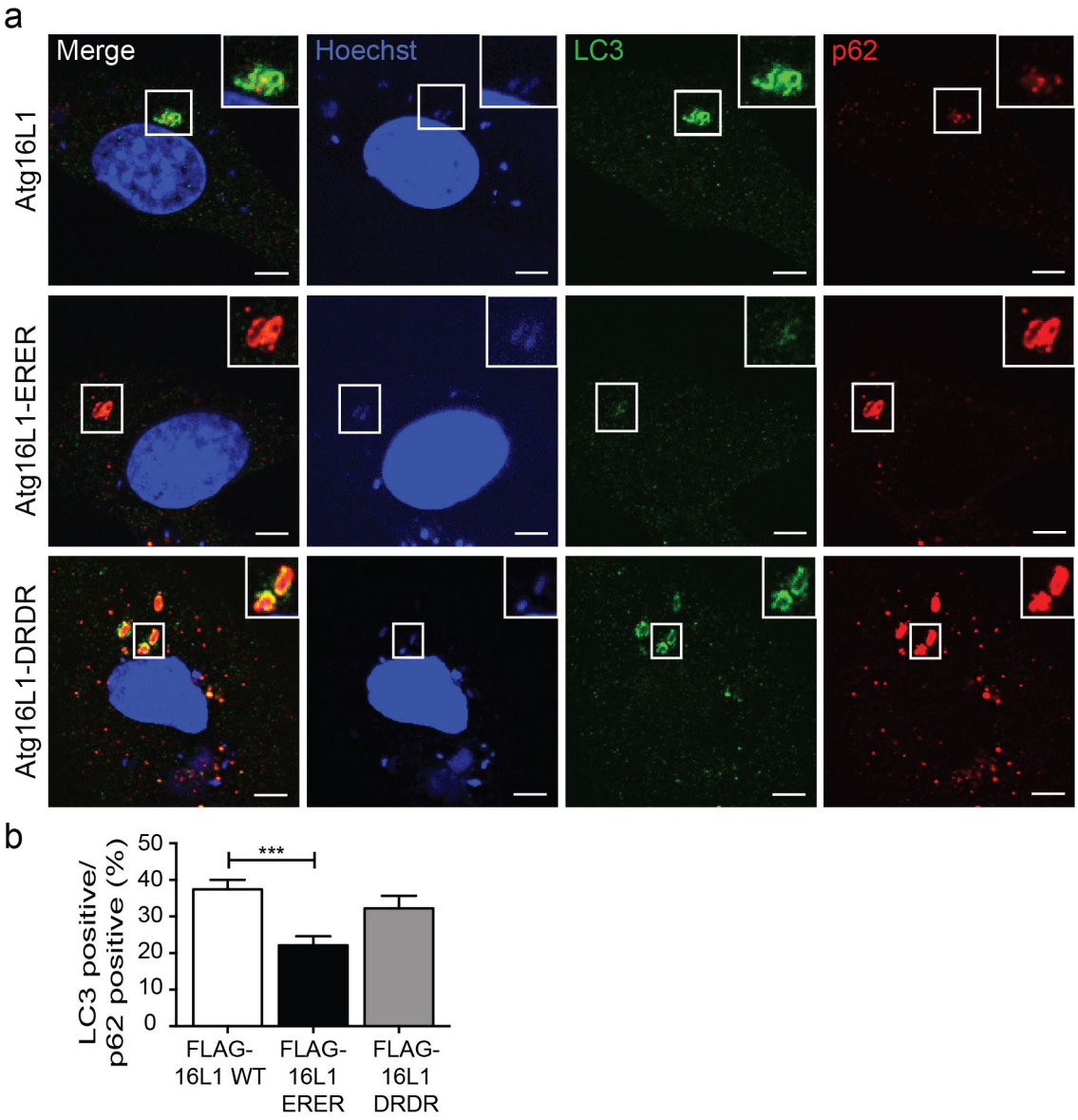

Figure 4.17 Atg16L1 ERER shows impaired LC3 recruitment to the SCV

(a) Atg16L1$^{\Delta/\Delta}$ MEFs were transiently transfected with FLAG-Atg16L1 WT, ERER or DRDR for 24 hours before being infected with *Salmonella* (MOI of 25) for one hour. Cells were fixed, labelled with the indicated antibodies and analysed by confocal microscopy. Scale bars are 5 µm. **(b)** Statistical analysis of **(a)**. The SEM for four independent experiments is shown. Statistical analysis was performed by one-way ANOVA with Dunn's post text. ***, $p \leq 0.001$.

4.6.4 Wortmannin does not inhibit WIPI1 or WIPI2 localisation to *Salmonella*

The requirement for PtdIns(3)P in xenophagy is unclear. It is well established that Beclin1 is required for *Salmonella* clearance through xenophagy both at the organism

(Jia et al., 2009) and cellular level (Sun et al., 2008). Similarly, wortmannin treatment of cells before and during *Salmonella* infection results in increased intracellular bacteria (Steele-Mortimer et al., 2002, Brumell et al., 2002). However, the reason for this requirement for PtdIns(3)P production by the Beclin1-continaing Vps34 complex during xenophagy is unknown. In macroautophagy, wortmannin treatment completely inhibits LC3 recruitment to the forming autophagosomes. This does not seem to be the case during xenophagy. Instead, the requirement of PtdIns(3)P for LC3 recruitment is under debate. While one study found no effect on the percentage of LC-positive salmonella (Kageyama et al., 2011), others found that wortmannin treatment causes a significant decrease, but not complete inhibition, in LC3 recruitment to the salmonella (Huang et al., 2011, Birmingham et al., 2006). GFP-WIPI1 recruitment requires PtdIns(3)P; wortmannin treatment abolishes GFP-WIPI1 localisation to *Salmonella* (Kageyama et al., 2011). I used immunofluorescence to investigate WIPI1 and WIPI2 recruitment to *Salmonella* in cells treated with wortmannin (Figure 4.18). Surprisingly, although wortmannin treatment abolished WIPI2 and LC3 puncta formation during starvation (Figure 4.18a), WIPI1 and WIPI2 localisation to *Salmonella* were not inhibited by wortmannin (Figure 4.18b and c). This is in contrast to previous work by Kageyama *et al*., 2011 described above (Kageyama et al., 2011). I repeated this experiment three times, and each time saw no effect on WIPI2 recruitment to *Salmonella*. The possible reasons for this disagreement are not clear. The HeLa cells that I used for wortmannin treatment were treated with RISC-free siRNA as they were from the same pool of cells used for colony counting (Figure 4.16), but this RISC-free treatment does not interfere with normal WIPI2 behaviour (Figure 4.16b and 4.18a). Due to time constraints, I did not carry out statistical analysis on the number of p62-labelled *Salmonella* that were also positive for WIPI1 or WIPI2. It is therefore possible that wortmannin treatment causes a decrease, but not a complete abolition, in WIPI1 and WIPI2 recruitment, as is the case for LC3 recruitment after wortmannin treatment.

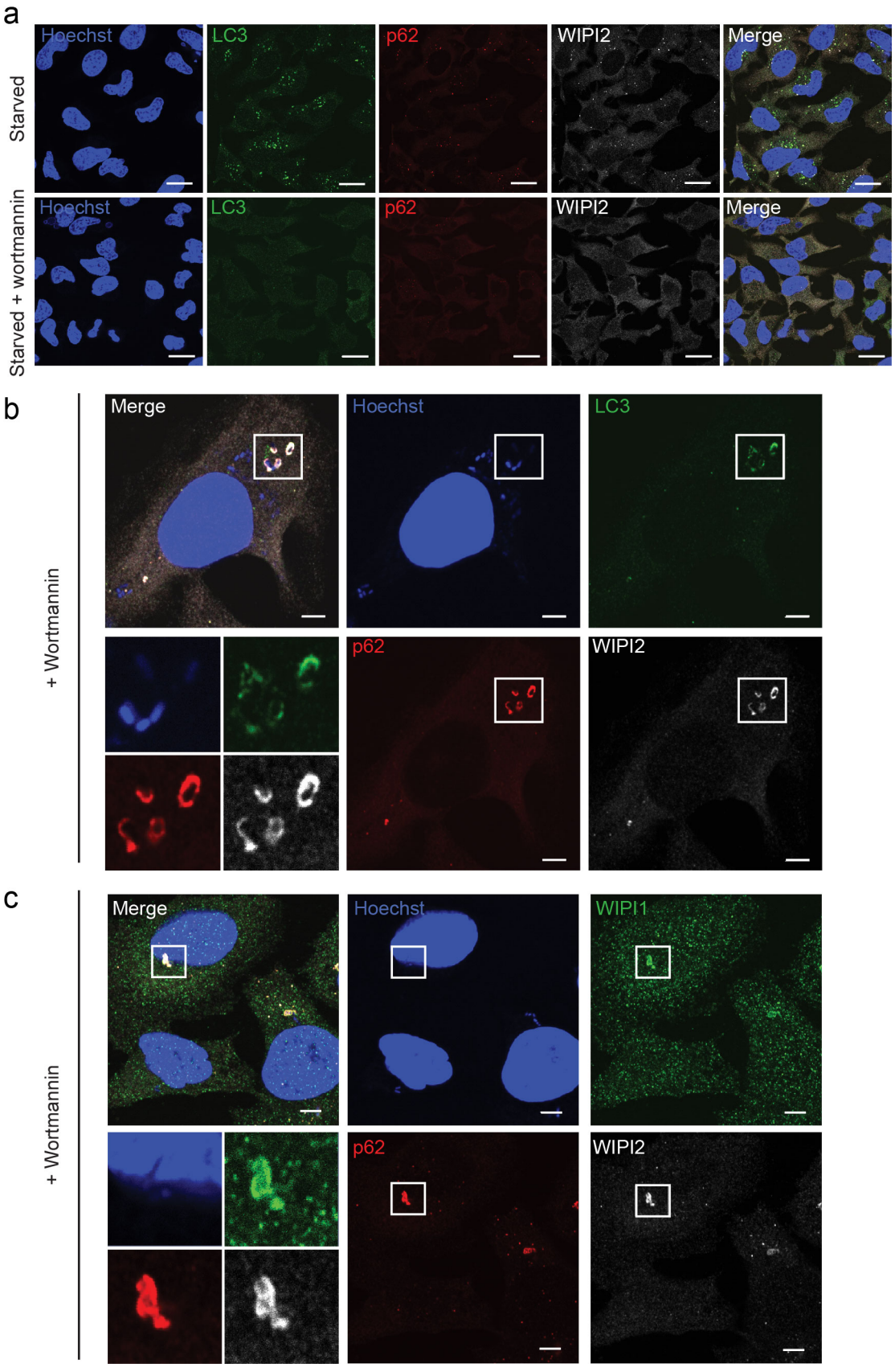
a
Starved
Starved + wortmannin
Hoechst
LC3
p62
WIPI2
Merge
b
+ Wortmannin
Merge
Hoechst
LC3
p62
WIPI2
c
+ Wortmannin
Merge
Hoechst
WIPI1
p62
WIPI2

Figure 4.18 Wortmannin treatment does not inhibit WIPI1 or WIPI2 recruitment during xenophagy

(a) HeLa cells were treated with RF siRNA for 72 hours were starved in EBBS with or without wortmannin for 1 hour before fixing and staining with the indicated antibodies for immunofluorescence. Scale bars are 20 μm. **(b,c)** HeLa cells treated with RF siRNA for 72 hours were infected with Salmonella with an MOI of 100 for 1 hour before fixing and labelling for immunofluorescence with Hoechst dye, anti-p62, anti-WIPI2 and anti-LC3 **(b)** or anti-WIPI1 **(c)**. Scale bars are 5 μm

4.7 Discussion

In this chapter I have demonstrated that WIPI2b functions in autophagy by recruiting the Atg12–5-16L1 complex to forming autophagosomes (Figure 4.18). This helps explain two incompletely understood areas of autophagosome biogenesis: the function of PtdIns(3)P in autophagy initiation, and the PtdIns(3)P-dependence of Atg12–5-16L1 recruitment, by connecting PtdIns(3)P to the Atg12–5-16L1 complex via WIPI2b.

Previous work has shown that FIP200 is required for Atg12–5-16L1 recruitment in both starvation-induced autophagy and targeted autophagy of latex beads and *Salmonella* (Nishimura et al., 2013, Gammoh et al., 2013, Fujita et al., 2013). However, my results suggest that FIP200 is not involved in Atg12–5-16L1 recruitment. As discussed in Chapter 3.8, Atg16L1 mutants used by Nishimura *et al.*, and Gammoh *et al*., will have disrupted WIPI2b binding as well as FIP200 binding. The point mutants of Atg16L1 used in this chapter for rescue of Atg16L1$^{\Delta/\Delta}$ MEFs dissociated Atg16L1-FIP200 binding from Atg16L1-WIPI2b binding and showed that Atg16L1 interaction with WIPI2b, but not FIP200 is required for Atg16L1 function in autophagy. I could detect no significant autophagy impairment in cells rescued with the FIP200 binding mutant of Atg16L1. However, recent work showing that Atg16L1 can bind FIP200 and ubiquitin, and through these binding partners be recruited to *Salmonella* and latex beads, has raised the possibility that the mechanisms of Atg16L1 recruitment have become more complex in higher organisms, possibly to allow for more complex autophagy pathways than are found in yeast (Fujita et al., 2013). Therefore, the Atg16L1-FIP200 binding may have a function in cargo-specific autophagy, or in some other regulatory or redundant function in macroautophagy. Although requiring further investigation, this hypothesis is supported by the evolutionary conservation of the WIPI2b and FIP200

binding sites of Atg16L1 (observation by Michael Wilson, personal communication). The WIPI2b binding site is found in most metazoans, whereas the FIP200 binding site is missing in metazoans pre-dating zebrafish, and may not be present at all in invertebrates (observation by Michael Wilson). Although binding site for WIPI2b (and FIP200) on Atg16L1 is missing in yeast, and *S. cerevisiae* Atg18 does not bind Atg16 (Fulvio Reggiori, personal communication), *S. pombe* Atg18a binds Atg5 and is thought to recruit the Atg12–5-16 complex to the PAS through this interaction (Sun et al., 2013). Therefore, it may be that the mechanism of recruiting the Atg12–5-16 complex through Atg18/WIPI2b is conserved between *S. pombe* and mammals.

Results in this chapter show that WIPI2 binding to Atg16L1 is required for xenophagy and LC3 recruitment to *Salmonella*. The requirement for PtdIns(3)P binding proteins in control of intracellular bacteria and for the recruitment of LC3 to *Salmonella* was previously not known. However, I also found that WIPI1 and WIPI2 could be recruited to *Salmonella* even in the presence of wortmannin. As discussed in Chapter 4.6.4, the reason for the difference between my results (Figure 4.18) and published work showing that GFP-WIPI1 localisation to *Salmonella* is inhibited by wortmannin treatment is not known. Similarly, the reasons behind different findings for the dependence of LC3 recruitment to *Salmonella* on PtdIns(3)P is unclear (Kageyama et al., 2011, Birmingham et al., 2006, Huang et al., 2011). It seems to be the case that the dependence on PtdIns(3)P for recruitment of LC3 is not absolute, but perhaps instead is partial (Huang et al., 2011). Given more time I would have quantified WIPI1 and WIPI2 recruitment to p62-positive *Salmonella* under wortmannin-treated conditions as these proteins may similarly be partially dependent on PtdIns(3)P for their recruitment during xenophagy. As discussed above, Atg16L1 appears to be recruited to *Salmonella* via multiple binding partners. WIPI2 may also be recruited to *Salmonella* through unknown binding partners. To investigate this further I would use our GFP-WIPI2b stably expressing cell line for Salmonella infection followed by GFP-Trap and mass spectrometry to identify novel proteins that bind WIPI2b during xenophagy. Furthermore, I would use siRNA knockdown of WIPI2 followed by rescue with siRNA resistant WT WIPI2, WIPI2b RERE (Atg16L1 binding mutant), WIPI2b FTTG (PtdIns(3)P binding mutant) and WIPI2b FTTG RERE (PtdIns(3)P and Atg16L1 binding mutant) to determine the PtdIns(3)P- and Atg16L1-binding requirements of

WIPI2b in xenophagy. If Atg16L1 itself is a binding partner through which WIPI2b can be recruited in the absence of PtdIns(3)P (as Atg16L1 can also be recruited through binding FIP200 and ubiquitin (Fujita et al., 2013)) WIPI2b FTTG RERE should not be recruited to p62-positive *Salmonella*. Furthermore, if WIPI2b is the major protein responsible for Atg12–5-16L1 recruitment during xenophagy then overexpression of WIPI2b RERE after endogenous WIPI2 depletion may inhibit LC3 recruitment, as seen in macroautophagy. Generally, the recruitment mechanisms of Atg proteins during xenophagy seem to be more complex, possibly with partially redundant mechanisms, than macroautophagy. As work to understand xenophagy continues it will be interesting to see which of the autophagy proteins in higher eukaryotes have evolved features that are not present in their yeast counter parts and that support more complex recruitment and/or regulation mechanisms.

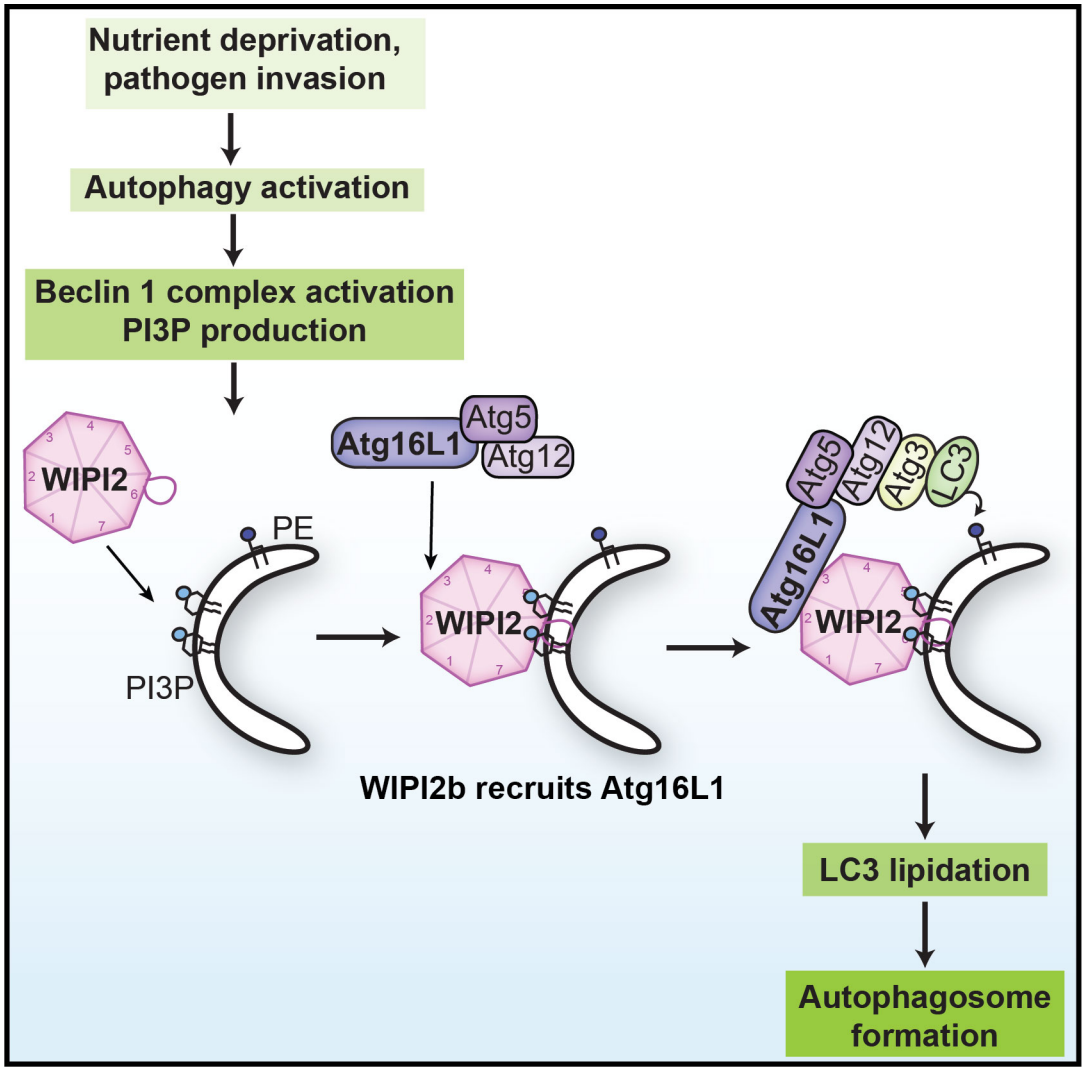

Figure 4.19 WIPI2b recruits the Atg12–5-16L1 complex to forming autophagosomes

Model of WIPI2b-mediated Atg12–5-16L1 recruitment to PtdIns(3)P-positive site of autophagosome formation. Figure from (Dooley et al., 2014).

Chapter 5. Preliminary investigation of WIPI2 phosphorylation

5.1 Introduction and Aim

5.1.1 Introduction

As discussed in Chapter 3, the Atg16L1-WIPI2b interaction appears to be starvation-independent. This raises the question of whether the Atg16L1-WIPI2b interaction is regulated and if it is, how it is. Similarly, WIPI2 can bind PtdIns(3)P and PtdIns(3,5)P_2 but forms PtdIns(3)P-dependent starvation-induced puncta at the omegasome (Polson et al., 2010). PtdIns(3)P is found on early and late endosomes as well as on omegasomes and PtdIns(3,5)P_2 is found on late endosomes (Vicinanza et al., 2008). The regulation behind the specific localisation of WIPI2 to PtdIns(3)P positive omegasomes upon starvation is not known. Atg18 (*S. cerevisiae*) is required for starvation-induced autophagy and for the regulation of vacuole morphology, and localises to PtdIns(3)P on the PAS and PtdIns(3,5)P_2 on the vacuole, respectively, for these functions (Barth et al., 2001, Efe et al., 2007). Recruitment of Atg18 to the PtdIns(3)P-positive PAS requires Atg2 binding by Atg18 (Suzuki et al., 2007, Rieter et al., 2013) and recruitment to the PtdIns(3,5)P_2 positive vacuole requires binding to Vac7 (Efe et al., 2007). It is possible that WIPI2 has an analogous binding partner, or is post-translationally modified to allow proper recruitment to PtdIns(3)P positive omegasome upon starvation-induced autophagy.

Work in our group (Hannah Polson, unpublished data) has suggested that WIPI2 may be phosphorylated within its C-terminus. In the mass spectrometry screen for WIPI interactors using GFP-tagged stable cell lines of WIPI1a and WIPI2b (see Chapter 3.1) a phosphorylation of WIPI2b at serine 395 was found in all three experiments. There was no clear fed/starved dependence of the phosphorylation: S395 was phosphorylated in starved conditions of experiments 1 and 3, but in fed conditions for experiment 2 (See Figure 5.1a). Protein phosphorylation is thought to be one of the most prevalent posttranslational modifications and is responsible for altering the function of a protein in a number of ways including disrupting or inducing protein-protein, protein-membrane and protein-DNA interactions, changing the activity state of enzymes, and

stabilising or destabilising proteins (Cohen, 2002). The reversible nature of protein phosphorylation makes it suitable for switching a protein between two states. Phosphorylation of the C-terminus of WIPI2 may provide a mechanism through which WIPI2 interaction with membranes or proteins can be modulated. Serine 395 of WIPI2b is found in the C-terminus of WIPI2a and WIPI2b (Figure 1.8 and 1.9) and is conserved in mouse, chicken and *Xenopus* (observation by Michael Wilson, personal communication). The same site was identified as a potential mTOR phosphorylation site by Hsu *et al.*, who used quantitative mass spectrometry in a proteomic screen for Torin1-sensitive phosphorylation sites and subsequently defined a mTOR consensus motif (Hsu et al., 2011). WIPI2 serine 395 fits this consensus (Figure 5.1b) (Hsu et al., 2011). mTOR is a master controller of cell growth that forms two kinase complexes, mTORC1 and mTORC2 (see Chapter 1.3.1). WIPI2 S395 may be phosphorylated by mTORC1, mTORC2 or another kinase downstream of these master regulators. Indeed, this potential WIPI2 phosphorylation site has been identified in a number of phosphoprotein screens, as indexed by PhosphoSitePlus® (Hornbeck et al., 2012), and kinase predication resources such as PhosphoNET: Kexus Kinase Predictor suggest that kinases other than mTOR may recognise this site.

In addition to this potential phosphorylation site, Atg2 was identified in one of Hannah Polson's mass spectrometry experiments as an interactor of GFP-WIPI2b. Although Atg2 binding by WIPI2b was only found in one mass spectrometry result and was not further confirmed, Atg18 binds Atg2 in yeast and is required for proper Atg18 localisation to the PAS (Suzuki et al., 2007) and the Atg18-Atg2 complex regulates Atg9 trafficking (Obara et al., 2008, Wang et al., 2001, Reggiori et al., 2004). Binding of WIPI2 to Atg2 may be conserved and required for correct WIPI2 localisation to the omegasome as in yeast.

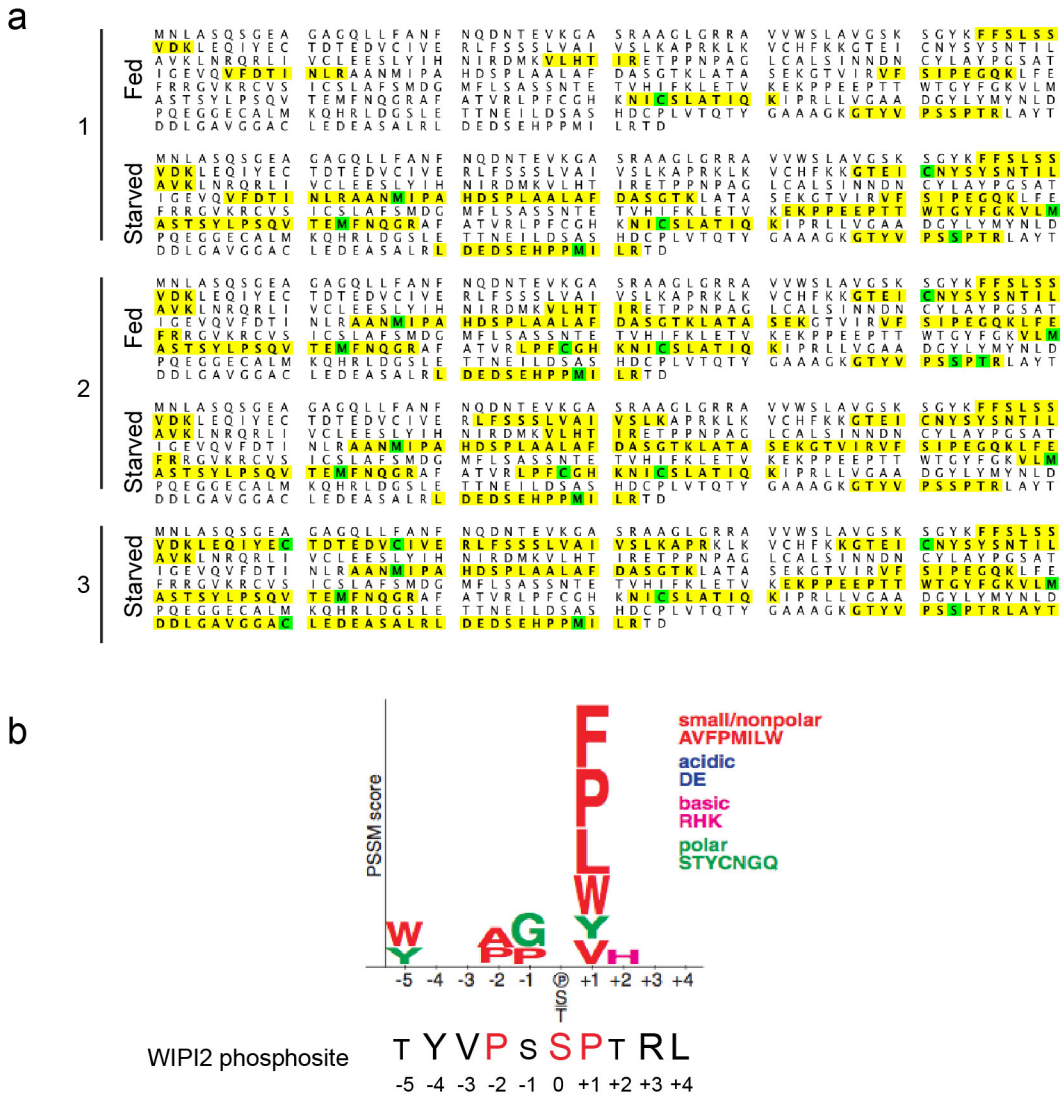

Figure 5.1 Potential phosphorylation of WIPI2 serine 395

(a) Figure showing mass spectroscopy detection of WIPI2 peptides from Hannah's GFP-WIPI2b GFP-Trap and mass spectroscopy screen. Yellow indicates peptides detected. Green indicates modified amino acids. 1, 2, and 3 indicate the experiment number. Experiment performed by and figure provided by Hannah Polson. (b) WIPI2b serine 395 conforms to the mTOR phosphorylation consensus. PSSM, position-specific scoring matrix. Pannel showing mTOR consensus is from (Hsu et al., 2011). Reprinted with permission from AAAS.

5.1.2 Aim

I sought to substantiate data from our lab and from published work that WIPI2 is phosphorylated at serine 395 and determine if phosphorylation has any effect on WIPI2 function in autophagy. To do this I began by validating rabbit serum produced against

the phosphosite, and generating and testing WIPI2b phosphomutants to probe the effect of phosphorylation on Atg16L1 binding. I investigated the function of Atg2 on autophagy and WIPI2 function using Atg2 knockdown. I performed this work before a study on the role of Atg2 in starvation induced autophagy and lipid droplet formation was published (Velikkakath et al., 2012).

5.2 Phosphospecific antibody validation

5.2.1 Antibody validation by Western blot

Rabbits were immunised with an 11 amino acid phosphopeptide corresponding to the human WIPI2 phosphosite (Figure 5.2). Cysteine or lysine was used for peptide conjugation to the carrier protein in the production of STO 313, 314 and 315, and STO 316, 317 and 318, respectively. The peptide was made and conjugated by LRI peptide synthesis unit and the serum generated by LRI polyclonal antisera services.

I validated the antiserum against endogenous WIPI2 by using cell lysates from WIPI2 siRNA treated HEK293A and western blot analysis. The anti-WIPI2 polyclonal rabbit antibody serum that was previously developed by our lab (Polson et al., 2010) is used at a concentration of 1:250 and gives a very clear band corresponding to WIPI2 just below the marker for 52 kDa (WIPI2 has a molecular weight of 49 kDa) (Figure 5.3, top panel). I tested serums STO 313-318 over a range of concentrations: 1-100 – 1:1000 (Figure 5.3). STO 313, 314, 317 and 319 did not give any specific bands that decreased with WIPI2 knockdown. STO 315, 316 and 318 all showed a band at the correct molecular weight for WIPI2 that decreased upon knockdown that was not present in the pre-immune (PI) serum. Therefore it is likely that these sera recognise endogenous WIPI2 protein from human cells. These sera showed a clear WIPI2 signal at 1:200 or 1:1000.

WIPI2 is well conserved between mouse and human. The peptide used for polyclonal antibody production differs by two amino acids when compared to mouse WIPI2 over the same stretch (the extreme N-terminus is an alanine and the extreme C-terminus is a glycine in the mouse peptide). I used cell lysates from wild-type and TSC2 knock out ($TSC2^{-/-}$) MEFs to validate recognition of mouse WIPI2 by STO 315, 316

and 318. TSC2 is one member of TSC1/TSC2, a heterodimeric complex that, together with TDC1D17, is a GAP for Rheb (Chapter 1.3.1). TSC2 loss results in increased mTORC1 signalling (Zhang et al., 2003). If WIPI2 is phosphorylated by mTORC1, or via a downstream pathway activated by mTORC1, WIPI2 phosphorylation should also be increased in $TSC2^{-/-}$ MEFs. I used both the wild type and knockout cell lysates to investigate if there was any difference in the WIPI2 as detected by phosphospecific antibody serum in mTORC1 activated cell lysates. As a control for WIPI2 recognition, I used HEK293A lysates from RISC-free and WIPI2 siRNA treated cells (Figure 5.4). Again, all three antibodies showed a WIPI2 band just below the 52 kDa marker (shown in yellow) that decreased after WIPI2 knockdown in HEK293A cells and all three recognised mouse WIPI2. However, there was no difference in WIPI2 signals between WT and $TSC2^{-/-}$ lysates, indicating that there is no change in WIPI2 phosphorylation between the two cell types or that the phosphoantibodies require optimising for phospho-WIPI2 recognition. Although WIPI2 S395 has been reported to be mTOR regulated, with a decrease in phospho-detection by mass spectrometry after Torin1 treatment (Hsu et al., 2011), I also saw no difference in signal when cells were treated with the mTOR inhibitor Torin1 (data not shown). Because the conditions under which WIPI2 is phosphorylated were unclear, I decided to use ELISA (enzyme-linked immunosorbent assay) for further optimisation and validation of phosphopeptide recognition by the phospho-antibodies. Serum STO 316 and 318 were used for further optimisation; STO 315 was not optimised further due to the non-specific band seen just above the WIPI2 band, which may render interpretation of western blots with this antibody difficult.

STO 313, 314, 315: K-TYVPSS_PPTRLA-$CONH_2$

STO 316, 317, 318: C-TYVPSS_PPTRLA-$CONH_2$

Figure 5.2 WIPI2 peptides used for rabbit immunisation

An 11 amino acid phosphopeptide was used for immunisation. Either lysine (STO 313, 314 and 315) or cysteine (STO 316, 317 and 318) was used for conjugation of the peptide to the carrier protein.

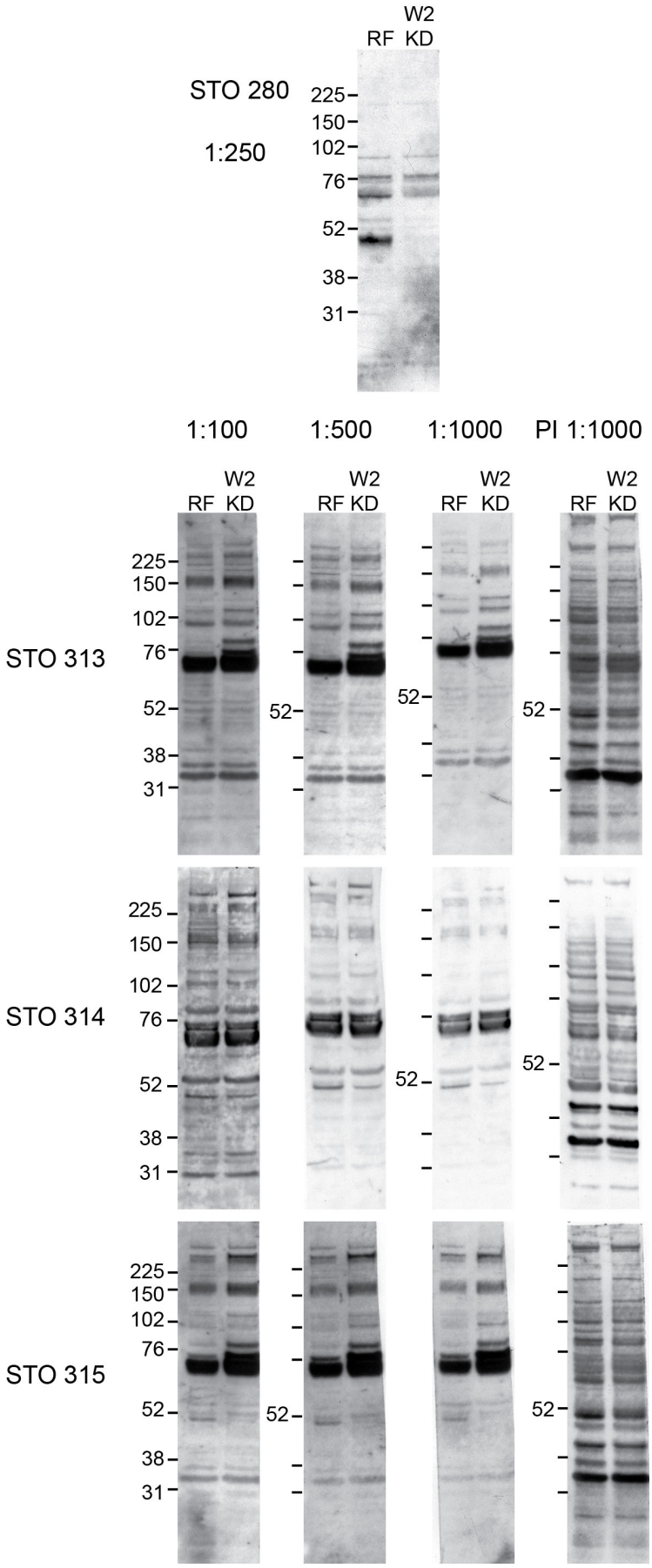
STO 280
1:250
RF
W2 KD
225
150
102
76
52
38
31
1:100
1:500
1:1000
PI 1:1000
STO 313
STO 314
STO 315

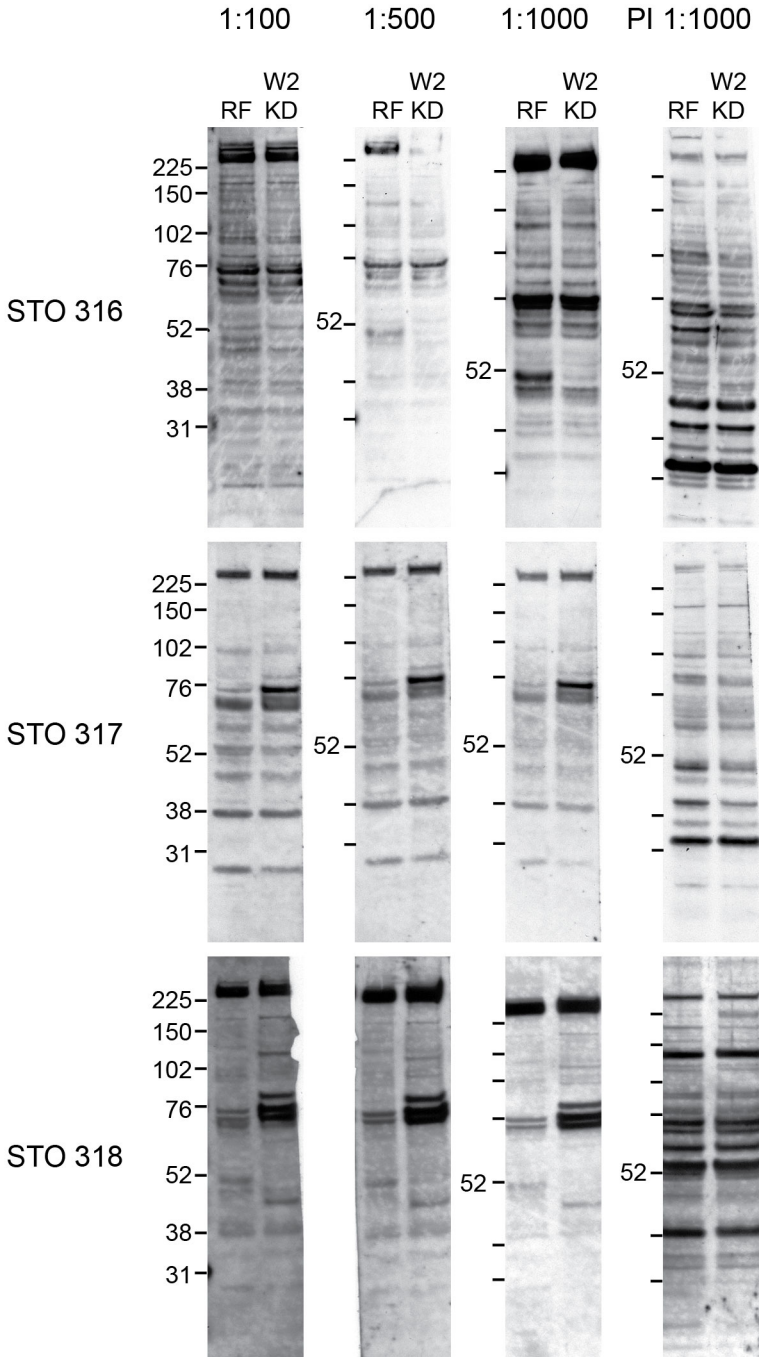

Figure 5.3 STO 315, 316 and 318 recognise human WIPI2

Cell lysates from HEK293A cells treated with RISC-free (RF) or WIPI2 siRNA for 72 hours were used for western blot analysis of the indicated immunoserum. STO 280 is a positive control for a rabbit polyclonal serum that recognises WIPI2. Molecular weight markers are in kDa. WIPI2 has a molecular weight of 49 kDa and runs just below the 52 kDa marker.

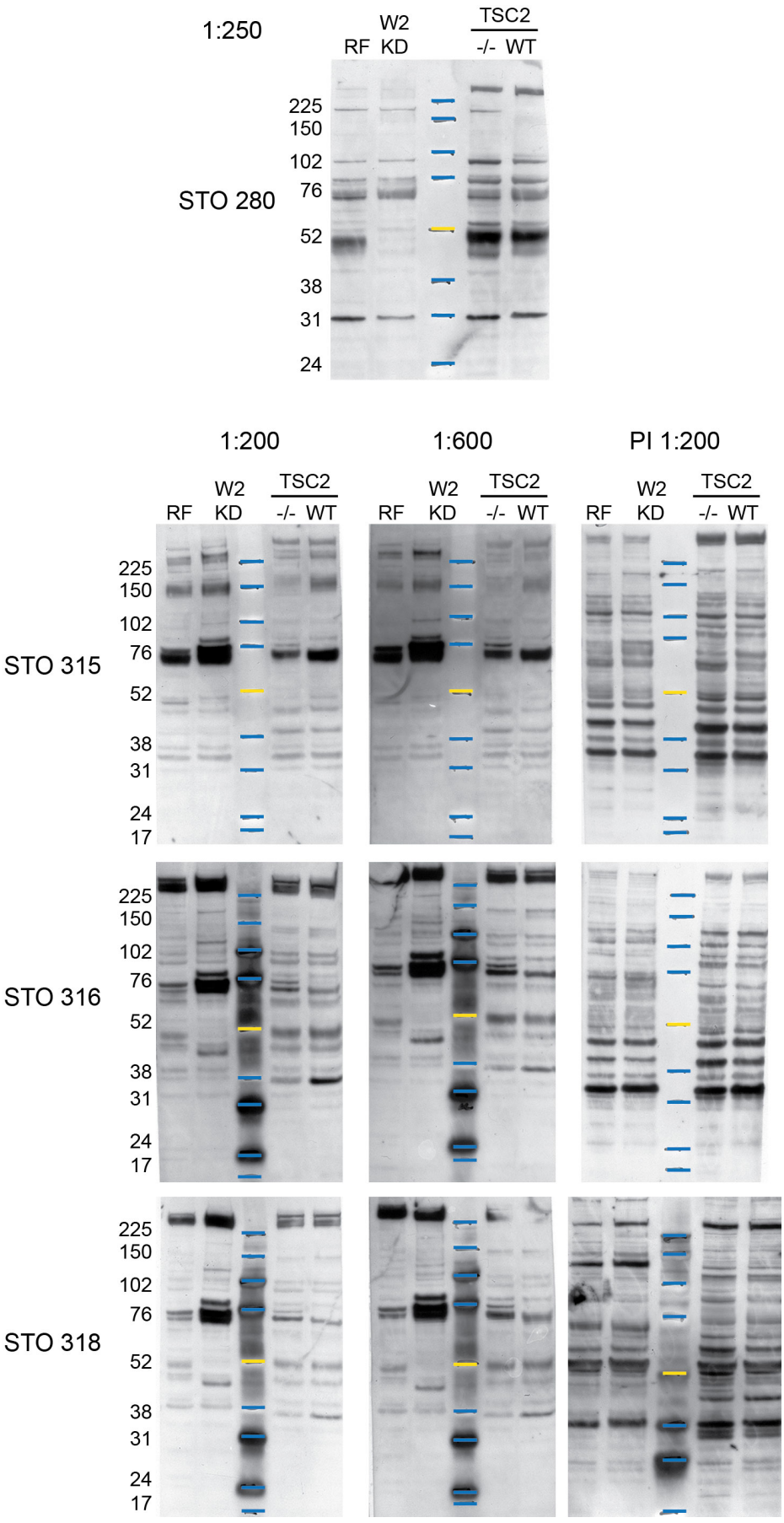
1:250
W2
RF KD
TSC2
-/- WT
225
150
102
76
52
38
31
24
STO 280
1:200
1:600
PI 1:200
W2
RF KD
TSC2
-/- WT
225
150
102
76
52
38
31
24
17
STO 315
STO 316
STO 318

Figure 5.4 STO 315, 316 and 318 recognise mouse WIPI2

Cell lysates from HEK293A cells treated with RISC-free (RF) or WIPI2 siRNA for 72 hours, and cell lysates from TSC2 knockout (-/-) or wild-type (WT) MEFs were used for western blot analysis of recognition of mouse WIPI2 by the indicated serum. Serum were used at the indicated dilution. Molecular weight markers are in kDa.

5.2.2 Antibody validation by ELISA

The 11 amino acid polypeptide (Figure 5.2) used for antibody production will have a number of epitopes, resulting in the production of a polyclonal antiserum and probably the production of antibodies that can recognise the peptide irrespective of its phosphorylation status (i.e. non-phosphospecific). Preincubating the polyclonal serum with a non-phosphorylated version of the peptide used for immunisation results in formation of peptide-antibody complexes between the non-phospho peptide and non-phosphospecific antibodies present in the polyclonal serum. Therefore, preincubation of serum with non-phosphopeptide can be used to remove the non-phosphospecific antibodies from the ELISA reaction. After removal of the non-phospho antibodies from the ELISA reaction, the titre of the phosphospecific antibodies in STO 316 and STO 318 serum can be compared.

Before investigating the relative titre of phosphospecific antibodies in STO 316 and STO 318, I found the peptide concentration over which epitope recognition by the whole sera (with no preincubation) increase linearly with increase of peptide on the ELISA well surface. I used serum dilutions of 1:250, 1:2000 and 1:20000 and phosphopeptide range of 0.01 – 100 ng per well (concentration range: 0.0002 – 2 ng/μL) in duplicate. The increase in absorption at 490 nm (the absorption wavelength for the substrate, OPD) was roughly linear between 0.01-1 ng (0.0002 – 0.002 ng/μL) of peptide for both STO 316 and 318 for all serum dilutions before levelling off for higher peptide amounts (Figure 5.5a, b and c). Results are shown on a logarithmic scale so that the data points at low peptide concentrations can be distinguished. Left hand panels shown show no serum control, right hand panel show serum results in more detail. Serum dilution of 1:20000 showed the greatest difference in A490 between the peptide concentrations in this range.

I subsequently wanted to validate phosphopeptide recognition by the two antisera. I decided to use 0.01, 0.05 and 0.1 ng of peptide per well (concentration range

of 0.0002 – 0.002 ng/μL) in an attempt to ensure that the increase in antibody binding is linear with increase in peptide. I used serum dilutions of 1:250, 1:2000 and 1:20000. No peptide controls and no serum controls were used for each serum concentration and peptide amount, respectively. I used three conditions for each set of peptide concentrations and serum dilutions: no preincubation with peptide, preincubation with non-phosphopeptide to remove non-phosphospecific antibodies, and preincubation with non-phospho and phosphopeptide to remove all antibody from the sera and reduce absorbance to background levels (Figure 5.6a, b and c). Preincubation peptide was added at a final concentration of 1 μg/mL. I did not conduct this ELISA in duplicate, limiting its accuracy and making the results difficult to interpret.

For both STO 316 and 318, the increase of absorbance with peptide concentration (with no preincubation) was as expected: as the concentration of peptide increased, so did the absorbance (Figure 5.6a, b and c). However, the increase in absorbance with peptide concentration was not linear, and it may be that the substrate (OPD) became saturated at the higher peptide concentrations. Generally, serum at 1:250 and 1:200 had similar absorbances over the peptide concentration range, and this was similar between the two sera (with a maximum OD A490 of approximately 2.5 for both STO 316 and 318). However, at a dilution of 1:20000 STO 318 resulted in a higher OD_{490} than for STO316, suggesting that the antibody tire may be higher in STO318.

For both sera, peptide competition with both the phospho and non-phosphopeptide reduced absorbance to basal levels for serum at 1:20000 dilution, and almost basal levels for 1:2000 dilution. This indicates that the reactivity between the antisera and peptide on the ELISA plate is specific. However, at a dilution of 1:250 both STO 316 (Figure 5.5b) and STO 318 (Figure 5.5c) showed above basal absorbance when preincubated with both peptides. This above basal absorbance was consistent for all concentrations of peptides attached to the ELISA plate, including no peptide control, but was not seen for no peptide on the ELISA plate when the antiserum was not preincubated with peptide. It could be that the sera at a dilution of 1:250, when preincubated with peptide, are being retained in the wells between washes. Similarly, sera at 1:250 in wells with no peptide produced above basal absorbance when pre-incubated with just the non-phosphopeptide.

Preincubation with non-phosphopeptide alone did not reduce absorbance to basal levels, but did reduce the absorbance range for each antiserum dilution compared to the absorbance seen with no peptide competition. This suggests that non-phosphospecific antibodies are being successfully removed from the antisera and that there are phosphospecific antibodies present. Generally, the absorbance seen with STO 316 and 318 after preincubation with non-phosphopeptide was similar, suggesting that they have a similar titre of phosphospecific antibodies. This ELISA needs repeating in duplicate or triplicate, using a lower range of peptide concentrations for coating the ELISA plate, in order to be able to distinguish which is the better phosphospecific antiserum.

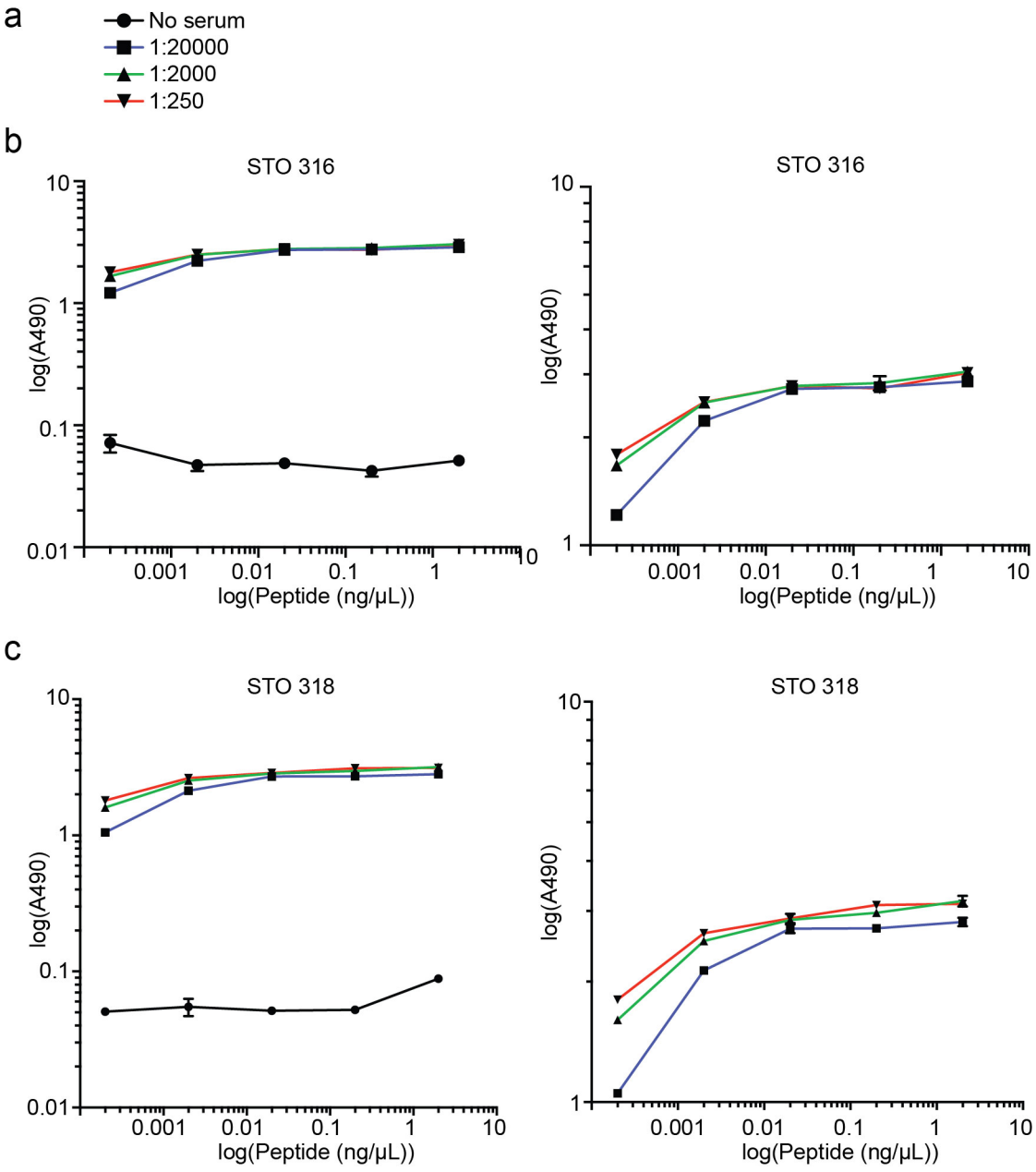

Figure 5.5 STO 316 and 318 validation by ELISA

(a) Key for ELISA graphs. Black line with black circular points: serum control, blue line with black square points, 1:20000 dilution; green line with upright black triangle, 1:2000 dilution; and red line with upside down black triangle, 1:250 dilution. **(b)** STO 316 was used at the indicated dilutions for ELISA against phosphopeptide at the indicated concentrations. **(c)** STO 316 was used at the indicated dilutions for ELISA against phosphopeptide at the indicated concentrations.

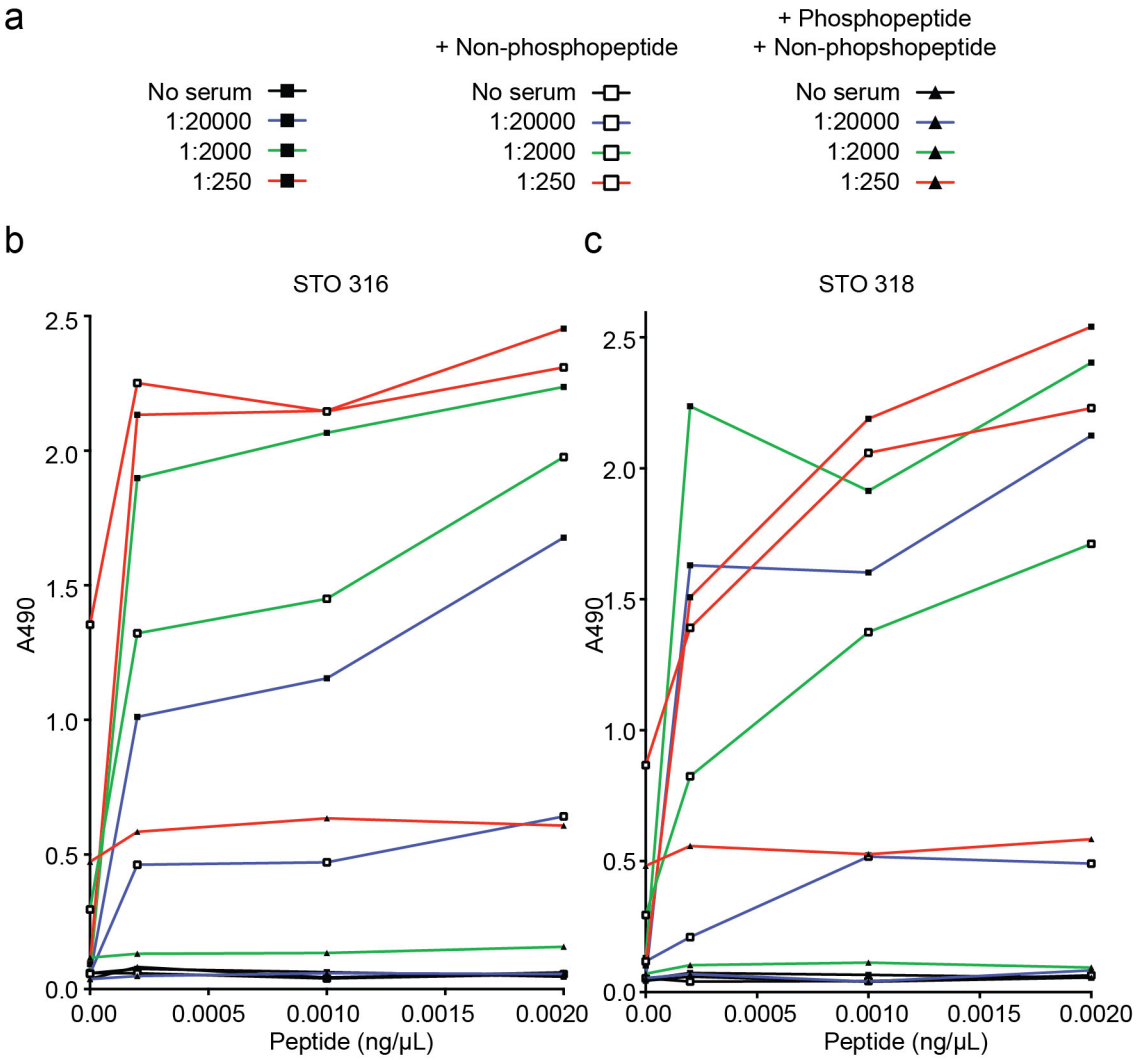

Figure 5.6 STO 316 and 318 show some phospho-specificity by ELISA

(a) Key for ELISA graphs. Black boxed points indicate no peptide competition, white boxes incicate non-phosphopeptide competition, and black triangles indicate completion with both non-phospho and phosphopeptide. Serum dilutions: black line, serum control; blue line, 1:20000; green lines, 1:2000; red line, 1:250. **(b)** STO 316 was used at the indicated dilutions for ELISA against phosphopeptide at the indicated concentrations with the indicated peptide competition. **(c)** STO 316 was used at the indicated dilutions for ELISA against phosphopeptide at the indicated concentrations with the indicated peptide competition.

5.3 Phosphomutant effect on Atg16L1 binding

The C-terminus of WIPI2 is thought to be unstructured (Krick et al., 2012) and so is it possible that this region of the protein could affect Atg16L1 binding. It may be that the C-terminus hinders Atg16L1 binding through binding to the Atg16L1-binding region on

the surface of the β-propeller of WIPI2, or it may enhance Atg16L1 binding by forming a secondary Atg16L1 binding site. Serine 395 could therefore play a role in regulation of Atg16L1 binding through the phosphorylation of this residue altering the interaction between the C-terminus and the β-propeller of WIPI2 or between the WIPI2 C-terminus and Atg16L1.

In order to test the effect of phosphorylation of Serine 395 on Atg16L1 binding, I produced GFP-tagged phospho-null (alanine) and phospho-mimetic (glutamic acid) point mutants of GFP-WIPI2b. Serine 395 is immediately preceded by another serine (394), therefore I made single mutants (S395A and S396E) and double mutants (S394A 3S95A, and S394E S395E) in case serine 394 can be phosphorylated in situations where S395 is mutated. I used these mutants for GFP-Trap and analysed endogenous Atg16L1 co-immunoprecipitation by western blot (Figure 5.7). There was no difference in Atg16L1 co-immunoprecipitation, suggesting that the phosphorylation state of serine-395 has no effect on Atg16L1 binding. Note: removing the whole C-terminus of WIPI2b increases Atg16L1 binding (Chapter 3.6.1). These experiments were performed in the same experimental set as C-terminus deletion experiments which show that removing the whole C-terminus of WIPI1 or WIPI2 significantly increases Atg16L1 binding (Figure 3.21), this experiment set was performed three times and I have shown a different experiment below from that used for Figure 3.21. I have separated the phosphomutant and C-terminal deletions results for clarity. GFP-WIPI2a cannot be seen in the input as this protein does not overexpress well, even though it is in the same vector as other GFP-WIPI constructs.

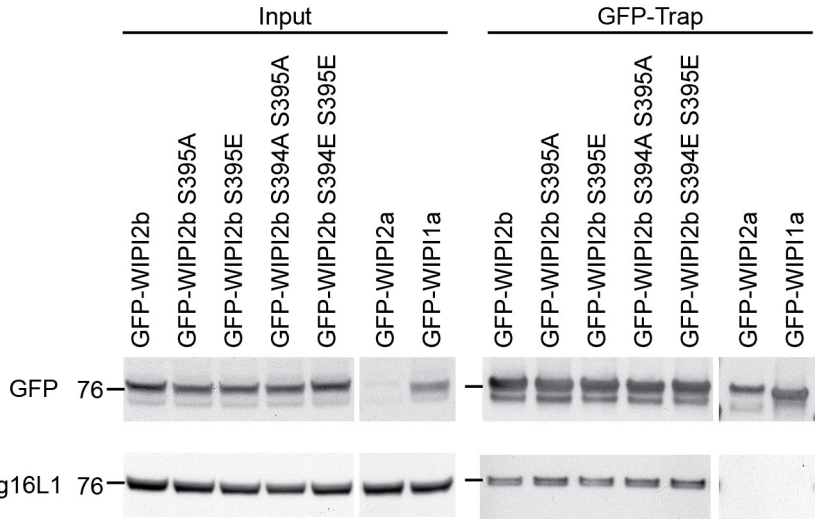

Figure 5.7 Phospho-null and -mimetic mutants have no effect on Atg16L1 binding

HEK293A cells were transiently transfected with the indicated GFP-tagged constructs for 24 hours before GFP-Trap and western blot analysis. Molecular markers are in kDa.

5.4 Atg2

5.4.1 Atg2 knockdown optimisation

Mammals have two Atg2 homologues. Atg2a and Atg2b have 44.5% amino acid identity and have redundant funcitons (Velikkakath et al., 2012). I used siRNA for each homologue simultaneously to knockdown both proteins at the same time. As no commercial antibodies that worked for western blot were available, I assessed mRNA depletion using qPCR (quantitative PCR) (Figure 5.8). Atg2a was significantly depleted by Atg2a siRNA duplexes 17, 19 and 20 (Figure 5.8a) and Atg2b was significantly depleted by all four Atg2b siRNAs (Figure 5.8b). Atg2a siRNA had no significant effect on Atg2b mRNA levels, however Atg2b siRNA generally decreased Atg2a levels (this was statistically significant for Atg2b duplex 18 and 21). Consistently, published work has subsequently shown that depletion of Atg2a mRNA upon Atg2b knockdown is reflected at the protein level; Atg2b knockdown reduces Atg2a protein (Velikkakath et al., 2012). This depletion of Atg2a protein was seen after using a different siRNA duplex to the one that I used in work for this thesis, suggesting that it is a biological rather than an off-target effect. I used the siRNAs that most effectively depleted their target proteins; therefore I used Atg2a siRNA duplex #20 and Atg2b siRNA deplex #21 to knockdown Atg2a and Atg2b for autophagy assays.

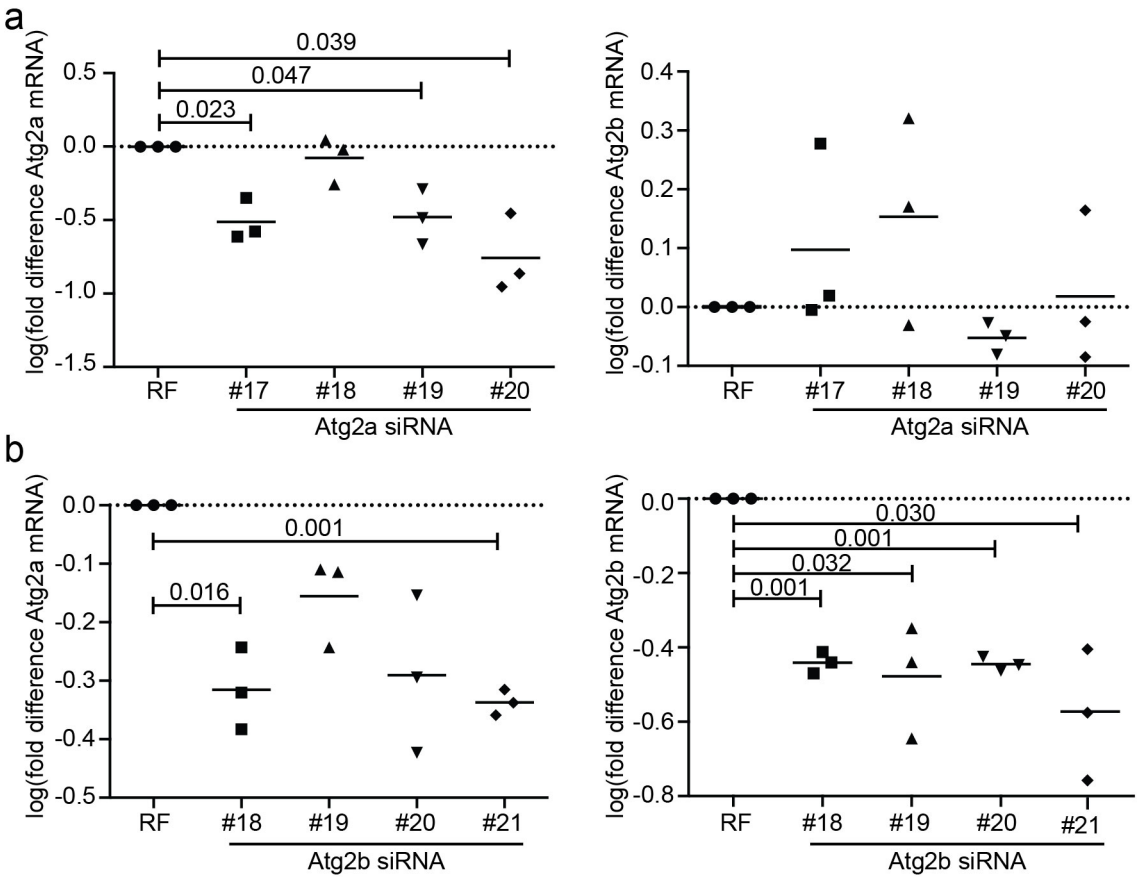

Figure 5.8 Optimisation of Atg2a and Atg2b knockdown

HEK293A cells were treated with RISC-free (RF) control, the indicated Atg2a siRNA **(a)** or Atg2b siRNA **(b)** for 72 hours before RNA extraction and qPCR analysis for change in Atg2a levels (left hand panels) and change in Atg2b levels (right hand panels). The mean is shown from three independent experiments in triplicate. Statistical analysis performed by student's t-test. Where the difference is significant, the p value is shown.

5.4.2 Atg2 knockdown increases LC3 lipidation and LC3 and WIPI2 puncta

The function of Atg2 and its position within the sequential and hierarchical action of mammalian Atg proteins was not published when I started this work. It has since been published that Atg2 acts during the late stages of autophagosome formation, after LC3 recruitment and lipidation but before autophagosome closure. Atg2a and b depletion leads to an accumulation of LC3-II and unclosed LC3 positive autophagosomes in fed

and starved conditions, with no further accumulation with lysosomal inhibitors, suggestive of a maturation block (Velikkakath et al., 2012).

I found that knockdown of Atg2a and b resulted in a consistent increase in LC3-II in fed conditions (Figure 5.9a and b). Furthermore, LC3 and puncta increased significantly in fed and starved conditions, while WIPI2 puncta were significantly increased in starved conditions (Figure 5.9c, d and e). LC3 puncta further increased with Bafilomycin A treatment, however Bafilomycin A treatment was only used in two of the three experiments and so was not included in the statistical analysis (shown as a grey bars in Figure 5.9d and e). LC3 and WIPI2 puncta appeared larger in Atg2a and b knockdown cells than in RISC-free control. My results support an enhancement of autophagy when Atg2a and b are depleted as I repeatedly see a further increase in LC3 lipidation and puncta formation with Bafilomycin A treatment. However, in light of published data, it may be that the knockdown that I was achieving was not sufficient to fully block autophagosome formation.

The data shown in Figure 5.9 is from the same set of experiments as that shown in Figure 4.3. The immunofluorescence images are from the same experiment repeat.

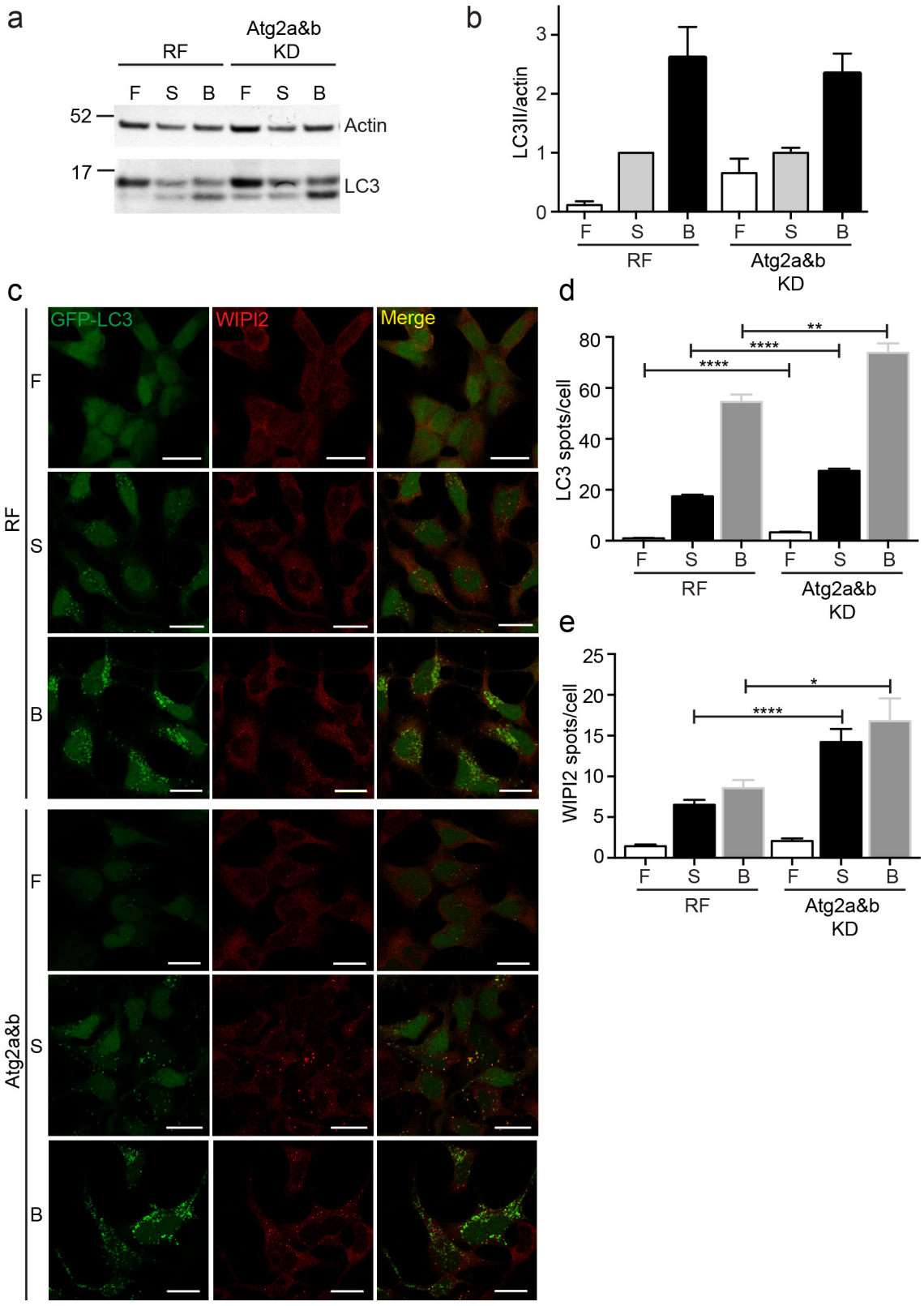

Figure 5.9 Atg2a and b knockdown increases LC3 lipidation and LC3 and WIPI2 puncta formation

(a) 2GL9 cells treated with RISC-free or Atg2a and b siRNA for 72 hours were treated with full medium (F), starvation medium (S) or starvation medium with Bafilomycin A (B) for two hours before LC3 lipidation analysis by western blot. Molecular weight markers are in kDa. **(b)** Quantification of **(a)**. The SEM for three independent experiments is shown. **(c)** Cells treated as in **(a)** were analysed by confocal microscopy for GFP-LC3 and endogenous WIPI2 puncta formation. Scale bars are 10 μm. **(d)** Statistical analysis of GFP-LC3 puncta from **(c)**. The SEM from three (outlined in black) or two (outlined in grey) independent experiments is shown. Statistical analysis was performed by Student's t test. *, $p \leq 0.05$; **, $p \leq 0.01$; ****, $p \leq 0.0001$.

5.5 Discussion

In this chapter I have begun investigations into the possible function of WIPI2b phosphorylation on Serine 395 and the function of Atg2. I have validated two polyclonal antibodies for recognition of endogenous WIPI2. Further work is needed to fully characterise the specificity of these antibody for phosphorylated WIPI2. Given more time I would use ELISAs to validate the specificity of STO 316 and 318 for the 11 amino acid phosphopeptide used for antibody production, using a lower peptide concentration on the ELISA wells to ensure a proper linear relationship between increasing the peptide concentration and increased antibody binding. Once I had found the peptide concentration range over which a linear relationship is shown, I would use peptide competition to determine which immunoserum has the highest tire of phosphospecific antibodies. As the conditions under which WIPI2 Serine 395 is phosphorylated are unknown, following selection of the better phosphospecific antibody, immunoprecipitation of WIPI2 and *in vitro* dephosphorylation using calf intestinal phosphatase could be used for validation of the phosphospecific antibody by western blot.

I have shown that phospho-mimetic and phospho-null point mutants of WIPI2b do not affect Atg16L1 binding. This suggests that phosphorylation of serine 395 does not play a role in regulating the Atg16L1-WIPI2b interaction. However, removal of the whole C-terminus of WIPI2b does increase Atg16L1 binding (Figure 3.21). Similarly, removal of the C-terminal of WIPI1a increases Atg16L1 binding to WIPI1a. Clearly the C-termini of these proteins affect Atg16L1 binding in some manner. Whether this plays a functional role requires further work. Although it is seems likely that Serine 395 phosphorylation does not affect Atg16L1 binding, phosphorylation at this site may

affect WIPI2 binding to the membrane or to PtdIns(3)P. Using the WIPI2 Serine 395 point mutants for phospholipid binding assays and membrane fractionation would help determine whether this is the case. Furthermore, this site may affect some other as yet undiscovered autophagy-related function of WIPI2. Using the phospho-mimetic and phospho-null WIPI2b mutants for rescue experiments following WIPI2 knockdown would give an indication of whether this is the case.

I began to characterise the function of Atg2 in autophagy and have shown that knockdown results in an increase in WIPI2 and LC3 puncta and LC3 lipidation. Published work from another lab has shown that Atg2 acts downstream of LC3 lipidation and is required for autophagosome closure (Velikkakath et al., 2012), putting it downstream of WIPI2 function. The same study also showed that Atg2 binds WIPI4, and that Atg2 localisation to the forming autophagosome requires PtdIns(3)P. WIPI4 is a homologue of WIPI2, and the WIPI4 homologue in *C. elegans*, Epg-6, has been shown to act downstream of *C. elegans* Atg18 (WIPI2 homolgoue) (Lu et al., 2011), suggesting that WIPI4 and Epg-6 have conserved functions. It is possible that each member of the WIPI family performs a different function, perhaps each recruiting its own subset of interacting proteins to the omegasome in a PtdIns(3)P dependent manner. I did not look for WIPI2 binding of Atg2, which would have to be done before an Atg2-WIPI2 interaction could be discounted, but it possible that Atg2 present in Hannah Polson's mass spectrometry results could have been pulled down as a false positive through an intermediate interacting protein or through immunoprecipitating autophagosomal membranes.

Chapter 6. Discussion

In my PhD work I have sought to identify the molecular functions of mAtg9 and WIPI2 in autophagy. To do this I attempted to identify novel mAtg9 and WIPI2 interactors before concentrating my efforts on validating and characterising interacting partners previously identified within the lab. In the preceding chapters I have described the function of WIPI2b as a PtdIns(3)P effector whose function is to directly bind and recruit the Atg12–5-16L1 complex to forming autophagosomes. This function of WIPI2b explains both why Atg12–5-16L1 recruitment to forming autophagosome is PtdIns(3)P-dependent and also why PtdIns(3)P is so essential for autophagosome formation. Previous chapters also detail work done to validate TfR as a mAtg9 binding partner. This work contributed to Andrea Orsi's study describing mAtg9 localisation to tubular-vesicular compartments and the importance of these in autophagy (Orsi et al., 2012).

Using the limited approaches that I set up, I did not identify any novel mAtg9 or WIPI2 interactors, which was disappointing. Given more time I would use BioID technology in combination with mass spectrometry to screen for new interacting proteins (Roux et al., 2012). BioID is a technology involving fusion of a promiscuous *E. coli* biotin ligase to a target protein (in this instance either WIPI2b or mAtg9). Once expressed in cells, this fusion protein then biotinylates neighbouring proteins in a proximity-dependent manner. These proteins can be isolated by biotin affinity capture using streptavidin-conjugated beads and subsequently identified using mass spectrometry (Roux et al., 2012). In terms of the mass spectra produced, this technique is much simpler than using crosslinking and has now been successfully used in our lab. Identification of new mAtg9 interactors is still an important problem as this will shed some light on the function of this protein, and characterisation of additional WIPI2b interactors may help explain some of the remaining questions about this protein (see below).

Given that WIPI2 is a WD-40 domain containing protein that forms a 7-bladed β-propeller, it is likely that it functions to mediate protein interactions. Indeed, it seems probable that the other PROPPIN proteins similarly mediate protein interactions. The combination of the PtdIns(3)P- and protein-binding ability of the PROPPIN family

makes them ideally suited to recruiting Atg proteins during the early stages of autophagy, where the activation signal comprises PtdIns(3)P production at the ER. Consistently, Atg18, WIPI4 and EPG-6 all bind Atg2 (Obara et al., 2008, Velikkakath et al., 2012, Lu et al., 2011). The PROPPIN family are thought to be the first group of β-propeller proteins acting to mediate protein-lipid complexes (Rieter et al., 2013). Intriguingly, Atg18 and WIPI2b seem to be binding their interacting partners (Atg2 and Atg16L1, respectively) at similar locations within their β-propellers. The loops between β-sheets of each blade of the β-propeller are often where interactions occur. Loops in blades 2 that are proximal blade 3 and the loop connecting blades 2 and 3 are important for Atg2 binding (Watanabe et al., 2012, Rieter et al., 2013). Atg2 binds to two sites within blade 2 of Atg18: at F54 S55 and P72 R73 (Watanabe et al., 2012). These residues are conserved in WIPI2b (Figure 1.9). Results in Chapter 3 show that Arginines 108 and 125 within loops of blade 3 of WIPI2b are essential for Atg16L1 binding. These Arginines are in loops of blade 3 that form a solute-expose basically charged cleft between blades 2 and 3 of WIPI2. Interestingly, modelling of WIPI2b by Michael Wilson (based on a crystal structure of Hsv2 (Watanabe et al., 2012)) shows that R108 and R125 are proximal to F65 and S66 (corresponding to Atg2 binding site F54, S55 on Atg18) (Figure 6.1). Blades 5 and 6 of proteins in the PROPPIN family mediate membrane interactions (Krick et al., 2012, Baskaran et al., 2012, Watanabe et al., 2012). Therefore, blades 1, 2 and 3 are well positioned to mediate interactions when the β-propeller is membrane bound and it is possible that other PROPPIN proteins function in autophagy by binding their interacting partners at binding sites formed by the loops of blades 2 and 3. Consistently, WIPI1a R110 (the equivalent of WIPI2b R108) is required for WIPI1a function in autophagy (Gaugel et al., 2012). WIPI1a R110A mutants formed starvation- and PtdIns(3)P-independent puncta although the PtdIns(3)P binding ability of this mutant is not changed. These puncta and their effect on autophagy has not been fully characterised, but they are Atg12 positive during starvation conditions. Further work on identifying interacting partners of the PROPPIN family and characterising the functions of these interactions will shed light on the molecular functions of uncharacterised PROPPIN family members such as WIPI1, 3 and 4.

Our model for WIPI2b function is that WIPI2b is recruited to the PtdIs(3)P-positive omegasome, where it subsequently binds Atg16L1 and consequently recruits the Atg12–5-16L1 complex. Evidence for this sequential recruitment comes from live cell imaging: starvation-induced WIPI2b puncta become Atg16L1 positive over time (Dooley et al., 2014). However, in a manner similar to interactions between Atg18 and Atg2 or PtdIns(3)P, the WIPI2b-Atg16L1 and WIPI2b-PtdIns(3)P interactions seem to be independent of each other (Rieter et al., 2013, Obara et al., 2008) (Figures 3.22 and 4.6d). Furthermore, the WIPI2b-Atg16L1 interaction seems to be starvation independent (Figure 3.6). This raises the question of how this interaction is regulated. Although the Atg18-Atg2 interaction is independent of PtdIns(3)P at the whole-cell level, the interaction between these two proteins at the PAS is PtdIns(3)P dependent (Rieter et al., 2013). This was shown using bimolecular fluorescence complementation (BiFC), an assay in which N- and C-terminal fragments of Venus (a yellow fluorescent protein protein) are each fused to the proteins of interest. When the fusion proteins form a complex, the N- and C-terminal fragments are brought into close enough proximity to form a functional fluorescent protein. WIPI2b and Atg16L1 may transiently interact under all conditions, which would make an increase in interaction during starvation or inhibition of PtdIns(3)P binding hard to detect. BiFC assays using fusion proteins of Atg16L1 and WIPI2b could be used to assay the ability of WT WIPI2b and WIPI2b FTTG to form a complex *in vivo* with Atg16L1. Preliminary observations suggest that clustering of WIPI2b, perhaps as a result of concentrated PtdIns(3)P production, may itself be required for Atg16L1 binding. WIPI2b cannot bind to Atg16L1 that does not form dimers even when the residues required for WIPI2b interaction (E226 and E230) are present (Figure 3.11d). The inability of WIPI2b to bind Atg16L1 Δ69-213 could either be because there is a second Atg16L1 binding site within Atg16L1 69-230 (N-terminal to the site that we have identified) or because the weak interaction of WIPI2b and Atg16L1 must be stabilised by two WIPI2b molecules interacting with a dimer of Atg16L1 (Figure 6.2). Validation of this would require detailed mutation analysis of Atg16L1 to disrupt coiled-coil homodimerisation and subsequent analysis of WIPI2b binding. If true, WIPI2b oligomerisation at the omegasome could theoretically be needed to achieve a 2:2 stoichiometry for binding.

Alternatively, WIPI2b-Atg16L1 interaction could be regulated by some as yet undiscovered mechanism. Phosphorylation of WIPI2b S395 does not seem to affect Atg16L1 binding, but paradoxically removing the C-terminus of WIPI2 increases Atg16L1 binding (Figures 5.7 and 3.21). As discussed in Chapter 5.5, investigation of the function of this potential phosphorylation site requires more extensive functional assays. The C-termini of WIPI1 and WIPI2 are not well conserved (Figure 1.9). Therefore, the C-terminus of WIPI1 and WIPI2 may modulate the function of these proteins, as seems to be the case with their ability to bind Atg16L1. The C-terminus of WIPI2b is predicted to be unstructured (Krick et al., 2012) and it is possible that it could function in obscuring binding sites on WIPI2 or enhancing WIPI2 interactions.

Similarly to regulation of Atg16L1 binding, the mechanisms controlling WIPI2-localisation, and that of other PROPPIN family members, to membranes are very poorly understood. Hsv2 binds PtdIns(3)P through a conserved PtdIns(3)P binding FRRG motif and through a membrane insertion loop (Krick et al., 2012, Baskaran et al., 2012, Watanabe et al., 2012) and it is probable that WIPI2 also associates with the membrane through both the FRRG and membrane insertion loop. However, WIPI2 localisation is restricted to PtdIns(3)P pools at the omegasome, rather than other PtdIns(3)P-positive endomembrane structures (Polson et al., 2010). Hydroponic residues within the membrane insertion loop of HSV2 are required for membrane binding (Baskaran et al., 2012). However, whether or not the membrane insertion loop itself plays a role determining the membrane to which PROPPIN proteins are localised remains to be seen. Localisation of Atg18 is restricted both by its binding partner and by PtdIns(3)P binding (Obara et al., 2008, Efe et al., 2007). Although WIPI2b does not need to bind Atg16L1 to localise to omegasomes (Figures 4.4 and 4.7), perhaps its localisation is similarly controlled by an additional interaction partner. Interestingly, a number of ER-localised proteins were identified in Hannah Polson's mass spectrometry screen for WIPI2b interactors (data not shown). Furthermore, Atg18 binding to PtdIns(3,5)P_2 is controlled by phosphorylation within a loop in blade 7 of the β-propeller (Chapter 1.3.4.2) (Tamura et al., 2013). WIPI2 binding to PtdIns(3)P may similarly be controlled by phosphorylation, as discussed in Chapter 5.5. Alternatively, other post-translational modifications may be involved in regulating WIPI2 localisation to the omegasome. Ambra1-dependent ubiquitination of ULK1 promotes ULK1 stabilisation, self-

association and function in autophagy (Nazio et al., 2013). Three sites in WIPI2 were identified in a global screen for ubiquitinated proteins (K198, K205 and K219) (Kim et al., 2011b). These three sites are within blade five of the β-propeller and could potentially interfere with PtdIns(3)P binding if modified with ubiquitin (the FRRG motif is within blade 5).

Results in Chapter 4 show that WIPI2b binding, rather than FIP200 binding, is required for autophagy rescue in Atg16$^{\Delta/\Delta}$ MEFs (Figures 4.13 and 4.14). This raises the question of what the function of FIP200 in starvation-induced autophagy is. Atg16L1 binds FIP200 and ubiquitin and, although when these interactions are inhibited separately there is no effect on starvation-induced autophagy, Atg16L1 unable to bind either protein is not fully functional in starvation-induced autophagy (Fujita et al., 2013). This suggests that FIP200 and ubiquitin binding of Atg16L1 are redundant. PtdIns(3)P production at the omegasome is required for stabilisation of the ULK1 complex (Karanasios et al., 2013a) and it is conceivable that Atg16L1 binding by FIP200 is needed for this stabilisation. ULK1 activation and PtdIns(3)P production on omegasomes by the Vps34 PtdIns(3) kinase complex recruits WIPI2b and subsequently the Atg12–5-16L1 complex. Atg16L1 binding to FIP200 could stabilise ULK1 complex association with the forming autophagosome and, as Atg16L1 recruitment is PtdIns(3)P dependent (through its interaction with WIPI2b), any stabilisation would be PtdIns(3)P dependent. Further work is needed to clarify the function of the Atg16L1-FIP200 interaction.

Atg16L1$^{\Delta/\Delta}$ MEFs have been extremely useful in rescue experiments dissecting the requirement for WIPI2b binding by Atg6L1. Production of a WIPI2 knock out mouse and subsequently a WIPI2$^{-/-}$ cell line would allow further validation of the function of WIPI2b in autophagy and would also be useful in the continuing characterisation of WIPI2. I found that the effect of rescue experiments with WIPI2b RERE (Atg16L1 binding mutant) on autophagy were markedly different in RISC-free treated cells compared to WIPI2 knockdown cells (Figure 4.5). The inhibitory effect of WIPI2b RERE is dependent on depletion of endogenous WIPI2. Using WIPI2$^{-/-}$ MEFs for rescue experiments would ensure that cells contain no residual WIPI2.

In combination with crystal structures of Hsv2, identification of the WIPI2b-Atg16L1 interaction and the mechanism of Atg12–5-16L1 complex recruitment raises

some interesting questions about the orientation of these proteins on the omegasome and forming autophagosome. The orientation of Hsv2 on PtdIns(3)P-positive membrane is restricted by its PtdIns(3)P binding domain and membrane insertion loop, resulting in Hsv2 docking on the membrane through the sides of the β-propeller (rather than face down) with blades 5 and 6 in contact with the membrane (Figure 1.7) (Krick et al., 2012, Baskaran et al., 2012, Watanabe et al., 2012). WIPI2 is probably similarly orientated on PtdIns(3)P-positive omegasomes. Molecular modelling of WIPI2b and Atg16L1 207-165 by Michael Wilson suggests that when WIPI2b binds dimers of Atg16L1 (Atg16L1 forms a parallel coiled-coil dimer (Fujioka et al., 2010)) Atg16L1 must be positioned perpendicular to the membrane on which WIPI2b is docked (Michael Wilson, personal communication). If this is correct, binding of Atg16L1 to WIPI2b in this manner would position the Atg12–5 complex away from the membrane onto which WIPI2b is docked (Figure 6.2) (Michael Wilson, personal communication). Phagophores can form between two leaves of ER cisternae (probably the omegasome) in a manner by which lipidated LC3 does not spread from the phagophore to the ER and PtdIns(3)P is only produced on the omegasome and does not spread to the phagophore (as labelled by DFCP1 localisation) (Yla-Anttila et al., 2009, Hayashi-Nishino et al., 2009, Karanasios et al., 2013a). This arrangement suggests that PtdIns(3)P and its binding partners are spatially distinct from LC3 lipidation and this could be achieved by Atg16L1 being positioned perpendicularly to the omegasome membrane (Figure 6.2). This is a very speculative model and further structural analysis of the positioning of the WIPI2b-Atg16L1 complex on forming autophagosomes will hopefully shed light on this area.

In summary, I have demonstrated that WIPI2b is responsible for Atg16L1 recruitment to PtdIns(3)P-positive forming autophagosomes. Detailed mapping of WIPI2b and FIP200 binding sites on Atg16L1 has enabled me to differentiate between the functions of WIPI2b- and FIP200-binding to Atg16L1 in both starvation- and *Salmonella*-induced autophagy. The close proximity of the WIPI2b and FIP200 binding sites on Atg16L1 suggest that Atg16L1, WIPI2b and FIP200 may be interconnected in some functional or regulatory manner. Furthermore, further work on the PtdIns(3)P-dependent anchoring of the Atg12–5-16L1 complex to membranes by WIPI2b may shed light on the complex membrane dynamics underpinning formation of the autophagosome double membrane.

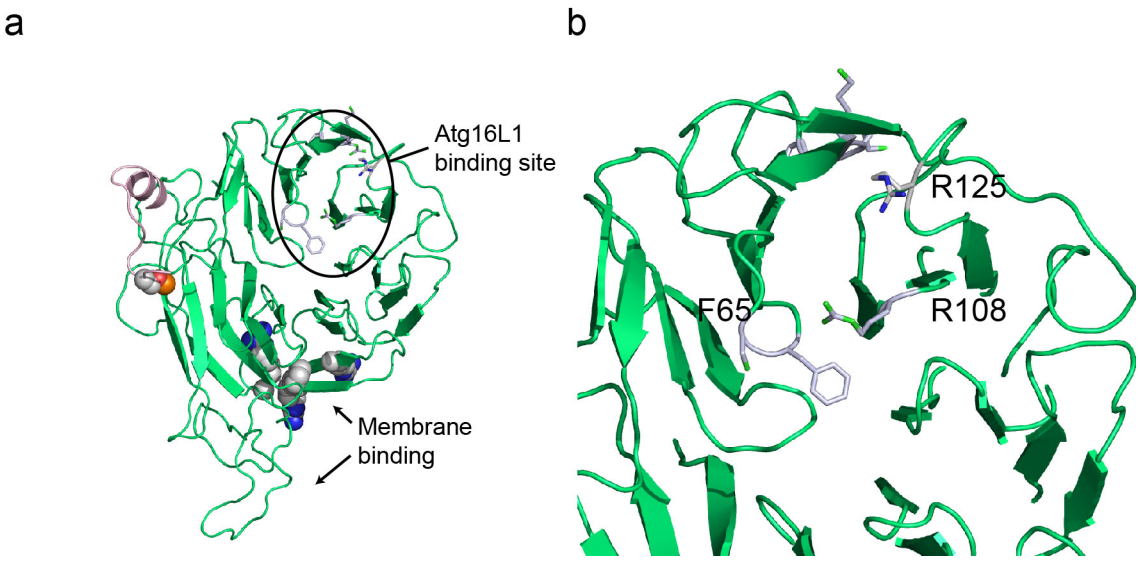

Figure 6.1 Model of WIPI2b

(a) Model for human WIPI2b (14-377) based on the X-ray structure of Hsv2 ((Watanabe et al., 2012);3vu4.pdb) made with the iterative threading assembly refinement (I-TAASER;(Roy et al., 2010)). The Atg16L1-binding cleft between blades 2 and 3 and the membrane binding region in blades 5 and 6 are labelled. **(b)** Zoom of the Atg16L1 binding region circled in **(a)**. F65 is *S. cerevisiae* Atg18 F54. Modelling done and figure provided by Michael Wilson.

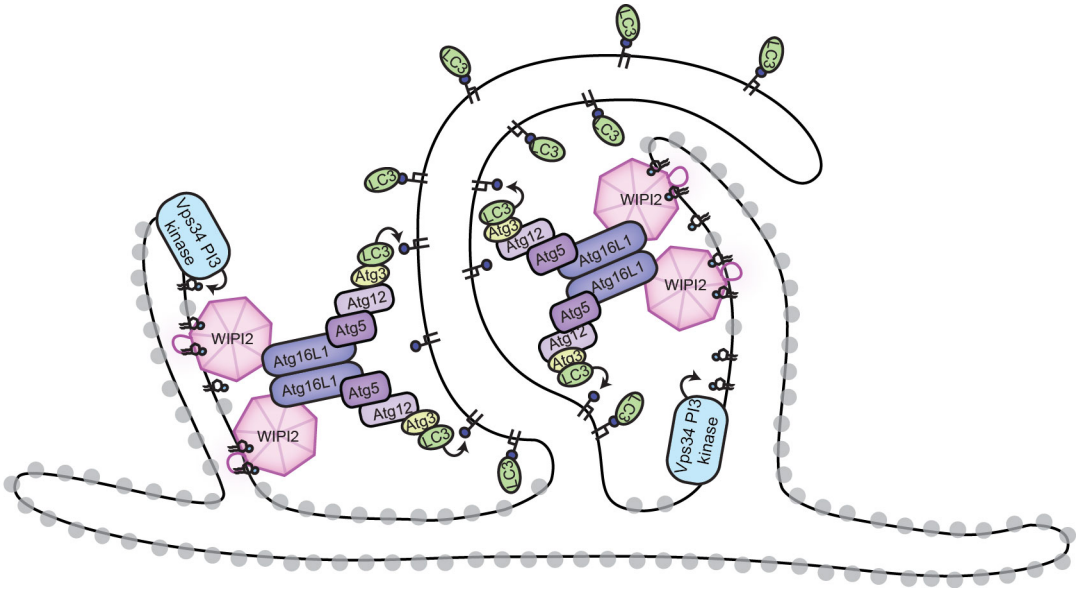

Figure 6.2 Possible arrangement of autophagy proteins on the forming autophagosome

Phagophores can form between two cisternae of the ER (shown with ribosomes). PtdIns(3)P production by the Beclin1 Vps34 PtdIns(3) kinase complex leads to WIPI2b binding. WIPI2b recruits the Atg12–5-16L1 complex, possibly in a perpendicular orientation to the omegasome.

Reference List

AITA, V. M., LIANG, X. H., MURTY, V. V., PINCUS, D. L., YU, W., CAYANIS, E., KALACHIKOV, S., GILLIAM, T. C. & LEVINE, B. 1999. Cloning and genomic organization of beclin 1, a candidate tumor suppressor gene on chromosome 17q21. *Genomics,* 59**,** 59-65.

ALERS, S., LOFFLER, A. S., WESSELBORG, S. & STORK, B. 2012. Role of AMPK-mTOR-Ulk1/2 in the regulation of autophagy: cross talk, shortcuts, and feedbacks. *Mol Cell Biol,* 32**,** 2-11.

AXE, E. L., WALKER, S. A., MANIFAVA, M., CHANDRA, P., RODERICK, H. L., HABERMANN, A., GRIFFITHS, G. & KTISTAKIS, N. T. 2008. Autophagosome formation from membrane compartments enriched in phosphatidylinositol 3-phosphate and dynamically connected to the endoplasmic reticulum. *J Cell Biol,* 182**,** 685-701.

BAR-PELED, L., SCHWEITZER, L. D., ZONCU, R. & SABATINI, D. M. 2012. Ragulator is a GEF for the rag GTPases that signal amino acid levels to mTORC1. *Cell,* 150**,** 1196-208.

BARTH, H., MEILING-WESSE, K., EPPLE, U. D. & THUMM, M. 2001. Autophagy and the cytoplasm to vacuole targeting pathway both require Aut10p. *FEBS Lett,* 508**,** 23-8.

BASKARAN, S., RAGUSA, M. J., BOURA, E. & HURLEY, J. H. 2012. Two-site recognition of phosphatidylinositol 3-phosphate by PROPPINs in autophagy. *Mol Cell,* 47**,** 339-48.

BIRMINGHAM, C. L., SMITH, A. C., BAKOWSKI, M. A., YOSHIMORI, T. & BRUMELL, J. H. 2006. Autophagy controls Salmonella infection in response to damage to the Salmonella-containing vacuole. *J Biol Chem,* 281**,** 11374-83.

BJORKOY, G., LAMARK, T., BRECH, A., OUTZEN, H., PERANDER, M., OVERVATN, A., STENMARK, H. & JOHANSEN, T. 2005. p62/SQSTM1 forms protein aggregates degraded by autophagy and has a protective effect on huntingtin-induced cell death. *J Cell Biol,* 171**,** 603-14.

BRUMELL, J. H., TANG, P., ZAHARIK, M. L. & FINLAY, B. B. 2002. Disruption of the Salmonella-containing vacuole leads to increased replication of Salmonella enterica serovar typhimurium in the cytosol of epithelial cells. *Infect Immun,* 70**,** 3264-70.

CALLAGHAN, J., SIMONSEN, A., GAULLIER, J. M., TOH, B. H. & STENMARK, H. 1999. The endosome fusion regulator early-endosomal autoantigen 1 (EEA1) is a dimer. *Biochem J,* 338 (Pt 2)**,** 539-43.

CAO, Y., NAIR, U., YASUMURA-YORIMITSU, K. & KLIONSKY, D. J. 2009. A multiple ATG gene knockout strain for yeast two-hybrid analysis. *Autophagy,* 5**,** 699-705.

CHAN, E. Y., KIR, S. & TOOZE, S. A. 2007. siRNA screening of the kinome identifies ULK1 as a multidomain modulator of autophagy. *J Biol Chem,* 282**,** 25464-74.

CHAN, E. Y., LONGATTI, A., MCKNIGHT, N. C. & TOOZE, S. A. 2009. Kinase-inactivated ULK proteins inhibit autophagy via their conserved C-terminal domains using an Atg13-independent mechanism. *Mol Cell Biol,* 29**,** 157-71.

CHEUNG, P. C., SALT, I. P., DAVIES, S. P., HARDIE, D. G. & CARLING, D. 2000. Characterization of AMP-activated protein kinase gamma-subunit isoforms and their role in AMP binding. *Biochem J,* 346 Pt 3**,** 659-69.

CIECHANOVER, A. 2005. Intracellular protein degradation: from a vague idea, through the lysosome and the ubiquitin-proteasome system, and onto human diseases and drug targeting (Nobel lecture). *Angew Chem Int Ed Engl,* 44**,** 5944-67.

COHEN, P. 2002. The origins of protein phosphorylation. *Nat Cell Biol,* 4**,** E127-30.

DE DUVE, C. & WATTIAUX, R. 1966. Functions of lysosomes. *Annu Rev Physiol,* 28**,** 435-92.

DI BARTOLOMEO, S., CORAZZARI, M., NAZIO, F., OLIVERIO, S., LISI, G., ANTONIOLI, M., PAGLIARINI, V., MATTEONI, S., FUOCO, C., GIUNTA, L.,

D'AMELIO, M., NARDACCI, R., ROMAGNOLI, A., PIACENTINI, M., CECCONI, F. & FIMIA, G. M. 2010. The dynamic interaction of AMBRA1 with the dynein motor complex regulates mammalian autophagy. *J Cell Biol,* 191**,** 155-68.

DOOLEY, H. C., RAZI, M., POLSON, H. E., GIRARDIN, S. E., WILSON, M. I. & TOOZE, S. A. 2014. WIPI2 Links LC3 Conjugation with PI3P, Autophagosome Formation, and Pathogen Clearance by Recruiting Atg12-5-16L1. *Mol Cell,* 55**,** 238-52.

DUNLOP, E. A., HUNT, D. K., ACOSTA-JAQUEZ, H. A., FINGAR, D. C. & TEE, A. R. 2011. ULK1 inhibits mTORC1 signaling, promotes multisite Raptor phosphorylation and hinders substrate binding. *Autophagy,* 7**,** 737-47.

DUNN, W. A., JR. 1990. Studies on the mechanisms of autophagy: formation of the autophagic vacuole. *J Cell Biol,* 110**,** 1923-33.

EFE, J. A., BOTELHO, R. J. & EMR, S. D. 2007. Atg18 regulates organelle morphology and Fab1 kinase activity independent of its membrane recruitment by phosphatidylinositol 3,5-bisphosphate. *Mol Biol Cell,* 18**,** 4232-44.

EGAN, D. F., SHACKELFORD, D. B., MIHAYLOVA, M. M., GELINO, S., KOHNZ, R. A., MAIR, W., VASQUEZ, D. S., JOSHI, A., GWINN, D. M., TAYLOR, R., ASARA, J. M., FITZPATRICK, J., DILLIN, A., VIOLLET, B., KUNDU, M., HANSEN, M. & SHAW, R. J. 2011. Phosphorylation of ULK1 (hATG1) by AMP-activated protein kinase connects energy sensing to mitophagy. *Science,* 331**,** 456-61.

FAN, W., NASSIRI, A. & ZHONG, Q. 2011. Autophagosome targeting and membrane curvature sensing by Barkor/Atg14(L). *Proc Natl Acad Sci U S A,* 108**,** 7769-74.

FIMIA, G. M., STOYKOVA, A., ROMAGNOLI, A., GIUNTA, L., DI BARTOLOMEO, S., NARDACCI, R., CORAZZARI, M., FUOCO, C., UCAR, A., SCHWARTZ, P., GRUSS, P., PIACENTINI, M., CHOWDHURY, K. & CECCONI, F. 2007. Ambra1 regulates autophagy and development of the nervous system. *Nature,* 447**,** 1121-5.

FINLAY, B. B. & BRUMELL, J. H. 2000. Salmonella interactions with host cells: in vitro to in vivo. *Philos Trans R Soc Lond B Biol Sci,* 355**,** 623-31.

FOSTER, F. M., TRAER, C. J., ABRAHAM, S. M. & FRY, M. J. 2003. The phosphoinositide (PI) 3-kinase family. *J Cell Sci,* 116**,** 3037-40.

FUJIOKA, Y., NODA, N. N., NAKATOGAWA, H., OHSUMI, Y. & INAGAKI, F. 2010. Dimeric coiled-coil structure of Saccharomyces cerevisiae Atg16 and its functional significance in autophagy. *J Biol Chem,* 285**,** 1508-15.

FUJITA, N., ITOH, T., OMORI, H., FUKUDA, M., NODA, T. & YOSHIMORI, T. 2008. The Atg16L complex specifies the site of LC3 lipidation for membrane biogenesis in autophagy. *Mol Biol Cell,* 19**,** 2092-100.

FUJITA, N., MORITA, E., ITOH, T., TANAKA, A., NAKAOKA, M., OSADA, Y., UMEMOTO, T., SAITOH, T., NAKATOGAWA, H., KOBAYASHI, S., HARAGUCHI, T., GUAN, J. L., IWAI, K., TOKUNAGA, F., SAITO, K., ISHIBASHI, K., AKIRA, S., FUKUDA, M., NODA, T. & YOSHIMORI, T. 2013. Recruitment of the autophagic machinery to endosomes during infection is mediated by ubiquitin. *J Cell Biol,* 203**,** 115-28.

FUJITA, N., SAITOH, T., KAGEYAMA, S., AKIRA, S., NODA, T. & YOSHIMORI, T. 2009. Differential involvement of Atg16L1 in Crohn disease and canonical autophagy: analysis of the organization of the Atg16L1 complex in fibroblasts. *J Biol Chem,* 284**,** 32602-9.

FUKUDA, M. & ITOH, T. 2008. Direct link between Atg protein and small GTPase Rab: Atg16L functions as a potential Rab33 effector in mammals. *Autophagy,* 4**,** 824-6.

GAMMOH, N., FLOREY, O., OVERHOLTZER, M. & JIANG, X. 2013. Interaction between FIP200 and ATG16L1 distinguishes ULK1 complex-dependent and -independent autophagy. *Nat Struct Mol Biol,* 20**,** 144-9.

GAN, B., PENG, X., NAGY, T., ALCARAZ, A., GU, H. & GUAN, J. L. 2006. Role of FIP200 in cardiac and liver development and its regulation of TNFalpha and TSC-mTOR signaling pathways. *J Cell Biol,* 175**,** 121-33.

GAUGEL, A., BAKULA, D., HOFFMANN, A. & PROIKAS-CEZANNE, T. 2012. Defining regulatory and phosphoinositide-binding sites in the human WIPI-1 beta-propeller responsible for autophagosomal membrane localization downstream of mTORC1 inhibition. *J Mol Signal,* 7**,** 16.

GE, L., MELVILLE, D., ZHANG, M. & SCHEKMAN, R. 2013. The ER-Golgi intermediate compartment is a key membrane source for the LC3 lipidation step of autophagosome biogenesis. *Elife,* 2**,** e00947.

GENG, J., NAIR, U., YASUMURA-YORIMITSU, K. & KLIONSKY, D. J. 2010. Post-Golgi Sec proteins are required for autophagy in Saccharomyces cerevisiae. *Mol Biol Cell,* 21**,** 2257-69.

GOMES, L. C. & DIKIC, I. 2014. Autophagy in Antimicrobial Immunity. *Mol Cell,* 54**,** 224-233.

GORVEL, J. P. & MERESSE, S. 2001. Maturation steps of the Salmonella-containing vacuole. *Microbes Infect,* 3**,** 1299-303.

HAMASAKI, M., FURUTA, N., MATSUDA, A., NEZU, A., YAMAMOTO, A., FUJITA, N., OOMORI, H., NODA, T., HARAGUCHI, T., HIRAOKA, Y., AMANO, A. & YOSHIMORI, T. 2013. Autophagosomes form at ER-mitochondria contact sites. *Nature,* 495**,** 389-93.

HARA, T., TAKAMURA, A., KISHI, C., IEMURA, S., NATSUME, T., GUAN, J. L. & MIZUSHIMA, N. 2008. FIP200, a ULK-interacting protein, is required for autophagosome formation in mammalian cells. *J Cell Biol,* 181**,** 497-510.

HARDING, T. M., MORANO, K. A., SCOTT, S. V. & KLIONSKY, D. J. 1995. Isolation and characterization of yeast mutants in the cytoplasm to vacuole protein targeting pathway. *J Cell Biol,* 131**,** 591-602.

HAYASHI-NISHINO, M., FUJITA, N., NODA, T., YAMAGUCHI, A., YOSHIMORI, T. & YAMAMOTO, A. 2009. A subdomain of the endoplasmic reticulum forms a cradle for autophagosome formation. *Nat Cell Biol,* 11**,** 1433-7.

HORNBECK, P. V., KORNHAUSER, J. M., TKACHEV, S., ZHANG, B., SKRZYPEK, E., MURRAY, B., LATHAM, V. & SULLIVAN, M. 2012. PhosphoSitePlus: a comprehensive resource for investigating the structure and function of experimentally determined post-translational modifications in man and mouse. *Nucleic Acids Res,* 40**,** D261-70.

HOSOKAWA, N., HARA, T., KAIZUKA, T., KISHI, C., TAKAMURA, A., MIURA, Y., IEMURA, S., NATSUME, T., TAKEHANA, K., YAMADA, N., GUAN, J. L., OSHIRO, N. & MIZUSHIMA, N. 2009a. Nutrient-dependent mTORC1 association with the ULK1-Atg13-FIP200 complex required for autophagy. *Mol Biol Cell,* 20**,** 1981-91.

HOSOKAWA, N., SASAKI, T., IEMURA, S., NATSUME, T., HARA, T. & MIZUSHIMA, N. 2009b. Atg101, a novel mammalian autophagy protein interacting with Atg13. *Autophagy,* 5**,** 973-9.

HSU, P. P., KANG, S. A., RAMESEDER, J., ZHANG, Y., OTTINA, K. A., LIM, D., PETERSON, T. R., CHOI, Y., GRAY, N. S., YAFFE, M. B., MARTO, J. A. & SABATINI, D. M. 2011. The mTOR-regulated phosphoproteome reveals a mechanism of mTORC1-mediated inhibition of growth factor signaling. *Science,* 332**,** 1317-22.

HUANG, J., BIRMINGHAM, C. L., SHAHNAZARI, S., SHIU, J., ZHENG, Y. T., SMITH, A. C., CAMPELLONE, K. G., HEO, W. D., GRUENHEID, S., MEYER, T., WELCH, M. D., KTISTAKIS, N. T., KIM, P. K., KLIONSKY, D. J. & BRUMELL, J. H. 2011. Antibacterial autophagy occurs at PI(3)P-enriched domains of the endoplasmic reticulum and requires Rab1 GTPase. *Autophagy,* 7**,** 17-26.

ICHIMURA, Y., KIRISAKO, T., TAKAO, T., SATOMI, Y., SHIMONISHI, Y., ISHIHARA, N., MIZUSHIMA, N., TANIDA, I., KOMINAMI, E., OHSUMI, M., NODA, T. & OHSUMI, Y. 2000. A ubiquitin-like system mediates protein lipidation. *Nature,* 408**,** 488-92.

IHLING, C., SCHMIDT, A., KALKHOF, S., SCHULZ, D. M., STINGL, C., MECHTLER, K., HAACK, M., BECK-SICKINGER, A. G., COOPER, D. M. & SINZ, A. 2006. Isotope-labeled cross-linkers and Fourier transform ion cyclotron resonance mass spectrometry for structural analysis of a protein/peptide complex. *J Am Soc Mass Spectrom,* 17**,** 1100-13.

ISHIBASHI, K., FUJITA, N., KANNO, E., OMORI, H., YOSHIMORI, T., ITOH, T. & FUKUDA, M. 2011. Atg16L2, a novel isoform of mammalian Atg16L that is not essential for canonical autophagy despite forming an Atg12-5-16L2 complex. *Autophagy,* 7**,** 1500-13.

ITAKURA, E., KISHI, C., INOUE, K. & MIZUSHIMA, N. 2008. Beclin 1 forms two distinct phosphatidylinositol 3-kinase complexes with mammalian Atg14 and UVRAG. *Mol Biol Cell,* 19**,** 5360-72.

ITAKURA, E., KISHI-ITAKURA, C. & MIZUSHIMA, N. 2012. The hairpin-type tail-anchored SNARE syntaxin 17 targets to autophagosomes for fusion with endosomes/lysosomes. *Cell,* 151**,** 1256-69.

ITAKURA, E. & MIZUSHIMA, N. 2010. Characterization of autophagosome formation site by a hierarchical analysis of mammalian Atg proteins. *Autophagy,* 6**,** 764-76.

ITAKURA, E. & MIZUSHIMA, N. 2011. p62 Targeting to the autophagosome formation site requires self-oligomerization but not LC3 binding. *J Cell Biol,* 192**,** 17-27.

ITOH, T., KANNO, E., UEMURA, T., WAGURI, S. & FUKUDA, M. 2011. OATL1, a novel autophagosome-resident Rab33B-GAP, regulates autophagosomal maturation. *J Cell Biol,* 192**,** 839-53.

JIA, K., THOMAS, C., AKBAR, M., SUN, Q., ADAMS-HUET, B., GILPIN, C. & LEVINE, B. 2009. Autophagy genes protect against Salmonella typhimurium infection and mediate insulin signaling-regulated pathogen resistance. *Proc Natl Acad Sci U S A,* 106**,** 14564-9.

JIANG, P. & MIZUSHIMA, N. 2014. Autophagy and human diseases. *Cell Res,* 24**,** 69-79.

JIANG, P., NISHIMURA, T., SAKAMAKI, Y., ITAKURA, E., HATTA, T., NATSUME, T. & MIZUSHIMA, N. 2014. The HOPS complex mediates autophagosome-lysosome fusion through interaction with syntaxin 17. *Mol Biol Cell,* 25**,** 1327-37.

JUNG, C. H., JUN, C. B., RO, S. H., KIM, Y. M., OTTO, N. M., CAO, J., KUNDU, M. & KIM, D. H. 2009. ULK-Atg13-FIP200 complexes mediate mTOR signaling to the autophagy machinery. *Mol Biol Cell,* 20**,** 1992-2003.

KABEYA, Y., KAMADA, Y., BABA, M., TAKIKAWA, H., SASAKI, M. & OHSUMI, Y. 2005. Atg17 functions in cooperation with Atg1 and Atg13 in yeast autophagy. *Mol Biol Cell,* 16**,** 2544-53.

KABEYA, Y., MIZUSHIMA, N., UENO, T., YAMAMOTO, A., KIRISAKO, T., NODA, T., KOMINAMI, E., OHSUMI, Y. & YOSHIMORI, T. 2000. LC3, a mammalian homologue of yeast Apg8p, is localized in autophagosome membranes after processing. *EMBO J,* 19**,** 5720-8.

KABEYA, Y., MIZUSHIMA, N., YAMAMOTO, A., OSHITANI-OKAMOTO, S., OHSUMI, Y. & YOSHIMORI, T. 2004. LC3, GABARAP and GATE16 localize to autophagosomal membrane depending on form-II formation. *J Cell Sci,* 117**,** 2805-12.

KAGEYAMA, S., OMORI, H., SAITOH, T., SONE, T., GUAN, J. L., AKIRA, S., IMAMOTO, F., NODA, T. & YOSHIMORI, T. 2011. The LC3 recruitment mechanism is separate from Atg9L1-dependent membrane formation in the autophagic response against Salmonella. *Mol Biol Cell,* 22**,** 2290-300.

KAMADA, Y., FUNAKOSHI, T., SHINTANI, T., NAGANO, K., OHSUMI, M. & OHSUMI, Y. 2000. Tor-mediated induction of autophagy via an Apg1 protein kinase complex. *J Cell Biol,* 150**,** 1507-13.

KAMADA, Y., YOSHINO, K., KONDO, C., KAWAMATA, T., OSHIRO, N., YONEZAWA, K. & OHSUMI, Y. 2010. Tor directly controls the Atg1 kinase complex to regulate autophagy. *Mol Cell Biol,* 30**,** 1049-58.

KARANASIOS, E., STAPLETON, E., MANIFAVA, M., KAIZUKA, T., MIZUSHIMA, N., WALKER, S. A. & KTISTAKIS, N. T. 2013a. Dynamic association of the ULK1 complex with omegasomes during autophagy induction. *J Cell Sci,* 126**,** 5224-38.

KARANASIOS, E., STAPLETON, E., WALKER, S. A., MANIFAVA, M. & KTISTAKIS, N. T. 2013b. Live cell imaging of early autophagy events: omegasomes and beyond. *J Vis Exp*.

KAWAMATA, T., KAMADA, Y., KABEYA, Y., SEKITO, T. & OHSUMI, Y. 2008. Organization of the pre-autophagosomal structure responsible for autophagosome formation. *Mol Biol Cell,* 19**,** 2039-50.

KIM, J., KIM, Y. C., FANG, C., RUSSELL, R. C., KIM, J. H., FAN, W., LIU, R., ZHONG, Q. & GUAN, K. L. 2013. Differential regulation of distinct Vps34 complexes by AMPK in nutrient stress and autophagy. *Cell,* 152**,** 290-303.

KIM, J., KUNDU, M., VIOLLET, B. & GUAN, K. L. 2011a. AMPK and mTOR regulate autophagy through direct phosphorylation of Ulk1. *Nat Cell Biol,* 13**,** 132-41.

KIM, P. K., HAILEY, D. W., MULLEN, R. T. & LIPPINCOTT-SCHWARTZ, J. 2008. Ubiquitin signals autophagic degradation of cytosolic proteins and peroxisomes. *Proc Natl Acad Sci U S A,* 105**,** 20567-74.

KIM, W., BENNETT, E. J., HUTTLIN, E. L., GUO, A., LI, J., POSSEMATO, A., SOWA, M. E., RAD, R., RUSH, J., COMB, M. J., HARPER, J. W. & GYGI, S. P. 2011b. Systematic and quantitative assessment of the ubiquitin-modified proteome. *Mol Cell,* 44**,** 325-40.

KOBAYASHI, T., SUZUKI, K. & OHSUMI, Y. 2012. Autophagosome formation can be achieved in the absence of Atg18 by expressing engineered PAS-targeted Atg2. *FEBS Lett,* 586**,** 2473-8.

KRICK, R., BUSSE, R. A., SCACIOC, A., STEPHAN, M., JANSHOFF, A., THUMM, M. & KUHNEL, K. 2012. Structural and functional characterization of the two phosphoinositide binding sites of PROPPINs, a beta-propeller protein family. *Proc Natl Acad Sci U S A,* 109**,** E2042-9.

KRICK, R., HENKE, S., TOLSTRUP, J. & THUMM, M. 2008. Dissecting the localization and function of Atg18, Atg21 and Ygr223c. *Autophagy,* 4**,** 896-910.

KRICK, R., TOLSTRUP, J., APPELLES, A., HENKE, S. & THUMM, M. 2006. The relevance of the phosphatidylinositolphosphat-binding motif FRRGT of Atg18 and Atg21 for the Cvt pathway and autophagy. *FEBS Lett,* 580**,** 4632-8.

KUMA, A., HATANO, M., MATSUI, M., YAMAMOTO, A., NAKAYA, H., YOSHIMORI, T., OHSUMI, Y., TOKUHISA, T. & MIZUSHIMA, N. 2004. The role of autophagy during the early neonatal starvation period. *Nature,* 432**,** 1032-6.

LAMB, C. A., YOSHIMORI, T. & TOOZE, S. A. 2013. The autophagosome: origins unknown, biogenesis complex. *Nat Rev Mol Cell Biol,* 14**,** 759-74.

LAPLANTE, M. & SABATINI, D. M. 2012. mTOR signaling in growth control and disease. *Cell,* 149**,** 274-93.

LI, W. W., LI, J. & BAO, J. K. 2012. Microautophagy: lesser-known self-eating. *Cell Mol Life Sci,* 69**,** 1125-36.

LIANG, C., FENG, P., KU, B., DOTAN, I., CANAANI, D., OH, B. H. & JUNG, J. U. 2006. Autophagic and tumour suppressor activity of a novel Beclin1-binding protein UVRAG. *Nat Cell Biol,* 8**,** 688-99.

LIANG, C., LEE, J. S., INN, K. S., GACK, M. U., LI, Q., ROBERTS, E. A., VERGNE, I., DERETIC, V., FENG, P., AKAZAWA, C. & JUNG, J. U. 2008. Beclin1-binding UVRAG targets the class C Vps complex to coordinate autophagosome maturation and endocytic trafficking. *Nat Cell Biol,* 10**,** 776-87.

LIANG, X. H., JACKSON, S., SEAMAN, M., BROWN, K., KEMPKES, B., HIBSHOOSH, H. & LEVINE, B. 1999. Induction of autophagy and inhibition of tumorigenesis by beclin 1. *Nature,* 402**,** 672-6.

LIU, H., HE, Z., VON RUTTE, T., YOUSEFI, S., HUNGER, R. E. & SIMON, H. U. 2013. Down-regulation of autophagy-related protein 5 (ATG5) contributes to the pathogenesis of early-stage cutaneous melanoma. *Sci Transl Med,* 5**,** 202ra123.

LONGATTI, A., LAMB, C. A., RAZI, M., YOSHIMURA, S., BARR, F. A. & TOOZE, S. A. 2012. TBC1D14 regulates autophagosome formation via Rab11- and ULK1-positive recycling endosomes. *J Cell Biol,* 197**,** 659-75.

LU, J., HE, L., BEHRENDS, C., ARAKI, M., ARAKI, K., JUN WANG, Q., CATANZARO, J. M., FRIEDMAN, S. L., ZONG, W. X., FIEL, M. I., LI, M. & YUE, Z. 2014. NRBF2 regulates autophagy and prevents liver injury by modulating Atg14L-linked phosphatidylinositol-3 kinase III activity. *Nat Commun,* 5**,** 3920.

LU, Q., YANG, P., HUANG, X., HU, W., GUO, B., WU, F., LIN, L., KOVACS, A. L., YU, L. & ZHANG, H. 2011. The WD40 repeat PtdIns(3)P-binding protein EPG-6 regulates progression of omegasomes to autophagosomes. *Dev Cell,* 21**,** 343-57.

LYSKOV, S. & GRAY, J. J. 2008. The RosettaDock server for local protein-protein docking. *Nucleic Acids Res,* 36**,** W233-8.

MARI, M., GRIFFITH, J., RIETER, E., KRISHNAPPA, L., KLIONSKY, D. J. & REGGIORI, F. 2010. An Atg9-containing compartment that functions in the early steps of autophagosome biogenesis. *J Cell Biol,* 190**,** 1005-22.

MARINO, G., URIA, J. A., PUENTE, X. S., QUESADA, V., BORDALLO, J. & LOPEZ-OTIN, C. 2003. Human autophagins, a family of cysteine proteinases potentially implicated in cell degradation by autophagy. *J Biol Chem,* 278**,** 3671-8.

MATSUNAGA, K., MORITA, E., SAITOH, T., AKIRA, S., KTISTAKIS, N. T., IZUMI, T., NODA, T. & YOSHIMORI, T. 2010. Autophagy requires endoplasmic reticulum targeting of the PI3-kinase complex via Atg14L. *J Cell Biol,* 190**,** 511-21.

MATSUNAGA, K., SAITOH, T., TABATA, K., OMORI, H., SATOH, T., KUROTORI, N., MAEJIMA, I., SHIRAHAMA-NODA, K., ICHIMURA, T., ISOBE, T., AKIRA, S., NODA, T. & YOSHIMORI, T. 2009. Two Beclin 1-binding proteins, Atg14L and Rubicon, reciprocally regulate autophagy at different stages. *Nat Cell Biol,* 11**,** 385-96.

MAUTHE, M., JACOB, A., FREIBERGER, S., HENTSCHEL, K., STIERHOF, Y. D., CODOGNO, P. & PROIKAS-CEZANNE, T. 2011. Resveratrol-mediated autophagy requires WIPI-1-regulated LC3 lipidation in the absence of induced phagophore formation. *Autophagy,* 7**,** 1448-61.

MCALPINE, F., WILLIAMSON, L. E., TOOZE, S. A. & CHAN, E. Y. 2013. Regulation of nutrient-sensitive autophagy by uncoordinated 51-like kinases 1 and 2. *Autophagy,* 9**,** 361-73.

MEILING-WESSE, K., BARTH, H., VOSS, C., ESKELINEN, E. L., EPPLE, U. D. & THUMM, M. 2004. Atg21 is required for effective recruitment of Atg8 to the preautophagosomal structure during the Cvt pathway. *J Biol Chem,* 279**,** 37741-50.

MIJALJICA, D., PRESCOTT, M. & DEVENISH, R. J. 2011. Microautophagy in mammalian cells: revisiting a 40-year-old conundrum. *Autophagy,* 7**,** 673-82.

MIZUSHIMA, N., KUMA, A., KOBAYASHI, Y., YAMAMOTO, A., MATSUBAE, M., TAKAO, T., NATSUME, T., OHSUMI, Y. & YOSHIMORI, T. 2003. Mouse Apg16L, a novel WD-repeat protein, targets to the autophagic isolation membrane with the Apg12-Apg5 conjugate. *J Cell Sci,* 116**,** 1679-88.

MIZUSHIMA, N., SUGITA, H., YOSHIMORI, T. & OHSUMI, Y. 1998. A new protein conjugation system in human. The counterpart of the yeast Apg12p conjugation system essential for autophagy. *J Biol Chem,* 273**,** 33889-92.

MIZUSHIMA, N., YAMAMOTO, A., HATANO, M., KOBAYASHI, Y., KABEYA, Y., SUZUKI, K., TOKUHISA, T., OHSUMI, Y. & YOSHIMORI, T. 2001. Dissection of autophagosome formation using Apg5-deficient mouse embryonic stem cells. *J Cell Biol,* 152**,** 657-68.

MOREAU, K., RAVIKUMAR, B., RENNA, M., PURI, C. & RUBINSZTEIN, D. C. 2011. Autophagosome precursor maturation requires homotypic fusion. *Cell,* 146**,** 303-17.

MURTHY, A., LI, Y., PENG, I., REICHELT, M., KATAKAM, A. K., NOUBADE, R., ROOSE-GIRMA, M., DEVOSS, J., DIEHL, L., GRAHAM, R. R. & VAN LOOKEREN CAMPAGNE, M. 2014. A Crohn's disease variant in Atg16l1 enhances its degradation by caspase 3. *Nature,* 506**,** 456-62.

NAIR, U., CAO, Y., XIE, Z. & KLIONSKY, D. J. 2010. Roles of the lipid-binding motifs of Atg18 and Atg21 in the cytoplasm to vacuole targeting pathway and autophagy. *J Biol Chem,* 285**,** 11476-88.

NAIR, U., YEN, W. L., MARI, M., CAO, Y., XIE, Z., BABA, M., REGGIORI, F. & KLIONSKY, D. J. 2012. A role for Atg8-PE deconjugation in autophagosome biogenesis. *Autophagy,* 8**,** 780-93.

NAKAMURA, T., HAYASHI, T., NASU-NISHIMURA, Y., SAKAUE, F., MORISHITA, Y., OKABE, T., OHWADA, S., MATSUURA, K. & AKIYAMA, T. 2008. PX-RICS mediates ER-to-Golgi transport of the N-cadherin/beta-catenin complex. *Genes Dev,* 22**,** 1244-56.

NAKATOGAWA, H., ICHIMURA, Y. & OHSUMI, Y. 2007. Atg8, a ubiquitin-like protein required for autophagosome formation, mediates membrane tethering and hemifusion. *Cell,* 130**,** 165-78.

NAZIO, F., STRAPPAZZON, F., ANTONIOLI, M., BIELLI, P., CIANFANELLI, V., BORDI, M., GRETZMEIER, C., DENGJEL, J., PIACENTINI, M., FIMIA, G. M. & CECCONI, F. 2013. mTOR inhibits autophagy by controlling ULK1 ubiquitylation, self-association and function through AMBRA1 and TRAF6. *Nat Cell Biol,* 15**,** 406-16.

NISHIMURA, T., KAIZUKA, T., CADWELL, K., SAHANI, M. H., SAITOH, T., AKIRA, S., VIRGIN, H. W. & MIZUSHIMA, N. 2013. FIP200 regulates targeting of Atg16L1 to the isolation membrane. *EMBO Rep,* 14**,** 284-91.

NODA, N. N., FUJIOKA, Y., HANADA, T., OHSUMI, Y. & INAGAKI, F. 2013. Structure of the Atg12-Atg5 conjugate reveals a platform for stimulating Atg8-PE conjugation. *EMBO Rep,* 14**,** 206-11.

NODA, T., KIM, J., HUANG, W. P., BABA, M., TOKUNAGA, C., OHSUMI, Y. & KLIONSKY, D. J. 2000. Apg9p/Cvt7p is an integral membrane protein required for transport vesicle formation in the Cvt and autophagy pathways. *J Cell Biol,* 148**,** 465-80.

NOJIMA, H., TOKUNAGA, C., EGUCHI, S., OSHIRO, N., HIDAYAT, S., YOSHINO, K., HARA, K., TANAKA, N., AVRUCH, J. & YONEZAWA, K. 2003. The mammalian target of rapamycin (mTOR) partner, raptor, binds the mTOR substrates p70 S6 kinase and 4E-BP1 through their TOR signaling (TOS) motif. *J Biol Chem,* 278**,** 15461-4.

OBARA, K., SEKITO, T., NIIMI, K. & OHSUMI, Y. 2008. The Atg18-Atg2 complex is recruited to autophagic membranes via phosphatidylinositol 3-phosphate and exerts an essential function. *J Biol Chem,* 283**,** 23972-80.

OGAWA, M., YOSHIKAWA, Y., KOBAYASHI, T., MIMURO, H., FUKUMATSU, M., KIGA, K., PIAO, Z., ASHIDA, H., YOSHIDA, M., KAKUTA, S., KOYAMA, T., GOTO, Y., NAGATAKE, T., NAGAI, S., KIYONO, H., KAWALEC, M., REICHHART, J. M. & SASAKAWA, C. 2011. A Tecpr1-dependent selective autophagy pathway targets bacterial pathogens. *Cell Host Microbe,* 9**,** 376-89.

OHASHI, Y. & MUNRO, S. 2010. Membrane delivery to the yeast autophagosome from the Golgi-endosomal system. *Mol Biol Cell,* 21**,** 3998-4008.

OHSUMI, Y. 2014. Historical landmarks of autophagy research. *Cell Res,* 24**,** 9-23.

ORENSTEIN, S. J. & CUERVO, A. M. 2010. Chaperone-mediated autophagy: molecular mechanisms and physiological relevance. *Semin Cell Dev Biol,* 21**,** 719-26.

ORSI, A., RAZI, M., DOOLEY, H. C., ROBINSON, D., WESTON, A. E., COLLINSON, L. M. & TOOZE, S. A. 2012. Dynamic and transient interactions of Atg9 with autophagosomes, but not membrane integration, are required for autophagy. *Mol Biol Cell,* 23**,** 1860-73.

OTTO, G. P., RAZI, M., MORVAN, J., STENNER, F. & TOOZE, S. A. 2010. A novel syntaxin 6-interacting protein, SHIP164, regulates syntaxin 6-dependent sorting from early endosomes. *Traffic,* 11**,** 688-705.

PANARETOU, C., DOMIN, J., COCKCROFT, S. & WATERFIELD, M. D. 1997. Characterization of p150, an adaptor protein for the human phosphatidylinositol (PtdIns) 3-kinase. Substrate presentation by phosphatidylinositol transfer protein to the p150.Ptdins 3-kinase complex. *J Biol Chem,* 272**,** 2477-85.

PANKIV, S., CLAUSEN, T. H., LAMARK, T., BRECH, A., BRUUN, J. A., OUTZEN, H., OVERVATN, A., BJORKOY, G. & JOHANSEN, T. 2007. p62/SQSTM1 binds directly to Atg8/LC3 to facilitate degradation of ubiquitinated protein aggregates by autophagy. *J Biol Chem,* 282**,** 24131-45.

PAPINSKI, D., SCHUSCHNIG, M., REITER, W., WILHELM, L., BARNES, C. A., MAIOLICA, A., HANSMANN, I., PFAFFENWIMMER, T., KIJANSKA, M., STOFFEL, I., LEE, S. S., BREZOVICH, A., LOU, J. H., TURK, B. E., AEBERSOLD, R., AMMERER, G., PETER, M. & KRAFT, C. 2014. Early steps in autophagy depend on direct phosphorylation of Atg9 by the Atg1 kinase. *Mol Cell,* 53**,** 471-83.

PIERCE, B. G., HOURAI, Y. & WENG, Z. 2011. Accelerating protein docking in ZDOCK using an advanced 3D convolution library. *PLoS One,* 6**,** e24657.

POLSON, H. E., DE LARTIGUE, J., RIGDEN, D. J., REEDIJK, M., URBE, S., CLAGUE, M. J. & TOOZE, S. A. 2010. Mammalian Atg18 (WIPI2) localizes to omegasome-anchored phagophores and positively regulates LC3 lipidation. *Autophagy,* 6.

PREKERIS, R., KLUMPERMAN, J., CHEN, Y. A. & SCHELLER, R. H. 1998. Syntaxin 13 mediates cycling of plasma membrane proteins via tubulovesicular recycling endosomes. *J Cell Biol,* 143**,** 957-71.

PROIKAS-CEZANNE, T., WADDELL, S., GAUGEL, A., FRICKEY, T., LUPAS, A. & NORDHEIM, A. 2004. WIPI-1alpha (WIPI49), a member of the novel 7-bladed WIPI protein family, is aberrantly expressed in human cancer and is linked to starvation-induced autophagy. *Oncogene,* 23**,** 9314-25.

PURI, C., RENNA, M., BENTO, C. F., MOREAU, K. & RUBINSZTEIN, D. C. 2013. Diverse autophagosome membrane sources coalesce in recycling endosomes. *Cell,* 154**,** 1285-99.

QUAN, W., LIM, Y. M. & LEE, M. S. 2012. Role of autophagy in diabetes and endoplasmic reticulum stress of pancreatic beta-cells. *Exp Mol Med,* 44**,** 81-8.

RAVIKUMAR, B., MOREAU, K., JAHREISS, L., PURI, C. & RUBINSZTEIN, D. C. 2010. Plasma membrane contributes to the formation of pre-autophagosomal structures. *Nat Cell Biol,* 12**,** 747-57.

REGGIORI, F., TUCKER, K. A., STROMHAUG, P. E. & KLIONSKY, D. J. 2004. The Atg1-Atg13 complex regulates Atg9 and Atg23 retrieval transport from the pre-autophagosomal structure. *Dev Cell,* 6**,** 79-90.

RIETER, E., VINKE, F., BAKULA, D., CEBOLLERO, E., UNGERMANN, C., PROIKAS-CEZANNE, T. & REGGIORI, F. 2013. Atg18 function in autophagy is regulated by specific sites within its beta-propeller. *J Cell Sci,* 126**,** 593-604.

ROMANOV, J., WALCZAK, M., IBIRICU, I., SCHUCHNER, S., OGRIS, E., KRAFT, C. & MARTENS, S. 2012. Mechanism and functions of membrane binding by the Atg5-Atg12/Atg16 complex during autophagosome formation. *EMBO J,* 31**,** 4304-17.

ROUX, K. J., KIM, D. I., RAIDA, M. & BURKE, B. 2012. A promiscuous biotin ligase fusion protein identifies proximal and interacting proteins in mammalian cells. *J Cell Biol,* 196**,** 801-10.

ROY, A., KUCUKURAL, A. & ZHANG, Y. 2010. I-TASSER: a unified platform for automated protein structure and function prediction. *Nat Protoc,* 5**,** 725-38.

RUSSELL, R. C., TIAN, Y., YUAN, H., PARK, H. W., CHANG, Y. Y., KIM, J., KIM, H., NEUFELD, T. P., DILLIN, A. & GUAN, K. L. 2013. ULK1 induces autophagy by phosphorylating Beclin-1 and activating VPS34 lipid kinase. *Nat Cell Biol,* 15**,** 741-50.

SABATINI, D. D. & ADESNIK, M. 2013. Christian de Duve: Explorer of the cell who discovered new organelles by using a centrifuge. *Proc Natl Acad Sci U S A,* 110**,** 13234-5.

SAGIV, Y., LEGESSE-MILLER, A., PORAT, A. & ELAZAR, Z. 2000. GATE-16, a membrane transport modulator, interacts with NSF and the Golgi v-SNARE GOS-28. *EMBO J,* 19**,** 1494-504.

SAITOH, T., FUJITA, N., HAYASHI, T., TAKAHARA, K., SATOH, T., LEE, H., MATSUNAGA, K., KAGEYAMA, S., OMORI, H., NODA, T., YAMAMOTO, N., KAWAI, T., ISHII, K., TAKEUCHI, O., YOSHIMORI, T. & AKIRA, S. 2009. Atg9a controls dsDNA-driven dynamic translocation of STING and the innate immune response. *Proc Natl Acad Sci U S A,* 106**,** 20842-6.

SAITOH, T., FUJITA, N., JANG, M. H., UEMATSU, S., YANG, B. G., SATOH, T., OMORI, H., NODA, T., YAMAMOTO, N., KOMATSU, M., TANAKA, K., KAWAI, T., TSUJIMURA, T., TAKEUCHI, O., YOSHIMORI, T. & AKIRA, S. 2008. Loss of the autophagy protein Atg16L1 enhances endotoxin-induced IL-1beta production. *Nature,* 456**,** 264-8.

SAITSU, H., NISHIMURA, T., MURAMATSU, K., KODERA, H., KUMADA, S., SUGAI, K., KASAI-YOSHIDA, E., SAWAURA, N., NISHIDA, H., HOSHINO, A., RYUJIN, F., YOSHIOKA, S., NISHIYAMA, K., KONDO, Y., TSURUSAKI, Y., NAKASHIMA, M., MIYAKE, N., ARAKAWA, H., KATO, M., MIZUSHIMA, N. & MATSUMOTO, N. 2013. De novo mutations in the autophagy gene WDR45 cause static encephalopathy of childhood with neurodegeneration in adulthood. *Nat Genet,* 45**,** 445-9, 449e1.

SAKOH-NAKATOGAWA, M., MATOBA, K., ASAI, E., KIRISAKO, H., ISHII, J., NODA, N. N., INAGAKI, F., NAKATOGAWA, H. & OHSUMI, Y. 2013. Atg12-Atg5 conjugate enhances E2 activity of Atg3 by rearranging its catalytic site. *Nat Struct Mol Biol,* 20**,** 433-9.

SANCAK, Y., BAR-PELED, L., ZONCU, R., MARKHARD, A. L., NADA, S. & SABATINI, D. M. 2010. Ragulator-Rag complex targets mTORC1 to the lysosomal surface and is necessary for its activation by amino acids. *Cell,* 141**,** 290-303.

SANCAK, Y., PETERSON, T. R., SHAUL, Y. D., LINDQUIST, R. A., THOREEN, C. C., BAR-PELED, L. & SABATINI, D. M. 2008. The Rag GTPases bind raptor and mediate amino acid signaling to mTORC1. *Science,* 320**,** 1496-501.

SEKITO, T., KAWAMATA, T., ICHIKAWA, R., SUZUKI, K. & OHSUMI, Y. 2009. Atg17 recruits Atg9 to organize the pre-autophagosomal structure. *Genes Cells,* 14**,** 525-38.

SINZ, A. 2010. Investigation of protein-protein interactions in living cells by chemical crosslinking and mass spectrometry. *Anal Bioanal Chem,* 397**,** 3433-40.

STEELE-MORTIMER, O., BRUMELL, J. H., KNODLER, L. A., MERESSE, S., LOPEZ, A. & FINLAY, B. B. 2002. The invasion-associated type III secretion system of Salmonella enterica serovar Typhimurium is necessary for intracellular proliferation and vacuole biogenesis in epithelial cells. *Cell Microbiol,* 4**,** 43-54.

STROMHAUG, P. E., REGGIORI, F., GUAN, J., WANG, C. W. & KLIONSKY, D. J. 2004. Atg21 is a phosphoinositide binding protein required for efficient lipidation and localization of Atg8 during uptake of aminopeptidase I by selective autophagy. *Mol Biol Cell,* 15**,** 3553-66.

SUN, L. L., LI, M., SUO, F., LIU, X. M., SHEN, E. Z., YANG, B., DONG, M. Q., HE, W. Z. & DU, L. L. 2013. Global analysis of fission yeast mating genes reveals new autophagy factors. *PLoS Genet,* 9**,** e1003715.

SUN, Q., FAN, W., CHEN, K., DING, X., CHEN, S. & ZHONG, Q. 2008. Identification of Barkor as a mammalian autophagy-specific factor for Beclin 1 and class III phosphatidylinositol 3-kinase. *Proc Natl Acad Sci U S A,* 105**,** 19211-6.

SUN, Q., WESTPHAL, W., WONG, K. N., TAN, I. & ZHONG, Q. 2010. Rubicon controls endosome maturation as a Rab7 effector. *Proc Natl Acad Sci U S A,* 107**,** 19338-43.

SUZUKI, K., KUBOTA, Y., SEKITO, T. & OHSUMI, Y. 2007. Hierarchy of Atg proteins in pre-autophagosomal structure organization. *Genes Cells,* 12**,** 209-18.

TABATA, K., MATSUNAGA, K., SAKANE, A., SASAKI, T., NODA, T. & YOSHIMORI, T. 2010. Rubicon and PLEKHM1 negatively regulate the endocytic/autophagic pathway via a novel Rab7-binding domain. *Mol Biol Cell,* 21**,** 4162-72.

TAKAHASHI, Y., COPPOLA, D., MATSUSHITA, N., CUALING, H. D., SUN, M., SATO, Y., LIANG, C., JUNG, J. U., CHENG, J. Q., MULE, J. J., PLEDGER, W. J. & WANG, H. G. 2007. Bif-1 interacts with Beclin 1 through UVRAG and regulates autophagy and tumorigenesis. *Nat Cell Biol,* 9**,** 1142-51.

TAKAHASHI, Y., MEYERKORD, C. L., HORI, T., RUNKLE, K., FOX, T. E., KESTER, M., LOUGHRAN, T. P. & WANG, H. G. 2011. Bif-1 regulates Atg9 trafficking by mediating the fission of Golgi membranes during autophagy. *Autophagy,* 7**,** 61-73.

TAMURA, N., OKU, M., ITO, M., NODA, N. N., INAGAKI, F. & SAKAI, Y. 2013. Atg18 phosphoregulation controls organellar dynamics by modulating its phosphoinositide-binding activity. *J Cell Biol,* 202**,** 685-98.

TANIDA, I., TANIDA-MIYAKE, E., KOMATSU, M., UENO, T. & KOMINAMI, E. 2002. Human Apg3p/Aut1p homologue is an authentic E2 enzyme for multiple substrates, GATE-16, GABARAP, and MAP-LC3, and facilitates the conjugation of hApg12p to hApg5p. *J Biol Chem,* 277**,** 13739-44.

TANIDA, I., TANIDA-MIYAKE, E., UENO, T. & KOMINAMI, E. 2001. The human homolog of Saccharomyces cerevisiae Apg7p is a Protein-activating enzyme for multiple substrates including human Apg12p, GATE-16, GABARAP, and MAP-LC3. *J Biol Chem,* 276**,** 1701-6.

TATTOLI, I., SORBARA, M. T., VUCKOVIC, D., LING, A., SOARES, F., CARNEIRO, L. A., YANG, C., EMILI, A., PHILPOTT, D. J. & GIRARDIN, S. E. 2012. Amino acid starvation induced by invasive bacterial pathogens triggers an innate host defense program. *Cell Host Microbe,* 11**,** 563-75.

THURSTON, T. L., RYZHAKOV, G., BLOOR, S., VON MUHLINEN, N. & RANDOW, F. 2009. The TBK1 adaptor and autophagy receptor NDP52 restricts the proliferation of ubiquitin-coated bacteria. *Nat Immunol,* 10**,** 1215-21.

THURSTON, T. L., WANDEL, M. P., VON MUHLINEN, N., FOEGLEIN, A. & RANDOW, F. 2012. Galectin 8 targets damaged vesicles for autophagy to defend cells against bacterial invasion. *Nature,* 482**,** 414-8.

TSUKADA, M. & OHSUMI, Y. 1993. Isolation and characterization of autophagy-defective mutants of Saccharomyces cerevisiae. *FEBS Lett,* 333**,** 169-74.

VAN DAM, E. M. & STOORVOGEL, W. 2002. Dynamin-dependent transferrin receptor recycling by endosome-derived clathrin-coated vesicles. *Mol Biol Cell,* 13**,** 169-82.

VAN DER VAART, A., GRIFFITH, J. & REGGIORI, F. 2010. Exit from the Golgi is required for the expansion of the autophagosomal phagophore in yeast Saccharomyces cerevisiae. *Mol Biol Cell,* 21**,** 2270-84.

VAN MEER, G., VOELKER, D. R. & FEIGENSON, G. W. 2008. Membrane lipids: where they are and how they behave. *Nat Rev Mol Cell Biol,* 9**,** 112-24.

VELIKKAKATH, A. K., NISHIMURA, T., OITA, E., ISHIHARA, N. & MIZUSHIMA, N. 2012. Mammalian Atg2 proteins are essential for autophagosome formation and important for regulation of size and distribution of lipid droplets. *Mol Biol Cell,* 23**,** 896-909.

VICINANZA, M., D'ANGELO, G., DI CAMPLI, A. & DE MATTEIS, M. A. 2008. Function and dysfunction of the PI system in membrane trafficking. *EMBO J,* 27**,** 2457-70.

WANG, C. W., KIM, J., HUANG, W. P., ABELIOVICH, H., STROMHAUG, P. E., DUNN, W. A., JR. & KLIONSKY, D. J. 2001. Apg2 is a novel protein required for the cytoplasm to vacuole targeting, autophagy, and pexophagy pathways. *J Biol Chem,* 276**,** 30442-51.

WATANABE, Y., KOBAYASHI, T., YAMAMOTO, H., HOSHIDA, H., AKADA, R., INAGAKI, F., OHSUMI, Y. & NODA, N. N. 2012. Structure-based analyses reveal

distinct binding sites for Atg2 and phosphoinositides in Atg18. *J Biol Chem,* 287**,** 31681-90.

WEBBER, J. L. & TOOZE, S. A. 2010. Coordinated regulation of autophagy by p38alpha MAPK through mAtg9 and p38IP. *EMBO J,* 29**,** 27-40.

WEIDBERG, H., SHVETS, E., SHPILKA, T., SHIMRON, F., SHINDER, V. & ELAZAR, Z. 2010. LC3 and GATE-16/GABARAP subfamilies are both essential yet act differently in autophagosome biogenesis. *EMBO J,* 29**,** 1792-802.

WHITE, E. 2012. Deconvoluting the context-dependent role for autophagy in cancer. *Nat Rev Cancer,* 12**,** 401-10.

WILD, P., FARHAN, H., MCEWAN, D. G., WAGNER, S., ROGOV, V. V., BRADY, N. R., RICHTER, B., KORAC, J., WAIDMANN, O., CHOUDHARY, C., DOTSCH, V., BUMANN, D. & DIKIC, I. 2011. Phosphorylation of the autophagy receptor optineurin restricts Salmonella growth. *Science,* 333**,** 228-33.

WRIGHT, L. P. & PHILIPS, M. R. 2006. Thematic review series: lipid posttranslational modifications. CAAX modification and membrane targeting of Ras. *J Lipid Res,* 47**,** 883-91.

XIAO, B., SANDERS, M. J., UNDERWOOD, E., HEATH, R., MAYER, F. V., CARMENA, D., JING, C., WALKER, P. A., ECCLESTON, J. F., HAIRE, L. F., SAIU, P., HOWELL, S. A., AASLAND, R., MARTIN, S. R., CARLING, D. & GAMBLIN, S. J. 2011. Structure of mammalian AMPK and its regulation by ADP. *Nature,* 472**,** 230-3.

XU, C. & MIN, J. 2011. Structure and function of WD40 domain proteins. *Protein Cell,* 2**,** 202-14.

YAN, Y., FLINN, R. J., WU, H., SCHNUR, R. S. & BACKER, J. M. 2009. hVps15, but not Ca2+/CaM, is required for the activity and regulation of hVps34 in mammalian cells. *Biochem J,* 417**,** 747-55.

YLA-ANTTILA, P., VIHINEN, H., JOKITALO, E. & ESKELINEN, E. L. 2009. 3D tomography reveals connections between the phagophore and endoplasmic reticulum. *Autophagy,* 5**,** 1180-5.

YOUNG, A. R., CHAN, E. Y., HU, X. W., KOCHL, R., CRAWSHAW, S. G., HIGH, S., HAILEY, D. W., LIPPINCOTT-SCHWARTZ, J. & TOOZE, S. A. 2006. Starvation and ULK1-dependent cycling of mammalian Atg9 between the TGN and endosomes. *J Cell Sci,* 119**,** 3888-900.

ZHANG, H., CICCHETTI, G., ONDA, H., KOON, H. B., ASRICAN, K., BAJRASZEWSKI, N., VAZQUEZ, F., CARPENTER, C. L. & KWIATKOWSKI, D. J. 2003. Loss of Tsc1/Tsc2 activates mTOR and disrupts PI3K-Akt signaling through downregulation of PDGFR. *J Clin Invest,* 112**,** 1223-33.

ZHENG, Y. T., SHAHNAZARI, S., BRECH, A., LAMARK, T., JOHANSEN, T. & BRUMELL, J. H. 2009. The adaptor protein p62/SQSTM1 targets invading bacteria to the autophagy pathway. *J Immunol,* 183**,** 5909-16.

ZHONG, Y., WANG, Q. J., LI, X., YAN, Y., BACKER, J. M., CHAIT, B. T., HEINTZ, N. & YUE, Z. 2009. Distinct regulation of autophagic activity by Atg14L and Rubicon associated with Beclin 1-phosphatidylinositol-3-kinase complex. *Nat Cell Biol,* 11**,** 468-76.

ZONCU, R., BAR-PELED, L., EFEYAN, A., WANG, S., SANCAK, Y. & SABATINI, D. M. 2011. mTORC1 senses lysosomal amino acids through an inside-out mechanism that requires the vacuolar H(+)-ATPase. *Science,* 334**,** 678-83.